

---

# **Retrogression of eclogites to blueschists: a record of fluid infiltration during uplift in subduction zones**

---

Dissertation  
zur Erlangung des Doktorgrades  
der Mathematisch-Naturwissenschaftlichen Fakultät  
der Christian-Albrechts-Universität  
zu Kiel

vorgelegt von  
François van der Straaten



Kiel, 2008



---

# Eklogit-Blauschiefer Umwandlung: Hinweise auf Fluidinfiltrierung während des Aufstiegs in Subduktionszonen

---

Dissertation  
zur Erlangung des Doktorgrades  
der Mathematisch-Naturwissenschaftlichen Fakultät  
der Christian-Albrechts-Universität  
zu Kiel

vorgelegt von  
François van der Straaten



Wappen der Familie van der Straaten

Kiel, 2008

Referent: *Prof. Dr. Volker Schenk*

Korreferent/in: *Prof. Dr. Astrid Holzheid.*

Tag der mündlichen Prüfung: *04. November 2008*

Zum Druck genehmigt: *Kiel, .....*

Der Dekan

# Vorwort

Die vorliegende Arbeit ist eine monographische Dissertation und beinhaltet drei von einander getrennte Kapitel mit einer vorangestellten Einleitung. Die Gesamtheit aller Kapitel spiegelt das Thema der Dissertation wieder. Jedes Kapitel für sich kann oder wurde bereits in Fachzeitschriften publiziert. Daher sei für den Leser angemerkt, dass jedes Kapitel eine Zusammenfassung, Einleitung, Diskussion und Literaturangabe enthält. Mögliche thematische Überschneidungen oder Wiederholungen sind daher zu berücksichtigen.

Kiel, September 2008

*Man setzt der Finsternis ein  
Ende und durchforscht bis zur  
äußersten Grenze das Gestein der  
Dunkelheit und Finsternis.*

Buch Hiob: 28,3

*Und er öffnete den Schlund des  
Abgrundes; und ein Rauch stieg  
auf aus dem Schlund... und die  
Luft wurden von dem Rauch des  
Schlundes verfinstert.*

Offenbarung: 9,2

*Der tiefe Fluss ist ruhig – der wis-  
sende Mensch ist bescheiden.*

aus der Mongolei

*In Wirklichkeit erkennen wir  
nichts; denn die Wahrheit liegt in  
der Tiefe.*

Demokrit

# Contents

<b>Zusammenfassung</b>	<b>xi</b>
<b>Abstract</b>	<b>xiii</b>
<b>1 Introduction</b>	<b>1</b>
1.1 The slab-mantle interface and subduction channel . . . . .	1
1.2 Aim of study . . . . .	2
1.3 Study approach and analytical techniques . . . . .	3
1.4 Outline of the thesis . . . . .	4
References . . . . .	6
<b>2 Fluid-rock interaction in the subduction channel</b>	<b>7</b>
2.1 Introduction . . . . .	8
2.2 Geology . . . . .	9
2.3 Analytical methods . . . . .	11
2.4 Field area . . . . .	12
2.5 Petrology . . . . .	12
2.5.1 Mineral chemistry . . . . .	16
2.5.2 Metamorphic reaction history . . . . .	26
2.5.3 P-T evolution . . . . .	27
2.6 Bulk rock geochemistry . . . . .	30
2.6.1 Eclogite domain . . . . .	30
2.6.2 Blueschist domains . . . . .	30
2.7 Discussion . . . . .	35
2.7.1 Evidence for pre-metamorphic seafloor alteration? . . . . .	35
2.7.2 Mass-balance calculation . . . . .	36
2.7.3 Mineral reactions and element mobility . . . . .	38
2.7.4 Characteristics of the infiltrating fluid . . . . .	41
2.7.5 Fluid infiltration & eclogite-blueschist transformation . . . . .	44
2.7.6 Influence of the eclogite-blueschist transformation on fluid-rock interaction in the subduction channel . . . . .	45
2.8 Summary and conclusion . . . . .	46
2.9 Acknowledgement . . . . .	47

References . . . . .	48
<b>3 Chemical and petrophysical changes during exhumation</b>	<b>53</b>
3.1 Abstract . . . . .	53
3.2 Introduction . . . . .	53
3.3 Geological and petrological description . . . . .	55
3.3.1 Tian Shan . . . . .	55
3.3.2 Sifnos . . . . .	56
3.4 Analytical methods . . . . .	60
3.5 Geochemistry . . . . .	62
3.5.1 Whole rock major and trace elements . . . . .	64
3.6 Mineral chemistry . . . . .	66
3.6.1 Garnet . . . . .	66
3.6.2 Clinopyroxene . . . . .	68
3.6.3 Amphibole . . . . .	70
3.6.4 White mica . . . . .	73
3.6.5 Epidote mineral . . . . .	74
3.6.6 Other minerals . . . . .	75
3.7 Discussion . . . . .	76
3.7.1 Nature of the eclogite protholiths . . . . .	76
3.7.2 P-T path and metamorphic evolution . . . . .	77
3.7.3 Element mobility, mass-balance and metasomatism during the eclogite-blueschist transformation . . . . .	85
3.7.4 Exhumation processes in the subduction channel . . . . .	88
3.7.5 Conclusions . . . . .	90
3.8 Acknowledgement . . . . .	91
References . . . . .	92
<b>4 Isotope variations: constraints on fluid source</b>	<b>97</b>
4.1 Abstract . . . . .	97
4.2 Introduction . . . . .	98
4.3 Eclogite-blueschist transformation on Sifnos (Greece) . . . . .	99
4.4 Blueschist-facies overprint of eclogites in Tian Shan (China) . . . . .	103
4.5 Analytical methods . . . . .	105
4.6 Isotope geochemistry results . . . . .	105
4.7 Discussion . . . . .	109
4.7.1 Stable oxygen isotopes: constraints on metamorphic equilibrium and metamorphic temperatures . . . . .	109
4.7.2 Evidence for inherited seawater alteration? . . . . .	114
4.7.3 Evidence for serpentinite-derived fluids . . . . .	117
4.7.4 Fluid-rock interaction and isotope constraints on fluid source . . . . .	119
4.7.5 Implications for element budget of subduction zones . . . . .	121
4.8 Conclusions . . . . .	121



4.9 Acknowledgements . . . . .	122
References . . . . .	123
<b>List of Figures</b>	<b>130</b>
<b>List of Tables</b>	<b>131</b>
<b>A Appendix related to Chapter 2 and 3</b>	<b>133</b>
<b>Addendum</b>	<b>139</b>



# Zusammenfassung

Während der Subduktion ozeanischer Platten in den Erdmantel entstehen durch metamorphe Entwässerungsprozesse Fluide, die in den darüber liegenden Mantelkeil gelangen und den dort vorliegenden Peridotit teilweise serpentinisieren. Der direkt über der subduzierten ozeanischen Lithosphäre liegende partiell serpentinierte Teil des Mantelkeiles wird Subduktionskanal (englisch: *subduction channel*) genannt. Er ist wegen der geänderten rheologischen Eigenschaften gegenüber dem nicht hydratisierten Mantelperidotit mobil. So ist der Serpentin im *subduction channel*, aufgrund des großen Dichteunterschiedes zwischen diesen beiden Gesteinstypen in der Lage, Bruchstücke der eklogitisierten ozeanischen Kruste nach oben in oberflächennahe Tiefen zu transportieren. Dabei werden die aufsteigenden, weitgehend entwässerten Hochdruckgesteine partiell wieder hydratisiert.

Diese Arbeit liefert einen Beitrag über die Zusammensetzung und Wirkungsweise der Fluide, die auf Eklogite einwirken, wenn sie retrograd in Blauschiefer umgewandelt werden. Dabei wird untersucht, wie die Fluidinfiltration sich auf die petrophysikalischen Eigenschaften der Eklogite auswirkt und wie aus den chemischen Daten Rückschlüsse auf die Zusammensetzung und die Herkunft des Fluids gezogen werden können.

Zu diesem Zweck wurden partiell zu Blauschiefer umgewandelte Eklogite von Sifnos in Griechenland und aus dem chinesischen Teil des südlichen Tian Shan gesammelt. Drei repräsentative Proben-Sequenzen mit lateralem Eklogit-Blauschiefer-Übergang im dm- bis m-Bereich wurden petrografisch, gesteins- und mineralchemisch untersucht. Die petrografischen Gesteins-Dünnschliffe liefern Informationen über die Mineralreaktionen während der Eklogit-Blauschiefer-Überprägung. Die Gesamtgesteinsanalyse zur Bestimmung der Haupt- und Spurenelemente erfolgte mit der RFA, ICP-MS oder ICP-OES. Die Analyse der gleichen Elementgruppen wurden in situ an Mineralen durch die Kombination von Mikrosonde und LA-ICP-MS durchgeführt. Von jedem Gestein wurde zudem die Gesamtgesteinsdichte mit Pyknometern nach dem Prinzip der Verdrängung bestimmt. Der prograde und retrograde Druck- und Temperaturpfad der blauschieferüberprägten Eklogite wurde mit Hilfe dieser Daten und dem thermodynamischen Kalkulationsprogramm *Perple\_X* rekonstruiert. Aus den chemischen Daten der reliktsch erhaltenen Eklogite und den assoziierten Blauschiefern lässt sich durch Massenbilanzierung auf die Zusammensetzung der eindringenden Fluide schließen. Strontium- und Neodymisotopie der Eklogit- und Blauschiefer-Gesamtgesteinszusammensetzung dienen als Tracer, um die mögliche Quelle der Fluide zu bestimmen oder diese unter den potentiellen lithologischen Einheiten einzugrenzen.

Alle drei untersuchten Sequenzen zeigen einen Übergang von Eklogit zu Blauschiefer. Blauschieferfazieller Glaukophan, Hellglimmer und das Karbonat wachsen auf Kosten der eklogitfaziellen Paragenese Granat und Omphazit. Der retrograde P-T Pfad ist durch Abkühlung bei gleichzeitigem Druckabfall gekennzeichnet. Diese Konstellation lässt auf den Aufstieg dieser Gesteine im *subduction channel* schließen. Dabei können sowohl Serpentine als auch subduzierte Marmore oder Metapelite die Rolle des Transportmediums im *subduction channel* übernehmen. Die Sauerstoffisotopie der Minerale zeigen ein isotopisches Gleichgewicht der eklogitfaziellen Minerale Granat und Omphazit (in Fällen auch mit Phengit) und ebenso zwischen den blauschieferfaziellen Mineralen Glaukophan und Hellglimmer. In der Sifnos-Sequenz ist zusätzlich eine grünschieferfazielle Überprägung erkennbar. Die Fluidinfiltrierung bewirkte eine Veränderung des Elementhaushaltes in den Gesteinen. Vor allem **Large Ion Lithophile Elements (LILE: Cs, Rb, Ba, K)**, CO<sub>2</sub>, Mg, Ni und Co wurden den Blauschiefern hinzugefügt, während seltene Erdelemente, Si und Ca mobilisiert und aus dem System entfernt wurden. Dabei verhielten sich die **High Field Strength Elements (HFSE: Zr, Hf, Ti, Nb, Ta)** immobil. Dieser Elementaustausch lässt auf eine Fluide schließen, die im Gleichgewicht mit Gesteinen peridotitischer Zusammensetzung stand. Die Serpentine, Chlorit- und Talkschiefer aus der Zone des Übergangs von der abtauchenden Platte zum darüber liegenden Mantel und im *subduction channel* werden als die wahrscheinlichsten peridotitischen Gesteinsquellen der Fluide angesehen. Die erhöhte Nd-Isotopen Signatur von Blauschiefer gegenüber Eklogit in einer Eklogit-Blauschiefer-Sequenz des Tian Shans zeigt deutlich eine Gleichgewichtseinstellung mit einer peridotitischen Matrix. Erhöhte Sr-Isotopenwerte in den Eklogit-Blauschiefer-Übergängen lassen auf die Einwirkung von metamorphen Fluiden schließen, die eine ererbte Sr-Isotopen Signatur von Seewasser-alterierten und entwässerten ozeanischen Gesteinen aufweist. Die hier dargestellten chemischen Charakteristika der Fluide entsprechen der letzten Gleichgewichtseinstellung, bevor diese die Eklogite infiltrierte und in Blauschiefer umwandelte. Über die Entwicklung und die Herkunft der Fluide lässt sich wie folgt spekulieren: Die Fluide wurde aus der Entwässerung von subduzierten serpentinierten Mantelperidotiten gebildet und ist anschließend durch die abtauchende ozeanische Kruste geströmt und wurde dort mit LILE und CO<sub>2</sub> angereichert, die aus der Entwässerung der alterierten ozeanischen Kruste oder den aufliegenden Sedimenten stammen.

# Abstract

Fluids in subduction zones were formed by metamorphic devolatilisation processes, during the subduction of the oceanic plate into the mantle. The fluids enter the mantle wedge and cause the partial serpentinisation of the mantle peridotite above the descending oceanic lithosphere. This part of the mantle wedge is called the *subduction channel*. The present serpentinite in the subduction channel is capable to flow, due to its changed rheological properties and compared to the non-hydrated mantle peridotite. The serpentinite is able to transport fragments of the eclogitised oceanic crust to shallower depths of the fore arc, due to the large density difference of both rock types. The ascending nearly dehydrated HP rocks may rehydrate partially.

This study gives a contribution to the composition and behaviour of the fluid that affected eclogites, which were transformed retrogradly to blueschists. Hereby the effects to the petrophysical properties induced by the fluid-infiltration will be analysed. Chemical data should give insights to the composition, characteristic and possible source of the fluid.

For these purposes we sampled blueschist-facies overprinted eclogites from the island Sifnos in Greece and from the Chinese part of the South Tian Shan. Three representative eclogite-blueschist transformation sequences in dm- and m-size were investigated by petrography, whole rock and mineral chemistry. Thin sections provide petrographic information about mineral reactions during the eclogite-blueschist transition. Major and trace elements were analysed by XRF, ICP-MS and ICP-OES. In situ mineral analyses were determined by electron-microprobe and LA-ICP-MS. The whole rock density was estimated by pycnometer after the principle of displacement. Based on this data and under application of the thermodynamical calculation program *Perple\_X*, the P-T path of the blueschist-facies overprinted eclogites was reconstructed. The chemical composition of the infiltrating fluid was estimated, based on mass-balance calculations from the element content of the partially preserved eclogite and the associated blueschist. Whole rock Sr and Nd isotope signatures of eclogites and blueschists were used as tracer to determine the possible source of the fluid or to constrain it from the potential lithological units.

All three investigated sequences show retrogradly the transformation from eclogite to blueschist. The blueschist-facies minerals glaucophane, white mica and carbonate growing newly at the expense of the eclogite-facies assemblage omphacite and garnet. The calculated P-T path is characterised by contemporaneous cooling and decompression, which is crucial for the exhumation within the subduction channel. Serpentinite, but as well subducted marbles or metapelite can take over the role of the transport matrix in the subduction channel. The oxygen isotope composition of mineral separates shows an equi-

librium in the eclogite-facies assemblage omphacite and garnet (in cases phengite) and in the blueschist-facies assemblage glaucophane and white mica. In addition, the Sifnos-sequence shows a greenschist-facies overprint. The fluid infiltration causes a change in the element budget of the infiltrated HP rocks. Particularly a gain in **Large Ion Lithophile Elements (LILE: Cs, Rb, Ba, K)**,  $\text{CO}_2$ , Mg, Ni and Co and a loss of REE, Si and Ca is observed, while **High Field Strength Elements (HFSE: Zr, Hf, Ti, Nb, Ta)** behave immobile. This element exchange during the eclogite-blueschist transformation implies a fluid composition, which was in equilibrium with rocks of peridotitic composition. Serpentine, chlorite and talc schist are the most conceivable types of peridotitic rocks in the transition between the descending slab and the mantle wedge and in the subduction channel. Elevated Nd isotopic compositions of the blueschist compared to the eclogite in one sequence of the Tian Shan, shows clearly the equilibration of the peridotitic rock-source. Elevated Sr isotopic compositions of the eclogite-blueschist sequences in the Tian Shan may suggest on the derivation of metamorphic fluids with inherited Sr signature caused by devolatilisation from seawater altered and subducted oceanic rocks. The here described chemical characteristics of the fluid show the latest equilibration stage prior to the infiltration of the eclogites and the transformation to blueschists. The development and the source of the fluid is speculative to discuss as follows: The fluids derived from devolatilisation processes of the subducted lithospheric peridotite with subsequent flow through the subducting slab, where it was enriched with LILE and  $\text{CO}_2$  from the altered oceanic crust or the above lying sediments.

# Chapter 1

## Introduction

### 1.1 The slab-mantle interface and subduction channel

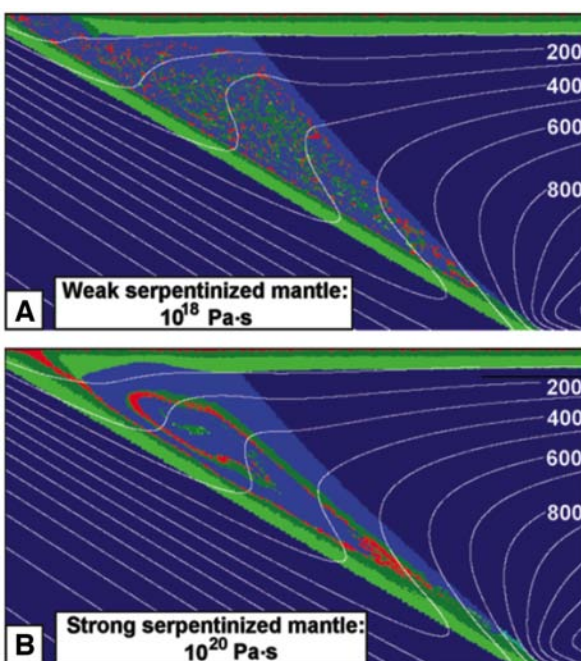


**Figure 1.1:** Numerical model of the subduction channel at A: low viscosity of the serpentinised mantle peridotite and B: high viscosity, modified after [Gerya et al. \(2002\)](#). Colours: red = sedimentary rocks; dark green = basaltic upper oceanic crust; light green = gabbroic lower oceanic crust; dark blue = unhydrated mantle; light blue = serpentinized mantle; turquoise = hydrated mantle beyond stability field of antigorite.

The slab-mantle interface in subduction zones may be defined as the zone between the upper crust of the down going oceanic slab and the peridotite of the mantle wedge above the slab (e.g. [Bebout and Barton, 2002](#)). During the descent of the slab in the mantle, parts of the upper oceanic crust split off and concentrate in the slab-mantle interface. During subduction several devolatilisation reactions occur in the different lithological parts of the slab, which are from the upper to the lower crust: the marine sediment layer, the altered and unaltered oceanic basaltic crust and the unaltered or partially serpentinised lithospheric slab mantle. At the prevailing pressures and temperatures in the deep subduction zone the released volatiles behave as fluids and migrate upwards to the slab-mantle interface and into the mantle wedge. Thus, the separated rocks at the slab-mantle interface are exposed to a fluid-rich environment. The slab-mantle interface was described in detail e.g. by [Bebout and Barton \(2002\)](#) and is also labelled as subduction zone *mélange* ([King et al., 2003, 2006](#)).

[Shreve and Cloos \(1986\)](#) and [Cloos and Shreve \(1988\)](#) introduced the term *subduction channel* for this *mélange* zone. Based on the hypothesis of the formation of the *subduction*

channel Gerya et al. (2002) developed thermo-mechanical models, which supported the hypothesis. Gerya et al. (2002) defined the *subduction channel* as the partially serpentinised mantle peridotite above the subducting slab that has changed rheological characteristics, mainly in viscosity and in buoyancy forces (Figure 1.1). Gerya et al. (2002) modelled in addition P-T paths of sheared, cut and incorporated HP rocks during their ascent within the subduction channel, in which the serpentinite is able to transport subduction zone rocks to shallower levels (Schwartz et al., 2001; Gerya et al., 2002; Warren et al., 2008) of the subduction zone. The retrograde P-T paths are characterised by cooling during uplift (Figure 1.2) and thus verify the field and petrological observations made by Ernst (1979), who summarised the P-T paths of uplifted HP rocks of paleo-subduction zones, worldwide.

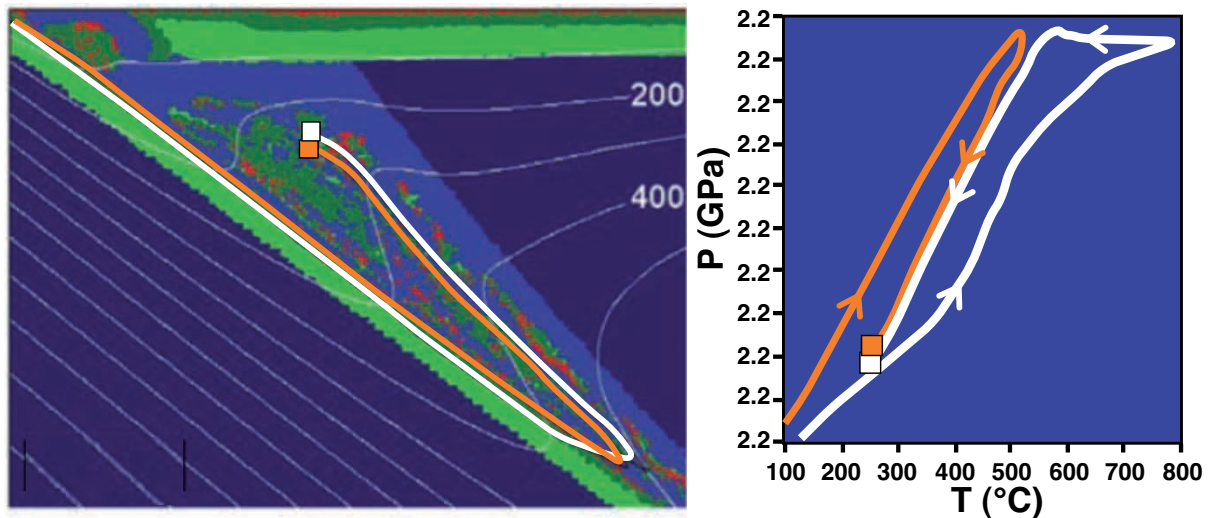


**Figure 1.2:** Subduction channel model and calculated P-T paths of two different slab fragments, modified after Gerya et al. (2002). Left: Formation of the subduction channel in the mantle wedge above a descending slab; same colour code as in Figure 1.1; right: P-T paths, white: anticlockwise path of an early incorporated slab fragment; orange: clockwise path of mature subducted and incorporated slab fragment.

## 1.2 Aim of study

The *Sonderforschungsbereich 574* (special collaborative research center) of the university of Kiel, founded in 2001, investigates the fluid and volatile cycles in subduction zones. Subproject C1, of which this thesis is a part, analyses the metamorphic devolatilisation and volatilisation processes within the descending slab and within the subduction channel. Details about the processes and the evolution of HP/UHP rocks that are incorporated in the subduction channel are not well known until now. In addition, there are only few data available about the fluids that react within the subduction channel with the incorporated HP/UHP rocks, which are surrounded predominantly by a serpentinite matrix. This thesis is aimed to give insights into the processes that HP/UHP rocks experience during their



ascent within a subduction channel. Details about the chemical composition and the reactivity of the fluids will be given that react with the ascending HP/UHP rocks. Chemical tracer should help to constrain possible source-rocks of the infiltrating fluids. In this study I investigated eclogites, which became overprinted by a blueschist-facies mineralogy. Eclogites that are free of prograde hydrous minerals are ideal subjects for this study, as all volatile-bearing phases had broken down during their subduction. In addition, many eclogites display a MORB chemistry, which is well characterised, and therefore better when chemical changes have to be discussed. Sampling areas were chosen on the island of Sifnos as part of the Tertiary Cycladic archipelago in Greece and from the Chinese part of the late Carboniferous Southern Tian Shan. Both areas are assumed to contain rocks of paleo-subduction zones that are outcropping in tectonic mélanges.

### 1.3 Study approach and analytical techniques

The work for this Ph.D. thesis started with extensive field work in the Cyclades (Greece) and in the Tian Shan (China). The sampling was focused on eclogites that show partial overprinting by blueschist-facies metamorphism. In the Tian Shan the use of a rock driller was preferred if outcrops showed detailed structures, which would have been destroyed when slashed with a hammer. Thin sections of all rocks were examined by polarising microscopy. Samples showing clear textures of the retrograde eclogite-blueschist transformation were used for further studies. In total, three sequences of eclogite-blueschist transformation (one from Sifnos in Greece and two from the South Tian Shan in China) were analysed. Coexisting eclogite and blueschist domains in one sample or drilling core were separated by hand with a preparation stone saw. Major and trace element contents of all separated eclogite and blueschist domains were determined by X-ray fluorescence (XRF) and Inductively Coupled Plasma Mass Spectrometry (ICP-MS). The mineral chemistry of selected samples was determined on polished thin sections using an electron microprobe and a Laser Ablation ICP-MS. Whole rock densities were determined with pycnometers that worked after the principle of displacement. These data were used in combination with the petrographical observations to estimate the P-T history of the rocks, by using thermobarometric calculations. P-T pseudosections, calculated with the thermodynamical calculation program *Perple\_X* (Connolly, 1990), were dominantly used. These calculations required an intensive practice in the use of the program in advance. Element concentrations in eclogite and blueschist domains of the certain sample sequence were compared in mass-balance calculations, following the method of Ague (2003). When the first results had been obtained and some parts of the infiltration process had been understood, oxygen isotope analyses of mineral separates of eclogite and blueschist domains and whole rock Sr and Nd isotope analyses were performed to constrain the source of the fluids, which infiltrated the eclogites and caused the blueschist-facies overprint.

## 1.4 Outline of the thesis

The following main part of this thesis is subdivided into three chapters, which already have been published (Chapter 2) or have been submitted for publication (Chapter 3) or will be submitted soon (Chapter 4). The present study focused on a few keypoints:

*Chapter 2* describes the processes and the implications of the fluid infiltration on pillow basalts of former eclogite-facies mineralogy of the Tian Shan, metamorphosed under eclogite-facies conditions, where the pillow rims were partially transformed to blueschists. Detailed geochemical whole rock and mineral analyses allow the investigation of element mobility during the eclogite-blueschist transformation and the composition of the infiltrating fluid. P-T pseudosections were calculated, which support the hypothesis that these pillow basalts were exhumed within a subduction channel, which requires a specific P-T path. This chapter is already published as:

van der Straaten, F., Schenk, V., John, T., Gao, J. (2008): Blueschist-facies rehydration of eclogites (Tian Shan, NW-China): implications for fluid-rock interaction in the subduction channel. *Chemical Geology*, **255** (1-2): 195-219.

*Chapter 3* describes in detail two sample sequences in which eclogites became increasingly transformed to blueschists. The first sequence is from Sifnos and a second one is from the Tian Shan (FTS 9–1 seq). From both sequences the P-T paths were deduced by P-T pseudosection calculations. The mineral chemistry gives details about the element mobility during the eclogite-blueschist transformation. The Tian Shan eclogite-blueschist transformation is compared to the Sifnos sample sequence in their chemistry, P-T evolution and exhumation. Finally, it is discussed whether the theoretical concept of uplift within the serpentinite matrix of the subduction channel applies to the studied samples.

This chapter has been submitted to *Contributions to Mineralogy and Petrology*:

van der Straaten, F., Schenk, V., John, T.: Fluid-induced chemical and petrophysical changes associated with the retrograde eclogite-blueschist transformation: Constraints for metasomatism and exhumation within a subduction channel. *Contributions to Mineralogy and Petrology*.

*Chapter 4* combines the results of the two previous chapters with stable and radiogenic isotope analyses of three eclogite-blueschist transformation sequences from Sifnos and the Tian Shan. The isotope analyses were made to evaluate the possible lithological source of the infiltrating fluid. The chemical characteristics of the fluids were obtained by the combining element chemistry with the results of the mineral oxygen isotope composition and the whole rock Sr and Nd isotope composition.

This chapter will be submitted to *Chemical Geology*:

---

van der Straaten, F., Schenk, V., John, T., Halama, R.: The chemical and Sr-Nd-O isotopic compositions of subduction channel fluids: Constraints from eclogites partially transformed to blueschists. *Chemical Geology*.

This thesis gives a detailed look at the geochemical signature of subduction channel fluids and the element mobility during the eclogite-blueschist transformation induced by infiltrating fluids, which were not much studied until now. The results show that the fluids acting within the subduction channel have obtained their characteristics by interaction with serpentinite or rocks of peridotitic composition prior to infiltration into eclogites. The presented results enhance the understanding of fluid processes in subduction channels.

## References

- Ague, J. J., 2003. Fluid infiltration and transport of major, minor, and trace elements during regional metamorphism of carbonate rocks, Wepawaug Schist, Connecticut, USA. *American Journal of Science* 303, 753–816.
- Bebout, G. E., Barton, M. D., 2002. Tectonic and metasomatic mixing in a high-T, subduction-zone melange; insights into the geochemical evolution of the slab-mantle interface. *Chemical Geology* 187 (1-2), 79–106.
- Cloos, M., Shreve, R. L., 1988. Subduction-channel model of prism accretion, melange formation, sediment subduction, and subduction erosion at convergent plate margins; Part I, Background and description. *Pure and Applied Geophysics* 128 (3-4), 455–500.
- Connolly, J. A. D., 1990. Multivariable phase diagrams; an algorithm based on generalized thermodynamics. *American Journal of Science* 290 (6), 666–718.
- Ernst, W. G., 1979. Coexisting sodic and calcic amphiboles from high-pressure metamorphic belts and the stability of barroisitic amphibole. *Mineralogical Magazine* 43 (326), 269–278.
- Gerya, T. V., Stöckhert, B., Perchuk, A. L., 2002. Exhumation of high-pressure metamorphic rocks in a subduction channel; a numerical simulation. *Tectonics* 21 (6), 1056, doi:10.1029/2002TC001406.
- King, R. L., Bebout, G. E., Moriguti, T., Nakamura, E., 2006. Elemental mixing systematics and Sr-Nd isotope geochemistry of melange formation: Obstacles to identification of fluid sources to arc volcanics. *Earth and Planetary Science Letters* 246, 288–304.
- King, R. L., Kohn, M. J., Eiler, J. M., 2003. Constraints on the petrologic structure of the subduction zone slab-mantle interface from Franciscan Complex exotic ultramafic blocks. *Geological Society of America Bulletin* 115 (9), 1097–1109.
- Schwartz, S., Allemand, P., Guillot, S., 2001. Numerical model of the effect of serpentinites on the exhumation of eclogitic rocks; insights from the Monviso ophiolitic massif (Western Alps). *Tectonophysics* 342 (1-2), 193–206.
- Shreve, R. L., Cloos, M., 1986. Dynamics of sediment subduction, melange formation, and prism accretion. *Journal of Geophysical Research*. B 91 (10), 10229–10245.
- Warren, C. J., Beaumont, C., Jamieson, R. A., 2008. Modelling tectonic styles and ultra-high pressure (UHP) rock exhumation during the transition from oceanic subduction to continental collision. *Earth and Planetary Science Letters* 267 (1-2), 129–145.

# Chapter 2

## BLUESCHIST-FACIES REHYDRATION OF ECLOGITES (TIAN SHAN, NW-CHINA): IMPLICATIONS FOR FLUID-ROCK INTERACTION IN THE SUBDUCTION CHANNEL

### Abstract

Chemical changes associated with the rehydration of dry eclogites to form blueschists were studied to obtain information about the chemistry of the fluids infiltrating during this retrograde metamorphic overprint. The studied eclogites of the Tian Shan were formed during Carboniferous subduction of pillow basalts that show typical ocean island basalt geochemical signatures. The retrograde P-T path is characterised by decompression associated with cooling, typical for fragments of a subducting slab that are ascending in the cool and hydrated subduction channel. The fluids infiltrating the eclogites are interpreted to represent dehydration fluids of the down going slab that ascended to the overlying subduction channel. The rehydration of the eclogites proceeded from the pillow margins producing two concentric shells consisting of glaucophane-dominated blueschists (inner shell) and phengite-ankerite blueschists (outer shell) replacing omphacite and garnet of the eclogite. Mass-balance calculations based on major and trace element compositions of eclogites and blueschists point to high element mobility during fluid infiltration and associated metamorphic reactions. Blueschists show lower contents of REE, Y, Sr, Pb, U, P, Ca, Na, Al and Si compared to eclogites, indicating a loss of these elements, but they show higher contents of volatiles, Mg, transition metals and LILE, indicating a gain of these elements. The chemical changes point to a composition of the infiltrating fluid that has an affinity to fluids derived from serpentinites, i.e. with low concentrations in Si, Al, Ca and Na and high concentrations in Mg, Co and Ni. The gain of Cu, Mn, Zn and LILE in the blueschists points to an addition of a sediment-derived component in the serpentinite-derived fluid. The pronounced enrichment of  $K_2O$  and of Ba at constant Ba/Th ratios in the blueschists resembles those of island arc basalts derived from a fluid-enriched source. The low element load of the fluid equilibrated with Mg-rich *mélange* zones induces the mo-

bility of most of the elements during the eclogite-blueschist transformation to compensate for disequilibrium between the mafic rock and the infiltrating fluid. The associated volume loss enhances the fluid infiltration into the eclogite interior. Increasing precipitation rates and/or diminishing diffusion rates for element removal brought the eclogite-blueschist transformation to an end, which resulted in the preservation of eclogite in the pillow cores.

## 2.1 Introduction

Slab-released volatiles in subduction zones are believed to undergo several pathways at active continental margins. The fluids either expel from the down going plate by sediment compaction or diagenetic processes and are released through the fore arc (e.g. Fisher, 1996; Deyhle et al., 2004), or the chemically bound volatiles are successively released from the down going slab at greater depths due to metamorphic dehydration reactions (Peacock, 1993; Schmidt and Poli, 1998; Rüpke et al., 2002). In the latter case the volatiles pass in part through the volcanic arc system into the atmosphere (e.g. Plank and Langmuir, 1993). The amount of the mismatch between the volatile input into the subduction zone and the fluxes through the fore arc and the volcanic arc is believed to be recycled back into the mantle (Schmidt and Poli, 1998; Hacker et al., 2003; Rüpke et al., 2004; Savov et al., 2007). However, besides these well established fluid pathways, a probably significant, although not yet balanced amount of released fluids may flow back along the slab-wedge interface or penetrate the mantle wedge above the slab and cause hydration reactions, leading to serpentinisation of the mantle wedge peridotite (Peacock, 1996; Gerya et al., 2002; Hyndman and Peacock, 2003; Scambelluri et al., 2004). The associated changes in the rheology of the mantle wedge cause an upward movement within the newly formed subduction channel (Peacock, 1996; Gerya et al., 2002; Hyndman and Peacock, 2003; Scambelluri et al., 2004). Gerya et al. (2002) showed that the subduction channel is the most likely uplift pathway for subduction-related high-pressure rocks. Blocks of eclogites break off the slab and are incorporated into the hydrous mobile regime of the subduction channel (Cloos and Shreve, 1988; Gerya et al., 2002) and are transported upwards to the surface. The subduction channel or slab-wedge interface represents a highly reactive mechanical mixture of different lithologies that typically show metasomatised rinds around incorporated blocks (Bebout and Barton, 2002; King et al., 2006). Basaltic rocks of the oceanic slab typically experience a very tight P-T loop during their burial and uplift paths, crossing the blueschist facies, entering the eclogite facies and going back to the blueschist facies. In the highly hydrated environment of the subduction channel, dry eclogites may get in contact to wet lithologies and are affected by infiltrating fluids. The eclogite assemblage of omphacite and garnet may be transformed to the blueschist-facies assemblage of dominantly glaucophane, white mica and carbonate. The newly formed mineral assemblage may provide information about the composition of the infiltrating fluid and the characteristics of the rehydration process. Here we describe eclogitic oceanic pillow lava basalts from the Chinese Tian Shan high-pressure/low-temperature belt that experienced a blueschist-facies overprint during the uplift. This paper is addressed to give insights into the processes that

cause the rehydration of eclogites and the P-T-X conditions of the uplift path through the subduction channel. We examine the process of fluid-rock interaction related to the retrograde formation of hydrous minerals in eclogites.

## 2.2 Geology

The high mountains of the Tian Shan extend geographically with a total length of ca. 2500 km in WNW to ESE direction through the countries of Kyrgyzstan, Kazakhstan and the P. R. of China. The orogeny of the Tian Shan is related to the formation of the Central Asian Orogenic Belt (Ufimtsev, 1990), as a result of the complex Devonian to Carboniferous amalgamation of several fragments in Central Asia between the cratons of Siberia, Baltica and Tarim (Sobolev et al., 1986; Sengör and Natal'In, 1996; Bykadorov et al., 2003). The South Tian Shan Fold Belt was formed by the collision of the eastern part of the Kazakhstan Block (Yili Central Tian Shan Plate) and the Tarim Craton (Figure 2.1A) as a result of the closure of the Turkestan Ocean at the northern rim of the Paleo-Tethys Ocean (Bykadorov et al., 2003). During subduction of the South Tian Shan Ocean (marginal sea of Turkestan Ocean) the island arc of the future South Tian Shan was formed and welded with the Yili Central Tian Shan Plate (YCTP, Bykadorov et al., 2003). Relicts of the Paleo South Tian Shan Ocean and the island arc can be found in the South Tian Shan Fold Belt as a blueschist belt (first mentioned by Norin, 1941; Liou et al., 1989). This blueschist belt represents in parts a tectonic *mélange* and is enclosed between the main thrusts of the South Tian Shan Suture in the north and the Northern Haerkeshan Peak Fault in the south (Figure 2.1B). Between the South Tian Shan Suture and the southern margin of the YCTP a high-temperature/low-pressure zone of dominantly sillimanite-biotite gneisses, granulites and amphibolites occur together with subduction-related granitoids, which represent the relicts of a magmatic arc (Gao et al., 1995, 1998). The blueschist belt mainly consists of metamorphic mafic rocks formed under greenschist-, blueschist- and eclogite-facies conditions, together with minor Silurian marbles and peridotitic lenses. A zone of eclogite- and blueschist-facies rocks occurs in the centre between greenschist-facies metasediments and metabasalts (Figure 2.1B). Eclogite occurs in layers of variable thickness, as boudins or large blocks within the blueschists. Prograde blueschists comprise intercalations of eclogites that form massive blocks and prograde veins or reaction selvages (Gao and Klemd, 2001; Gao et al., 2007; John et al., 2008). Eclogites occur as relicts within retrograde blueschists as well, which are the topic of this study. Peak metamorphic conditions during eclogite-facies metamorphism were estimated, as well as the formation of a prograde dehydration vein-network of eclogites within the blueschists by dehydration (Gao and Klemd, 2001; Gao et al., 2007; John et al., 2008) at about 500 to 600°C and up to 20 kbar (Gao et al., 1999; Klemd et al., 2002). The occurrence of possible UHP metamorphic rocks was controversially discussed by Zhang et al. (2003) and Klemd (2003). Sm–Nd isochron data (omp–gln–grt–wr) of  $343 \pm 44$  Ma and an  $^{40}\text{Ar}/^{39}\text{Ar}$  age of  $344 \pm 1$  Ma of crossite indicate peak metamorphism in the Carboniferous (Gao and Klemd, 2003). White mica cooling ages (K–Ar, Ar–Ar, Rb–Sr) with a mean of 310–311 Ma (Klemd et al., 2005) and a lack of

blueschist detritus in Carboniferous sediments (Gao et al., 1995) lead to the assumption that the rocks were exhumed to the surface not earlier than during the Permian.

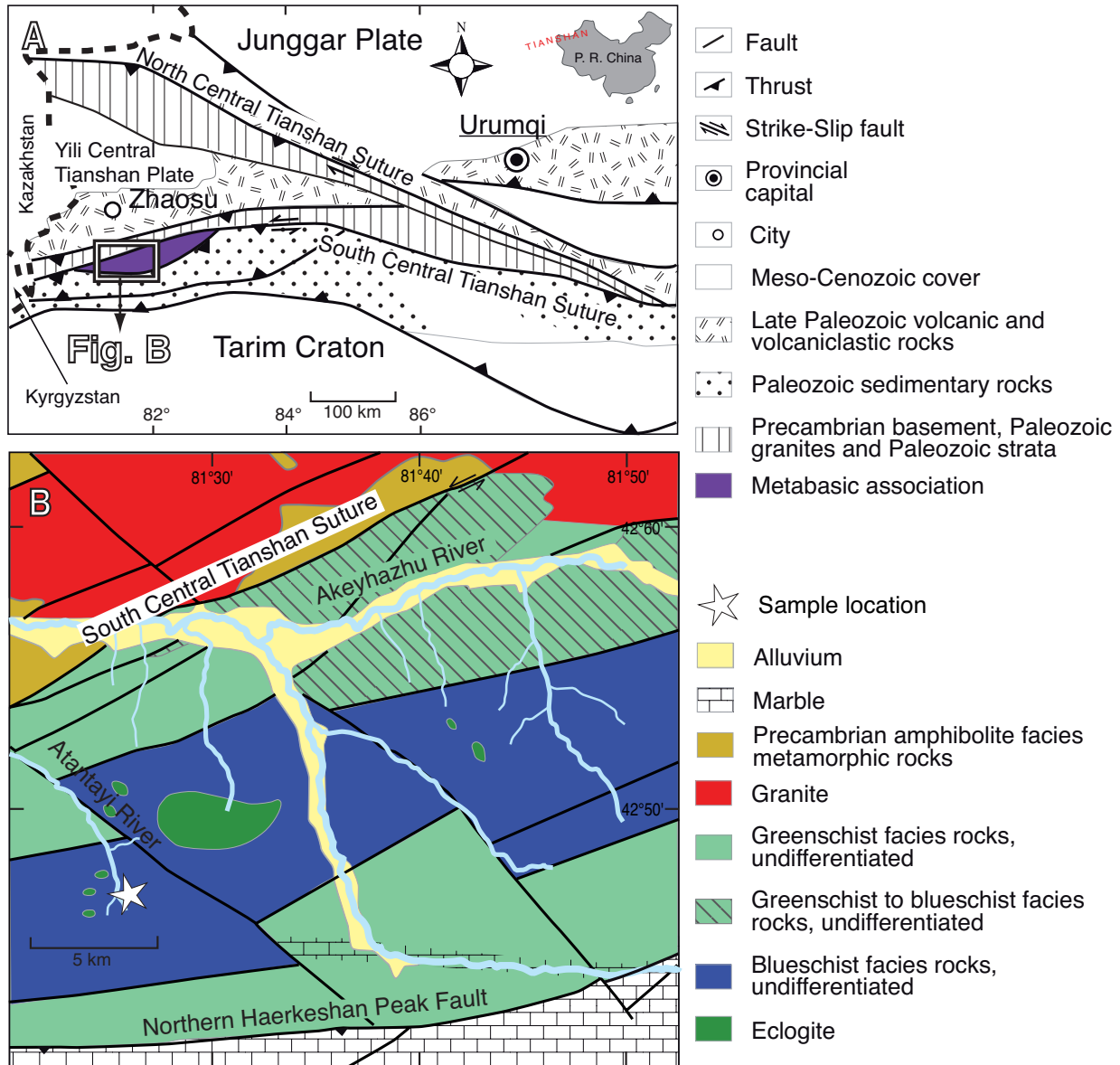


**Figure 2.1:** Geological map of the Southern Tian Shan, modified after Gao et al. (1999). Figure 2.1B shows the detailed part into the eastern part of the metabasic association. Sample location is indicated by star.



## 2.3 Analytical methods

Major elements were measured by X-ray fluorescence analysis (XRF, Philips PW 1480) on fused glass discs at the Institut für Geowissenschaften, University of Kiel. Values of BHVO.1 (Flanagan, 1976) was used for standardisation control. Accuracy and precision are better than 1% ( $1\sigma$ ) for the major oxides (Table A.1).

Trace elements were analysed by ICP-MS (Agilent 7500c) at the same institute. 100 mg pulverised and dried rock powder were digested by pure HF and HNO<sub>3</sub> in digestion bombs for four days at 180°C and fumed off with HClO<sub>4</sub>. The final 1% HNO<sub>3</sub> solution was diluted 20-fold and spiked with 2.5 ng/ml Beryllium (Be), Indium (In) and Rhenium (Re) for internal standardisation. Five replicate measurements of each sample were conducted with breaks for cleaning with a blank reagent. Further details of the procedure can be found in Garbe-Schönberg (1993) or John et al. (2008). The analytical precision is estimated to be <10% ( $1\sigma$ ) according to duplicate analysis of samples and standard (values of BHVO.2 (Wilson, 1997), see Table A.2).

In situ analysis by LA-ICP-MS (Agilent 7500i, quadrupole) were made at the Institut für Mineralogie, University of Würzburg. A Nd-YAG laser with 266 nm wavelength is used for ablation. Argon is used as carrier-gas. Apatite and ankerite were measured with 30% of the laser activity and silicates with 45% of laser activity. Each sample was measured 15 sec on the background and 20 sec on the mineral. External calibration was carried out with NIST 612 50 ppm glass disc with values of Pearce et al. (1997). NIST 610, 614 (Table A.3) and an in-house used standard GranatK23 were used for accuracy determination and further ablation of NIST 612 was used to obtain the reproducibility. Si concentrations were used for internal standardisation for silicate analyses and Ca concentrations were used for phosphate and carbonate analyses. Si and Ca were measured with the electron microprobe at the University of Kiel. The minimum detection limit equal to 99% confidence level is defined by  $2.3 * \sqrt{(2B)}$ , where  $B$  is the total counts on the background. The minimum detection is usually at 0.02–0.18 ppm for REE, 0.03–0.10 ppm for HFSE (Zr, Nb, Hf, Ta), 0.27–0.44 ppm for Li and Be, <2.8 ppm B, 0.07–1.7 for transition metals (except <7.3 ppm for Zn) and 0.02–0.30 ppm for LILE (Cs, Rb, Ba, Sr, Pb, Th). The REE concentrations of omphacite, glaucophane and white mica are up to 0.01–0.10 ppm above the detection limit, but usually below these values. LREE (La–Nd) concentrations of garnet are usually below the detection limit.

Major elements of an ankerite-apatite vein were measured with ICP-OES at the Institut für Geowissenschaften, University of Kiel, except for SiO<sub>2</sub>. The OES is equipped with the Spectro Ciros CCD SOP. The pulverised and dried rock powder was separated in four pieces, each of them 100 mg. Two separates were moistened with triple-distilled water and diluted in 5ml HCl and after fuming of in 5 ml HNO<sub>3</sub>. The other two separates and the standards were digested two times by 5 ml pure HNO<sub>3</sub> and fumed of at 190°C. Final 1% HNO<sub>3</sub> solution was diluted 10-fold. For standardisation control, the following standards were analysed: J-Do dolomite and JLS Limestone (Terashima et al., 1990), MAG.1 and BHVO.1 basalt (Flanagan, 1976), BCS-CRM 393 limestone (Jochum et al., 2005) and AC-E granite (Potts and Holbrook, 1987, Table A.4) and laboratory made HNO<sub>3</sub> with 100

ppm Y. The precision of the analyses ( $n = 4$ ) is  $\sim 5\%$  ( $1\sigma$ ), except for  $K_2O$ ,  $Na_2O$  and  $Al_2O_3$ , which are  $<0.2$  wt%, for which  $1\sigma$  is between 40 and 60%.

Mineral chemical data were obtained by electron microprobe (JEOL JXA 8900R) at Institut für Geowissenschaften, University of Kiel. The microprobe is equipped with five wavelengths-dispersive spectrometers (WDS). Depending on the analysed mineral phase, the following acceleration voltages and beam currents were used: 10 kV and 15 nA for apatite, 15 kV and 15 nA for garnet and phengite, 20 kV and 20 nA for amphibole, pyroxene, epidote and carbonate. CITZAF corrections were used for matrix correction.

Total carbon measurements were made with a Carlo-Erba instrument in a routine mode at IFM-GEOMAR, Kiel. Each sample was measured twice. The analytical precision is estimated to be  $<1.2\%$  ( $1\sigma$ ) according to standards, blanks and duplicate analyses.

Density determinations are based on measurements with a Gay-Lussac pycnometer with a calibrated volume of 2 ml. Each sample was measured three times and measurements were repeated if precision of the analysis was  $>2\%$  ( $1\sigma$ ).

## 2.4 Field area

The study area is located in Zhaosu County (NW-China). Samples were taken on the mountainsides at the upper part of the Atantayi River, which is a feeder river of the Akeyhazhu River, ca 80 km south of the city of Zhaosu (Figure 2.1). The sampling was focused on eclogitic rocks that were partially transformed to blueschist, which developed as veins or metasomatic rims within and around peak-metamorphic eclogites. Samples were taken as drilling cores from a meta-basaltic boulder of four to five meters in size. The boulder contains rounded relicts of eclogitic pillow structures in dm size, which are surrounded by blueschist (Figure 2.2A–D). Three main zones can be distinguished according to their mineralogy: in the centre 1) a homogeneous eclogite surrounded by a rim of 2) light blue homogeneous glaucophane-dominated blueschist and a wall rock of 3) carbonate and white mica-bearing, greyish, coarse-grained blueschist. In one eclogitic part of a drilling core a yellowish ankerite-dominated vein with a thickness of  $\sim 3$  mm size was found, which is called ankerite-apatite vein in the following sections.

## 2.5 Petrology

### Sample description

The samples derive from pillow-lava structures in which the dm-sized cores are eclogitic and the cm-sized rims are glaucophane-dominated blueschists. The overall wall rock is a blueschist, mainly consisting of glaucophane, white mica (phengite) and carbonate (ankerite). In total, 25 mechanically separated domains were analysed: 10 samples from the eclogite core domain, 4 samples from the glaucophane-dominated blueschist, 10 samples from the phengite-ankerite blueschist domain and one sample from an ankerite-apatite vein. The constituent minerals occur in different amounts, but the mineral assemblage of all

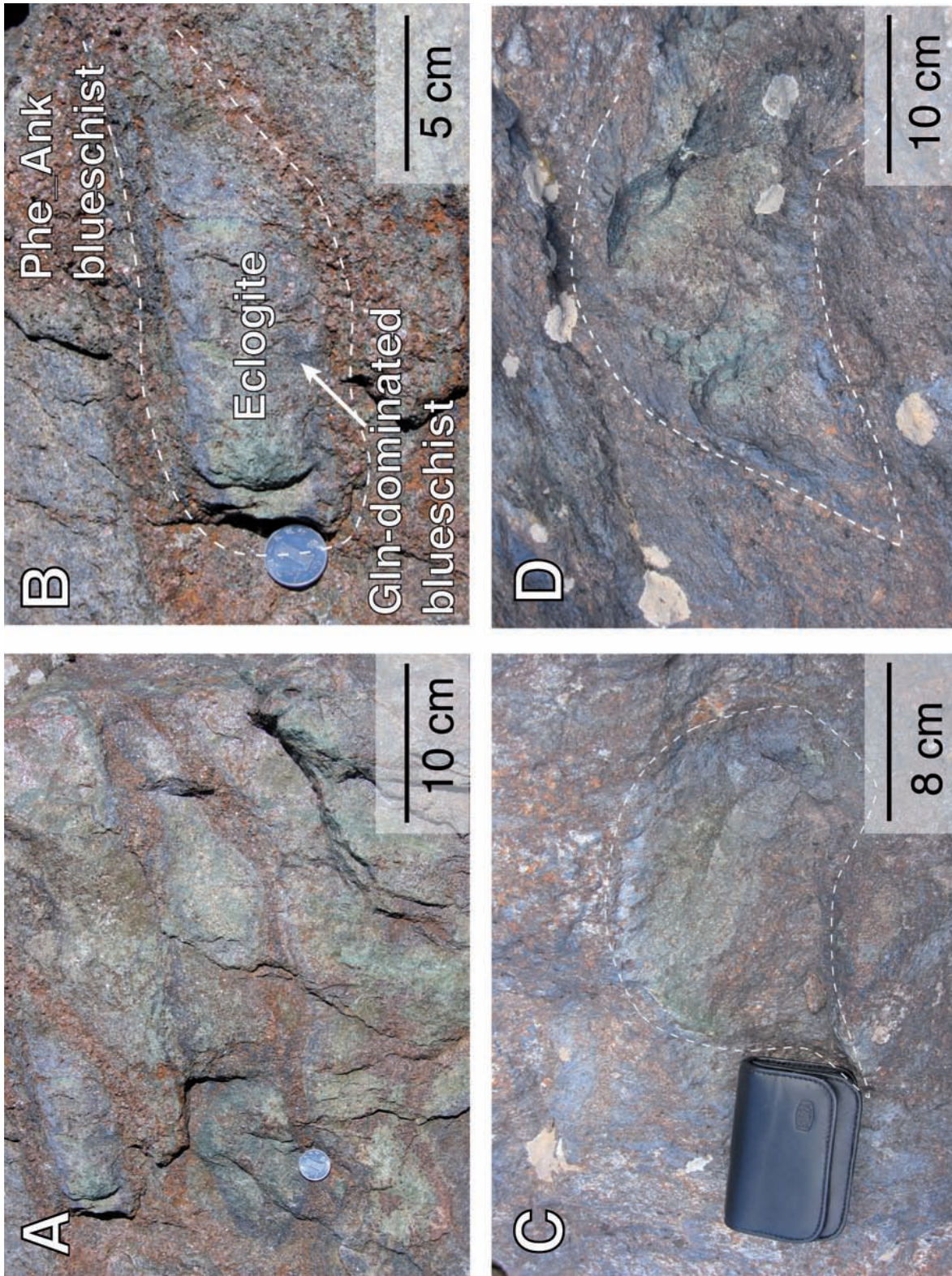


**Figure 2.2:** A–D: Photographs of eclogites of former oceanic pillow-lava basalts, partially transformed to blueschists (dashed white lines mark the pillow margin). B: Detail of A; eclogite is remaining in the pillow core surrounded by a glaucophane-dominated blueschist (light blue).

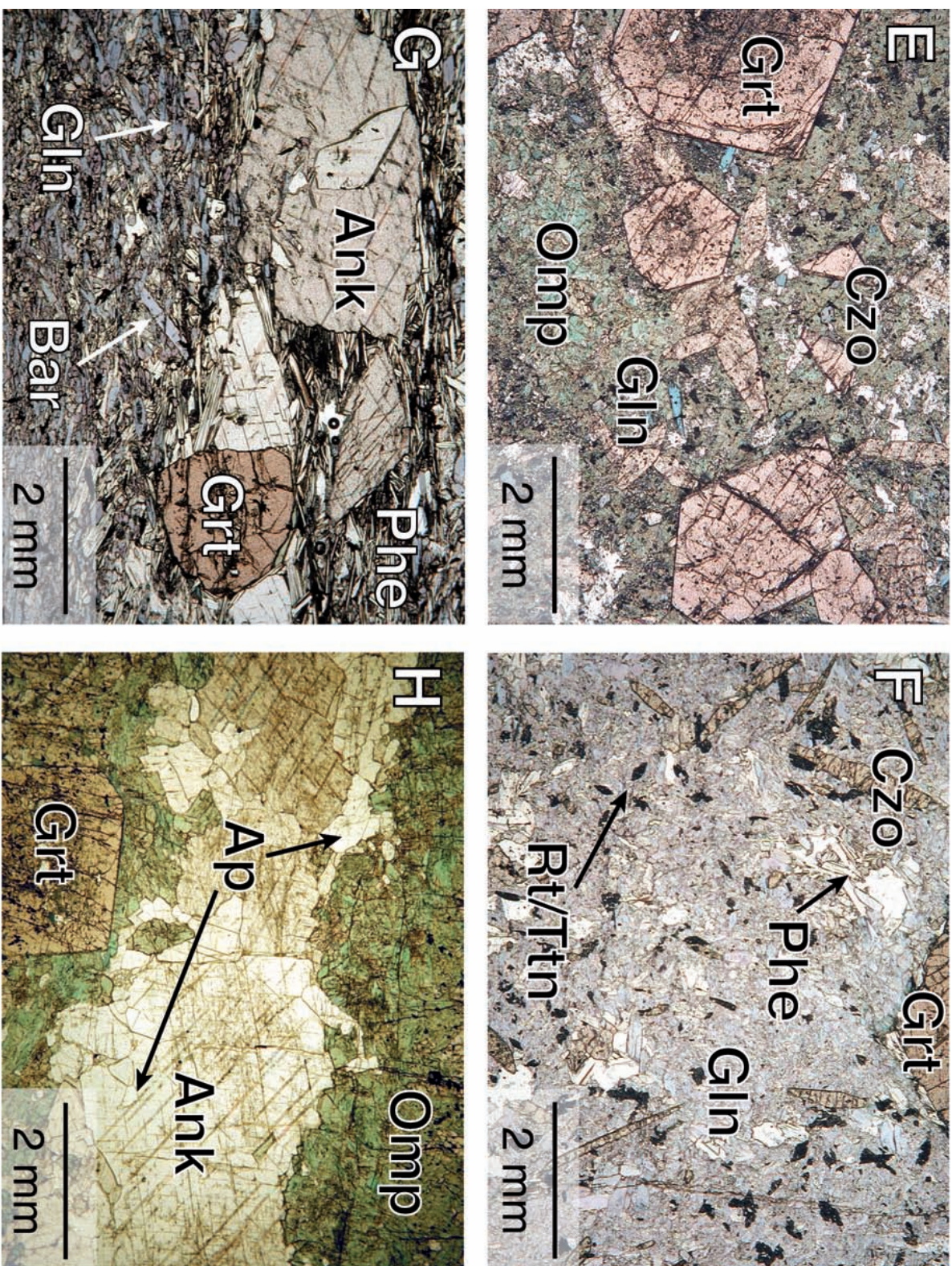


**Figure 2.2:** (cont.) E: Photomicrograph of the eclogite domain (Grt = garnet, Omp = omphacite, Czo = clinzoisite, Gln = glaucophane). F: Photomicrograph of the glaucophane-dominated blueschist (Phe = phengite, Rt/Ttn = rutile/titanite). G: Photomicrograph of the phengite-ankerite blueschist (Ank = ankerite, Bar = barroisite, titanite is present but not shown). H: Photomicrograph of an ankerite-apatite vein found within relict eclogite domain (Ap = apatite).

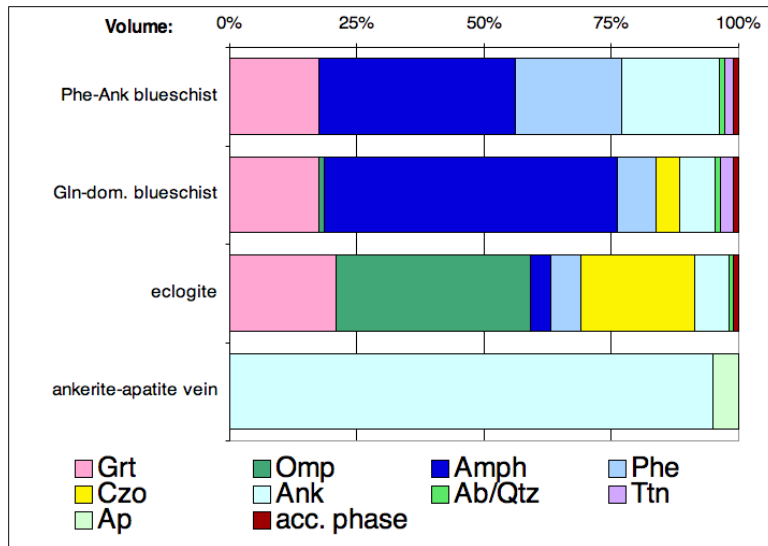


**Figure 2.3:** Estimated modal amounts of minerals in petrographically recognised domains, based on microscopical investigations. Accessory phases that occur in Phe-Ank blueschist: Rt, Czo, Ap & opaque phases; glaucophane-dominated blueschist: Omp, Rt, Ap & opaque phases; eclogite: Rt, Ttn, Ap & opaque phases.

domains is the same (Figure 2.3): garnet, omphacite, glaucophane (partly replaced by barroisite), clinozoisite, ankerite (minor calcite), phengite, albite, quartz, apatite, rutile, titanite, zircon and opaque phases. Main phases in the eclogite domain are garnet, omphacite, clinozoisite, rutile and apatite. Locally, the eclogite has higher abundances of phengite, amphibole and ankerite. Glaucophane is the dominant mineral in the glaucophane-dominated schist, whereas phengite, ankerite and glaucophane are dominant in the phengite-ankerite blueschist, which forms the main part of the rock boulder.

### Eclogite (Ec):

Garnet occurs as euhedral mm-sized porphyroblast with straight grain boundaries (Figure 2.2E and 2.4A) in a matrix of medium-grained omphacite and evenly distributed rutile. No foliation or preferred orientation of the minerals is found. Sometimes the eclogite is pervaded by cracks, which are vanishing in the surrounding blueschist (Figure 2.4A). Quartz, epidote minerals, sodic and sodic-calcic amphiboles, white mica and rutile are minor components in the matrix and enclosed in garnet, too. Intergrowths of white mica with epidote minerals, chlorite and quartz are found as inclusions in garnet and are interpreted as a replacement after lawsonite. They are similar to pseudomorphs after lawsonite described by Fry and Fyfe (1971) and Okrusch et al. (1978). Omphacite is the main phase in the matrix and also occurs as inclusion in garnet. Some fragments of omphacite in <0.1mm-size are visible in phengite, glaucophane and ankerite, indicating a replacement or resorption of omphacite by these minerals. Rutile, if not included in other phases, is partially or totally replaced by poikiloblastic titanite. Glaucophane shows locally a chemical zonation indicated by variations in the birefringence. It is marginally surrounded by sodic-calcic amphibole, primarily barroisite. Epidote minerals form euhedral, inclusion-rich porphyroblasts and are irregularly arranged. Mineral inclusions are omphacite, glaucophane or barroisite and rutile. Ankerite usually occurs in clusters with variable grain size (up to

3 mm). Albite is very fine-grained and occurs interstitially, but is usually not visible under the microscope but was often detected in back-scattered electron images. Quartz also occurs as an interstitial phase.

### **Glaucofane-dominated blueschist (GDB):**

Glaucofane is the dominant mineral in this blueschist domain followed by phengite (Figure 2.2F). Both minerals are fine- to medium-grained. Locally omphacite occurs as relict inclusions in glaucofane, phengite and ankerite or in the matrix. Garnet forms porphyroblasts with uneven grain boundaries displaying a corroded shape. Some garnet is partially replaced by amphibole, phengite or iron-rich chlorite. Epidote minerals are less frequent than in the eclogite domain. Epidote minerals have minor inclusions of omphacite and amphibole. Rutile in the matrix is replaced by poikiloblastic titanite.

### **Phengite-ankerite blueschist (PAB):**

The phengite-ankerite blueschist looks similar to the glaucofane-dominated blueschist with the exception that here phengite and ankerite are the dominant minerals. Ankerite and garnet form the largest porphyroblasts in a matrix of glaucofane with barroisite rims, barroisite, phengite and titanite (Figure 2.2G). The latter often contains relicts of rutile. Garnet is highly resorbed compared to garnet in the eclogite domain. Epidote minerals and omphacite are generally absent in the matrix. Several minerals, mostly omphacite, glaucofane, rutile and opaque phases are enclosed in ankerite. Omphacite relicts are found in amphiboles and phengite.

### **Ankerite-apatite vein (AAV):**

The drilling core FTS 4–2.5 shows a yellowish-greyish vein up to 3 mm in thickness cutting the eclogite domain. It predominantly consists of ankerite (up to 95%) and some apatite (see Figure 2.2H and Figure 2.3). Ankerite forms the granoblastic matrix with ~1 mm grain sizes, shows a lot of twins and is often inclusion-rich. Apatite occurs interstitially as tiny (<0.5 mm) grains.

## **2.5.1 Mineral chemistry**

Major and trace element contents of minerals have been analysed to discuss possible mobilisations of these elements during the eclogite-blueschist transformation and the replacement of eclogitic minerals by blueschist-facies assemblages. Concentrations of selected trace elements will be described in each mineral subsection of this chapter.

### **Garnet**

Garnet of the eclogite domain has an average core composition of  $\text{alm}_{67}\text{-prp}_7\text{-grs}_{24}\text{-sps}_2\text{-adr}_0$  with a  $X_{Fe} [\text{Fe}^{2+}/(\text{Fe}^{2+} + \text{Mg})] = 0.90$  and a rim average composition of  $\text{alm}_{61}\text{-prp}_{12}\text{-}$

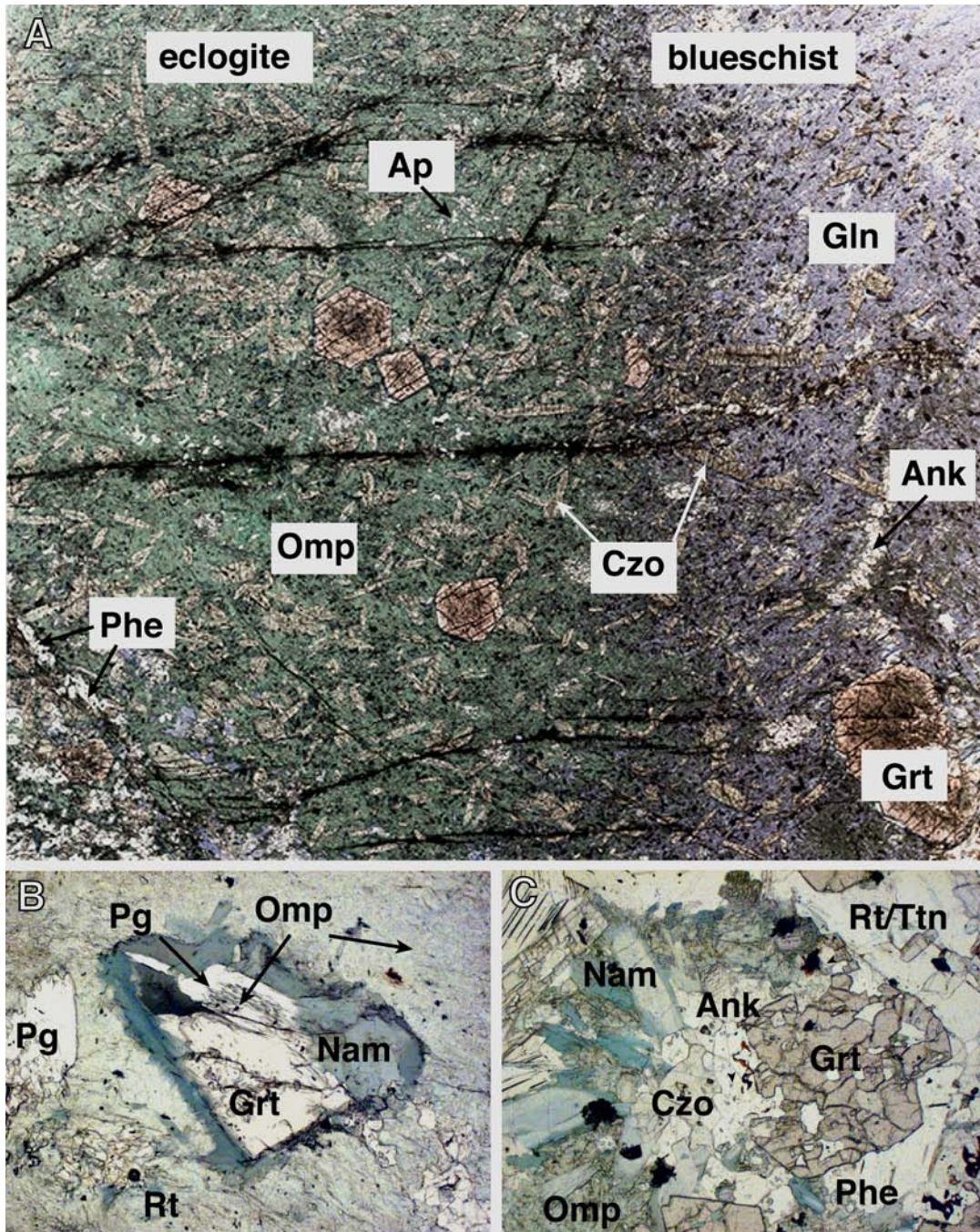


**Figure 2.4:** A: Photomicrograph of sample FTS 4-3.5. Eclogite domain surrounded by glaucophane-dominated blueschist (same mineral abbreviations used as in Figure 2.2). Boundary is not sharp. Garnet in the eclogite is euhedral, in the blueschist it is corroded and partially resorbed. Clinzoisite is euhedral in eclogite, but increasingly resorbed towards the blueschist. Cracks through the eclogite vanish in the blueschist. B: Photomicrograph of eclogite showing breakdown of garnet and omphacite to barroisite and paragonite due to reactions 2.2–2.5. Paragonite is replaced by phengite, presumably during fluid infiltration. C: Thin section photograph of phengite-ankerite blueschist. Displayed assemblage is a result of the eclogite-blueschist transformation. Garnet and omphacite are replaced by glaucophane, ankerite, phengite and clinzoisite. Glaucophane and remaining omphacite reacting to barroisite surrounding glaucophane. Rutile is replaced by titanite.

grs<sub>26</sub>-sps<sub>1</sub>-adr<sub>0</sub> with a  $X_{Fe} = 0.84$ . Garnet of the glaucophane-dominated blueschist has a similar composition of alm<sub>67</sub>-prp<sub>8</sub>-grs<sub>21</sub>-sps<sub>2</sub>-adr<sub>2</sub> with a  $X_{Fe} = 0.89$  in the core and alm<sub>62</sub>-prp<sub>11</sub>-grs<sub>25</sub>-sps<sub>1</sub>-adr<sub>1</sub> with a  $X_{Fe} = 0.85$  at the rim (Table 2.1).  $X_{Fe}$ , almandine and spessartine components decrease whereas pyrope and grossular components increase towards the rim. Semiquantitative element mappings for Mn show low-manganese rims in garnet of the eclogite domain as well as in the blueschist domain. The eclogite garnet with straight grain boundaries differs from the garnet in the glaucophane-dominated blueschist, which shows embayments due to corrosion (Figure 2.5). The Cr content is constant at  $\sim 170$  ppm, whereas contents of Y and Zr decrease towards the rim from  $\sim 900$  to 10 ppm and from  $\sim 220$  to 10 ppm, respectively (Table 2.2). Chondrite-normalised (Boynton, 1984) REE patterns of garnet cores show large enrichments in Tb–Lu and decreasing normalised ratios towards the La–Nd ( $< 1$  times chondrite, Figure 2.6A). HREE are 70–400 times (Dy) and 35–700 times (Lu) enriched compared to chondrite composition. Lu concentrations in garnet rims are similar to the cores, whereas Yb to Gd contents are lower and decrease towards the MREE, i.e. the  $(Tb/Yb)_N$  changes from  $\sim 0.5$  to  $\sim 0.1$ . The REE garnet rim patterns do not occur in garnet of the blueschist domains, as the rims are absent in the analysed samples, due to corrosion.

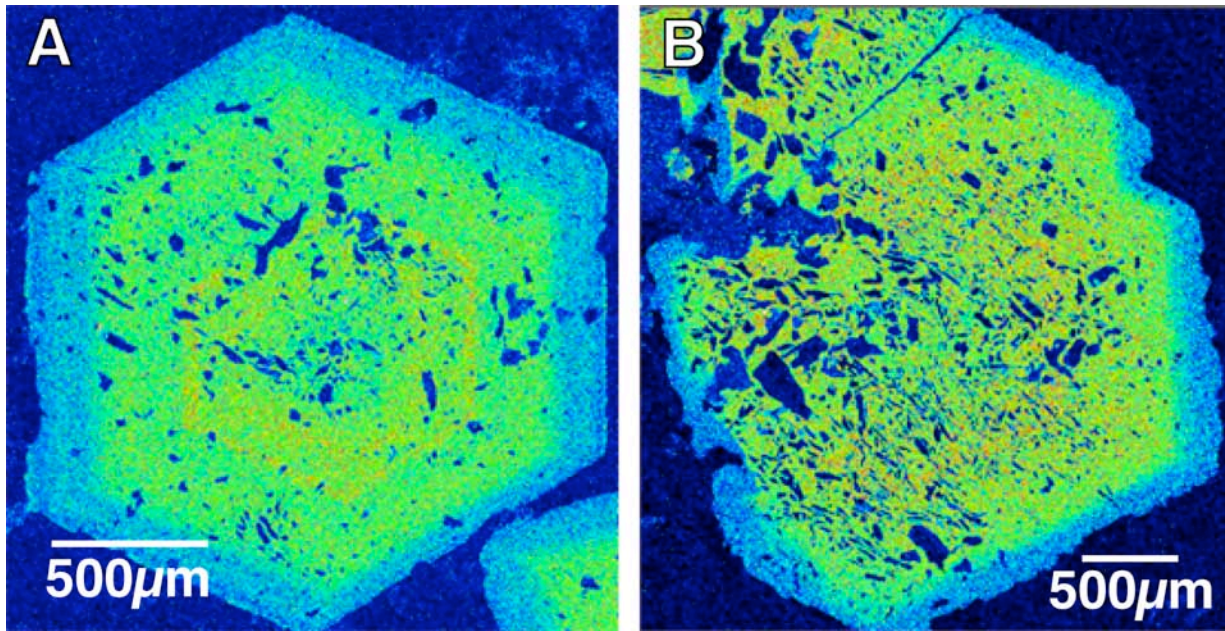


**Figure 2.5:** Semiquantitative microprobe mappings of Mn in garnet: A in eclogite domain, B in glaucophane schist domain of sample FTS 4–3.5 (yellow colours indicate higher Mn concentrations than green or blue colours). Eclogitic garnet is characterised by euhedral grains and distinct low Mn-rim. Blueschist-facies garnet has same composition as eclogite garnet, but has corroded grain boundaries, indicating resorption by metamorphic reactions.

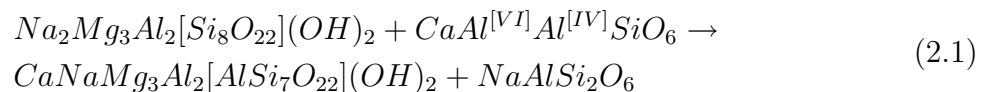


## Clinopyroxene

Nearly all pyroxenes of the eclogite and blueschist domains can be classified as omphacite according to the nomenclature of [Morimoto \(1988\)](#), Figure 2.7A. Omphacite in the eclogite domain is characterised by slightly higher calcium and higher acmite [ $Ae = (Na - Al^{VI}) / (Na + Ca)$ ] contents, compared to omphacite in the blueschist domains. Omphacite enclosed in garnet from both domains shows increasing jadeite [ $Jd = (Al^{VI}) / (Na + Ca)$ ] component from mean 25 mol.% in the core to mean 37 mol.% (max. 41 mol.%) in the rim of garnet, both with a mean acmite component of 13 to 16 mol.%. Matrix-omphacite and fragments enclosed in epidote minerals have mean jadeite and acmite contents of 37 mol.% and 8–14 mol.%, respectively, which is similar to omphacite enclosed in garnet rims. Omphacite relicts enclosed in glaucophane, phengite and ankerite have very similar jadeite (average 34 mol.%) and acmite components (10–15 mol.%) as the matrix grains (Table 2.1). LA-ICP-MS measurements show Li and B contents up to 130 and 27 ppm, respectively. Cr, Mn and Ni contents are about 200 and 300 ppm and Sr, Rb, Co and Cu contents are around 20 ppm.

## Amphibole

The analysed amphiboles are either glaucophane or barroisite (Figure 2.7B) according to the classification of [Leake et al. \(1997\)](#). Glaucophane in the matrix and grains that are enclosed by other minerals show no significant difference. The  $X_{Fe^{3+}}$  [ $Fe^{3+} / (Fe^{3+} + Al^{VI})$ ] values are between 0.07 and 0.25 with no visible zonation in the grains.  $X_{Fe}$  [ $Fe^{2+} / (Fe^{2+} + Mg)$ ] values are relatively constant and range from 0.24 to 0.32. There are two types of barroisite: the first type was formed earlier and is enclosed in garnet of the eclogites and blueschists and occasionally occurs as inclusion in epidote minerals; the second type was formed late and forms rims around matrix-glaucophane. The first type has a higher  $X_{Fe}$  of 0.4–0.5 and  $Al^{IV}$  of 0.85–1.3 pfu (per formula unit) whereas the second type has lower  $X_{Fe}$  of 0.25–0.35 and  $Al^{IV}$  of 0.5–1.0 pfu (Table 2.1). The chemical variation found in barroisite surrounding glaucophane can be explained by a reaction involving the plagioclase-substitution expressed as  $NaSiCa_{-1}Al_{-1}^{[IV]}$  together with the Ca-tschermak component of adjacent omphacite to form barroisite and jadeite (Reaction 2.1).



glaucophane + ca-tschermak  $\rightarrow$  barroisite + jadeite

According to this reaction the A position of the newly formed amphibole should not contain Na. This is in agreement with the mineral chemical data (Table 2.1). The reaction of glaucophane with omphacite forming barroisite produces also a jadeite component, which can explain the higher jadeite content in omphacite of the blueschist domains (Figure 2.7A). Chondrite-normalised REE concentrations of glaucophane and omphacite show slightly

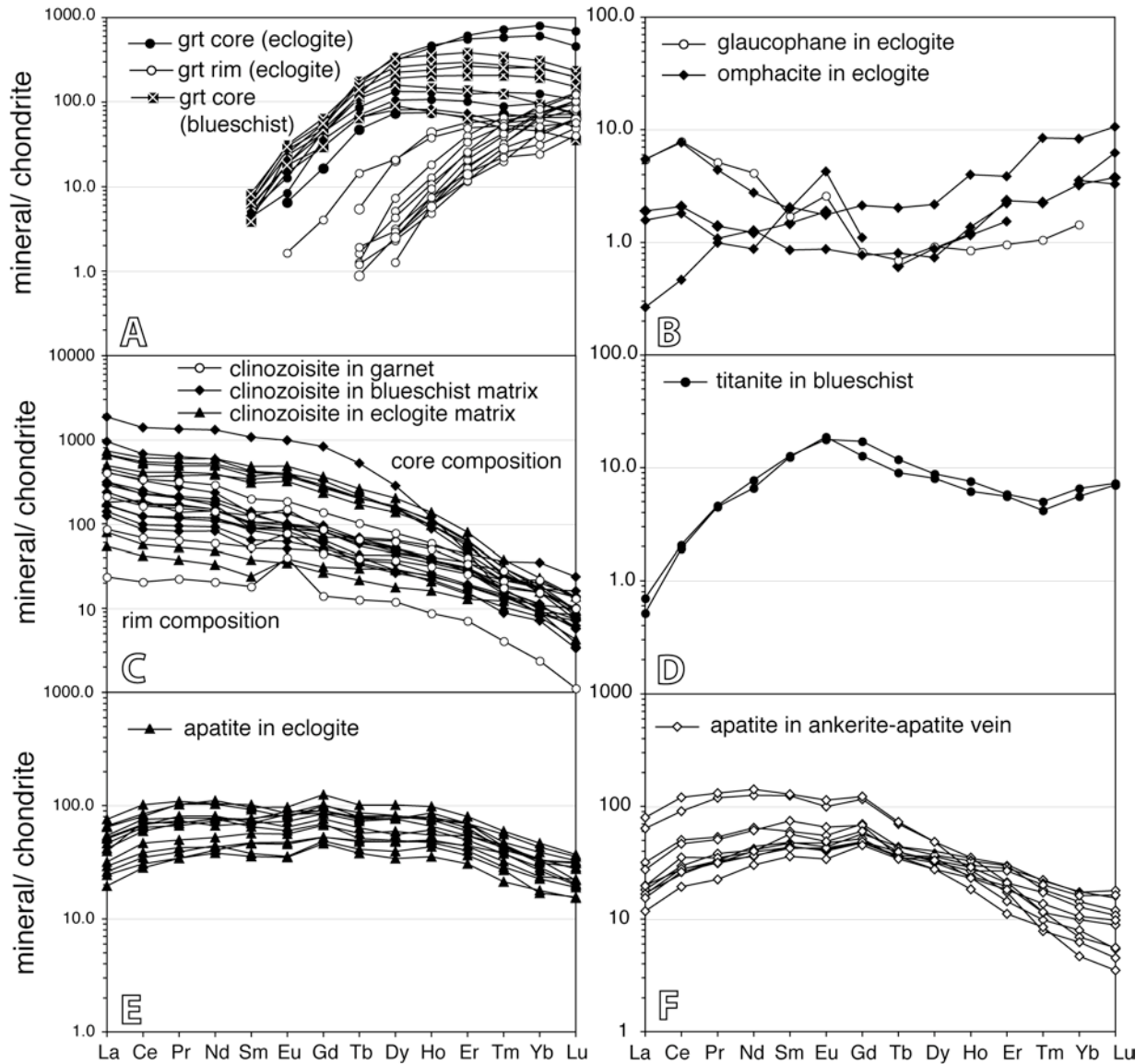


**Figure 2.6:** Chondrite-normalised (Boynton, 1984) REE concentrations of A garnet, B omphacite and glaucophane, C clinozoisite, D titanite, E apatite in eclogite domain and F in ankerite-apatite vein. A: Filled circles show core composition of garnets in eclogite as well as in blueschist. Concentrations of Gd to Yb decrease toward the rims composition. Rim composition is absent in resorbed garnet of blueschist. B: Omphacite and glaucophane show nearly identical concave pattern. C: clinozoisite enclosed in garnet show distinct Eu anomaly, clinozoisite in eclogite and in blueschist do not differ significantly in composition. D: Titanite newly formed in blueschist at the expense of rutile shows slightly enriched concentrations. E & F: Newly precipitated apatite differs from apatite in eclogite by lower HREE concentrations. Both apatites are important carrier for LREE.

Table 2.1: Electron microprobe analyses of eclogite- and blueschist-facies minerals.

Mineral Domain Analysis-No. Comment	Grt blueschist		Grt eclogite		Grt core		Bar blueschist		Bar in grt matrix		Gln blueschist matrix		Czo blueschist rim		Czo blueschist core		Czo eclogite in grt		Omp eclogite in grt matrix	
	223 rim	195 core	38.04 rim	130 eclogite	37.70 core	161 eclogite	48.48 in grt	277 matrix	351 blueschist	287 matrix	287 matrix	66 rim	81 core	200 in grt	196 in grt	216 matrix				
SiO <sub>2</sub>	38.40	37.82	38.04	37.70	37.70	37.70	48.48	51.90	56.99	38.04	37.51	38.36	38.36	54.39	55.60					
TiO <sub>2</sub>	0.00	0.00	0.07	0.18	0.18	0.18	0.21	0.16	0.04	0.13	0.09	0.15	0.07	0.00						
Al <sub>2</sub> O <sub>3</sub>	21.40	20.88	21.27	20.94	20.94	20.94	10.80	8.43	10.60	26.81	24.96	27.18	5.82	9.39						
Fe[ <i>tot</i> ]	28.68	30.59	27.71	29.82	29.82	29.82	17.03	13.15	10.82	8.23	10.97	8.31	12.44	6.90						
FeO	28.41	30.14	27.71	29.82	29.82	29.82	12.13	8.67	7.73	0.00	0.99	0.75	6.42	4.26						
Fe <sub>2</sub> O <sub>3</sub>	0.00	0.00	0.00	0.00	0.00	0.00	5.44	4.98	3.43	8.23	9.87	7.48	6.70	2.94						
Cr <sub>2</sub> O <sub>3</sub>	0.00	0.00	0.00	0.02	0.02	0.02	0.06	0.00	0.07	0.11	0.00	0.07	0.03	0.02						
MgO	2.88	2.05	2.96	1.85	1.85	1.85	9.01	12.42	10.24	0.10	0.10	0.17	6.85	7.66						
MnO	0.44	1.04	0.31	0.82	0.82	0.82	0.14	0.07	0.00	0.04	0.04	0.07	0.05	0.01						
CaO	9.31	8.10	9.37	8.24	8.24	8.24	6.59	7.24	1.09	23.51	22.90	23.21	12.58	12.37						
Na <sub>2</sub> O	-	-	-	-	-	-	4.44	3.76	6.63	0.01	0.00	0.01	6.53	7.04						
K <sub>2</sub> O	-	-	-	-	-	-	0.23	0.18	0.02	0.01	0.00	0.00	0.00	0.01						
SrO	-	-	-	-	-	-	0.04	-	0.04	0.10	0.45	0.14	-	-						
BaO	-	-	-	-	-	-	0.04	-	0.01	-	-	-	-	-						
NiO	-	-	-	-	-	-	-	0.03	-	-	-	-	0.02	0.03						
Total	100.86	100.06	99.73	99.57	99.57	99.57	97.61	97.85	96.88	97.09	96.91	97.58	99.46	99.34						
Si	3.005	3.007	3.010	3.017	3.017	3.017	7.065	7.371	7.892	2.999	2.993	3.002	2.012	2.007						
Ti	0.000	0.000	0.004	0.011	0.011	0.011	0.023	0.017	0.004	0.008	0.005	0.009	0.002	0.000						
Al[ <i>IV</i> ]	0.000	0.000	0.000	0.000	0.000	0.000	0.935	0.629	0.108	0.001	0.007	0.000	0.000	0.000						
Al[ <i>VI</i> ]	1.974	1.956	1.983	1.975	1.975	1.975	0.920	0.782	1.622	2.490	2.340	2.507	0.254	0.399						
Fe <sup>3+</sup>	0.017	0.030	0.000	0.000	0.000	0.000	0.597	0.532	0.358	0.488	0.654	0.480	0.186	0.080						
Fe <sup>2+</sup>	1.859	2.004	1.833	1.996	1.996	1.996	1.478	1.030	0.895	0.000	0.073	0.053	0.198	0.128						
Cr	0.000	0.000	0.000	0.001	0.001	0.001	0.007	0.000	0.007	0.000	0.000	0.004	0.001	0.001						
Mg	0.336	0.243	0.349	0.221	0.221	0.221	1.957	2.630	2.114	0.012	0.012	0.020	0.378	0.412						
Mn	0.029	0.070	0.021	0.056	0.056	0.056	0.018	0.009	0.000	0.002	0.002	0.004	0.002	0.000						
Ca	0.781	0.690	0.794	0.707	0.707	0.707	1.029	1.102	0.162	1.986	1.958	1.946	0.499	0.478						
Na	-	-	-	-	-	-	1.254	1.035	1.780	0.002	0.000	0.002	0.468	0.493						
K	-	-	-	-	-	-	0.042	0.033	0.003	0.001	0.000	0.000	0.000	0.001						
Sr	-	-	-	-	-	-	0.004	0.000	0.003	0.004	0.021	0.006	-	-						
Ba	-	-	-	-	-	-	0.002	0.000	0.000	-	-	-	-	-						
Ni	-	-	-	-	-	-	0.000	0.004	0.000	-	-	-	0.001	0.001						
Total	8.000	8.000	7.995	7.984	7.984	7.984	15.331	15.174	14.948	8.001	8.066	8.033	4.000	4.000						
Basis of O	11.5	11.5	11.5	11.5	11.5	11.5	23	23	23	13	13	13	6	6						
X <sub>Alm</sub>	0.62	0.67	0.61	0.67	0.67	0.67	-	-	-	-	-	-	-	-						
X <sub>SpS</sub>	0.01	0.02	0.01	0.02	0.02	0.02	-	-	-	-	-	-	-	-						
X <sub>Prp</sub>	0.11	0.08	0.12	0.07	0.07	0.07	-	-	-	-	-	-	0.001	0.001						
X <sub>Grs</sub>	0.25	0.21	0.26	0.24	0.24	0.24	-	-	-	-	-	-	0.001	0.001						
X <sub>Adr</sub>	0.01	0.02	0.01	0.02	0.02	0.02	-	-	-	-	-	-	0.000	0.000						
X <sub>Fe</sub>	0.85	0.89	0.84	0.90	0.90	0.90	0.39	0.40	0.18	0.16	0.22	0.16	0.468	0.478						
				X <sub>Fe<sup>3+</sup></sub>	0.90	0.90	0.43	0.28	0.30	0.22	0.16	0.16	0.000	0.001						
													0.000	0.001						
													4.000	4.000						
													6	6						
													0.26	0.41						
													0.22	0.10						
													0.34	0.24						

Fe<sup>3+</sup>: calculated assuming stoichiometry; 0.00: under detection limit; n.c.: not calculated; -: not analysed; X<sub>Fe<sup>3+</sup></sub>: Fe<sup>3+</sup>/(Fe<sup>3+</sup>+Al[*VI*])

Table 2.1: (cont.) Electron microprobe analyses of eclogite- and blueschist-facies minerals.

Mineral Domain Analysis-No. Comment	Omp blueschist 15 in phe	Omp blueschist 33 in gln	Omp eclogite 35 in gln	Omp eclogite 40 in ep	Omp eclogite 52 in ank	Phe blueschist 19 rim	Phe blueschist 21 core	Phe blueschist 196 core	Phe blueschist 201 rim	Pg blueschist 98 in grt	Pg blueschist 117 in grt	Ank eclogite 52 core
SiO <sub>2</sub>	55.62	55.77	55.68	56.08	55.52	51.83	51.85	49.75	49.60	45.63	46.15	-
TiO <sub>2</sub>	0.02	0.03	0.05	0.04	0.00	0.24	0.28	0.38	0.25	0.03	0.01	-
Al <sub>2</sub> O <sub>3</sub>	9.17	8.04	9.13	9.22	8.69	26.52	26.65	28.17	29.06	40.84	39.93	-
Fe[total]	8.41	8.62	9.52	7.79	7.85	3.19	3.12	3.07	3.47	0.59	0.62	10.15
FeO	3.81	5.48	4.80	4.31	4.11	n.c.	n.c.	n.c.	n.c.	n.c.	n.c.	n.c.
Fe <sub>2</sub> O <sub>3</sub>	5.11	3.49	5.25	3.87	4.15	n.c.	n.c.	n.c.	n.c.	n.c.	n.c.	n.c.
Cr <sub>2</sub> O <sub>3</sub>	0.02	0.03	0.04	0.08	0.02	0.09	0.03	0.11	0.01	0.04	0.02	-
MgO	7.12	7.56	6.75	7.26	7.42	3.49	3.50	2.98	2.66	0.09	0.13	15.15
MnO	0.02	0.06	0.03	0.00	0.00	0.00	0.01	0.02	0.02	0.02	0.01	0.13
CaO	11.55	14.09	11.29	12.38	12.95	0.05	0.02	0.08	0.05	1.30	0.86	27.82
Na <sub>2</sub> O	7.35	6.40	7.61	7.32	7.00	0.45	0.52	0.63	0.77	6.52	6.79	-
K <sub>2</sub> O	0.37	0.00	0.00	0.02	0.00	10.18	10.40	10.10	10.10	0.01	0.31	-
SiO	0.02	0.01	0.04	0.00	0.01	0.37	0.32	0.36	0.35	0.18	0.18	0.07
BaO	0.03	0.04	0.02	0.01	0.02	0.05	0.00	0.02	0.00	0.00	0.00	0.02
NiO	0.00	0.00	0.00	0.00	0.00	0.13	0.12	0.14	0.12	0.01	0.00	-
ZnO	-	-	-	-	-	-	-	-	-	-	-	0.05
ChO	-	-	-	-	-	-	-	-	-	-	-	0.03
Total	100.22	100.99	100.68	100.58	99.90	96.59	96.82	95.81	96.47	95.25	94.95	53.42
Si	2.000	2.004	1.999	2.005	2.003	3.430	3.425	3.327	3.299	2.918	2.961	-
Ti	0.001	0.001	0.001	0.001	0.000	0.012	0.014	0.019	0.013	0.001	0.000	-
Al[IV]	0.000	0.000	0.001	0.000	0.000	2.069	2.075	2.220	2.278	3.078	3.020	-
Al[VI]	0.389	0.340	0.385	0.389	0.370	-	-	-	-	-	-	-
Fe <sup>3+</sup>	0.138	0.094	0.142	0.104	0.113	-	-	-	-	-	-	-
Fe <sup>2+</sup>	0.256	0.261	0.144	0.129	0.124	0.177	0.172	0.172	0.193	0.031	0.033	3.334
Cr	0.001	0.001	0.001	0.002	0.001	0.005	0.002	0.006	0.000	0.002	0.001	-
Mg	0.382	0.405	0.361	0.387	0.399	0.344	0.345	0.297	0.264	0.009	0.012	8.873
Mn	0.001	0.002	0.001	0.000	0.000	0.000	0.000	0.001	0.001	0.001	0.001	0.044
Ca	0.445	0.542	0.434	0.474	0.501	0.004	0.001	0.005	0.004	0.089	0.059	11.707
Na	0.512	0.446	0.530	0.508	0.490	0.058	0.067	0.082	0.099	0.808	0.845	-
K	0.017	0.000	0.000	0.001	0.000	0.860	0.876	0.862	0.857	0.001	0.025	-
Sr	-	-	-	-	-	0.014	0.012	0.014	0.013	0.007	0.016	0.016
Ba	-	-	-	-	-	0.001	0.000	0.001	0.000	0.000	0.000	0.003
Ni	0.000	0.000	0.000	0.000	0.000	0.007	0.006	0.008	0.007	0.000	0.001	-
Zn	-	-	-	-	-	-	-	-	-	-	-	0.014
Cu	-	-	-	-	-	-	-	-	-	-	-	0.010
Total	3.999	4.000	3.999	4.000	4.000	6.980	6.995	7.013	7.027	6.946	6.962	24.000
Basis of O	6	6	6	6	6	11	11	11	11	11	11	24
X <sub>Fe</sub>	0.23	0.29	0.29	0.25	0.24	0.34	0.33	0.37	0.42	0.78	0.78	0.27
X <sub>Jd</sub>	0.41	0.34	0.40	0.40	0.37	-	-	-	-	-	-	-
X <sub>Ae</sub>	0.13	0.11	0.15	0.12	0.12	-	-	-	-	-	-	-
					X <sub>N<sub>a</sub></sub>	0.06	0.07	0.09	0.10	0.90	0.91	-

Fe<sup>3+</sup>: calculated assuming stoichiometry; 0.00: under detection limit; n.c.: not calculated; -: not analysed; X<sub>N<sub>a</sub></sub>: Na/(Na+K+Ca)

Table 2.2: LA-ICP-MS analyses of trace elements of eclogite- and blueschist-facies minerals (in ppm).

Mineral No.	blueschist		blueschist		blueschist		blueschist		eclogite		eclogite		eclogite		eclogite		eclogite	
	Czo	Czo in Grt	Phe	Ttn	Omp	Omp	Omp	Gln	Ap	Ap	Ap	Grt D core	Grt E core	Grt E rim	Grt E rim	Ank	Ank	Ank
Li	6.72	2.19	41.7	24.9	90.3	112	15.8	<0.25	<0.43	6.12	6.12	6.12	1.88	4.13	<0.61	<0.12	<0.61	<0.12
Be	0.34	<0.16	3.11	0.83	2.68	4.34	6.22	<0.21	<0.19	<0.64	<0.64	<0.64	<0.39	<0.12	<0.61	<0.12	<0.61	<0.12
B	7.66	2.81	47.3	1.95	12.5	3.52	5.69	<0.66	<0.78	<2.7	<2.7	<2.7	3.15	2.67	<2.8	<2.8	<2.8	2.67
V	325	453	202	242	239	294	282	0.10	<0.12	86.7	86.7	86.7	52.8	13.3	41.2	41.2	41.2	13.3
Cr	707	640	711	140	394	203	221	<0.93	<0.88	229	229	229	140	3.26	131	131	131	3.26
Mn	691	113	8.04	67	124	207	210	63.7	141	5434	5434	5434	5808	1818	2562	2562	2562	1818
Co	3.18	0.98	15.2	9.78	21.1	21.1	44	0.17	<0.04	26.8	26.8	26.8	23.4	25.2	40.5	40.5	40.5	25.2
Ni	5.69	5.84	157	51.3	201	126	356	1.04	0.68	4.71	4.71	4.71	2.29	78.3	1.39	1.39	1.39	78.3
Cu	7.83	34.4	<0.83	4.98	14.9	16.7	3.73	2.47	0.623	<1.9	<1.9	<1.9	<1.7	135	<1.8	<1.8	<1.8	135
Zn	<6.8	8.39	39.3	22.4	72.6	74.3	136	<3.6	<3.2	33.3	33.3	33.3	<15	72	47.6	47.6	47.6	72
Rb	22.1	2.55	209	<0.05	47	<0.05	0.21	<0.03	<0.02	<0.09	<0.09	<0.09	<0.12	<0.03	<0.16	<0.16	<0.16	<0.03
Sr	2019	653	19.6	27.8	8.99	24.1	10.1	777	899	0.66	0.66	0.66	0.36	731	0.19	0.19	0.19	731
Y	108	16.8	0.10	9.9	0.19	2.33	0.52	1.36	65.7	195	195	195	878	7.89	26.5	26.5	26.5	7.89
Zr	574	20.4	6.01	41.6	0.65	35	148	0.13	<0.03	163	163	163	218	0.14	57.3	57.3	57.3	0.14
Nb	0.18	0.04	0.27	170	0.14	0.24	1.16	<0.02	<0.02	70.6	70.6	70.6	0.89	0.04	0.12	0.12	0.12	0.04
Mo	<0.14	<0.08	<0.10	0.27	<0.07	<0.08	<0.06	<0.09	<0.12	0.42	0.42	0.42	<0.44	0.26	<0.33	<0.33	<0.33	0.26
Cs	0.60	0.07	7.63	<0.02	1.52	<0.03	<0.02	<0.02	<0.02	<0.05	<0.05	<0.05	<0.05	<0.02	<0.06	<0.06	<0.06	<0.02
Ba	441	14.7	327	0.48	433	0.78	1.2	5.12	12.8	<0.63	<0.63	<0.63	<0.81	1.62	<0.53	<0.53	<0.53	1.62
La	51.2	7.31	0.18	0.16	<0.02	0.59	0.16	20.6	9.87	<0.08	<0.08	<0.08	<0.06	0.24	<0.09	<0.09	<0.09	0.24
Ce	98.5	16.6	0.26	1.55	<0.02	1.68	0.82	68.4	40.7	<0.07	<0.07	<0.07	0.19	0.61	0.06	0.06	0.06	0.61
Pr	14	2.73	0.05	0.55	<0.01	0.17	0.07	12.5	6.52	<0.05	<0.05	<0.05	<0.06	0.10	<0.06	<0.06	<0.06	0.10
Nd	65	12.3	0.32	3.95	0.09	0.73	<0.13	66.5	38.7	<0.19	<0.19	<0.19	<0.48	0.76	<0.39	<0.39	<0.39	0.76
Sm	17.4	3.54	<0.17	2.42	<0.07	0.29	<0.05	18.8	11.7	0.85	0.85	0.85	0.90	0.70	<0.41	<0.41	<0.41	0.70
Eu	6.54	2.94	0.10	1.38	0.06	0.14	<0.03	7.15	4.06	0.62	0.62	0.62	1.36	0.54	<0.10	<0.10	<0.10	0.54
Gd	17.8	3.62	<0.24	3.3	<0.13	<0.19	<0.10	32.4	18.1	9.27	9.27	9.27	11	1.23	0.48	0.48	0.48	1.23
Tb	3.26	0.6	<0.03	0.43	<0.02	0.03	<0.02	4.81	2.07	3.32	3.32	3.32	5.82	0.22	<0.08	<0.08	<0.08	0.22
Dy	20.7	3.85	<0.12	2.59	<0.05	0.29	0.12	32.6	11.9	33.9	33.9	33.9	100	1.63	1.66	1.66	1.66	1.63
Ho	3.92	0.63	0.05	0.44	<0.02	0.09	<0.02	7.07	2.35	7.75	7.75	7.75	31.7	0.33	0.92	0.92	0.92	0.33
Er	9.32	1.49	0.13	1.17	<0.05	0.49	0.10	16.8	6.24	21.5	21.5	21.5	129	0.74	7.11	7.11	7.11	0.74
Tm	1.16	0.13	<0.04	0.14	<0.02	0.07	<0.02	1.93	0.59	2.89	2.89	2.89	23.6	0.10	1.69	1.69	1.69	0.10
Yb	7.25	0.50	<0.10	1.16	0.10	0.68	0.18	9.73	2.98	20.1	20.1	20.1	169	0.59	18.8	18.8	18.8	0.59
Lu	0.76	0.04	<0.04	0.23	<0.02	0.12	0.08	1.19	0.38	2.39	2.39	2.39	22.4	0.08	4.13	4.13	4.13	0.08
Hf	11.2	1.64	<0.16	1.81	0.08	1.69	3.63	0.09	<0.03	5.01	5.01	5.01	6.06	<0.07	1.75	1.75	1.75	<0.07
Ta	<0.03	<0.03	0.11	17.6	<0.01	0.04	<0.03	<0.01	<0.02	5.05	5.05	5.05	<0.09	<0.02	<0.05	<0.05	<0.05	<0.02
Pb	12.4	7.17	<0.40	<0.23	0.27	0.24	<0.18	3.54	1.45	<0.78	<0.78	<0.78	<0.66	5.57	<0.64	<0.64	<0.64	5.57
Th	7.29	0.46	<0.05	<0.06	<0.02	0.05	0.21	<0.03	<0.02	0.18	0.18	0.18	<0.14	<0.03	0.14	0.14	0.14	<0.03

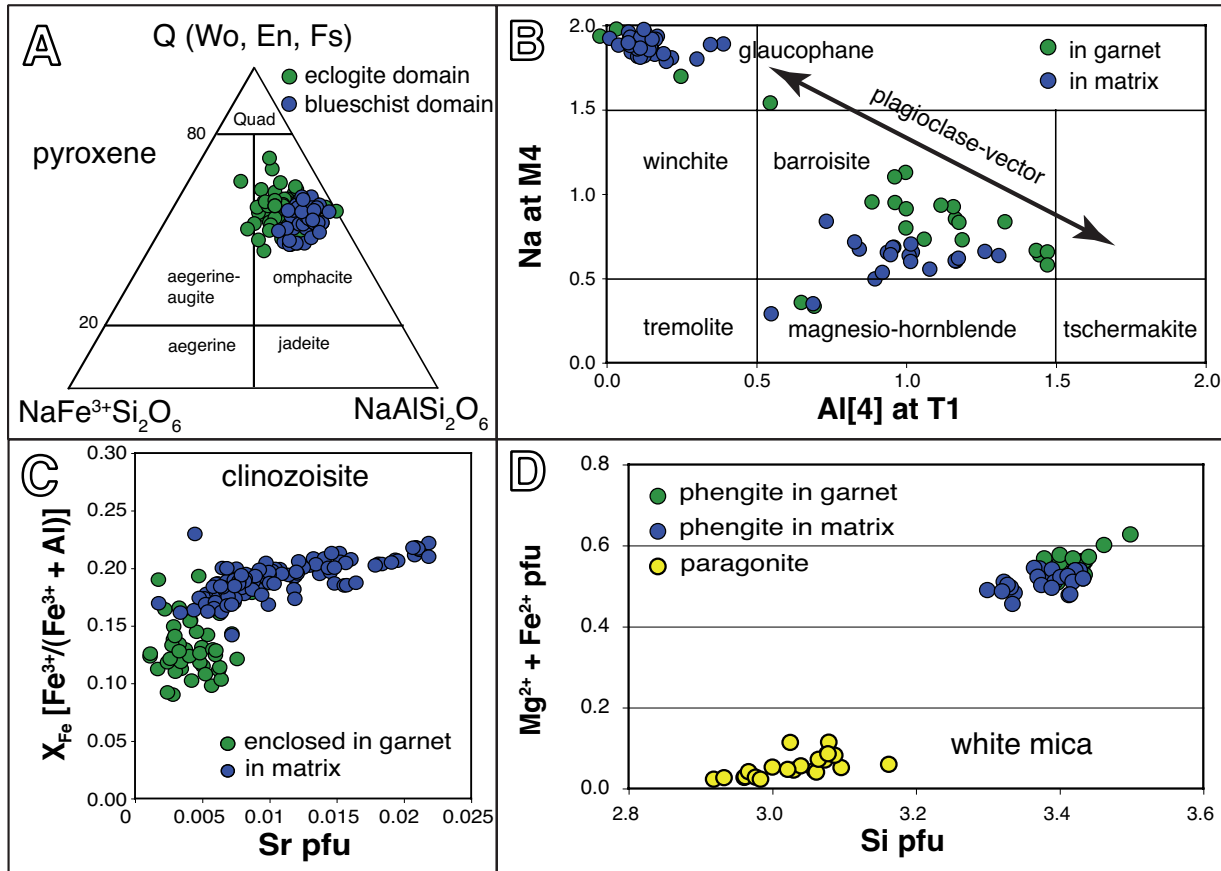


**Figure 2.7:** Mineral compositions of eclogite and blueschist domains. A: Triangle for clinopyroxene classification after Morimoto (1988). Eclogitic omphacite differ from omphacite in blueschist in slightly higher jadeite and lower aegerine component; Quad = Ca-Mg-Fe pyroxene. B: Amphibole classification after Leake et al. (1997), dark filled dots: Inclusions in garnet, light filled dots: matrix amphibole. C: Clinozoisite of matrix differs from clinozoisite enclosed in garnet in higher  $Fe^{3+}$  and Sr contents. D: White mica composition, phengite inclusions correspond to garnet in eclogite and blueschist domains.

enriched (1–10 times) concave pattern (Figure 2.6B). LREE and HREE are more enriched than Nd–Dy with  $(Ce/Tb)_N$  of  $\sim 3$ . Mean concentrations of Cr, Ni, V and Co are about 230, 300, 290 and 40 ppm, respectively, and Zn contents range between 100 and 145 ppm. These values are similar to those of clinopyroxene. Cu is very low in glaucophane.

### Epidote minerals

All analysed epidote minerals can be classified as clinozoisite according to the nomenclature of Armbruster et al. (2006). Two different types of clinozoisite can be distinguished based on texture and chemical characteristics: type 1) clinozoisite forms inclusions in garnet. The  $X_{Fe^{3+}} [Fe^{3+}/(Fe^{3+} + Al^{VI})]$  varies from 0.09 to 0.16 and the Sr content is low with values of up to 0.007 pfu (11.5 O basis), type 2) clinozoisite in the matrix differs from inclusions in garnet in  $X_{Fe^{3+}}$  (0.16 to 0.22) and a distinctly higher Sr content of up to 0.022 pfu (Figure

2.7C). Clinozoisite of the matrix shows a zonation with decreasing  $X_{Fe^{3+}}$  and Sr from core to rim and increasing Cr content (Table 2.1). Clinozoisite inclusions in garnet have lower contents of Pb (mean 10 ppm) and Y (mean 70 ppm) compared to clinozoisite in the matrix (Pb <40 ppm, Y <220 ppm) and higher Mn contents of about 500–1000 ppm compared to 100–150 ppm in clinozoisite enclosed in garnet. Chondrite-normalised REE patterns of clinozoisite in garnet (Figure 2.6C) show a clear positive Eu-anomaly possibly inherited from plagioclase. It has slightly lower REE concentrations (20–400 times of LREE and 1–20 times HREE) compared to those of the clinozoisite in the matrix (80–1900 times LREE, 3–16 times HREE). The fractionation between LREE and HREE expressed as  $(Ce/Yb)_N$  changes from  $\sim 10$  in inclusions to  $\sim 20$  in matrix grains.

### White mica

White mica occurs as paragonite and phengite. Paragonite generally occurs as isolated inclusions in garnet. In contrast phengite rarely occurs as isolated inclusion in garnet but is often intergrown with chlorite, quartz and clinozoisite forming inclusions in garnet. Phengite also occurs in the matrix, particularly of the blueschist domains.  $X_{Na}$  [ $Na/(Na + Ca + K)$ ] varies in paragonite between 0.80 and 0.97 whereas  $X_{Na}$  in phengite varies between 0.04 and 0.10. Two textural settings of phengite can be distinguished: 1) inclusions in garnet with Si contents of 3.38 to 3.50 pfu and 2) phengite in the matrix with Si contents of 3.30 to 3.43 pfu (Figure 2.7D). Some LILE are enriched in phengite as it contains 2000 to 3200 ppm Ba and on average, 200 ppm Rb, 7 ppm Cs and 40 ppm Li and B each.

### Carbonate

Carbonate is ankerite (nomenclature of Deer et al., 1992) and has  $X_{Fe}$  [ $Fe^{2+}/(Fe^{2+} + Mg)$ ] values of around 0.25. Calcite occurs interstitially between ankerite grains. Cr, Cu, Sr, Ba and Mn concentrations are higher in calcite than in ankerite. Mn concentrations are up to 2400 ppm. LA-ICP-MS data show high contents of transition metals (Co and Ni mean 50 ppm, Zn <90 ppm, Cu <140 ppm) and of Sr (400–700 ppm) and Pb (2.5–5.5 ppm). Ankerite in the ankerite-apatite vein has approximately the same composition as ankerite in the matrix of the eclogite and blueschist domains.

### Rutile/titanite

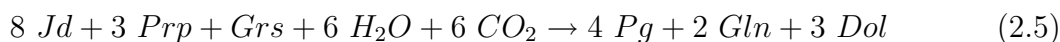
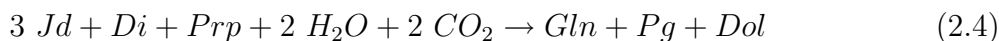
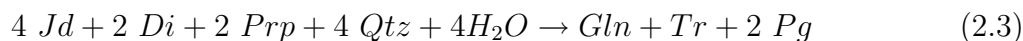
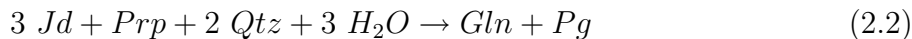
Rutile occurs in the matrix and is enclosed in every other rock-forming phase of the eclogites and blueschists. In back-scattered electron images, rutile can show exsolutions of ilmenite as very fine (<1mm) lamellae. Rutile inclusions in garnet having itself a titanite inclusion may indicate the prograde growth of rutile at the expense of titanite. Titanite shows slightly enriched chondrite-normalised REE pattern with a maximum between Sm and Tb, (12–18 times chondrite) with  $(Ce/Yb)_N$  of about 2 (Figure 2.6D). Titanite shows high contents of transition metals (e.g. 260 ppm V, 150 ppm Cr), and of Nb ( $\sim 160$  ppm), Ta ( $\sim 17$  ppm) and Li ( $\sim 24$  ppm, Table 2.1).

## Apatite

Apatite is common in the eclogite domain and almost absent in the blueschist domains. Apatite shows a slightly curved REE pattern with highest concentrations in the MREE (up to 100 times chondrite) (Figure 2.6E). The REE enrichment varies between 30–100 times with the maximum in Gd. HREE decrease towards Lu with  $(\text{Ce}/\text{Yb})_N$  of  $\sim 2$ . Mn and Y contents reach maximum values of 90 and 135 ppm, respectively, and maximum Sr and Pb contents are 780 and 3.5 ppm, respectively. The apatite in the ankerite-apatite vein differs in its REE pattern from those of the eclogite domain. LREE and MREE are strongly enriched in apatite of the vein (max. 140 times chondrite for Ce to Gd) with decreasing pattern towards Lu (4–18 times) with a  $(\text{Ce}/\text{Yb})_N$  of 20 (Figure 2.6F). Contents of mean Mn, Y, Sr and Pb are similar to contents in apatite of the eclogite domain (140, 72, 700 and 2 ppm, respectively; Table 2.2).

### 2.5.2 Metamorphic reaction history

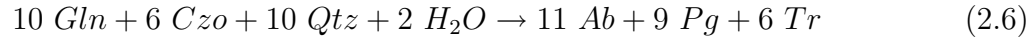
A prograde metamorphic evolution of the eclogites through the blueschist facies is indicated by inclusions in garnet, consisting of sodic-calcic amphibole, clinozoisite, white mica (paragonite) and pseudomorphs after lawsonite consisting of white mica (phengite with paragonite lamellae), clinozoisite and quartz. Inclusions of omphacite in garnet indicate the stable coexistence of both minerals under eclogite-facies conditions. During rehydration of the rock, glaucophane, white mica and ankerite were growing at the expense of the eclogitic assemblage garnet and omphacite. Relicts of the latter mineral are found as fragments in glaucophane, phengite, ankerite and clinozoisite. These textures occur in all three petrographically distinguished domains. The retrograde eclogite-blueschist transformation can be described by several reactions. For simplicity, all reactions are expressed for Mg-endmember compositions in a K-free system although white mica in eclogites and blueschists is dominantly phengite. The transformation from eclogite to blueschist can be deduced best from mineral reaction textures seen in the preserved eclogite domain, as this domain was affected least by the fluid infiltration. Reactions 2.2–2.5 (Evans, 1990; Gao and Klemm, 2001) and Figure 2.4B and 2.4C show the breakdown of omphacite and garnet to hydrous minerals as glaucophane and paragonite/phengite and to carbonate as dolomite/ankerite.



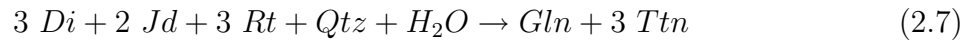
Reaction 2.3 describes the often observed late-stage formation of sodic-calcic amphibole intermediate between glaucophane and tremolite. Clinozoisite is rare in the glaucophane-dominated blueschist and is absent in the phengite-ankerite blueschist, which may indicate



that clinozoisite was stable in the eclogite and became successively replaced towards the blueschist domains. The consumption of clinozoisite can be related to reaction 2.6 (Evans, 1990). This reaction can only take place where water and glaucophane are present in sufficient amounts, which is the case in the GDB and in the PAB but not in the eclogite domain.



Titanite usually contains relicts of rutile as inclusions indicating the replacement of the latter. Titanite may be formed during the eclogite-blueschist transformation according to the reaction 2.7. Rutile occurs as inclusion in all other phases but most of the rutile in the matrix is replaced by titanite.



### 2.5.3 P-T evolution

The burial and uplift paths of high pressure rocks related to subduction channel processes, i.e. processes in the partially serpentinised mantle wedge, should describe a rather tight P-T loop either clockwise or anti-clockwise, where the uplift path is characterised by contemporaneous decompression and cooling (Gerya et al., 2002). In order to reconstruct the P-T evolution of the investigated samples several Fe-Mg exchange thermometers and the phengite-clinopyroxene-garnet barometer were applied and linked with P-T pseudosections generated with *Perple\_X* (Connolly, 1990, Table A.5). Peak-metamorphic conditions were calculated for a nearly unaltered eclogite composition in the KCNMFASH system (Figure 2.8). Information about P-T conditions during the prograde burial can be obtained from pseudomorphs after lawsonite included in garnet. The assemblage chlorite + omphacite + white mica + sodic-calcic amphibole + garnet + lawsonite + quartz (Stage A) was stable below 470°C (Figure 2.8E). Highest Si contents of 3.50 pfu in white mica (shown as isopleths in Figure 2.8C) restrict the pressure to <15.5 kbar at 450°C. Three textural different omphacite-garnet pairs give temperatures of three different eclogite-facies stages. Stage B (Figure 2.8E) can be obtained from omphacite inclusions in the core of garnet resulting in temperatures of 540±25°C (calibration of Powell, 1985) and 560±20°C (calibration of Ellis and Green, 1979).

The mineral assemblage chlorite + omphacite + white mica + sodic-calcic amphibole + garnet + lawsonite + quartz was replaced during prograde heating after passing intermediate stability fields, by the assemblage omphacite + white mica + garnet + zoisite + quartz (Figure 2.8A). Because kyanite is absent, but paragonite and omphacite are common as inclusions in garnet, an upper limit for the pressure during stage B and C can be obtained from the equilibrium  $\text{pg}=\text{ky}+\text{jd}_{50}+\text{H}_2\text{O}$  (Holland, 1979). This restricts the maximum pressure to <20 kbar in the range 500 to 650°C. Temperatures of 605±30°C

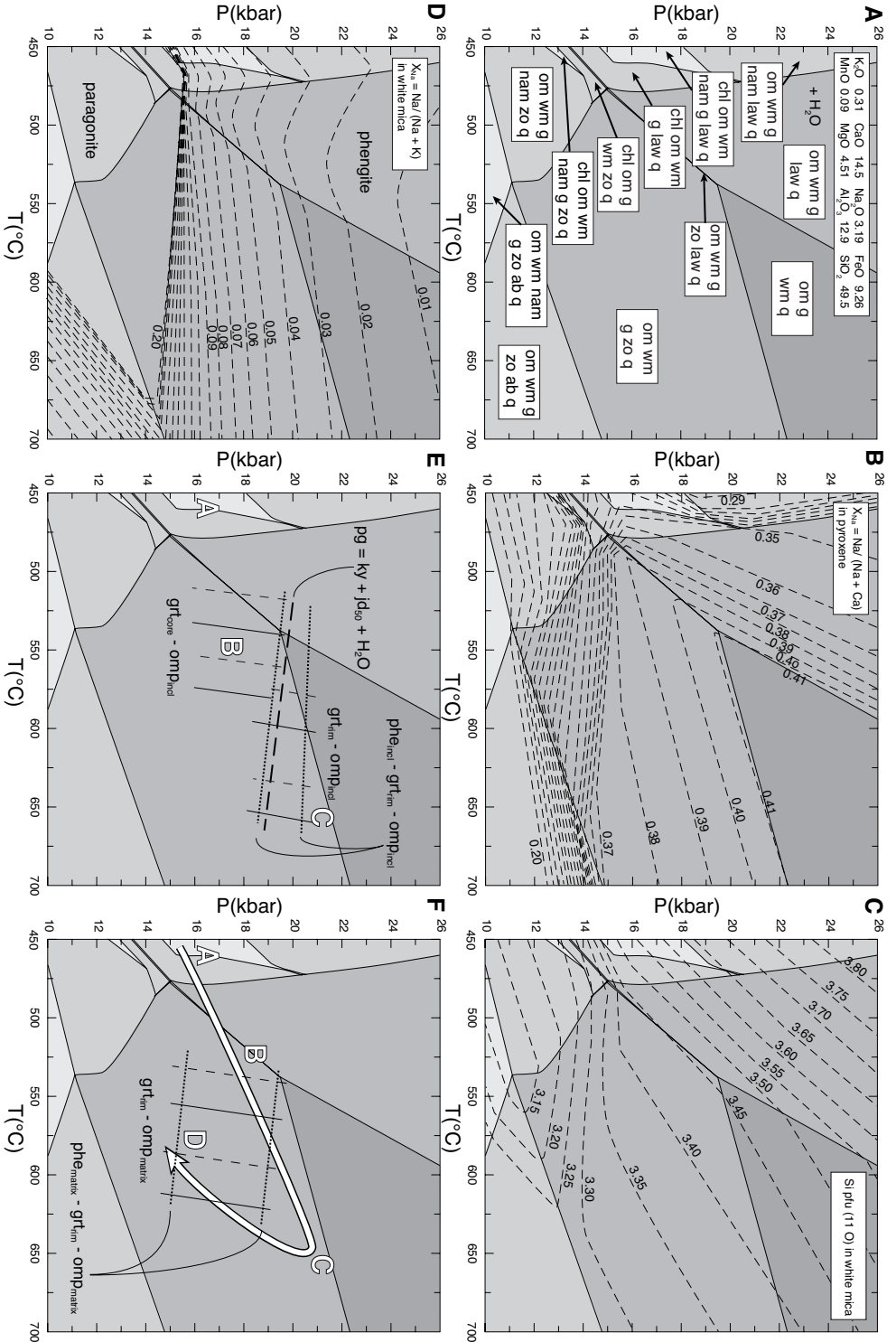


**Figure 2.8:** A: P-T pseudosection (Pepelke & Connolly, 1990) for eclogite calculated in the KCNFMASH system, using the bulk rock composition given in the white box.  $H_2O$  is in excess. Light to dark grey fields correspond to di-, tri-, quadri-, five- and six-variant fields, respectively. Narrow or small field labels are not mentioned for clarity ( $g$  = garnet,  $tr$  = quartz,  $flv$  = lawsonite,  $wm$  = white mica,  $nam$  = sodic-calcic amphibole,  $zo$  = zoisite,  $chl$  = chlorite,  $law$  = lawsonite,  $ab$  = albite,  $q$  = quartz). White mica composition is phengite (above 16 kbar, <1 Vol%) and paragonite under 16 kbar. B:  $X_{Na}$  [ $Na / (Na + Ca)$ ] isopleths of omphacite. C: Si pft in white mica isopleths. D:  $X_{Na}$  [ $Na / (Na + K)$ ] isopleths of white mica. E: Results from Fe-Mg exchange thermometry and phengite-garnet-pyroxene barometry. Stage A corresponds to the eclogite assemblage with stable lawsonite related from pseudomorphs after lawsonite enclosed in garnet. Stage B corresponds to  $grt_{core} - omp_{incl}$  pairs (in vertical dashed lines calibration after Powell (1985), in vertical drawn through lines calibration after (Ellis and Green, 1979) for the stage C and D, too). Stage C corresponds to  $grt_{trim} - omp_{incl}$  pairs. Horizontal dotted lines represent the pressure of  $phengite - grt_{trim} - omp_{incl}$  in the range between Si pft of 3.42 and 3.46 (calibration after Watson et al., 2006). Thick dotted line shows the paragonite breakdown after (Holland, 1979). F: Stage D corresponds to  $grt_{trim} - omp_{matrix}$  pairs and  $phengite - grt_{trim} - omp_{matrix}$  in the range of Si pft of 3.42 and 3.32.

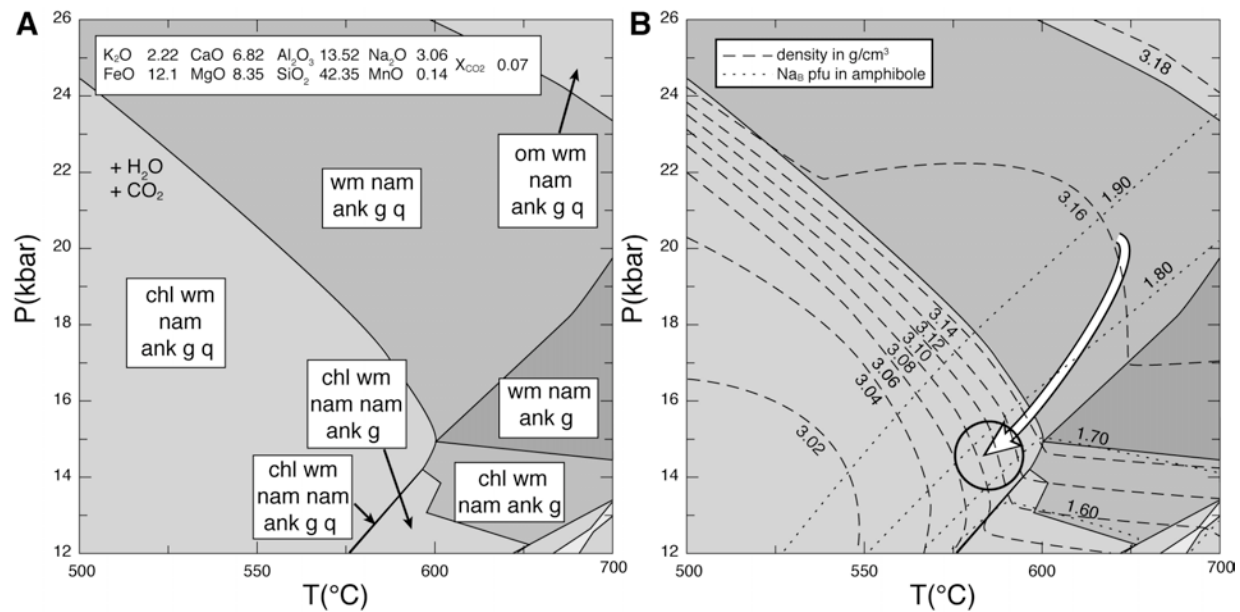


**Figure 2.9:** A: P-T pseudosection (Perple\_X; Connolly, 1990) for phengite-ankerite blueschist calculated in the KCNmFMASHC system, using the bulk rock composition given in the white box. H<sub>2</sub>O and CO<sub>2</sub> are in excess with X<sub>CO<sub>2</sub></sub> = 0.07. Light to dark grey fields correspond to tri-, quadri-, five- and six-variant fields, respectively (g = garnet, om = omphacite, nam = sodic-calcic amphibole, chl = chlorite, wm = white mica, ank = ankerite, q = quartz). B: in dashed lines: density isopleths; in dotted lines: Na<sub>B</sub> pfu in amphibole isopleths. The circle in D marks the possible P-T condition in agreement with the estimated mineral amounts and the pyknometer measurements. Arrow in D shows the retrograde P-T path from Figure 2.9B for comparison.

(Powell, 1985) and 640±15°C (Ellis and Green, 1979) were calculated with omphacite inclusions and garnet rims and are attributed to peak metamorphism (Stage C, Figure 2.8E and 2.8F). The associated pressure deduced from X<sub>Na</sub> [Na/ (Na + Ca)] isopleths of 0.41 in omphacite (highest observed jadeite content), and from phengite-clinopyroxene-garnet barometry (Waters and Martin, 1993) is at 19.5±1 kbar due to Si contents between 3.42 and 3.46 pfu in phengite. At peak-metamorphic temperatures of 650°C the isopleth of 3.40 Si pfu in white mica indicates a pressure of 21 kbar (Figure 2.8C). The stability field of the zoisite-free eclogite assemblage omphacite + white mica + garnet + quartz at P >22 kbar was not reached during peak metamorphism. The retrograde stage D, which is still in the omphacite + white mica + garnet + quartz stability field, shows lower conditions with temperatures of 560±30°C (Powell, 1985) and 590±30°C (Ellis and Green, 1979) derived from matrix-omphacite and garnet rim composition and pressures between 15 and 19.5 kbar derived from phengite-garnet-pyroxene barometry (Waters and Martin, 1993, garnet rim, matrix omphacite rim and matrix phengite with Si between 3.29 and 3.43 pfu, Figure 2.8F). The isopleth of 3.30 Si pfu in matrix white mica indicates a pressure of 14 kbar (Figure 2.8C) whereas the X<sub>Na</sub> = [Na/ (Na + K)] isopleth of 0.10 in matrix white mica gives a pressure of 16 kbar (Figure 2.8D). The X<sub>Na</sub> = [Na/ (Na + Ca)] isopleth of 0.37 in matrix pyroxene indicates a pressure of about 15 kbar (Figure 2.8B). In summary, the

latest preserved retrograde P-T conditions can be estimated at  $15\pm 1$  kbar and  $580\pm 50^\circ\text{C}$ . Conditions of the phengite-ankerite blueschist were calculated in the KCNMFASHC system.  $X_{\text{CO}_2}$  of the fluid phase was assumed at 0.07. With this  $X_{\text{CO}_2}$  value the calculated ankerite content of the ankerite-phengite blueschist during the metamorphic stage D corresponds to the modal proportion observed in the rock. The retrograde P-T path cannot be derived from P-T pseudosections alone, as the stability field of the assemblage chlorite + white mica + sodic-calcic amphibole + ankerite + garnet + quartz is very large (Figure 2.9A). Additional information is given by the measured density of  $3.09\text{ g/cm}^3$  (Table 2.3) and the Na contents between 1.70 and 1.80 in the B position ( $\text{Na}_B$ ) of the coexisting sodic amphibole (Table 2.1). The calculated isopleths (Perple\_X) of the density and of the  $\text{Na}_B$  contents of amphibole (Figure 2.9B), are crossing the P-T conditions of  $15\pm 1$  kbar and  $580\pm 10^\circ\text{C}$ . In conclusion, the density, the  $\text{Na}_B$  content of sodic amphibole and the mineral assemblage of the phengite-ankerite blueschist are in agreement with the retrograde P-T conditions (Stage D) deduced from the eclogite (Figure 2.8B–F). Subsequent to this stage the retrograde overprinting stopped and no new minerals were formed.

## 2.6 Bulk rock geochemistry

### 2.6.1 Eclogite domain

Eclogite domains ( $n = 10$ ) contain on average  $\sim 47\text{ wt}\%$   $\text{SiO}_2$ ,  $3.3\text{ wt}\%$   $\text{Na}_2\text{O}$  and  $0.9\text{ wt}\%$   $\text{K}_2\text{O}$ . This corresponds to a basaltic to trachybasaltic composition according to the  $\text{SiO}_2$  vs.  $\text{K}_2\text{O} + \text{Na}_2\text{O}$  relation. The Co vs. Th ratios, which might be more useful for altered rocks (Hastie et al., 2007), point to the same type of protholiths. The mean LOI is  $3.83\text{ wt}\%$  and the analysed  $\text{CO}_2$  content is  $3.14\text{ wt}\%$ . This results in a calculated  $\text{H}_2\text{O}$  content of  $0.69\text{ wt}\%$  (Table 2.3). The chondrite-normalised REE pattern shows a steep negative slope with  $(\text{Ce}/\text{Yb})_N$  of  $\sim 4$ , with LREE of about 52 times and HREE of about 11 times the chondritic values (Figure 2.10A). MORB-normalised trace element patterns show decreasing enrichments with decreasing incompatibility. Zr/Hf and Nb/Ta ratios are around 42 and 16 and are similar to those of OIB (ocean island basalt; Pfänder et al. (2007)). Gd–Lu concentrations are lower than those of MORB, whereas the concentrations of LILE are higher (e.g. Cs  $\sim 50$  times and Ba  $\sim 10$  times, Figure 2.10A). The MORB-normalised trace element pattern of an OIB (Wilson, 1997; Naumann et al., 2002) is very similar to the eclogite pattern (Figure 2.10B) except for highly fluid-mobile LILE (Cs, Rb, Ba and K). In conclusion, the MORB-normalised and chondrite-normalised trace element contents make it likely that OIB were the precursor rocks of the eclogites of the Tian Shan.

### 2.6.2 Blueschist domains

Compared to the composition of the eclogites the  $\text{SiO}_2$  and  $\text{Na}_2\text{O}$  concentrations in the glaucophane-dominated blueschist domains ( $N = 4$ ) do not differ significantly,

but the  $K_2O$  content increases from 0.87 to 1.88 wt%. In addition, the concentrations of all other major elements, with the exception of  $CaO$  and  $P_2O_5$ , increase.

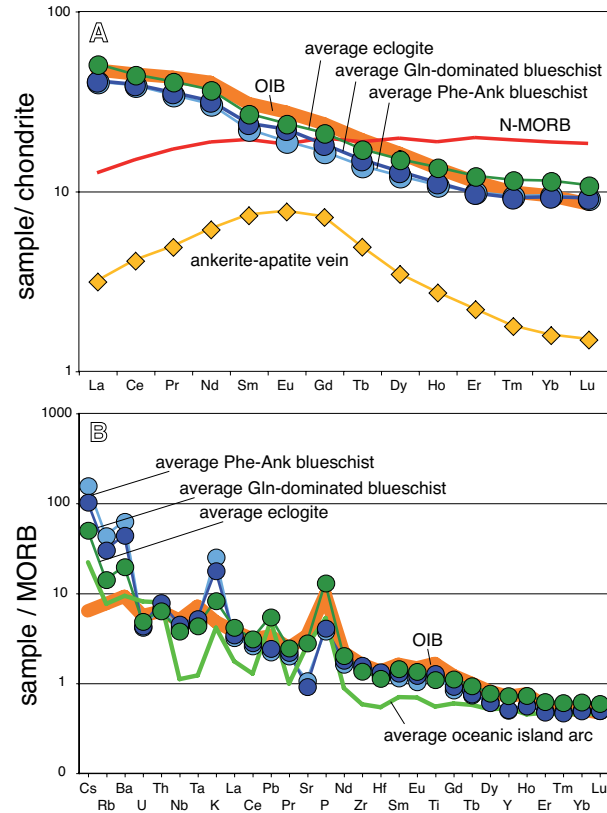


**Figure 2.10:** A: Chondrite-normalised (Boynton, 1984) REE patterns of all eclogite and blueschist domains, average composition are used. B: MORB-normalised multi-element diagram. MORB composition is that of Hart et al. (1999), OIB is represented by basalts from Hawaii (standard BHVO-2, USGS (Wilson, 1997)) and basalts from Galapagos (Naumann et al., 2002), and the average oceanic island arc is after Kelemen et al. (2003). Eclogite composition shows in both diagrams a strong affinity to OIB assumed to be the precursor rock of the eclogite.

HFSE ratios do not change (Figure 2.12A). Ratios of  $Zr/Hf$  and  $Nb/Ta$  of  $\sim 42$  and  $\sim 16$  of all three domains are in accordance with those ratios in OIB (Pfänder et al., 2007).

The LOI increases for 0.9 wt% to 4.72 wt%, with a slight increase of  $CO_2$  and  $H_2O$  to 3.40 wt% and 1.32 wt%, respectively. The phengite-ankerite blueschist ( $N = 10$ ) has, on average, 42.6 wt%  $SiO_2$ , which is much lower than in the eclogite domain.  $TiO_2$ ,  $Al_2O_3$ ,  $Fe_{tot}$ ,  $MgO$ ,  $P_2O_5$  and  $H_2O$  values are similar to those of the glaucophane-dominated blueschist, but are still higher than those of the eclogite domain, except for  $P_2O_5$ . Compared to the eclogite domain,  $MnO$ ,  $K_2O$  and  $CO_2$  contents are higher. The LOI increases from 3.8 to 7.5 wt% with 6.3 wt%  $CO_2$  and 1.2 wt%  $H_2O$  (Table 2.3). Chondrite-normalised REE patterns are similar to those of the eclogites but display lower concentrations (HREE  $\sim 9$  times and LREE  $\sim 40$ -43 times chondrite; Figure 2.10A). Both blueschist domains have almost identical Dy–Lu concentrations, but La–Tb concentrations are slightly higher in the glaucophane-dominated blueschist. MORB-normalised trace element patterns (Figure 2.10B) show a progressive increase of LILE (Cs, Rb, Ba and K) from the eclogite towards the phengite-ankerite blueschist domain (e.g. Cs up to 157 times enriched MORB) and a continuous decrease for Sr and P. HFSE contents increase slightly in the blueschist domains compared to the eclogite domains, but the

**Table 2.3:** Major and trace element analyses of mechanically separated eclogite and blueschist domains (E 81°15'38.3", N 42°28'59.1").

sample	<b>FTS</b> <b>4-1.1</b>	<b>FTS</b> <b>4-1.2</b>	<b>FTS</b> <b>4-1.3</b>	<b>FTS</b> <b>4-1.3</b>	<b>FTS</b> <b>4-1.4</b>	<b>FTS</b> <b>4-1.4</b>	<b>FTS</b> <b>4-1.5</b>	<b>FTS</b> <b>4-1.5</b>	<b>FTS</b> <b>4-2.1</b>	<b>FTS</b> <b>4-2.2</b>
domain	PAB	PAB	Ec	Ec	Ec	PAB	GDB	Ec	PAB	PAB
SiO <sub>2</sub>	42.32	47.11	49.67	49.48	44.64	36.46	51.56	49.75	44.65	42.35
TiO <sub>2</sub>	2.03	1.68	0.80	1.65	1.95	1.83	2.41	1.65	2.21	1.69
Al <sub>2</sub> O <sub>3</sub>	14.58	13.11	10.24	12.89	12.81	13.97	15.17	13.31	15.39	13.52
Fe[tot]	10.64	12.61	11.01	10.29	10.54	13.69	10.36	9.29	12.37	13.43
FeO [calc.]	9.57	11.35	9.91	9.26	9.48	12.32	9.32	8.36	11.13	12.08
MnO	0.11	0.13	0.10	0.09	0.12	0.25	0.07	0.06	0.12	0.14
MgO	8.40	8.82	5.33	4.51	6.13	7.22	7.30	5.23	7.52	8.35
CaO	6.83	4.90	15.29	14.45	13.97	13.11	3.06	12.70	5.27	6.82
Na <sub>2</sub> O	2.70	4.04	4.49	3.19	3.08	1.76	3.98	2.82	2.93	3.06
K <sub>2</sub> O	3.37	1.67	0.04	0.31	1.11	1.71	2.85	1.51	3.00	2.22
P <sub>2</sub> O <sub>5</sub>	0.02	0.04	1.93	0.52	0.23	0.12	0.11	0.58	0.09	0.07
CO <sub>2</sub>	7.73	4.35	1.24	1.70	4.95	10.05	0.57	2.29	4.67	7.12
H <sub>2</sub> O [calc.]	1.67	1.22	0.38	0.43	0.77	0.47	1.98	1.08	1.25	1.23
LOI	9.40	5.57	1.62	2.13	5.72	10.52	2.55	3.37	5.92	8.35
Density <sup>1</sup>	3.10	3.03	3.22	3.18	3.06	3.08	3.02	3.09	3.06	3.09
<b>sum</b>	<b>100.40</b>	<b>99.68</b>	<b>100.52</b>	<b>99.51</b>	<b>100.30</b>	<b>100.64</b>	<b>99.42</b>	<b>100.27</b>	<b>99.47</b>	<b>100.00</b>
Li	43.8	52.0	50.5	37.2	37.8	20.2	53.0	37.8	44.8	40.2
Sc	24.9	26.6	20.6	26.2	27.8	23.0	28.5	30.7	33.5	26.0
V	204	179	200	247	225	181	208	274	239	174
Cr*	290	244	131	236	289	256	336	248	312	242
Co	41.9	55.6	33.8	31.6	30.7	42.7	50.1	23.7	42.7	53.8
Ni	224	289	162	134	181	200	335	115	224	226
Cu	66.8	65.1	41.1	40.6	47.9	75.9	23.0	64.9	50.5	60.4
Zn	102	130	71.0	55.3	68.7	74.5	121.8	59.7	99.1	111
Ga	19.6	15.8	15.7	19.5	18.6	15.4	19.4	22.8	20.9	16.1
Rb	69.2	32.3	0.948	6.22	22.0	33.2	57.2	29.8	62.2	45.7
Sr	138	75.5	222	361	254	251	44.0	356	79.1	104
Y	10.4	9.84	30.0	33.2	20.1	20.1	14.1	28.8	21.3	13.9
Zr	157	135	64.7	131	155	141	197	134	175	130
Nb	14.4	13.0	6.2	12.5	14.0	12.4	19.1	12.2	16.9	11.7
Mo	0.32	0.34	0.29	0.18	0.29	0.47	0.18	0.19	0.23	0.36
Cd	0.09	0.07	0.12	0.12	0.14	0.12	n.a.	n.a.	0.09	0.09
Sn	1.37	0.96	1.12	1.40	1.50	1.22	1.48	1.91	1.46	1.13
Sb	0.12	0.10	0.12	0.17	0.12	0.11	0.12	0.11	0.16	0.11
Cs	2.66	1.33	0.07	0.36	0.87	1.35	2.41	1.24	2.49	2.03
Ba	1160	570	16.2	112	370	543	942	481	999	726
La	6.72	9.40	12.1	17.6	15.7	15.4	15.6	20.5	14.4	6.57
Ce	19.2	25.6	26.7	39.9	36.8	35.3	40.7	48.0	36.0	18.3
Pr	2.60	3.38	3.79	5.51	4.91	4.70	5.39	6.35	4.57	2.54
Nd	11.2	14.5	17.6	24.6	21.6	20.8	23.5	28.4	19.3	11.3
Sm	2.61	3.28	4.35	5.83	5.07	4.94	5.52	6.88	4.51	2.80
Eu	0.80	0.93	1.63	1.97	1.76	1.74	1.66	2.35	1.85	0.78
Gd	2.52	2.79	5.08	6.22	5.04	5.00	4.60	7.23	4.63	3.02
Tb	0.43	0.43	0.79	0.94	0.70	0.69	0.56	0.98	0.75	0.52
Dy	2.62	2.56	5.07	5.83	3.97	3.83	2.98	5.40	4.71	3.31
Ho	0.50	0.50	1.08	1.21	0.80	0.76	0.61	1.11	0.93	0.65
Er	1.36	1.36	2.95	3.29	2.15	2.04	1.79	2.97	2.51	1.74
Tm	0.21	0.21	0.43	0.48	0.32	0.29	0.27	0.43	0.38	0.27
Yb	1.42	1.40	2.62	2.99	2.09	1.92	1.86	2.75	2.47	1.75
Lu	0.21	0.22	0.38	0.43	0.31	0.30	0.29	0.40	0.35	0.25
Hf	3.64	3.27	1.58	3.08	3.83	3.38	4.65	3.13	4.19	3.18
Ta	0.89	0.81	0.37	0.77	0.93	0.84	1.20	0.79	1.05	0.76
W	0.57	0.53	0.63	0.34	0.72	0.77	0.24	0.16	0.94	0.71
Tl	0.23	0.11	0.01	0.03	0.07	0.18	0.19	0.11	0.21	0.16
Pb	1.35	0.66	1.54	2.35	1.92	1.85	0.69	2.97	0.82	0.86
Th	1.20	1.22	0.51	1.02	1.27	1.15	1.88	1.27	1.38	1.09
U	0.21	0.23	0.51	0.46	0.38	0.39	0.45	0.41	0.31	0.21

Major elements and LOI in % , Li to U in ppm , <sup>1</sup>in g/cm<sup>3</sup>, n.a. = not analysed, \*from XRF analyses, CO<sub>2</sub> calculated of TC, H<sub>2</sub>O difference between CO<sub>2</sub> and LOI, sum includes Fe[tot] and LOI. Domains: PAB = phengite-ankerite-blueschist; GDB = glaucophane-dominated blueschist; Ec = eclogite; AAV = ankerite-apatite-vein.

**Table 2.3:** (cont.) Major and trace element analyses of mechanically separated eclogite and blueschist domains (E 81°15'38.3", N 42°28'59.1").

sample	<b>FTS</b> <b>4-2.3</b>	<b>FTS</b> <b>4-2.3</b>	<b>FTS</b> <b>4-2.4</b>	<b>FTS</b> <b>4-2.4</b>	<b>FTS</b> <b>4-2.5</b>	<b>FTS</b> <b>4-2.5</b>	<b>FTS</b> <b>4-3.1</b>	<b>FTS</b> <b>4-3.1</b>	<b>FTS</b> <b>4-3.1</b>	<b>FTS</b> <b>4-3.2</b>
domain	PAB	PAB	PAB	Ec	Ec	AAV	PAB	GDB	Ec	Ec
SiO <sub>2</sub>	40.97	50.86	45.00	49.07	43.10	n.a.	39.58	47.16	52.33	47.67
TiO <sub>2</sub>	1.89	2.40	1.92	1.97	2.16	0.01	2.00	1.95	1.57	1.53
Al <sub>2</sub> O <sub>3</sub>	14.32	16.09	15.79	14.45	15.40	0.15	15.30	14.12	12.18	12.01
Fe[tot]	13.74	9.49	12.62	10.18	12.41	12.60	14.75	13.69	7.83	11.23
FeO [calc.]	12.36	8.54	11.36	9.16	11.17	11.33	8.54	13.27	12.32	7.05
MnO	0.17	0.05	0.13	0.06	0.14	0.25	0.19	0.12	0.02	0.10
MgO	7.84	6.58	6.24	4.97	4.31	15.11	6.96	7.88	5.99	6.87
CaO	7.31	3.48	6.83	10.78	14.65	29.29	8.16	5.40	12.37	12.10
Na <sub>2</sub> O	2.53	3.61	2.67	3.50	2.78	0.03	2.06	3.94	4.74	3.88
K <sub>2</sub> O	2.65	3.68	3.15	2.34	0.85	0.01	2.60	1.46	1.12	0.48
P <sub>2</sub> O <sub>5</sub>	0.03	0.20	0.34	0.29	0.25	1.53	0.08	0.14	0.37	0.34
CO <sub>2</sub>	7.85	0.58	3.78	1.13	3.26	41.31	7.41	3.07	0.61	3.61
H <sub>2</sub> O [calc.]	0.86	2.32	1.58	1.20	0.60	n.a.	0.76	1.20	1.22	0.68
LOI	8.71	2.90	5.36	2.33	3.86	n.a.	8.17	4.27	1.83	4.29
Density <sup>1</sup>	3.14	2.94	3.04	3.15	3.24	n.a.	3.15	3.15	n.a.	n.a.
<b>sum</b>	<b>100.16</b>	<b>99.34</b>	<b>100.05</b>	<b>99.94</b>	<b>99.91</b>	<b>100.29</b>	<b>99.85</b>	<b>100.13</b>	<b>100.35</b>	<b>100.50</b>
Li	34.0	44.9	26.1	41.6	29.7	n.a.	29.8	40.5	57.5	43.5
Sc	25.3	33.6	29.9	28.4	32.3	n.a.	27.5	n.a.	n.a.	n.a.
V	184	245	232	287	297	n.a.	181	150	283	204
Cr*	264	338	269	280	317	n.a.	272	278	247	223
Co	46.0	44.1	38.0	32.2	44.5	39.0	42.6	50.8	21.5	32.4
Ni	229	255	228	156	205	61	221	217	89	167
Cu	55.4	27.1	40.2	30.1	43.8	18.5	83.7	33.6	27.9	41.7
Zn	102	114	95.9	65.5	66.4	74.0	89.1	126	69.1	83.5
Ga	16.3	20.6	17.0	19.8	20.3	0.28	16.1	15.6	21.9	17.1
Rb	54.9	77.2	63.7	46.4	17.7	0.06	55.4	31.7	24.8	10.3
Sr	113	41.0	98.2	251	412	707	126	73.4	183	195
Y	9.92	15.5	31.7	22.6	31.1	5.49	21.1	22.6	13.3	28.1
Zr	146	190	157	160	174	0.20	156	156	121	123
Nb	13.8	18.6	14.2	15.2	16.0	0.02	14.2	16.0	12.6	11.9
Mo	0.25	0.19	0.21	0.18	0.25	0.09	0.45	0.21	0.17	0.25
Cd	0.10	0.09	n.a.	n.a.	0.13	n.a.	0.11	n.a.	n.a.	n.a.
Sn	1.22	1.70	1.38	1.77	1.54	0.07	1.21	0.85	1.59	0.94
Sb	0.13	0.12	0.10	0.15	0.17	0.01	0.13	0.12	0.13	0.11
Cs	2.20	3.24	2.56	1.81	0.73	0.01	2.07	1.07	0.83	0.38
Ba	861	1197	923	681	268	3.67	874	482	356	150
La	6.58	15.5	28.3	20.7	17.7	0.97	10.5	12.9	13.3	14.6
Ce	17.5	39.1	64.9	45.0	39.0	3.31	26.9	32.9	32.0	33.4
Pr	2.34	5.29	8.82	6.19	5.73	0.60	3.61	4.43	4.26	4.61
Nd	10.1	23.7	38.3	27.3	25.6	3.67	15.5	19.3	18.7	20.4
Sm	2.41	5.82	8.68	6.55	6.21	1.43	3.68	4.67	4.45	4.87
Eu	0.69	1.86	2.30	2.06	1.98	0.56	1.38	1.57	1.45	1.62
Gd	2.63	5.30	7.57	6.42	6.59	1.86	4.36	4.68	4.35	5.12
Tb	0.43	0.67	1.03	0.85	1.00	0.23	0.74	0.72	0.56	0.79
Dy	2.41	3.59	6.23	4.65	5.84	1.11	4.46	4.33	2.84	4.93
Ho	0.46	0.71	1.29	0.89	1.17	0.20	0.86	0.86	0.51	1.00
Er	1.27	1.95	3.45	2.37	3.08	0.46	2.23	2.18	1.17	2.53
Tm	0.20	0.29	0.48	0.34	0.44	0.06	0.32	0.33	0.16	0.38
Yb	1.39	1.92	2.94	2.19	2.77	0.33	2.04	2.16	1.00	2.43
Lu	0.22	0.29	0.42	0.32	0.41	0.05	0.30	0.33	0.15	0.36
Hf	3.55	4.60	3.55	3.71	4.09	0.01	3.74	3.75	2.88	2.95
Ta	0.87	1.17	0.91	0.94	1.02	-	0.90	0.94	0.73	0.73
W	0.78	0.46	0.28	0.30	0.63	0.04	0.69	n.a.	n.a.	n.a.
Tl	0.19	0.26	0.27	0.19	0.06	-	0.18	0.13	0.08	0.04
Pb	0.90	0.90	1.09	2.42	3.20	4.59	1.00	0.71	1.52	1.63
Th	1.13	1.51	1.60	1.27	1.34	0.02	1.21	1.34	1.13	1.03
U	0.22	0.43	0.52	0.49	0.41	0.01	0.21	0.26	0.24	0.21

Major elements and LOI in %, Li to U in ppm, <sup>1</sup>in g/cm<sup>3</sup>, n.a. = not analysed, \*from XRF analyses, CO<sub>2</sub> calculated of TC, H<sub>2</sub>O difference between CO<sub>2</sub> and LOI, sum includes Fe[tot] and LOI. Domains: PAB = phengite-ankerite-blueschist; GDB = glaucophane-dominated blueschist; Ec = eclogite; AAV = ankerite-apatite-vein.

**Table 2.3:** (cont.) Major and trace element analyses of mechanically separated eclogite and blueschist domains (E 81°15'38.3", N 42°28'59.1").

sample	<b>FTS</b> <b>4-3.2</b>	<b>FTS</b> <b>4-3.3</b>	<b>FTS</b> <b>4-3.3</b>	<b>FTS</b> <b>4-3.4</b>	<b>FTS</b> <b>4-3.5</b>	<b>FTS</b> <b>4-3.5</b>	<b>PAB</b> <b>av.</b>	<b>GDB</b> <b>av.</b>	<b>Ec av.</b>
domain	GDB	PAB	Ec	Ec	Ec	GDB			
SiO <sub>2</sub>	41.55	36.98	43.87	40.56	49.82	49.11	42.63	47.35	47.03
TiO <sub>2</sub>	1.98	1.89	1.96	1.79	1.49	1.91	1.95	2.06	1.77
Al <sub>2</sub> O <sub>3</sub>	14.26	14.84	14.36	13.12	11.83	13.03	14.69	14.15	13.24
Fe[tot]	13.77	14.13	11.84	12.20	10.26	10.50	12.75	12.08	10.61
FeO [calc.]	12.39	12.71	10.65	10.98	9.23	9.45	11.47	10.87	9.54
MnO	0.17	0.21	0.13	0.19	0.06	0.07	0.15	0.11	0.10
MgO	7.45	7.23	5.44	5.20	5.96	7.61	7.52	7.56	5.46
CaO	8.40	10.08	15.17	17.02	14.07	8.37	7.28	6.31	13.73
Na <sub>2</sub> O	2.70	1.71	3.14	1.58	4.64	4.30	2.71	3.73	3.34
K <sub>2</sub> O	1.93	2.66	0.35	0.43	0.24	1.28	2.67	1.88	0.87
P <sub>2</sub> O <sub>5</sub>	0.13	0.05	0.25	0.35	0.39	0.07	0.10	0.11	0.36
CO <sub>2</sub>	7.07	9.67	3.82	8.56	1.43	2.89	6.32	3.40	3.14
H <sub>2</sub> O [calc.]	0.44	0.84	0.40	0.01	0.51	1.65	1.22	1.32	0.69
LOI	7.51	10.51	4.22	8.57	1.94	4.54	7.54	4.72	3.83
Density <sup>1</sup>	3.12	3.14	3.17	3.19	3.14	3.03	3.08	3.08	3.15
<b>sum</b>	<b>99.85</b>	<b>100.29</b>	<b>100.73</b>	<b>101.01</b>	<b>100.70</b>	<b>100.79</b>	<b>99.99</b>	<b>100.05</b>	<b>100.32</b>
Li	32.6	41.2	37.6	18.7	56.7	45.7	37.7	42.9	39.8
Sc	28.5	23.4	30.3	n.a.	24.6	23.9	27.4	27.0	28.6
V	169	176	272	194	241	193	199	180	252
Cr*	279	259	266	257	218	260	275	288	258
Co	48.4	44.3	36.1	28.8	28.8	40.9	45.2	47.6	31.0
Ni	272	210	195	104	113	265	231	272	146
Cu	73.8	89.4	43.6	31.2	34.5	33.9	61.5	41.1	40.6
Zn	98.8	83.3	66.1	49.6	74.7	112	100	115	65.9
Ga	14.9	15.6	19.9	18.4	18.1	16.6	17.4	16.6	19.6
Rb	37.8	56.9	7.23	9.09	4.97	25.8	55.1	38.1	17.8
Sr	128	180	402	514	246	170	121	104	318
Y	22.6	25.9	29.8	29.6	23.5	13.8	18.0	18.2	26.0
Zr	151	145	154	140	123	156	153	165	142
Nb	15.3	14.2	14.5	12.7	11.7	13.1	14.3	15.9	13.3
Mo	0.36	0.54	0.25	0.20	0.22	0.25	0.33	0.25	0.22
Cd	0.11	0.11	0.13	n.a.	n.a.	n.a.	0.09	0.04	0.10
Sn	1.16	1.21	1.64	0.99	1.72	1.49	1.28	1.24	1.50
Sb	0.11	0.11	0.14	0.12	0.12	0.17	0.12	0.13	0.13
Cs	1.38	2.16	0.27	0.32	0.23	0.94	2.21	1.45	0.70
Ba	627	878	109	132	75.2	392	873	611	273
La	11.6	11.5	14.7	14.4	13.4	13.5	12.5	13.4	16.3
Ce	28.9	28.9	34.9	33.0	30.5	32.5	31.2	33.8	37.3
Pr	3.98	3.83	4.87	4.51	4.23	4.47	4.17	4.57	5.12
Nd	17.7	16.9	21.6	19.8	18.7	19.9	18.2	20.1	22.7
Sm	4.25	4.17	5.24	4.66	4.58	4.94	4.29	4.85	5.43
Eu	1.52	1.53	1.80	1.57	1.53	1.77	1.38	1.63	1.81
Gd	4.70	4.94	5.73	5.09	4.76	4.70	4.27	4.67	5.65
Tb	0.78	0.84	0.93	0.81	0.73	0.62	0.65	0.67	0.83
Dy	4.78	5.27	5.74	4.99	4.52	3.26	3.90	3.84	4.87
Ho	0.95	1.04	1.16	1.03	0.92	0.58	0.77	0.75	0.98
Er	2.49	2.72	3.12	2.69	2.43	1.44	2.06	1.98	2.58
Tm	0.36	0.39	0.46	0.42	0.35	0.20	0.30	0.29	0.38
Yb	2.32	2.46	2.93	2.75	2.18	1.32	1.97	1.91	2.41
Lu	0.35	0.36	0.42	0.41	0.30	0.20	0.29	0.29	0.35
Hf	3.88	3.47	3.78	3.35	2.82	3.59	3.66	3.97	3.36
Ta	0.97	0.86	0.93	0.80	0.72	0.89	0.91	1.00	0.84
W	0.51	0.69	0.39	n.a.	0.17	0.20	0.64	0.24	0.39
Tl	0.13	0.19	0.03	0.03	0.03	0.12	0.20	0.14	0.07
Pb	1.09	1.43	3.34	4.67	2.53	2.28	1.09	1.19	2.66
Th	1.34	1.15	1.29	1.17	1.11	1.33	1.26	1.47	1.19
U	0.24	0.24	0.33	0.26	0.27	0.29	0.30	0.31	0.35

Major elements and LOI in %, Li to U in ppm, <sup>1</sup>in g/cm<sup>3</sup>, n.a. = not analysed, \*from RFA analyses, CO<sub>2</sub> calculated of TC, H<sub>2</sub>O difference between CO<sub>2</sub> and LOI, sum includes Fe[tot] and LOI. Domains: PAB = phengite-ankerite-blueschist; GDB = glaucophane-dominated blueschist; Ec = eclogite; AAV = ankerite-apatite-vein.



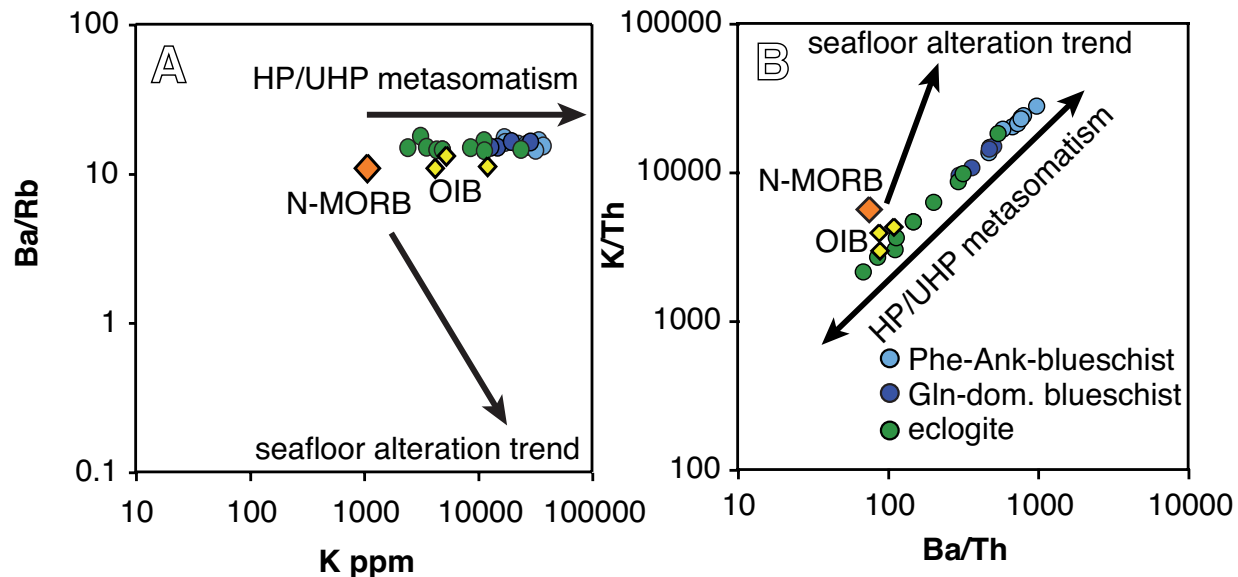


**Figure 2.11:** Ba/Rb vs. K and Ba/Th vs. K/Th diagrams to differentiate between enrichments by seawater alteration and those by HP/UHP metasomatism after [Bebout \(2007\)](#). A: Eclogites and blueschists of the Tian Shan are enriched in K at constant Ba/Rb ratios indicating enrichment due to HP/UHP metasomatism. B: Similar enrichments of Ba and K normalised to Th (fluid-immobile), follows the HP/UHP metasomatism trend, in contrast to the seafloor alteration trend, in which K is more enriched than Ba.

## 2.7 Discussion

### 2.7.1 Evidence for pre-metamorphic seafloor alteration?

The petrological observations as described before, indicate that the blueschist replaced the eclogite under retrograde blueschist-facies conditions. Chemical differences between the eclogite-facies cores and the blueschist-facies pillow-rims might not be a metamorphic feature, but could also refer to early, pre-metamorphic, seawater alteration. Seawater alteration is associated in many cases with a decrease of Si and Ca and an increase of Mg, K, Cs, Rb, Pb, U and CO<sub>2</sub> (e.g. [Bednarz and Schmincke, 1989](#); [Alt and Teagle, 2003](#); [Staudigel et al., 1996](#); [Staudigel, 2003](#)). The enrichment of Rb and K in the blueschist rim compared to the eclogite core seems to be in agreement with seawater alteration. However, it is expected that Ba enrichment by seafloor alteration is much smaller than that for Rb and K ([Bebout, 2007](#)). Barium is strongly enriched in the blueschists relative to the eclogites. This enrichment is similar to that of Rb and K and supports the contention that these enrichments occurred during HP metasomatism (Figure 2.12). CO<sub>2</sub> enrichment during seafloor alteration is related to carbonate formation and should therefore correlate with a distinct increase in Ca ([Alt and Teagle, 1999](#)). This is in contrast to the observed strong Ca decrease in the blueschists compared to the eclogites. Moreover, the Rb–Ba–K carrying mica ([Zack et al., 2001](#)) has been formed

during late stages of metamorphism, showing clearly their growth at the expense of garnet and omphacite (Figure 2.4), which indicates a late-stage addition of these elements. Seawater alteration would also not explain the depletions of LREE and the HREE in the blueschists compared to the eclogites. Even though many geochemical and petrological features indicate a HP metasomatic event during the eclogite-blueschist transformation, minor chemical changes during pre-metamorphic seafloor alteration cannot be excluded. These changes have been widely obliterated during subsequent metamorphism. For the following discussion we assume a homogenous composition of the pillow basalts prior to metamorphism.

### 2.7.2 Mass-balance calculation

The eclogite-facies pillow lavas of the Tian Shan developed a blueschist-facies mineral assemblage prior to the eclogite facies and were partially transformed to blueschists during retrogression. A  $\sim 2$  cm thick shell of a glaucophane-dominated blueschist marks the interface between the eclogite relict and the phengite-ankerite blueschist representing the overall wall rock. As the blueschist contains more volatile-rich minerals, rehydration reactions during the eclogite-blueschist transformation were induced by fluid infiltration. Glaucophane, phengite and ankerite could not have grown if not at least volatiles ( $\text{H}_2\text{O}$ ,  $\text{CO}_2$ ) and K had been added to the system. Hence, the rocks experienced prograde eclogite-facies dehydration reactions and a rehydration after peak-metamorphism under blueschist-facies conditions.

A mass-balance calculation is required to proof whether the change of element concentrations is a consequence of the mobility or

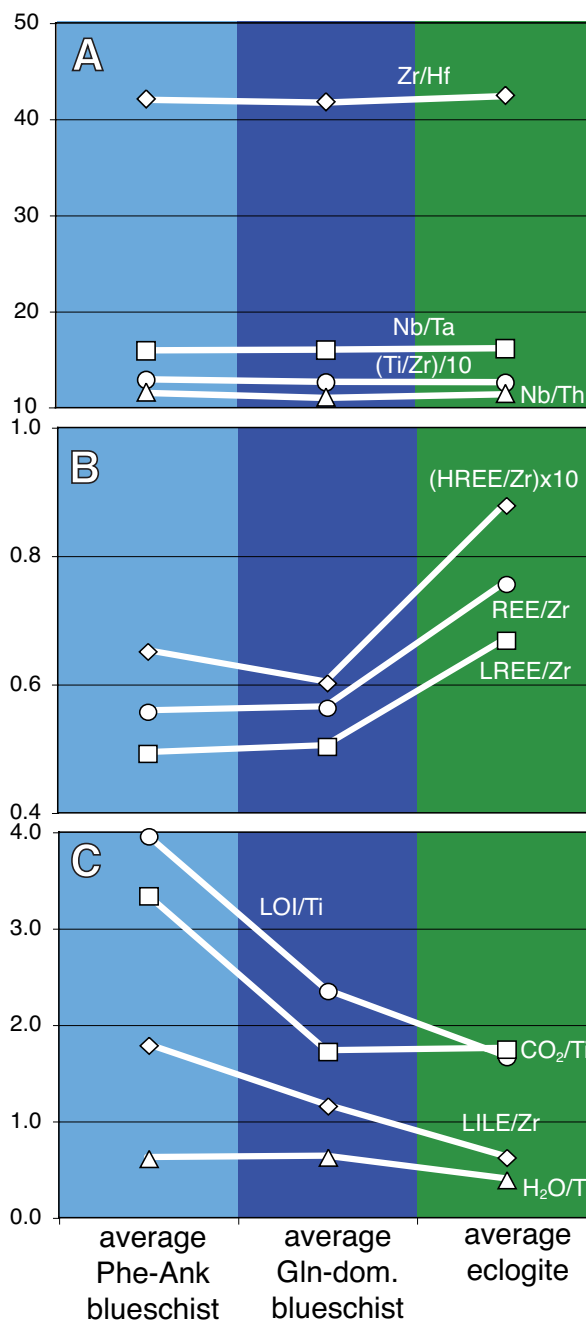


**Figure 2.12:** Various trace and volatile element ratios in eclogite domains compared to those ratios in adjoining glaucophane-dominated blueschist and phengite-ankerite blueschist domains. Differences in these ratios point to contrasting element mobilities during the retrograde eclogite-blueschist transformation due to fluid infiltration.

proof whether the change of element concentrations is a consequence of the mobility or

immobility of specific elements. It gives information about the mass and volume changes due to fluid-rock interaction and whether some pretended gain or loss of elements is actually controlled by overall mass gain or loss. The mass-balance calculation that follows below is based on the method described by [Ague \(2003\)](#). The calculation is based on the element concentration ratio  $r$  or  $r_{inv}$  of an immobile reference element group of the altered rock and the precursor rock:

$$r \equiv \frac{C_i'}{C_i^o} \text{ and } r_{inv} \equiv \frac{C_i^o}{C_i'}$$

where  $C_i'$  is the concentration of the immobile reference element  $i$  in the altered rock (superscript ') and in the precursor rock (superscript  $^o$ ). It is favourable to use more than one element to define the immobile reference frame ([Ague and van Haren, 1996](#); [Ague, 2003](#)). In this study the concentrations of HFSE and Th were chosen as the immobile reference because the ratios between HFSE (Zr/Hf, Nb/Ta, Ti/Zr, Nb/Th) did not change in the investigated samples (Figure 2.12A), although their concentrations are higher in both types of blueschist domains compared to the precursor eclogite. This increase of HFSE concentrations at constant ratios is explained by an overall mass loss, resulting in a relative enrichment of the HFSE. As Zr and Hf are dominantly incorporated in zircon, but Nb, Ta and Ti in rutile, a fractionation between the HFSE would occur if one of these two minerals became resorbed or grew newly. In fact, rutile is partially replaced by titanite but the Nb, Ta and Ti contents were locally redistributed. We discard the possibility of immobile behaviour of REE. The depletion of all REE in both blueschist domains is heterogeneous (Figure 2.12B) and the  $r_{inv}$  would be much below 1 indicating an overall mass gain of  $\sim 25\%$  and a calculated volume increase of  $\sim 30\%$ , implying also a  $\sim 40\%$  gain of the HFSE. This cannot be verified by petrographic observations, e.g. by new growth of zircon and titanite. LA-ICP-MS analyses show that clinozoisite and apatite are important trace element carrier as most of the REE are highly enriched in these minerals (Figure 2.6). There is a clear petrographic evidence that clinozoisite and apatite have been partially resorbed during the blueschist-facies overprint. This implies some loss of the REE if they are not redistributed into the newly grown blueschist minerals. However, according to the mineral chemical data and petrographic observations it is most likely that the REE were mobile and the HFSE immobile during the eclogite-blueschist transformation. Our observation of mobility of the REE is in accordance with data from other studies working on HP rocks ([John et al., 2004](#); [Gao et al., 2007](#); [Martin et al., 2007](#); [René, 2008](#); [Zack and John, 2007](#); [John et al., 2008](#)). On the other hand, at shallower, fore arc depths, the REE seem to be usually immobile ([Savov et al., 2007](#)). This contrasting behaviour of the REE may indicate that there is a mobility transition in the subduction zone, which is possibly dependent on temperature, pH, pressure or fluid composition. First we look at the element mobility in the glaucophane-dominated blueschist forming the  $\sim 2$  cm thick inner shell around the eclogite pillow. For the eclogite-GDB transformation  $r_{inv}$  is given by:

$$r_{inv} = \frac{C_{HFSE+Th}^{GDB}}{C_{HFSE+Th}^{Ec}} = 1.19$$

As this  $r_{inv}$  is 1.19 (i.e.  $>1$ ) an overall mass loss of 16% during the eclogite-GDB transformation is indicated (Figure 2.13). This means that 3–9% of the mass of Al, Fe, Na, Mn, CO<sub>2</sub> and Li were mobilised and removed from the system. All REE and Y were mobilised in significant amounts: about 25% of La–Gd and U, 32% of the Tb–Lu and even 40% of Y. 60–70% of Sr, Pb, P and Ca were lost. On the other hand, 16% Mg, 60% H<sub>2</sub>O and 80% LILE (Cs, Rb, Ba and K) were gained. For the eclogite-PAB transformation,  $r_{inv}$  is defined as:

$$r_{inv} = \frac{C_{HFSE+Th}^{PAB}}{C_{HFSE+Th}^{Ec}} = 1.08$$

The result of  $r_{inv} = 1.08$  points to an overall mass loss of 8%. This transformation shows higher gains in LILE (about 180%) than the eclogite-GDB transformation. H<sub>2</sub>O, Si, P, Sr, Pb, U and LREE were also efficiently mobilised. Approximately 25% of REE were released. 50 to 100% of Mn and CO<sub>2</sub> were gained. Mass changes in open systems are usually associated with volume changes, especially when rocks are in interaction with an external fluid (Ague and van Haren, 1996). The volume change  $\varepsilon_{\rho m}$  is given by:

$$\varepsilon_{\rho m} = \left( \frac{C_i^o}{C_i^i} \right) \left( \frac{\rho_g^o}{\rho_g^i} \right) - 1$$

in which  $\rho_g$  is the rock density (Ague, 2003). Calculated volume changes are about  $\varepsilon_{\rho m} = -6\%$  for the eclogite-PAB transformation and  $\varepsilon_{\rho m} = -13\%$  for eclogite-GDB transformation related to the decrease of the measured rock density from average 3.15 g/cm<sup>3</sup> in eclogite to 3.08 g/cm<sup>3</sup> in PAB and GDB. The overall mass and volume loss is higher in the GDB than in the PAB. This feature is related to different kinds of fluid infiltration and associated mineral reactions and will be discussed further on.

### 2.7.3 Mineral reactions and element mobility

Element mobility is dependent on metamorphic reactions and on the associated interaction with an infiltrating fluid. For this reason, trace element contents of minerals that are involved in reactions characterising the eclogite-blueschist transformation were analysed texturally controlled in thin sections (Table 2.1 and Table 2.2). The mineral chemical data will be correlated with the whole rock mass loss and the mobility of the specific elements as shown in Figure 2.13. First we will discuss the loss and mobility of some major elements, REE, Y, Sr, Pb, Ca, P, Na, Li and V correlated with the results of the bulk rock and the mineral chemistry (Table 2.1–2.3) and then we will discuss the gain of elements.

Phases with considerable amounts of REE and Y are clinozoisite, garnet and apatite in the samples. The Tb to Lu enriched garnet rim composition of eclogite was not found in garnet of the blueschist due to retrograde resorption. The amount of HREE and Y that were lost during the eclogite-blueschist transformation correlates well with the estimated amount of garnet that has been resorbed. The same is true for Ca, which becomes only partially incorporated, in the newly formed ankerite. Apatite has more or less flat chondrite-normalised REE patterns, with highest enrichments from La to Er. Apatite, the only phosphor-bearing phase, is nearly absent in the blueschist domains and its breakdown

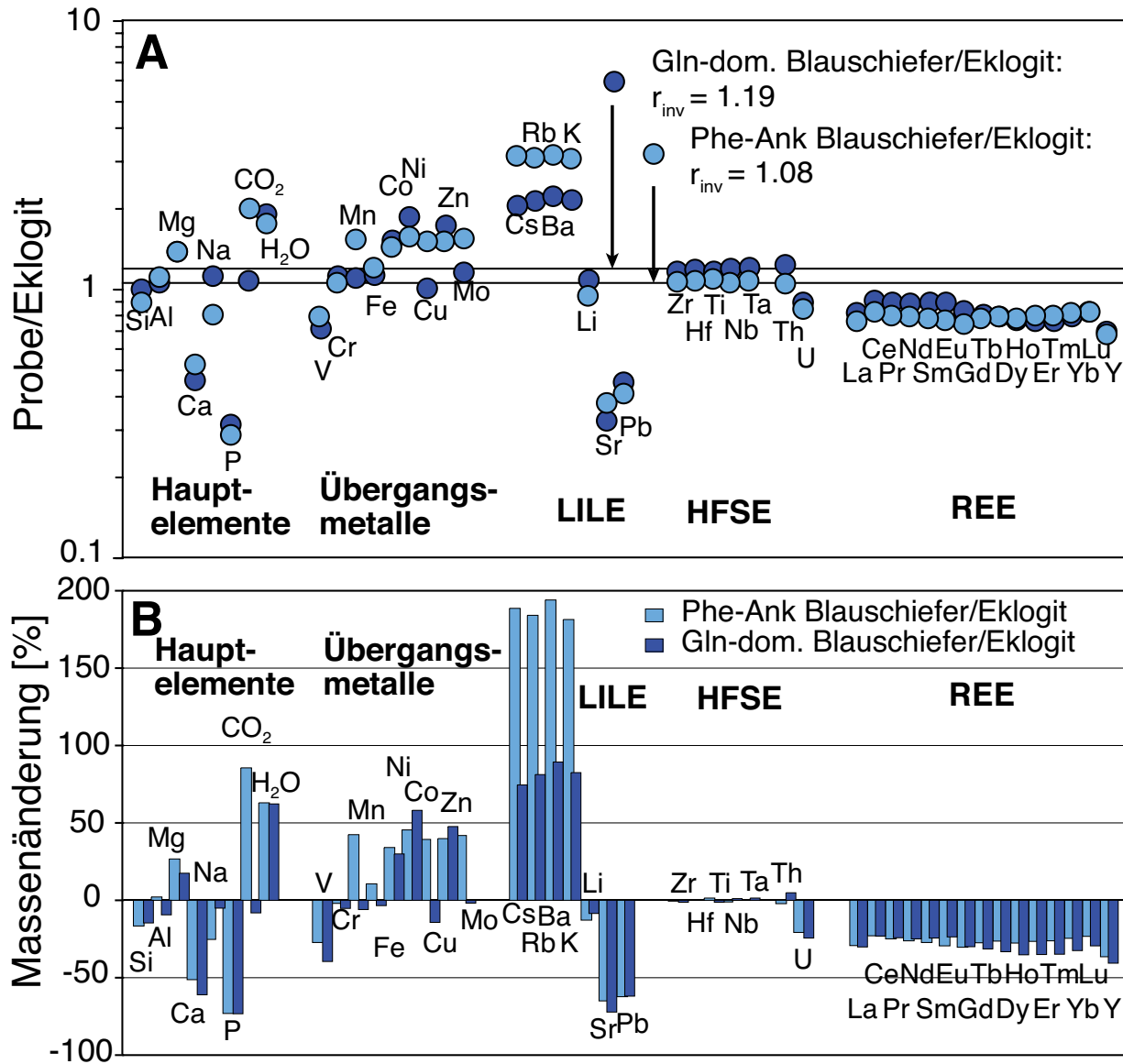


**Figure 2.13:** A: Major and trace element contents of average glaucophane-dominated blueschist and phengite-ankerite blueschist domains normalised to average eclogite composition demonstrating element mobility during the eclogite-blueschist transformation. For calculating  $r_{inv}$  after [Ague \(2003\)](#), the HFSE and Th have been assumed to be immobile. B: Gain and loss of elements during the eclogite-blueschist transformation given in percent of their contents in A.

may be responsible for the loss of 70% of phosphor. The loss of U and REE and of some Ca, Sr, Pb can also be associated with the breakdown of apatite. Up to 3000 ppm Sr were measured in a clinozoisite of an eclogite domain, which is higher than in any other phase. This is in agreement with the observation that clinozoisite is an important Sr carrier (Frei et al., 2004) and that up to 70% of the Sr of a whole rock can be attributed to epidote minerals of HP/ UHP metamorphic rocks (Enami et al., 2004). Chondrite-normalised REE patterns of clinozoisite have a decreasing slope from LREE towards the HREE (Figure 2.6C). Most of the mobility of LREE, Sr, Pb and Th seems to be associated with the resorption of clinozoisite, which is common in eclogite but absent in the phengite-ankerite blueschist (Figure 2.3). The loss of most LREE through the breakdown of clinozoisite and the loss of HREE mainly through the breakdown of garnet together with the general loss of all REE through resorption of apatite can explain the overall loss of ~30% of all REE during the formation of both types of blueschist domains. The incorporation of REE in newly formed minerals of the blueschist domains cannot be tracked by in-situ analyses and microscopical observations. Newly formed minerals are amphibole, ankerite, white mica and titanite. The latter is replacing rutile and could represent a possible HREE carrier. However, it shows only 10 times enrichment of REE compared to chondrite in the blueschist domain and has obviously not incorporated significant amounts of the mobilised REE.

An overall mobility of Li and V is evident from the mass-balance calculation. Li is mainly incorporated in omphacite (<130 ppm Li) and is partly lost due to the omphacite breakdown during retrogression. Sodic amphibole, phengite and titanite as newly formed minerals incorporate some of the mobilised Li (20–40 ppm). Vanadium is present in clinozoisite, omphacite, amphibole and phengite. Due to the formation of sodic amphibole and white mica at the expense of omphacite, most of the V is presumably redistributed into these newly formed minerals during the blueschist-facies transformation. However, a loss of calculated ~40% V presumably happened during the mobilisation of the V stored in dissolving clinozoisite, which disappeared during the blueschist transformation.

Besides these element losses, the blueschist domains gained some elements. Gain of CO<sub>2</sub> was apparently associated with the growth of ankerite, which allows the incorporation and possible gain of Mg, Fe and Mn. Co and Ni can be found in higher concentrations in sodic amphibole and in ankerite. The Cu content is high in ankerite and Zn is dominantly concentrated in sodic amphibole and also present in ankerite. All these transition metals occur in higher concentrations in the newly formed minerals than in their educt phases, which indicates that these elements were gained during the blueschist formation. Among the blueschist-facies minerals, phengite shows the highest concentrations of Ba, Rb and Cs, usual for white mica (Zack et al., 2001). In addition, phengite incorporates some amounts of Cr, Zn, B (<40 ppm) and Li (<40 ppm). The latter contents are in accordance to those in phengites (B ~35 ppm, Li ~80 ppm) from blueschist fragments exposed in the Izu-Bonin Mariana fore arc deriving from a depth of 20–40 km (Pabst et al., 2007).

The ankerite-apatite vein, crosscutting the relict eclogite in one drill-core, could represent the direct precipitation of some of the earlier dissolved elements. The vein is composed of ankerite incorporating Ca, Mg, Fe, Mn, CO<sub>2</sub> as major elements and V, Co, Ni, Zn, Sr and Pb as trace elements. Apatite is composed of P, Ca, REE and Y, some Mn, Sr, Pb and

Th. The elements incorporated in the newly formed apatite correspond to the elements that were lost and mobilised during the eclogite-blueschist transformation. The chondrite-normalised REE patterns (Figure 2.6F) of the vein apatite is slightly different from that of apatite in the eclogite domain (Figure 2.6E). The newly formed apatite has lower concentrations of the HREE, suggesting that the vein-forming fluid carried lower amounts of HREE or that the remaining HREE might have been removed from the system. However, the chemistry of the vein indicates that Mg, Fe, Mn, CO<sub>2</sub> and some transition metals (Co, Ni, Cu, Zn, Mo) were regular constituents of the fluid that infiltrated the eclogite and formed the ankerite-apatite vein; these elements were gained in both types of blueschists as well as in the ankerite-apatite vein. In addition, it indicates that some amounts of the REE were mobilised from the eclogites and were presumably precipitated directly in apatite in vein-like structures as the ankerite-apatite vein shows it. The REE would remain in solution until conditions are suitable for the precipitation of REE-carrying minerals, like apatite. Neither LILE (Rb, Ba, Cs, K, Li, B) nor HFSE could be found in the ankerite-apatite vein. The low HFSE contents in both ankerite and apatite of the vein indicate that these minerals did not incorporate large amounts of HFSE and that is in agreement with the assumption that the HFSE behaved immobile. The LILE could not be incorporated in the two phases of the ankerite-apatite vein and probably remained in the passing fluid.

#### 2.7.4 Characteristics of the infiltrating fluid

Fluids infiltrating the subduction channel may be enriched with elements and volatiles released by metamorphic dehydration reactions or partial melting of at least four different sources: 1) subducted sediments, 2) altered or unaltered subducted oceanic crust, 3) serpentinised parts of the upper mantle peridotite in the down going slab and 4) serpentinised mantle peridotite in the subduction channel. The incoming fluid is dominantly enriched in LILE, volatiles (Figure 2.11C) and transition metals. CO<sub>2</sub> release can be related to metamorphism of subducted carbonate-rich sediments, as limestones or other marine sediments, from organic material in the sediments, from carbonates in the altered mantle (Shaw et al., 2003; Gorman et al., 2006) or in the basaltic oceanic crust (Gao et al., 2007; John et al., 2008; Shaw et al., 2003).

During the eclogite-blueschist transformation in the Tian Shan, Cs, Rb, Ba and K behaved similarly and their concentrations increased at constant element ratios (Figure 2.14A). Increasing Ba and K<sub>2</sub>O contents and increasing Ba/Th ratios at constant low Th concentrations from the eclogite domain towards the phengite-ankerite blueschist are similar to trends found in island arc basalts interpreted to derive from a mantle wedge that has been enriched by aqueous fluids (Münker et al., 2004, Figure 2.14B). On the other hand, similar enrichments of Cs, Ba and K in the Kurile arc have been interpreted by Ryan et al. (1995) to result from mixing of hydrous fluids (Cs source) and sediment melts (Ba and K source). Possible LILE enrichment can be caused by the release of LILE from subducted sediments (Plank and Langmuir, 1993; Ryan et al., 1995; Domanik and Holloway, 1996), from subducted serpentinites (Scambelluri et al., 2001, 2004; Tenthorey and Hermann, 2004) or from subducted altered basaltic crust (Philipot, 1993; Ryan et al., 1995; Becker et al.,

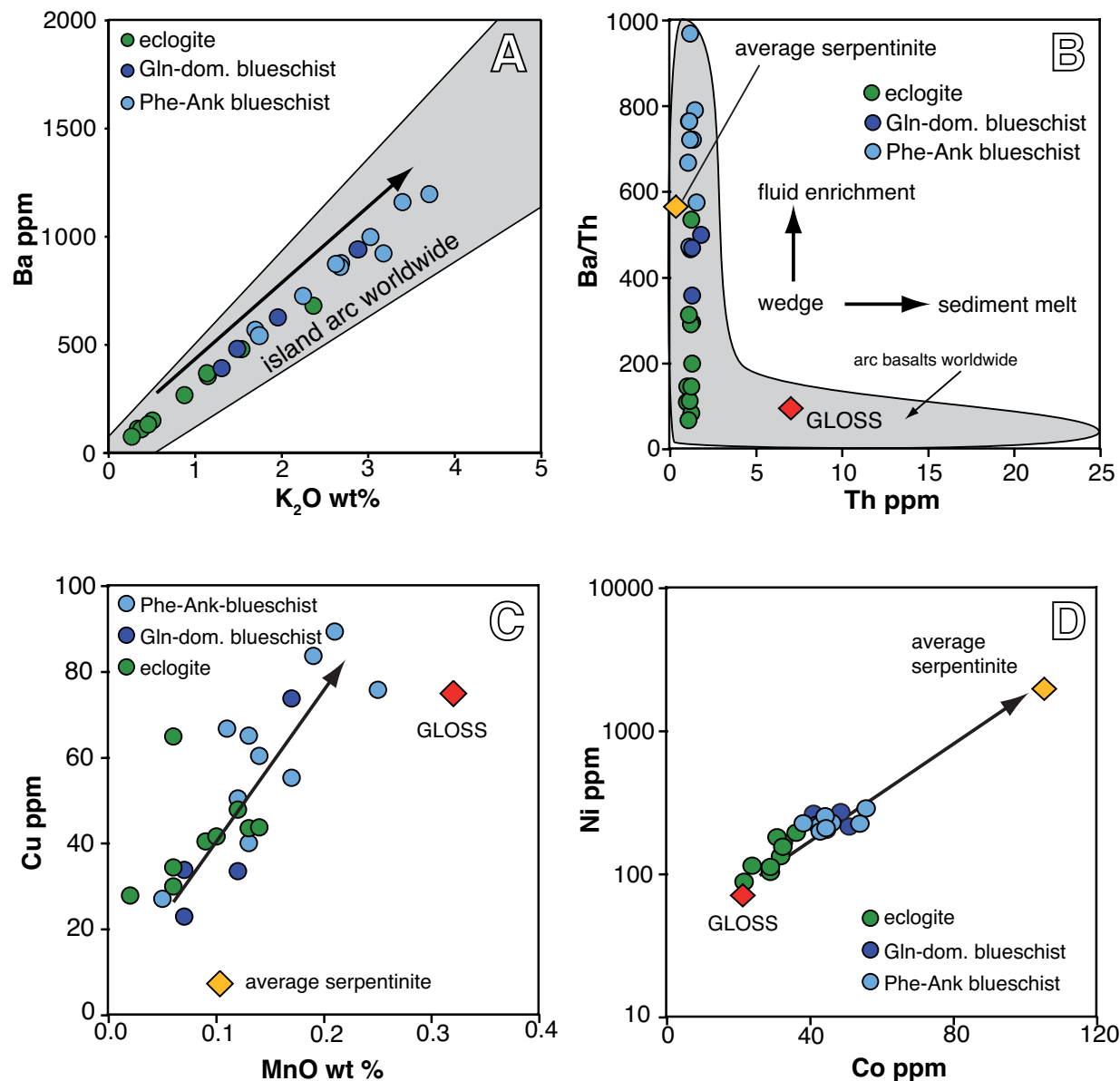


**Figure 2.14:** Trace element contents of relict eclogites and associated newly formed blueschists showing element mobility during the retrograde eclogite-blueschist transformation. A: Ba vs K<sub>2</sub>O enrichments in blueschists follows trend for island arc basalts worldwide (GEOROC, <http://georoc.mpch-mainz.gwdg.de>); B: Ba/Th ratio vs Th after (Münker et al., 2004), Ba increase in blueschists correlates with fluid induced Ba enrichments of island arc basalts at constant Ba/Th ratios; C: Cu and MnO enrichments can be explained by adding components derived from GLOSS (Plank and Langmuir, 1993) or altered oceanic crust (Kelemen et al., 2003); D: Ni and Co increase in blueschists compared to eclogite is explicable by adding a serpentinite component. Average serpentinite composition after Hattori and Guillot (2003); Savov et al. (2005); Paulick et al. (2006).



2000; John et al., 2004, 2008). In the case of fluid release from the partially serpentinised slab mantle it is conceivable that during the passing of the fluids through the oceanic crust and the above lying sediment layer, elements like LILE and CO<sub>2</sub> were leached and transported by the fluid into the mantle wedge (Malaspina et al., 2006; Zack and John, 2007). Becker et al. (2000) modelled, based on element flux calculations of N-MORB and altered oceanic crust of samples worldwide, that LILE are preferentially released from the altered or unaltered crust below 600°C except for U, Pb, Nd and Sr, which were released at temperatures above 600°C. John et al. (2008) show Sr, Nd and U mobility during prograde dehydration under eclogite-facies conditions below 600°C at 19–21 kbar. They assume a high concentration of LILE and Pb in the initial fluid composition. Gao et al. (2007) reported mobility of LILE and REE, among other elements, during a prograde dehydration that led to eclogite formation. Our investigations show clearly no gain of U, Pb, Nd and Sr during the retrograde eclogite-blueschist overprint. Instead these elements were mobilised and lost. This indicates that these elements were either simply not enriched in the fluid or if they were enriched, they were not incorporated into the newly formed minerals.

The higher Mn and Cu contents in blueschists compared to those in eclogites of the Tian Shan may indicate that the infiltrated fluids derived from subducted sediments (GLOSS in Figure 2.14C). The gain of Cr, Co and Ni in the blueschists shows a trend from eclogite composition towards the composition of serpentinite (Figure 2.14D). As serpentinite is the assumed transport matrix in subduction channels and partial mantle serpentinisation could also be present underneath the down going oceanic crust, enrichments of Co and Ni found in the blueschists of the Tian Shan suggests the interaction between serpentinite fluids and the eclogitic oceanic crust during uplift. In conclusion, the amounts of transition metals in the blueschist-facies fluid can be related to 1) a fluid release from subducted sediments and 2) from serpentinite either below the down going slab or directly from the eclogite-embedding serpentinite matrix in the subduction channel.

From the foregoing discussion on the chemical changes during the retrograde eclogite-blueschist transformation we develop the following scenario that is compatible with all observations: The fluids that interacted with the eclogite were dominantly related to fluid release from the hydrated and potentially serpentinised mantle peridotite below the subducting oceanic plate. This fluid infiltrated and penetrated the oceanic slab with its overlying marine sediments. This led to a strong leaching of transition metals and LILE, which were preferentially partitioned into the fluid. From whichever sources the fluid evolved, the element loss of Si, Al, Ca and Na, and the enrichment of Mg associated with the eclogite-blueschist transformation points to a composition of the infiltrated fluid that was in equilibrium with an ultramafic chemistry prior to infiltration into the eclogite-facies pillow lavas. These ultramafic rocks were presumably serpentinites or related rocks with low SiO<sub>2</sub> and high MgO contents like chlorite- or talc-rich schists, which likely represent the matrix in the subduction channel. These rocks imply a low load of the infiltrating fluid in many major and trace elements and strong chemical gradients between the fluid and the eclogite. To obtain equilibrium between the fluid and the eclogite, elements of the eclogite had to be mobilised.

### 2.7.5 Fluid infiltration & eclogite-blueschist transformation

According to the field observations the glaucophane-dominated blueschist domain forms a kind of reaction front between the relict eclogite and the phengite-ankerite blueschist domain. This reaction front is always about two cm thick (Figure 2.2A–D). Mass-balance calculations indicate an overall mass loss, implying also a volume loss during the eclogite-blueschist transformation. The volume loss is highest in the GDB and excludes pure rehydration reactions, which would lead to a volume increase. The mass loss indicates that the flux of elements out of the system was higher than the volume increase associated with a positive  $\Delta V$  of a hydration reaction. The reaction in progress and the volume loss created the permeability that enhanced the fluid infiltration into the interior of the eclogite pillow. The element flux had to be sufficiently high to guaranteed continuously open pathways for infiltrating fluids. Otherwise the pathways would have closed by swelling due to volume increasing reactions. The main fluid pathways presumably were developing along the former pillow boundaries. The infiltrating fluid was enriched in LILE, transition metals, but was also conditioned to the chemistry of the matrix serpentinite, which implies a low load with the major elements Si, Ca, Na and Al (Barnes et al., 2004). During uplift the eclogite reached P-T conditions where blue amphibole was stable, but rehydration reactions did not take place due to the absence of volatiles. When the fluid infiltration occurred it induced the formation of hydrous minerals and dissolved minerals that were not stable under the changed physical and chemical conditions. If the infiltrating fluids formed an interconnected system, element flux by diffusion within the fluid was possible. The outward flux of elements was driven by the chemical gradient between the composition of the incoming fluid along the pillow boundaries and the composition of the fluid at the reaction front, which always tried to reach equilibrium with the eclogite composition (Figure 2.15). However, the diffusion rate for elements leaving the system must have been more effective than the reaction rate controlling the formation of new minerals. This resulted in an overall volume loss, which provided space and triggered further fluid infiltration into the pillow. Infiltration of a fluid and the element diffusion within this fluid controlled the gain (LILE, transition metals) and loss (REE, Sr, Pb, U, Ca, Na, Si, P) of elements during metasomatism. High fluid-rock ratios allow for establishing a constant fluid composition (low element load) and fluid reservoir during the time of the fluid-infiltration. The element mobility (loss and gain) associated with the fluid-rock interaction during the eclogite-blueschist transformation, which resulted in the formation of two different concentric blueschist shells around eclogitic pillows is schematically summarised in Figure 2.15. Released Si, Al and Ca from eclogitic clinozoisite and garnet are partly consumed by newly formed silicates and carbonates in both blueschist domains or are lost from the system:  $\sim 15\%$  of the Si and  $\sim 50\%$  of the Ca were removed. Most of the Al is used to form phengite in the PAB but not in the GDB, which is poor in phengite. This results in a loss of  $10\%$  Al in the GDB compared to the eclogite. Na released due to the breakdown of omphacite is taken by the newly formed glaucophane, which is very abundant in the GDB ( $\sim 60$  Vol.%, Figure 2.3) but less abundant in the PAB with  $\sim 25$  Vol.% glaucophane. Low phosphor concentrations in the generally cation poor fluid might explain the dissolution of eclogitic

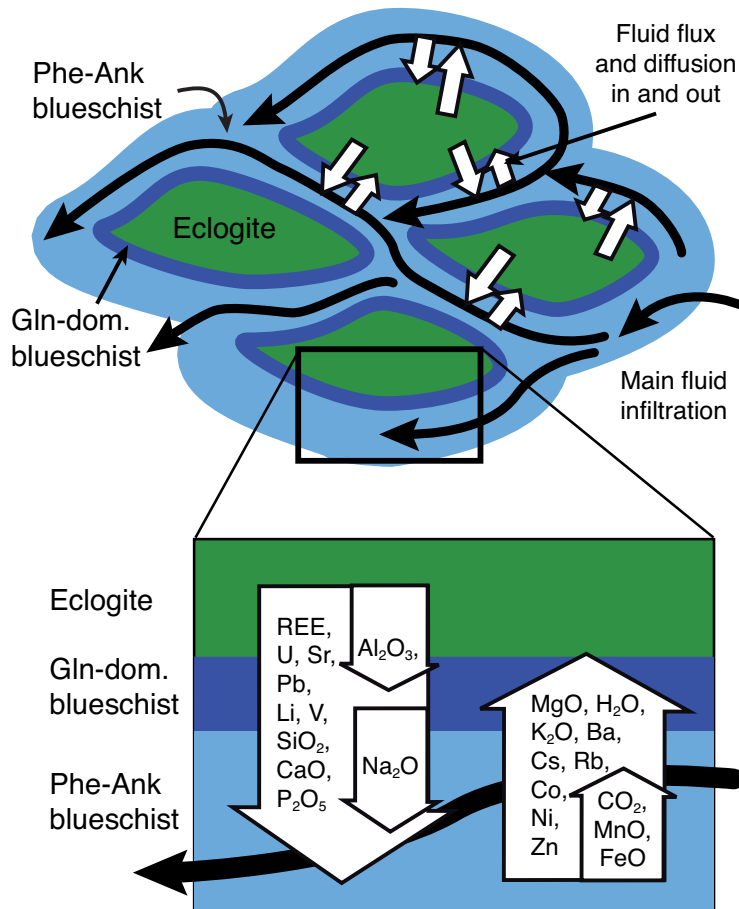


**Figure 2.15:** Schematic illustration of fluid infiltration into eclogitic pillow and the associated eclogite-blueschist transformation. Chemical changes were affiliated by the disequilibrium between the infiltrating fluid (low in SiO<sub>2</sub> and Na<sub>2</sub>O but high in MgO, CO<sub>2</sub> and LILE) compared to the composition of the eclogite. Loss of elements was higher than the gain resulted in overall volume loss, shrinkage and fluid flux into the eclogite. Fluid infiltration and element fluxes transformed the eclogite to phengite-ankerite blueschist (light grey) and a glaucophane-dominated blueschist as inner shell (dark grey). The transformation process and the chemical change terminated if diffusion pathways became too long. Final precipitation of newly formed blueschist-facies minerals inhibited further fluid infiltration and lead to the preservation of the eclogite (see Figure 2.2A–D, too). Element changes in detail correspond to the mass-balance calculation in Figure 2.13.

apatite and the loss of ~73% of the phosphor. In addition, the loss of ~30% of the REE, ~65% of the Sr, Pb and ~20% of the U can be explained by the resorption of apatite and clinzoisite that are the carrier of these elements. These elements were mobilised but not used for the formation of the newly formed minerals glaucophane, ankerite and phengite in the blueschist shells. The penetrating fluid removed them. Newly formed apatite in the ankerite-apatite vein represents a possible sink for REE, Sr, Pb, and U, as discussed before. The serpentinite-derived components (Mg, Ni, Co) and the sediment-derived components (Mn, Fe and Zn) were added to the system to form glaucophane and ankerite. Sediment-derived LILE (K, Ba, Cs, Rb) were incorporated in phengite, dominantly in the outer phengite-ankerite blueschist shell.

### 2.7.6 Influence of the eclogite-blueschist transformation on fluid-rock interaction in the subduction channel

The chemical processes associated with the retrograde eclogite-blueschist transformation illustrate that the composition and the reactivity of the infiltrating fluids in the hydrated mantle wedge above a subducting plate are most likely controlled by the interaction of metamorphic fluids with a lithological mixture of sediment, altered basaltic crust and

serpentinite. As we have shown, the infiltrating fluids are Si, Ca, Al and Na poor, but relatively Mg- and LILE-rich slab derived fluids with a flavour of transition metals. The subduction channel is that part of the subduction zone system where all lithologies of a subducting slab were mechanically mixed and combined with a matrix of partially serpentinised mantle peridotite. The latter derives from the mantle wedge above the slab. In such a reactive environment almost all elements can be mobilised. This demonstrates that for any subduction zone fluid and trace element budget, the material stored and trapped in the hydrated mantle wedge cannot be neglected. It represents a transient reservoir for fluids and elements that might contribute to the arc signature of fluid induced arc volcanism, if parts of the hydrated wedge would be dragged further down and dehydrate (McCulloch and Gamble, 1991; King et al., 2007). The hydrated mantle wedge provides high element and fluid contents not only in mélangé zones formed in shallower depths (e.g. King et al., 2003) but is also important at deeper levels, namely where the blueschist-eclogite transition occurs. High element mobility due to metamorphic processes do not only occur in the oceanic crust of the descending slab but also during ascent and retrograde rehydration of deeply subducted dry rocks, as shown in this study. The subduction channel represents therefore an important environment rich in fluids, which allows the mobilisation, transportation and even the storage of major and trace elements.

## 2.8 Summary and conclusion

Pillow-lava basalts with a chemical affinity to ocean-island basalts, assumed to represent the protholiths of the eclogites of the Tian Shan, were subducted with a down going oceanic slab to eclogite-facies conditions. The release of fluids from the slab into the overlying mantle wedge or subduction channel caused an interaction of highly reactive fluids with ascending eclogite bodies. The eclogites were metamorphically and metasomatically overprinted under blueschist-facies conditions. Indicative for this overprint is the growth of glaucophane, ankerite and the LILE-incorporation into newly formed phengite of the blueschists. REE, Y, Sr, Pb, U and P were mobilised and removed due to the breakdown of garnet and omphacite during the eclogite-blueschist transformation. Parts of the mobilised elements were most likely instantaneously precipitated in apatite or apatite-ankerite bearing fluid-veins crosscutting relict eclogite domains. Transition metals were incorporated in vein-ankerite as they were ubiquitous components of the fluid.

### Conclusions:

1. Mass-balance calculations point to an overall mass and volume loss during the retrograde eclogite-blueschist transformation, although the  $\Delta V$  of hydration reactions suggests a volume increase during the transformation. Enhanced fluid infiltration and associated metasomatism of the eclogite pillows was characterized by element loss that was more effective than the competitive precipitation of elements in newly formed minerals.

2. Element mobility due to mass-transfer during the fluid-rock interaction points to the likely source of the fluid, suggesting that it was in equilibrium with serpentinite and had a low element load of Si, Ca, Al and Na, but a relatively high Mg content. When passing the subducted altered basaltic crust and the overlying metasediments this fluid was able to liberate fluid mobile elements present in large amounts in the infiltrated rocks.
3. The subduction channel contains a mixture of fluids and lithologies deriving from the subducted sediments, the altered or unaltered basaltic crust and the partially serpentinised peridotite. Rehydration reactions taking place in the subduction channel induce high element mobility.
4. The LILE enrichment found in the newly formed blueschists is similar to that of island arc volcanic rocks for which wedge melting due to fluid influx is generally accepted. The trace element enrichments of subduction channel rocks may thus represent an additional source for element enrichments characterising arc volcanism.

## 2.9 Acknowledgement

This publication is contribution no. 133 of the Sonderforschungsbereich 574 Volatiles and Fluids in Subduction Zones at the University of Kiel, supported by the Deutsche Forschungsgemeinschaft. Financial support by the state Key Project for Basic Research of China (2001CB409803), the Funds for Hundred Outstanding Talents Plan of the Chinese Academy of Sciences is gratefully acknowledged. C.-D. Garbe-Schönberg is thanked for useful interpretations of the geochemical data and for assistance at the ICP-OES and during laboratory work. We thank P. Appel, B. Mader, for outstanding help at the microprobe, U. Westernströer, P. Fiedler, K. Kiesling, K. Bremer, A. Weinkauff, C. Kusebauch, A. Fehler and H. Brätz (Würzburg) for assistance during lab work. The petrologists at Kiel University and Bjørn Jamtveit at PGP in Oslo are thanked for useful discussions. We also thank R. Halama for proof-reading and R. Klemd is thanked for offering the opportunity for fieldwork in Tian Shan. We thank the reviewers for their constructive contributions and we thank R. L. Rudnick for editorial handling.

## References

- Ague, J. J., 2003. Fluid infiltration and transport of major, minor, and trace elements during regional metamorphism of carbonate rocks, Wepawaug Schist, Connecticut, USA. *American Journal of Science* 303, 753–816.
- Ague, J. J., van Haren, J. L. M., 1996. Assessing metasomatic mass and volume changes using the bootstrap, with application to deep crustal hydrothermal alteration of marble. *Economic Geology and the Bulletin of the society of economic geologists* 91 (7), 1169–1182.
- Alt, J. C., Teagle, D. A. H., 1999. The uptake of carbon during alteration of ocean crust. *Geochimica Et Cosmochimica Acta* 63 (10), 1527–1535.
- Alt, J. C., Teagle, D. A. H., 2003. Hydrothermal alteration of upper oceanic crust formed at a fast-spreading ridge: mineral, chemical, and isotopic evidence from ODP Site 801. *Chemical Geology* 201 (3-4), 191–211.
- Armbruster, T., Bonazzi, P., Akasaka, M., Bermanec, V., Chopin, C., Giere, R., Heuss, A. S., Liebscher, A., Menchetti, S., Pan, Y., Pasero, M., 2006. Recommended nomenclature of epidote-group minerals. *European Journal of Mineralogy* 18 (5), 551–567.
- Barnes, J. D., Selverstone, J., Sharp, Z. D., 2004. Interactions between serpentinite devolatilization, metasomatism and strike-slip strain localization during deep-crustal shearing in the Eastern Alps. *Journal of Metamorphic Geology* 22 (4), 283–300.
- Bebout, G. E., 2007. Metamorphic chemical geodynamics of subduction zones. *Earth and Planetary Science Letters* 260 (3-4), 373–393.
- Bebout, G. E., Barton, M. D., 2002. Tectonic and metasomatic mixing in a high-T, subduction-zone melange; insights into the geochemical evolution of the slab-mantle interface. *Chemical Geology* 187 (1-2), 79–106.
- Becker, H., Jochum, K. P., Carlson, R. W., 2000. Trace element fractionation during dehydration of eclogites from high-pressure terranes and the implications for element fluxes in subduction zones. *Chemical Geology* 163 (1-4), 65–99.
- Bednarz, U., Schmincke, H. U., 1989. Mass-Transfer during Sub-Seafloor Alteration of the Upper Troodos Crust (Cyprus). *Contributions to Mineralogy and Petrology* 102 (1), 93–101.
- Boynnton, W. V., 1984. Cosmochemistry of the rare earth elements; meteorite studies. In: Henderson, P. (Ed.), *Rare earth element geochemistry*. Vol. 2. Elsevier Sci Publ, Amsterdam, Netherlands, pp. 63–114.
- Bykadorov, V. A., Bush, V. A., Fedorenko, O. A., Filippova, I. B., Miltenko, N. V., Puchkov, V. N., Smirnov, A. V., Uzhkenov, B. S., Volozh, Y. A., 2003. Ordovician-Permian palaeogeography of Central Eurasia: Development of Paleozoic petroleum-bearing basins. *Journal of Petroleum Geology* 26 (3), 325–350.
- Cloos, M., Shreve, R. L., 1988. Subduction-channel model of prism accretion, melange formation, sediment subduction, and subduction erosion at convergent plate margins; Part II, Implications and discussion. *Pure and Applied Geophysics* 128 (3-4), 501–545.
- Connolly, J. A. D., 1990. Multivariable phase diagrams; an algorithm based on generalized thermodynamics. *American Journal of Science* 290 (6), 666–718.
- Deer, W. A., Howie, R. A., Zussman, J., 1992. *An introduction to the rock-forming minerals*. 2 ed. Longman Scientific Technical, Harlow, United Kingdom.
- Deyhle, A., Kopf, A., Pawlig, S., 2004. Cross-section through the frontal Japan Trench subduction zone; geochemical evidence for fluid flow and fluid-rock interaction from DSDP and ODP pore waters and sediments. In: *Ocean Drilling Program Leg 186; advanced results*. Vol. 13; 1. Blackwell Scientific Publications, Victoria, Australia, pp. 271–288.
- Domanik, K. J., Holloway, J. R., 1996. The stability and composition of phengitic muscovite and associated phases from 5.5 to 11 GPa; implications for deeply subducted sediments. *Geochimica et Cosmochimica Acta* 60 (21), 4133–4150.
- Ellis, D. J., Green, D. H., 1979. An experimental study of the effect of Ca upon garnet-clinopyroxene Fe-Mg exchange equilibria. *Contributions to Mineralogy and Petrology* 71 (1), 13–22.
- Enami, M., Liou, J. G., Mattinson, C. G., 2004. Epidote minerals in high P/ T metamorphic terranes; subduction zone and high- to ultrahigh-pressure metamorphism. In: Liebscher, A. (Ed.), *Epidotes*. Vol. 56. Mineralogical Society of America and Geochemical Society, Washington, DC, United States, pp. 347–398.
- Evans, B. W., 1990. Phase relations of epidote-blueschists. *Lithos* 25 (1-3), 3–23.
- Fisher, D. M., 1996. Fabrics and veins in the forearc; a record of cyclic fluid flow at depths of <15 km. In: *Subduction top to bottom*. Vol. 96;. American Geophysical Union, Washington, DC, United States, pp. 75–89.
- Flanagan, F. J., 1976. Description and analyses of eight new USGS rock standards. *USGS Professional Paper* 840, 1–192.
- Frei, D., Liebscher, A., Franz, G., Dulski, P., 2004. Trace element geochemistry of epidote minerals. In: *Epidotes*. Vol. 56;. Mineralogical Society of America and Geochemical Society, Washington, DC, United States, pp. 553–605.
- Fry, N., Fyfe, W., 1971. On the significance of the eclogite facies in alpine metamorphism. *Verhandlungen der geologischen Bundesanstalt, Wien (Vienna)* 2, 257–265.
- Gao, J., He, G., Li, M., Xiao, X., Tang, Y., Wang, J., Zhao, M., 1995. The mineralogy, petrology, metamorphic PTDt trajectory and exhumation mechanism of blueschists, South Tianshan, northwestern China. *Tectonophysics* 250 (1-3), 151–168.

- Gao, J., John, T., Klemd, R., Xiong, X., 2007. Mobilization of Ti-Nb-Ta during subduction: evidence from rutile-bearing dehydration segregations and veins hosted in eclogite, Tianshan, NW China. *Geochimica et Cosmochimica Acta* 71, 4974–4996.
- Gao, J., Klemd, R., 2001. Primary fluids entrapped at blueschist to eclogite transition; evidence from the Tianshan meta-subduction complex in northwestern China. *Contributions to mineralogy and petrology* 142 (1), 1–14.
- Gao, J., Klemd, R., 2003. Formation of HP-LT rocks and their tectonic implications in the western Tianshan Orogen, NW China; geochemical and age constraints. *Lithos* 66 (1-2), 1–22.
- Gao, J., Klemd, R., Zhang, L., Wang, Z., Xiao, X., 1999. P-T path of high-pressure/ low-temperature rocks and tectonic implications in the western Tianshan Mountains, NW China. *Journal of Metamorphic Geology* 17 (6), 621–636.
- Gao, J., Li, M., Xiao, X., Tang, Y., He, G., 1998. Paleozoic tectonic evolution of the Tianshan Orogen, northwestern China. *Tectonophysics* 287 (1-4), 213–231.
- Garbe-Schönberg, C. D., 1993. Simultaneous determination of thirty-seven trace elements in twenty-eight international rock standards by ICP-MS. *Geostandards Newsletter* 17 (1), 81–97.
- Gerya, T. V., Stöckhert, B., Perchuk, A. L., 2002. Exhumation of high-pressure metamorphic rocks in a subduction channel; a numerical simulation. *Tectonics* 21 (6), 1056, doi:10.1029/2002TC001406.
- Gorman, P. J., Kerrick, D. M., Connolly, J. A. D., 2006. Modeling open system metamorphic decarbonation of subducting slabs. *Geochemistry, Geophysics, Geosystems* (G3) 7 (4), 1–21.
- Hacker, B. R., Abers, G. A., Peacock, S. M., 2003. Subduction factory; 1, Theoretical mineralogy, densities, seismic wave speeds, and H<sub>2</sub>O contents. *Journal of Geophysical Research, B, Solid Earth and Planets* 2029 (doi:10.1029/2001JB001127).
- Hart, S. R., Blusztajn, J., Dick, H. J. B., Meyer, P. S., Muehlenbachs, K., 1999. The fingerprint of seawater circulation in a 500-meter section of ocean crust gabbros. *Geochimica et Cosmochimica Acta* 63 (4), 4059–4080.
- Hastie, A. R., Kerr, A. C., Pearce, J. A., Mitchell, S. F., 2007. Classification of altered volcanic island arc rocks using immobile trace elements: Development of the Th-Co discrimination diagram. *Journal of Petrology* 48 (12), 2341–2357.
- Hattori, K. H., Guillot, S., 2003. Volcanic fronts form as a consequence of serpentinite dehydration in the forearc mantle wedge. *Geology (Boulder)* 31 (6), 525–528.
- Holland, T. J. B., 1979. Experimental determination of the reaction paragonite = jadeite + kyanite + H<sub>2</sub>O and internally consistent thermodynamic data for part of the system Na<sub>2</sub>O-Al<sub>2</sub>O<sub>3</sub>-SiO<sub>2</sub>-H<sub>2</sub>O, with applications to eclogites and blueschists. *Contributions to Mineralogy and Petrology* 68 (3), 293–301.
- Hyndman, R. D., Peacock, S. M., 2003. Serpentinization of the forearc mantle. *Earth and Planetary Science Letters* 212 (3-4), 417–432.
- Jochum, K. P., Nohl, U., Herwig, K., Lammel, E., Stoll, B., Hofmann, A. W., 2005. GeoReM: A new geochemical database for reference materials and isotopic standards. *Geostandards and Geoanalytical Research* 29 (3), 333–338.
- John, T., Klemd, R., Gao, J., Garbe-Schönberg, C.-D., 2008. Trace-element mobilization in slabs due to non steady-state fluid-rock interaction: constraints from an eclogite-facies transport vein in blueschist (Tianshan, China). *Lithos* 103 (1-2), 1–24.
- John, T., Scherer, E. E., Haase, K., Schenk, V., 2004. Trace elements fractionation during fluid-induced eclogitization in a subducting slab: trace element and Lu-Hf-Sm-Nd isotope systematics. *Earth and Planetary Science Letters* 227, 441–456.
- Kelemen, P. B., Hanghøj, K., Greene, A. R., 2003. One view of the geochemistry of subduction-related magmatic arcs, with an emphasis on primitive andesite and lower crust. In: Rudnick, R. L. (Ed.), *The Crust*. Vol. 3 of *Treatise on Geochemistry*. Elsevier-Pergamon, Oxford, pp. 593–659.
- King, R. L., Bebout, G. E., Grove, M., Moriguti, T., Nakamura, E., 2007. Boron and lead isotope signatures of subduction-zone melange formation: Hybridization and fractionation along the slab-mantle interface beneath volcanic arcs. *Chemical Geology* 239 (3-4), 305–322.
- King, R. L., Bebout, G. E., Moriguti, T., Nakamura, E., 2006. Elemental mixing systematics and Sr-Nd isotope geochemistry of melange formation: Obstacles to identification of fluid sources to arc volcanics. *Earth and Planetary Science Letters* 246, 288–304.
- King, R. L., Kohn, M. J., Eiler, J. M., 2003. Constraints on the petrologic structure of the subduction zone slab-mantle interface from Franciscan Complex exotic ultramafic blocks. *Geological Society of America Bulletin* 115 (9), 1097–1109.
- Klemd, R., 2003. Ultrahigh-pressure metamorphism in eclogites from the western Tianshan high-pressure belt (Xinjiang, western China); comment. *American Mineralogist* 88 (7), 1153–1156.
- Klemd, R., Bröcker, M., Hacker, B. R., Gao, J., Gans, P., Wemmer, K., 2005. New Age Constraints on the Metamorphic Evolution of the High-Pressure/Low-Temperature Belt in the Western Tianshan Mountains, NW China. *Journal of Geology* 113, 157–168.

- Klemd, R., Schröter, F. C., Will, T. M., Gao, J., 2002. P-T evolution of glaucophane-omphacite bearing HP-LT rocks in the western Tianshan Orogen, NW China; new evidence for "Alpine-type" tectonics. *Journal of Metamorphic Geology* 20 (2), 239–254.
- Leake, B. E., Wooley, A. R., Arps, C. E. S., Birch, W. D., Gilbert, M. C., Grice, J. D., Hawthorne, F. C., Kato, A., Kisch, H. J., Krivovichev, V. G., Linthout, K., Laird, J., Mandarino, J., Maresch, W. V., Nickel, E. H., Rock, N. M. S., Schumacher, J. C., Smith, D. C., Stephenson, N. C. N., Ungaretti, L., Whittaker, E. J. W., Youzhi, G., 1997. Nomenclature of amphiboles; report of the Subcommittee on Amphiboles of the International Mineralogical Association Commission on New Minerals and Mineral Names. *European Journal of Mineralogy* 9 (3), 623–651.
- Liou, J. G., Graham, S. A., Maruyama, S., Wang, X., Xiao, X., Carroll, A. R., Chu, J., Feng, Y., Hendrix, M. S., Liang, Y. H., McKnight, C. L., Tang, Y., Wang, Z. X., Zhao, M., Zhu, B., 1989. Proterozoic blueschist belt in western China; best documented Precambrian blueschists in the world. *Geology (Boulder)* 17 (12), 1127–1131.
- Malaspina, N., Hermann, J., Scambelluri, M., Compagnoni, R., 2006. Multistage metasomatism in ultrahigh-pressure mafic rocks from the North Dabie Complex (China). *Lithos* 90, 19–42.
- Martin, C., Duchene, S., Luais, B., Deloule, E., 2007. REE and HFSE mobility from eclogite to amphibolite metamorphism (Vardalsneset, Norwegian Caledonides). *Geochimica Et Cosmochimica Acta* 71 (15), A626–A626.
- McCulloch, M. T., Gamble, A. J., 1991. Geochemical and geodynamical constraints on subduction zone magmatism. *Earth and Planetary Science Letters* 102 (3-4), 358–374.
- Morimoto, N., 1988. Nomenclature of pyroxenes; Subcommittee on Pyroxenes, Commission on New Minerals and Mineral Names (CNMMN), International Mineral Association (IMA). *Schweizerische Mineralogische und Petrographische Mitteilungen = Bulletin Suisse de Mineralogie et Petrographie* 68 (1), 95–111.
- Münker, C., Wörner, G., Yogodzinski, G., Churikova, T., 2004. Behaviour of high-field-strength elements in subduction zones; constraints from Kamchatka-Aleutian Arc lavas. *Earth and Planetary Science Letters* 224 (3-4), 275–293.
- Naumann, T., Geist, D., Kurz, M. D., 2002. Petrology and geochemistry of volcan Cerro Azul: Petrological diversity among the western Galapagos volcanoes. *Journal of Petrology* 43, 859–883.
- Norin, E., 1941. Geological reconnaissances in the chinese Tien-Shan; Reports from the Scientific Expedition to the North-Western Provinces of China under the leadership of Dr. Sven Hedin. Vol. 6 of III. *Geology, Stockholm*.
- Okrusch, M., Seidel, E., Davis, E. N., 1978. The assemblage jadeite - quartz in the glaucophane rocks of Sifnos (Cyclades Archipelago, Greece). *Neues Jahrbuch fuer Mineralogie Abhandlungen*. 132 (3), 284–308.
- Pabst, S., Zack, T., Savov, I. P., Rost, D., Vicenzi, E. P., 2007. In situ geochemical data from metamorphic rocks in the active Mariana subduction zone. *Geochimica Et Cosmochimica Acta* 71 (15), A746–A746.
- Paulick, H., Bach, W., Godard, M., de, H. J. C. M., Suhr, G., Harvey, J., 2006. Geochemistry of abyssal peridotites (Mid-Atlantic Ridge, 15 degrees 20'N, ODP Leg 209); implications for fluid-rock interaction in slow spreading environments. *Chemical Geology* 234 (3-4), 179–210.
- Peacock, S. M., 1993. The importance of blueschist to eclogite dehydration reactions in subducting oceanic crust. *Geological Society of America Bulletin* 105 (5), 684–694.
- Peacock, S. M., 1996. Thermal and petrologic structure of subduction zones. In: *Subduction top to bottom*. Vol. 96;. American Geophysical Union, Washington, DC, United States, pp. 119–133.
- Pearce, N. J. G., Perkins, W. T., Westgate, J. A., Gorton, M. P., Jackson, S. E., Neal, C. R., Chenery, S. P., 1997. A compilation of new and published major and trace element data for NIST SRM 610 and NIST SRM 612 glass reference materials. *Geostandards Newsletter-the Journal of Geostandards and Geoanalysis* 21 (1), 115–144.
- Pfänder, J. A., Münker, C., Stracke, A., Mezger, K., 2007. Nb/ Ta and Zr/ Hf in ocean island basalts; implications for crust-mantle differentiation and the fate of niobium. *Earth and Planetary Science Letters* 254 (1-2), 158–172.
- Philippot, P., 1993. Fluid-melt-rock interaction in mafic eclogites and coesite-bearing metasediments; constraints on volatile recycling during subduction. *Chemical Geology* 108 (1-4), 93–112.
- Plank, T., Langmuir, C. H., 1993. Tracing trace elements from sediment input to volcanic output at subduction zones. *Nature (London)* 362 (6422), 739–743.
- Potts, P. J., Holbrook, J. R., 1987. Alisa Craig - The history of a reference material. *Geostandards Newsletter* 11, 257–260.
- Powell, R., 1985. Regression diagnostics and robust regression in geothermometer/ geobarometer calibration; the garnet-clinopyroxene geothermometer revisited. *Journal of Metamorphic Geology* 3 (3), 231–243.
- René, M., 2008. Anomalous rare earth element, yttrium and zirconium mobility associated with uranium mineralization. *Terra Nova* 20, 52–58.
- Rüpke, L. H., Phipps, M. J., Hort, M., Connolly, J. A. D., 2002. Are the regional variations in Central American arc lavas due to differing basaltic versus peridotitic slab sources of fluids? *Geology (Boulder)* 30 (11), 1035–1038.
- Rüpke, L. H., Phipps, M. J., Hort, M., Connolly, J. A. D., 2004. Serpentine and the subduction zone water cycle. *Earth and Planetary Science Letters* 223 (1-2), 17–34.



- Ryan, J. G., Morris, J., Tera, F., Leeman, W. P., Tsvetkov, A., 1995. Cross-Arc Geochemical Variations in the Kurile Arc as a Function of Slab Depth. *Science* 270 (5236), 625–627.
- Savov, I. P., Ryan, J. G., D, A. M., Kelley, K., Mattie, P., 2005. Geochemistry of serpentinized peridotites from the Mariana forearc Conical Seamount, ODP Leg 125; implications for the elemental recycling at subduction zones. *Geochemistry, Geophysics, Geosystems* (G3) 6 (4), doi:10.1029/2004GC000777.
- Savov, I. P., Ryan, J. G., D'Antonio, M., Fryer, P., 2007. Shallow slab fluid release across and along the Mariana arc-basin system: Insights from geochemistry of serpentinized peridotites from the Mariana fore arc. *Journal of Geophysical Research-Solid Earth* 112 (B9), doi:10.1029/2006JB004749.
- Scambelluri, M., Bottazzi, P., Trommsdorff, V., Vannucci, R., Hermann, J., Gomez, P. M. T., Lopez, S. V. V., 2001. Incompatible element-rich fluids released by antigorite breakdown in deeply subducted mantle. *Earth and Planetary Science Letters* 192 (3), 457–470.
- Scambelluri, M., Fiebig, J., Malaspina, N., Muentener, O., Pettke, T., 2004. Serpentine subduction; implications for fluid processes and trace-element recycling. *International Geology Review* 46 (7), 595–613.
- Schmidt, M. W., Poli, S., 1998. Experimentally based water budgets for dehydrating slabs and consequences for arc magma generation. *Earth and Planetary Science Letters* 163 (1-4), 361–379.
- Sengör, A. M. C., Natal'In, B. A., 1996. Paleotectonics of Asia: fragments of a synthesis. In: Yin, A., Harrison, M. (Eds.), *The Tectonic Evolution of Asia*. World and Regional Geology Series. Cambridge University Press, Cambridge, New York, Melbourne, pp. 486–640.
- Shaw, A. M., Hilton, D. R., Fischer, T. P., Walker, J. A., Alvarado, G. E., 2003. Contrasting He-C relationships in Nicaragua and Costa Rica; insights into C cycling through subduction zones. *Earth and Planetary Science Letters* 214 (3-4), 499–513.
- Sobolev, N. V., Dobretsov, N. L., Bakirov, A. B., Shatsky, V. S., 1986. Eclogites from various types of metamorphic complexes in the USSR and the problems of their origin. In: Evans, B., Brown, E. (Eds.), *Blueschists and eclogites*. Vol. 164;. Geological Society of America (GSA), Boulder, CO, United States, pp. 349–363.
- Staudigel, H., 2003. Hydrothermal alteration processes in the oceanic crust. In: Rudnick, R. L. (Ed.), *The Crust*. Vol. 3 of *Treatise on Geochemistry*. Elsevier-Pergamon, Oxford, pp. 511–536.
- Staudigel, H., Plank, T., White, W. M., Schmincke, H. U., 1996. Geochemical fluxes during seafloor alteration of the upper crust: DSDP sites 417 and 418. In: Bebout, G. E., Kirby, S. H. (Eds.), *Subduction from Top to Bottom*. Vol. 96. American Geophysical Union, Washington, DC, pp. 19–38.
- Tenthorey, E., Hermann, J., 2004. Composition of fluids during serpentine breakdown in subduction zones; evidence for limited boron mobility. *Geology (Boulder)* 32 (10), 865–868.
- Terashima, S., Ando, A., Okai, T., Kanai, Y., Taniguchi, M., Takizawa, F., Itho, S., 1990. Elemental concentrations in nine new GSJ rock reference samples "sedimentary rock series". *Geostandards Newsletter* 14, 1–5.
- Ufimtsev, G. F., 1990. The recent central Asian orogenic belt. *Zeitschrift fuer Geomorphologie* 34 (2), 199–211.
- Waters, D. J., Martin, H. N., 1993. Geobarometry in phengite-bearing eclogites. Seventh meeting of the European Union of Geosciences; abstract supplement 5 (1), 410–411.
- Watson, E. B., Wark, D. A., Thomas, J. B., 2006. Crystallization thermometers for zircon and rutile. *Contributions to Mineralogy and Petrology* 151 (4), 413–433.
- Wilson, S., 1997. Data compilation for USGS reference material BHVO-2, Hawaiian Basalt. U.S. Geological Survey Open-File Report X, xxx.
- Zack, T., John, T., 2007. An evaluation of reactive fluid flow and trace-element mobility in subducting slabs. *Chemical Geology* 239, 199–216.
- Zack, T., Rivers, T., Foley, S. F., 2001. Cs-Rb-Ba systematics in phengite and amphibole; an assessment of fluid mobility at 2.0 GPa in eclogites from Trescolmen, Central Alps. *Contributions to Mineralogy and Petrology* 140 (6), 651–669.
- Zhang, L., Ellis, D. J., Williams, S., Jiang, W., 2003. Ultrahigh-pressure metamorphism in eclogites from the western Tianshan, China - Reply. *American Mineralogist* 88 (7), 1157–1160.



# Chapter 3

## FLUID-INDUCED CHEMICAL AND PETROPHYSICAL CHANGES ASSOCIATED WITH THE RETROGRADE ECLOGITE-BLUESCHIST TRANSFORMATION: CONSTRAINTS FOR METASOMATISM AND EXHUMATION PROCESSES WITHIN A SUBDUCTION CHANNEL

### 3.1 Abstract

Eclogites from Sifnos (Greece) and the Chinese Tian Shan showing a blueschist-facies overprint induced by infiltrating fluids were investigated to decipher their petrophysical, geochemical and metamorphic evolution. Both suites of rocks have in common a distinct fluid-induced chemical change that point to a fluid that was equilibrated with a Mg-rich rock of peridotitic composition prior to the infiltration. The density of the eclogites in both areas is reduced by the overprinting for 0.2 to 0.4 g/cm<sup>3</sup>. The density contrast of the HP rocks to an assumed serpentinite matrix in the subduction channel is high enough to allow for buoyancy-driven exhumation. Marble on Sifnos and metapelite in the Tian Shan are discussed as alternative buoyancy-driven transport matrix during the final exhumation to shallower levels (<40 km).

### 3.2 Introduction

Almost all oceanic basalts that enter subduction zones and convert to high-pressure metamorphic rocks will eventually be buried deep into the mantle, but in rare and special cases, some of these HP/UHP rocks become exhumed back to the surface. Concepts of exhumation processes of HP/UHP rocks were brought up from several authors. These are based either on petrological observations from ophiolitic/high-pressure occurrences (e.g. Cloos and Shreve, 1988a,b; Avigad et al., 1992; Hill and Baldwin, 1993; Hacker et al., 1995;

Mattauer and Ritz, 1996; Federico et al., 2004; Keiter et al., 2004; Willner et al., 2004) or on numerical or analogue modelling (Chemenda et al., 1996; Gerya et al., 2002; Warren et al., 2008). Recent studies focus on exhumation triggered by changed petrophysical properties of the rocks in subduction zones (Warren et al., 2008). Those changes are caused by infiltrating fluids released from the down going slab during dehydration reactions (e.g. Peacock, 1993; Poli and Schmidt, 1995), which allow for the formation of a subduction channel and associated rehydration of former dry high-pressure rocks (Cloos, 1982; Gerya et al., 2002; van der Straaten et al., 2008). The subduction channel describes the hydrated interface between the down going slab and the dry and hot mantle wedge. Outcrops of subduction channel rocks may be described as tectonic or subduction mélanges that are characterised by a mixture of subduction related rocks, like HP/UHP mafic rocks, meta-sediments, marbles and peridotites or their altered or transformed products, like serpentinites, talc or chlorite schists (e.g. Cloos, 1983; Fergusson, 1984; Shreve and Cloos, 1986; Bebout and Barton, 2002; Federico et al., 2007). Most of the rocks that are associated with a subduction channel provide geochemical information about fluid-rock interaction during exhumation, preserved in the constituent hydrous minerals or in fluid inclusions. Some rocks provide in addition geochemical information about the whole burial and exhumation process. Partially rehydrated eclogites are especially well suited for fluid-rock interaction studies as these rocks experienced “dry” peak-conditions and became eventually rehydrated under retrograde conditions. This rehydration in the subduction channel results in a partial or total overprint of the eclogites under blueschist- or greenschist-facies conditions (e.g. Burg and Philippot, 1991; Ganor et al., 1996; Lister and Raouzaïos, 1996; van der Straaten et al., 2008). A decreased density and associated decreased viscosity of the incorporated rocks and of the partially serpentinitised mantle peridotite that acts as transport matrix during uplift is decisive for movements and even circulations in the subduction channel (Schwartz et al., 2001; Gerya et al., 2002; Gorczyk et al., 2006) and results in the exhumation of the subduction mélange. Hence, buoyancy is a very crucial factor for uplift in subduction zones (Platt, 1993; Ernst et al., 1997; Hermann et al., 2000; Schwartz et al., 2001; Pilchin, 2005). In this study we compare partially blueschist-facies overprinted eclogite suites from two paleo-subduction zones: I) The Cenozoic tectonic mélange of north Sifnos (Cyclades, Greece) and II) the late Palaeozoic subduction mélange of the Chinese South Tian Shan. The aim is to constrain the causes of subduction related exhumation processes and the element mobility during fluid-rock interaction in subduction channels by analysing the P-T history, the geochemistry and density changes associated with the eclogite-blueschist transformation.

### 3.3 Geological and petrological description

#### 3.3.1 Tian Shan

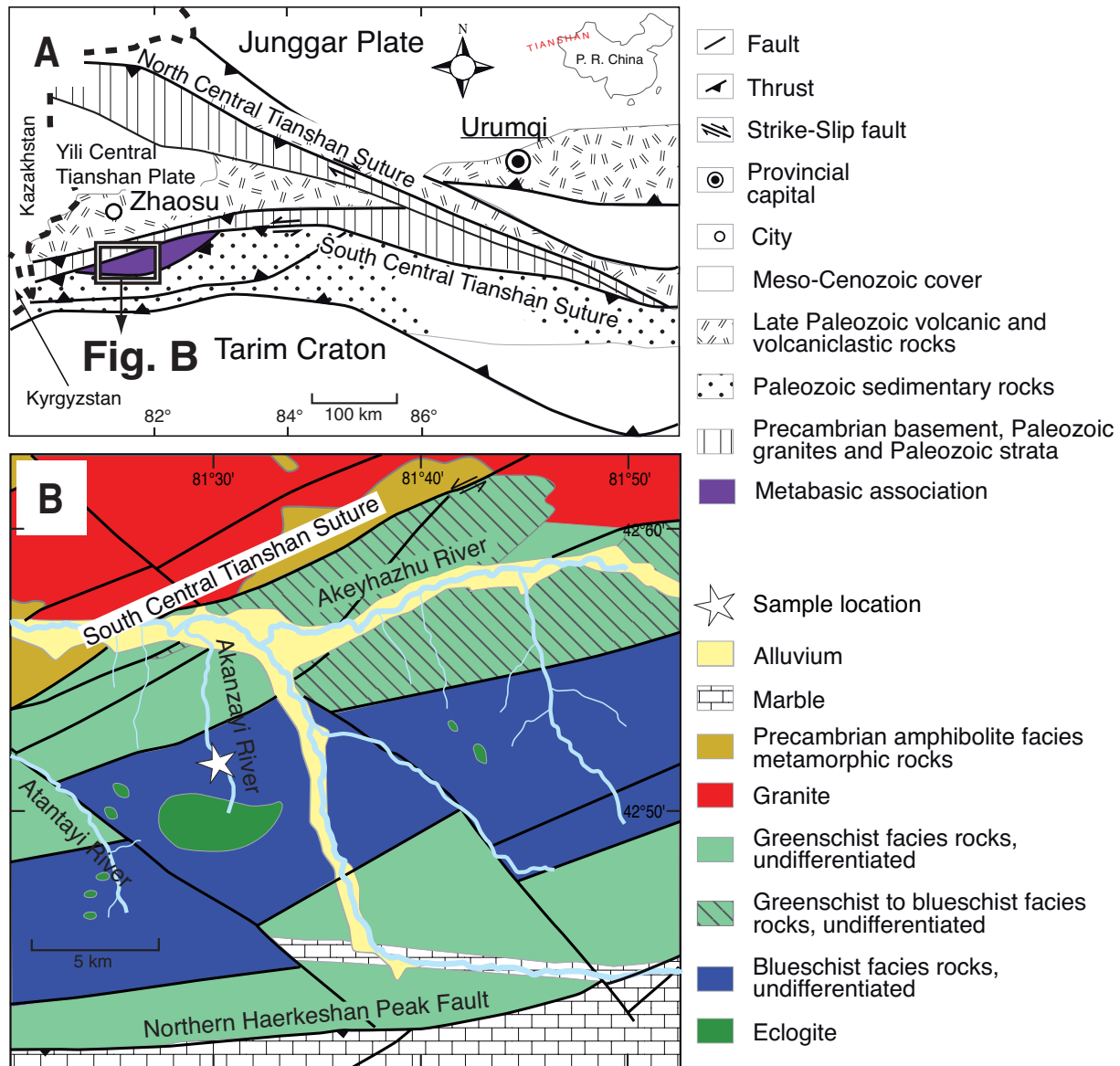


**Figure 3.1:** A) Geological map of the Chinese South Tian Shan modified after Gao et al. (1999). B) Detail of ophiolitic mélangé with sample locality (star).

The fold belt of the Chinese South Tian Shan developed as a result of the ocean closure and folding of Palaeozoic deposits and Precambrian basement between the Tarim craton and the Yili Central Tian Shan plate during the Variscan orogeny (Sobolev et al., 1986; Yang et al., 1986; Gao et al., 1995; Sengör and Natal'In, 1996; Bykadorov et al., 2003; Zhang

et al., 2005). A ~250 km long ESE–WNW striking ophiolitic mélangé (Figure 3.1A) results from the subduction and fragmental exhumation of the South Tian Shan Ocean, a marginal basin of the Turkestan Ocean, which is assigned to the northern branch of the Paleo-Tethys (Sengör and Natal’In, 1996; Bykadorov et al., 2003). Mainly metamafic rocks with greenschist-, blueschist- and eclogite-facies mineralogy, together with Silurian marbles and meta-ultramafic slices occur south of the Akeyhazhu River (Figure 3.1B; Gao et al., 1995, 1998). Peak-metamorphic conditions in eclogites and in eclogite-facies fluid veins within blueschist-facies host rocks were estimated at <20 kbar and between 500–650°C (Gao et al., 1998; Klemd et al., 2002; Gao et al., 2007; John et al., 2008; van der Straaten et al., 2008). Peak-metamorphic conditions in eclogites and blueschists occurred during early Carboniferous at  $343\pm 44$  Ma (Gao and Klemd, 2003). Cooling and the retrograde metamorphic evolution due to uplift began during the late Carboniferous at around 310–311 Ma. The latter age is based on white mica cooling ages (K–Ar, Ar–Ar, Rb–Sr; Klemd et al., 2005). Drill cores of an eclogite-blueschist sequence (in the following labelled as FTS 9–1 sequence) were taken from a m-sized boulder (Figure 3.2A) in the upper reaches of the Akanzayi River valley, which is located within the blueschist zone, close to the main eclogite-dominated occurrence of HP rocks (Figure 3.1B). Sample FTS 9–1.6 and 9–1.5A represent the best preserved eclogites of the whole eclogite-blueschist transition series (Figure 3.2A). A blueschist-facies overprint, i.e. increasing amounts of blueschist-facies minerals like glaucophane and white mica, increases up to sample FTS 9–1.1 (Figure 3.2A), which represents a pure blueschist with resorbed garnet and nearly complete replaced omphacite. The eclogite is composed of a fine-grained matrix of omphacite and accessory rutile; porphyroblasts are formed by garnet, blue amphibole and white mica (Figure 3.3A). Titanite grows poikiloblastically around matrix omphacite, a feature that is only visible with high magnification (Figure 3.4A). Omphacite, amphibole, rutile, quartz and minor amounts of white mica (phengite) and clinozoisite occur as inclusions in garnet. Clinozoisite is absent in the matrix. Calcite forms distinct aggregates in the matrix. The modal amounts of glaucophane, white mica and calcite increase significantly with increasing blueschist-facies overprint, whereas that of omphacite decreases. With increasing overprinting, garnet is resorbed and mostly replaced by Fe-rich chlorite and calcite and occurs only fragmental. Omphacite remains relictic in glaucophane and paragonite (Figure 3.3B). Fuchsite forms porphyroblasts in the glaucophane-dominated matrix. Titanite marginally replaces rutile.

### 3.3.2 Sifnos

The island Sifnos belongs to the eastern part of the Cyclades in the Attic-Cycladic Crystalline Complex (Dürr, 1986) as part of the Hellenic nappe stack in Greece (Aubouin, 1957). The orogen is divided into five N to NE dipping main nappes, which are from East to West: the Apulian, Ionian, Gavrovo-Tripolitza, Pindos-Olonos (including Cycladic blueschist) and the Pelagonian zone (Bornovas and Rontogianni-Tsiabaou, 1983, Figure 3.5A).

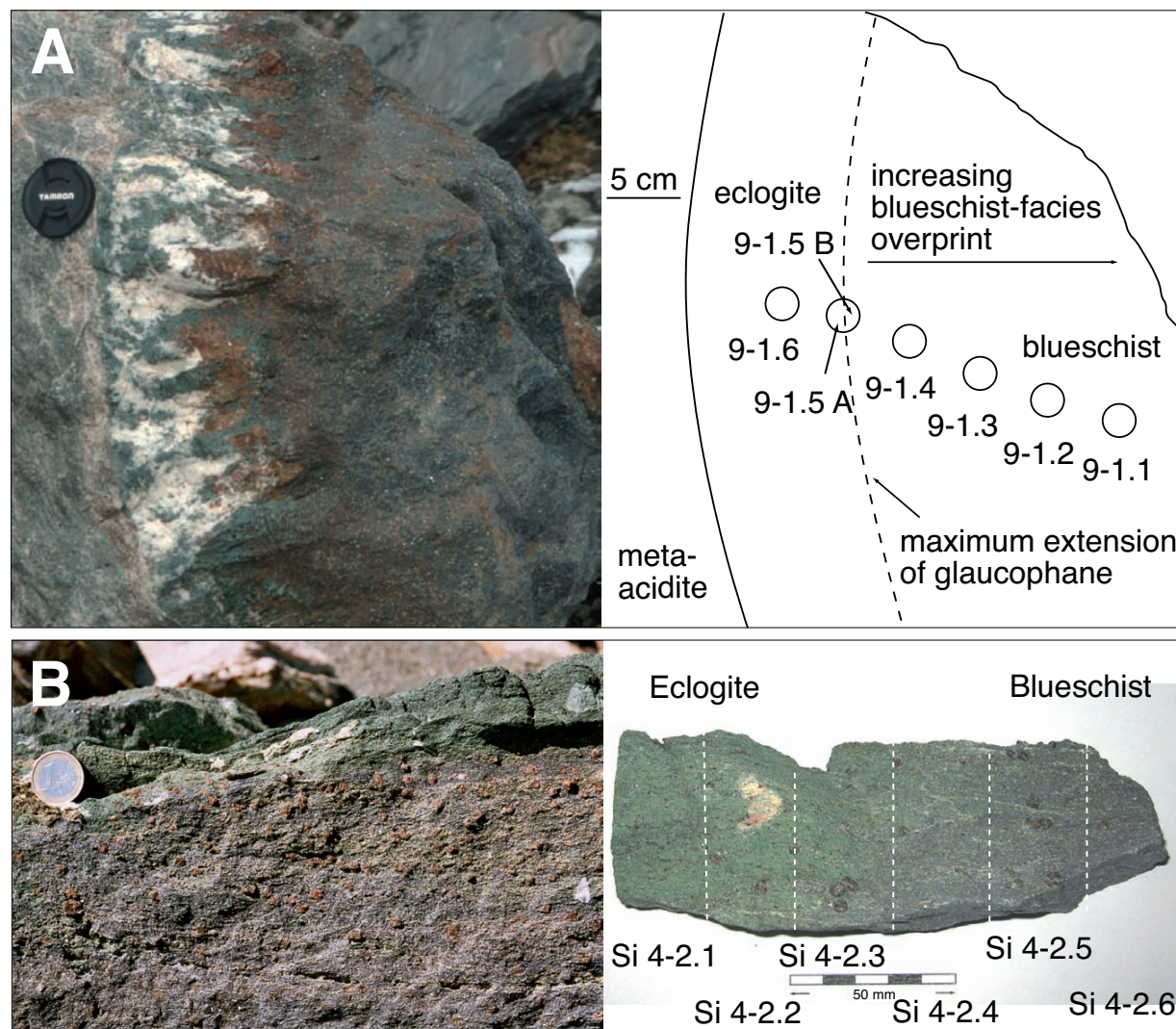


**Figure 3.2:** A) Photograph of eclogite boulder with increased blueschist overprint, Tian Shan (left); and schematic view of drilling holes (right). B) Photograph of eclogite with partial overprinted blueschist (left) and analysed sample (right); Bay of Vroulidia, Sifnos.

The main central and southern part of Sifnos represents the Basal Unit (Figure 3.5B; Dürr, 1986) and is composed of layered gneisses, schists and amphibolites together with Triassic to late Cretaceous thick-banded marbles and dolomite-marbles (Dürr, 1986). The sequence experienced an overprint during the Eocene (~42 Ma) under HP metamorphic conditions and subsequently in Miocene (25–20 Ma) under greenschist-facies conditions (Altherr et al., 1979, 1982; Maluski et al., 1987; Wijbrans et al., 1990). The northwestern and southwestern parts of Sifnos belong to the intermediate “blueschist unit” (Dürr, 1986). It is composed of Eocene HP metamorphosed (~42 Ma, Altherr et al., 1979) mafic to felsic volcano-sedimentary strata occurring as eclogite, blueschist, jadeite-gneiss and quartzite, which are over- and underlain by marbles (Dürr, 1986). The HP unit underwent peak-metamorphic conditions between 500–600°C and <20kbar, whereas the LP greenschist-

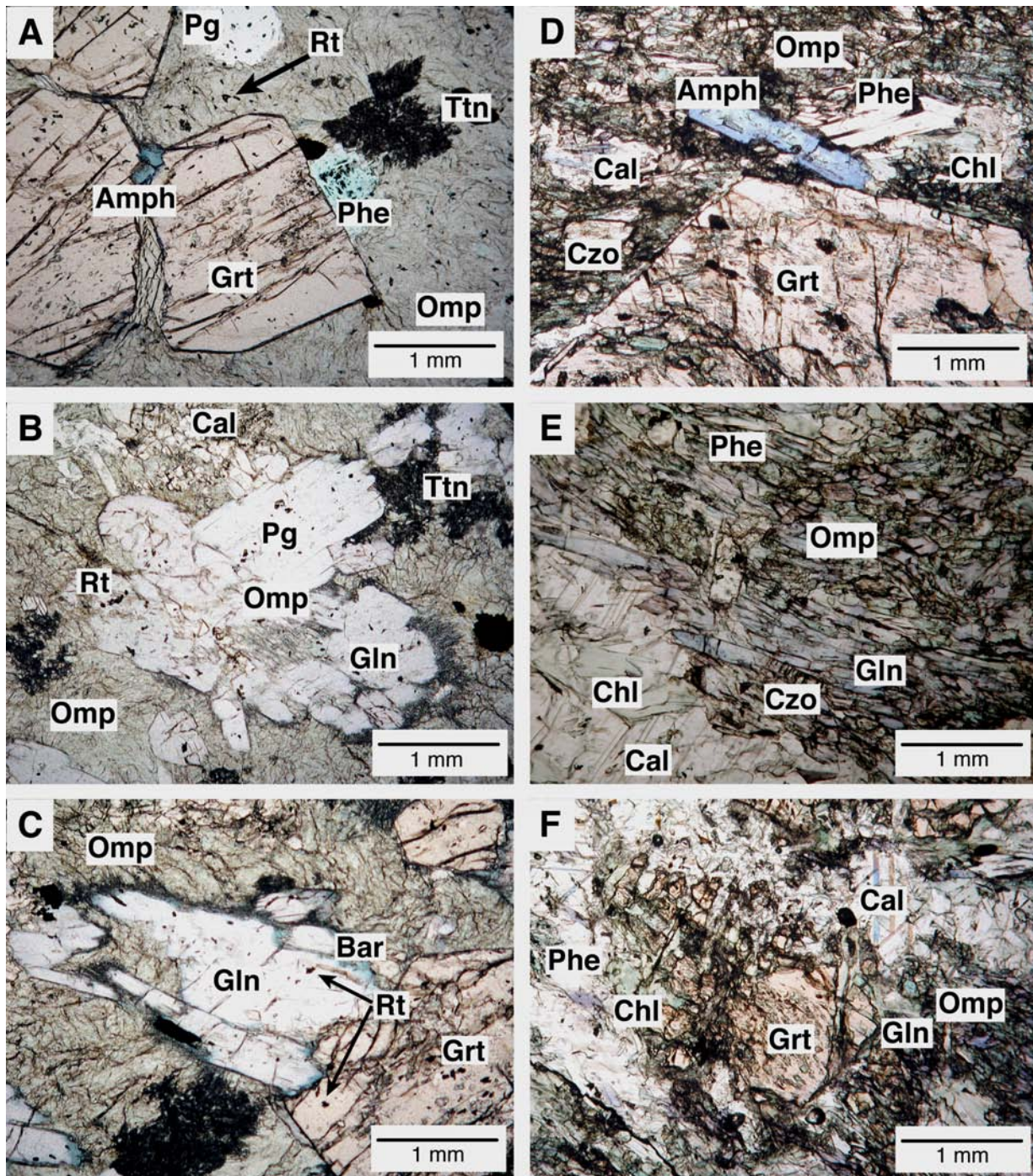


**Figure 3.3:** A–C) Microphotographs of eclogite (sample FTS 9–1.5). D–F) Microphotographs of eclogite to blueschist of Sifnos (sample Si 4–2). A) Eclogite-facies assemblage: garnet, omphacite, phengite (here fuchsite), sodic amphibole and rutile; B & C) retrograde blueschist-facies overprint, replacement of rutile by titanite and formation of glaucophane, paragonite and calcite at the expense of omphacite and garnet. D–F) Eclogite-facies mineral composition: garnet, omphacite, phengite and glaucophane with actinolite in core. Chlorite, clinozoisite, calcite and glaucophane in matrix are replacing retrogradely omphacite and garnet. Rutile is replaced by titanite but both are not indicated, also albite and quartz as they are too small.



facies overprint occurred at 360–380°C and  $5 \pm 2$  kbar (Schliestedt, 1980; Schliestedt and Okruch, 1988; Trotet et al., 2001; Schmädicke and Will, 2003; Spear et al., 2006). This late-stage metamorphic overprint was accompanied by infiltration of  $\text{CO}_2$ -,  $\text{Ca}^{2+}$ - and  $\text{H}_2\text{O}$ -rich fluids, presumably derived from plutons underlying Sifnos. The latter assumption is based on studies of the island Serifos (Dürr, 1986). At the northern shoreline of the Vroulidia Bay in north Sifnos (Figure 3.5B) well-preserved high-pressure rocks are outcropping, striking SW–NE and dipping about 40° to NW (Avigad et al., 1988). The rock-sequence contains blueschist, eclogite, chlorite-actinolite-fels, jadeite-gneiss and metasediment with changing silicate, calcite and dolomite contents (Mocek, 1994). Sample Si 4-2 is taken from the eclogite-blueschist unit and shows very clearly the late-stage transformation from eclogite to blueschist in hand-specimen (Figure 3.2B). The mineralogical composition of the eclogite as well as of the blueschist is Grt–Omp–Gln/Win/Act–Czo–Phe–Chl–Ab–Rt–Ttn–Cc–Qtz–Ap–opaque phase. Garnet and omphacite are the dominant minerals in the eclogite. Porphyroblasts of garnet are shaded with inclusions of omphacite, rutile, quartz, amphibole, chlorite and white mica. Fine-grained omphacite, porphyroblastic amphibole, clinozoisite, white mica and calcite are the main components in the matrix. Rutile is partially replaced by titanite. The porphyroblastic amphibole has a green-bluish pleochroitic core with a bluish pleochroitic rim (Figure 3.3D). Amphibole, omphacite, white mica, clinozoisite and rutile/titanite are also enclosed by calcite. Chlorite and albite are usually associated with garnet, white mica and blue amphibole. Quartz is rare and occurs mainly as inclusion. The amount of omphacite decreases with progressive blueschist-facies overprint and is replaced in part or in total by fine-grained and irregular arranged blue amphibole and white mica (Figure 3.3E). The amount of calcite increases strongly towards the blueschist. Calcite is either forming inclusion-rich porphyroblast, or is arranged in aggregates to elongated striae. Garnet shows minor to excessive replacement, in particular by chlorite but also by glaucophane, white mica and calcite (Figure 3.3F). The modal

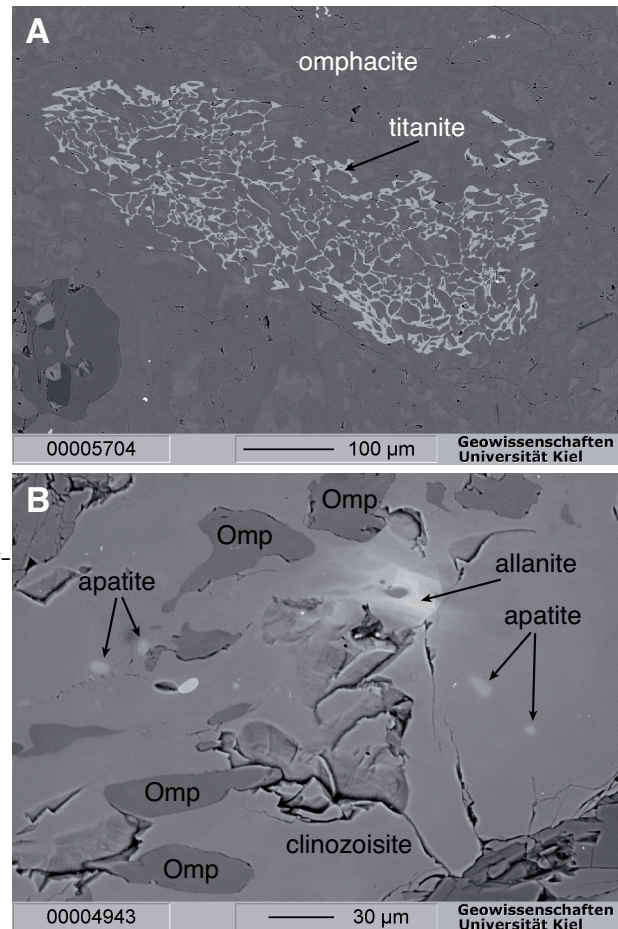


**Figure 3.4:** Backscattered-electron-image (BSE) of eclogite FTS 9–1.5A, Tian Shan showing fine-grained poikiloblastic growths of titanite overgrowing fine-grained omphacite in matrix. B) BSE-image of clinozoisite with allanitic core composition and omphacite and apatite inclusions, Sifnos blueschist Si 4–2.4.

amounts of sodic amphibole, chlorite, albite and titanite increase at the expense of garnet, omphacite and rutile. Apatite is partly enclosed in newly formed clinozoisite, which shows cores of allanitic composition (Figure 3.4B). Modal amounts of clinozoisite and white mica are approximately similar in the blueschist and in the eclogite. Matrix glaucophane in contact with calcite or with omphacite is marginally replaced by calcic amphibole.

### 3.4 Analytical methods

Major elements of whole rocks were measured by X-ray fluorescence spectrometry (XRF, Philips PW 1480) on fused glass discs at the Institut für Geowissenschaften, University of Kiel. Values of BHVO.1 (Flanagan, 1976) were used for internal standardisation (Table A.1). Accuracy and precision are better than 1% ( $1\sigma$ ) for the major oxides.

Trace elements were analysed by ICP-MS (Agilent 7500c) at the same institute. 100 mg pulverised and dried rock powder were digested by pure HF and HNO<sub>3</sub> in digestion bombs for four days at 180°C and fumed off with HClO<sub>4</sub>. The final 1% HNO<sub>3</sub> solution was diluted 20-fold and spiked with 2.5 ng/ml Beryllium (Be), Indium (In) and Rhenium (Re) for internal standardisation. Five replicate measurements of each sample were conducted with breaks for cleaning with a blank reagent. Further details of the procedure can be found in Garbe-Schönberg (1993) and John et al. (2008). The analytical precision is estimated to be <10% ( $1\sigma$ ) according to duplicate analysis of samples and standard (see Table A.2).

In situ analysis by LA-ICP-MS (Agilent 7500i, quadrupole) were made at the Institut für Mineralogie, University of Würzburg. A Nd-YAG laser with 266 nm wavelength is used for ablation. Argon is used as carrier-gas. Calcite was measured with 30% of the laser activity and silicates with 45% of laser activity. Each sample was measured 15 sec on the background and 20 sec on the mineral. External calibration was carried out with NIST 612 50 ppm glass disc with values of Pearce et al. (1997). For accuracy NIST 610 and 614 were used and further ablation of NIST 612 was used for reproducibility (Table A.3). Internal standardisation was carried out by Si concentration for analysing silicates and Ca concentrations for carbonates, both determined with the electron microprobe at Kiel University. The minimum detection limit equal to 99% confidence level is defined by  $2.3 * \sqrt{(2B)}$ , where  $B$  is the total counts on the background. The minimum detection is usually at 0.02–0.18 ppm for REE, 0.03–0.10 ppm for HFSE (Zr, Nb, Hf, Ta), 0.27–0.44 ppm for Li and Be, <2.8 ppm B, 0.07–1.7 for transition metals (except <7.3 ppm for Zn) and 0.02–0.30 ppm for LILE (Cs, Rb, Ba, Sr, Pb, Th). The REE concentrations of omphacite, glaucophane, calcite and white mica are up to 0.01–0.10 ppm above the detection limit, but usually below these values. LREE (La–Nd) concentrations of garnet are usually below the detection limit.

Mineral chemical data were obtained by electron microprobe (JEOL JXA 8900R) at Institut für Geowissenschaften, University of Kiel. The microprobe is equipped with five wavelengths-dispersive spectrometers (WDS). Depending on the analysed mineral phase, the following acceleration voltages and beam currents were used: 15 kV and 15 nA for

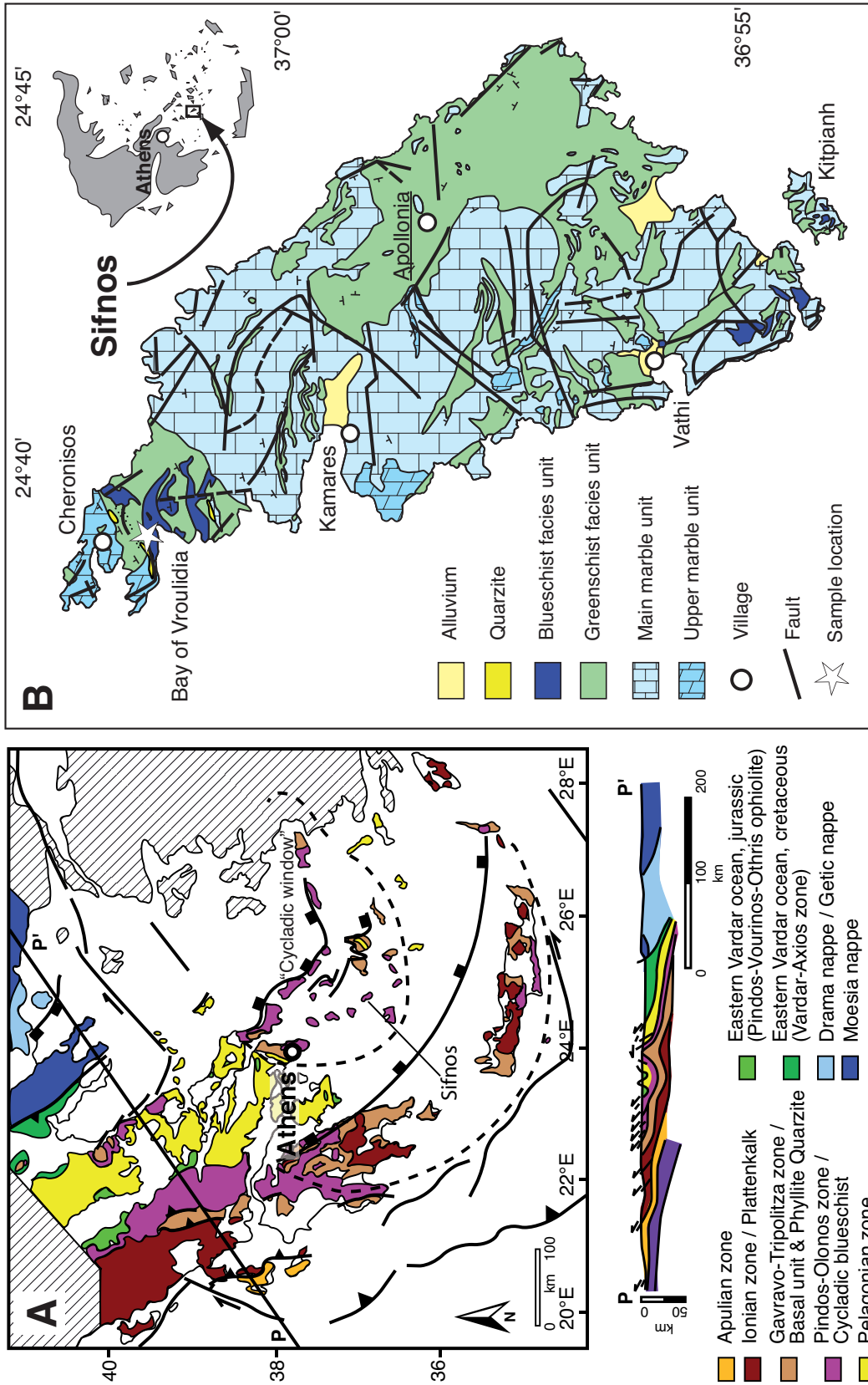
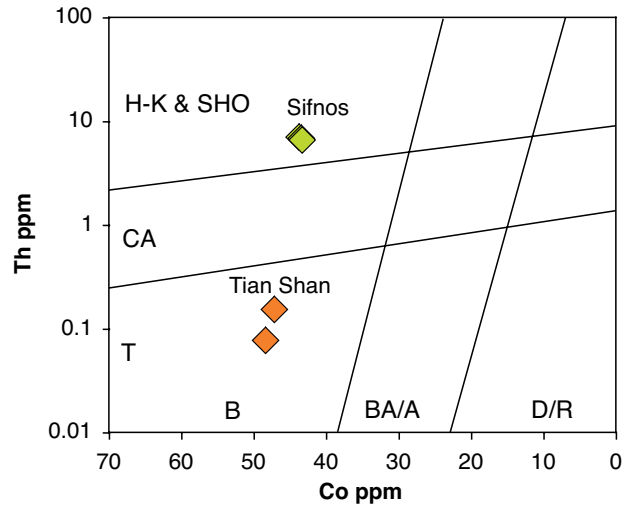


**Figure 3.5:** Geological map of Greece, modified after van Hinsbergen (2004). B) Geological map of Sifnos, modified after Davis (1966). Sample locality indicated by star at the northern shore of the Bay of Vroulidia.

**Figure 3.6:** Co vs. Th concentrations to estimate protholiths prior metamorphism for eclogite-blueschist samples of Sifnos and Tian Shan after [Hastie et al. \(2007\)](#). H-K: high-potassium, SHO: shoshonite, CA: calc-alkaline, T: tholeiite, B: basalt, BA/A: basalt-andesite/ andesite, D/R: dacite/ rhyolite.



garnet, phengite and feldspar and 20 kV and 20 nA for amphibole, pyroxene, epidote and carbonate. CITZAF corrections were used for matrix correction.

Total carbon measurements were made with a Carlo–Erba instrument in a routine mode at IFM-GEOMAR, Kiel. Each sample was measured twice. The analytical precision is estimated to be  $<1.2\%$  ( $1\sigma$ ) according to standards, blanks and duplicate analyses.

Density determinations are based on measurements with a Gay-Lussac pycnometer with a calibrated volume of 2 ml. Each sample was measured three times and measurements were repeated if precision of the analysis was  $>2\%$  ( $1\sigma$ ). The density calculation is based on the weighting and calculation of the displaced water by the powdered sample. Temperature measurements were made to obtain the specific water density at a given temperature.

### 3.5 Geochemistry

The field and the petrographical observations clearly indicate that the blueschists are the products of hydration and metasomatism of eclogites at both localities. Hence, the eclogite is interpreted to represent the precursor rock of the blueschist. For a better understanding of the effects of metasomatism and their petrophysical consequences, we first try to decipher the nature of the magmatic precursor prior to its subduction and then we will evaluate the chemical changes that occurred during the blueschist-facies overprint. The generally immobile behaviour of the HFSE ([Winchester and Floyd, 1977](#); [Corfu and Davis, 1991](#)) and occasionally also of the REE (e.g. [Savov et al., 2005](#)) may provide information about the magmatic protholith, as their concentrations may not have been changed during metamorphism. In addition, in situ mineral chemical trace element analyses by LA-ICP-MS (Table 3.1) were done for the most pristine eclogite of the Tian Shan (sample FTS 9–1.5B) on garnet, omphacite, glaucophane, white mica, calcite and titanite. Probable changes in concentrations and mobility of REE or transition metals could be predicted by combining petrographical observations with the trace element content in minerals. LA-

ICP-MS data from Sifnos were not considered because of the very fine-grained texture and inclusion-rich porphyroblasts of these rocks, which did not allow to obtain precise data. Major and trace element data of both eclogite-blueschist sequences are listed in Table 3.2.

**Table 3.1:** Selected mineral analyses by LA-ICP-MS of sample FTS 9-1.5 (Tian Shan).

No.	22	27	16	21	1	50	38	4	9	45
Mineral	ttn	ttn	grt	grt	omp	omp	omp	gln	fuc	pg
Comment	at grt	matrix	core	rim	in gln	in pg	matrix	matrix	matrix	matrix
Li	2	16.4	d.l.	d.l.	44.5	8.99	53.1	39.5	17.7	12.3
Be	d.l.	d.l.	d.l.	d.l.	d.l.	5.02	1.71	d.l.	2.19	2.41
B	d.l.	d.l.	d.l.	d.l.	d.l.	30.2	1.63	d.l.	15.2	14.1
V	121	119	33	41.7	200	86.9	192	153	264	87.5
Cr	403	444	462	638	1264	1110	921	887	38679	839
Mn	3172	349	11273	9947	271	40.3	528	207	202	346
Co	12.7	13.4	36.9	3.09	43.7	1.04	22.3	80	17.5	12.5
Ni	82.3	138	d.l.	7.5	297	5.25	149	823	68.6	39.4
Cu	11.7	6.91	d.l.	1.8	3.4	6.24	5.51	6.37	d.l.	5.39
Zn	d.l.	d.l.	d.l.	42.4	77.8	d.l.	51.9	144	392	31.8
Rb	0.225	0.16	d.l.	d.l.	0.08	7.49	0.33	d.l.	174	1.85
Sr	178	35.3	d.l.	0.09	10.5	1658	29.6	1	205	792
Y	84.5	6.98	204	54.3	0.36	d.l.	2.06	0.035	0.10	2.78
Zr	9.31	3.23	6.69	0.94	0.57	0.26	0.70	0.193	d.l.	1.1
Nb	61	11.1	d.l.	d.l.	d.l.	d.l.	d.l.	d.l.	0.08	d.l.
Mo	0.649	d.l.	d.l.	d.l.	d.l.	d.l.	d.l.	d.l.	d.l.	d.l.
Cs	d.l.	d.l.	d.l.	d.l.	d.l.	d.l.	d.l.	d.l.	5.29	0.09
Ba	2.66	0.94	d.l.	d.l.	0.50	285	1.43	d.l.	5750	81.8
La	3.3	1.37	d.l.	d.l.	d.l.	d.l.	d.l.	d.l.	d.l.	d.l.
Ce	15.2	4.36	d.l.	d.l.	d.l.	d.l.	d.l.	d.l.	d.l.	d.l.
Pr	2.32	0.74	d.l.	d.l.	d.l.	d.l.	d.l.	d.l.	d.l.	d.l.
Nd	14.8	3.32	d.l.	d.l.	d.l.	d.l.	d.l.	d.l.	d.l.	d.l.
Sm	4.81	0.77	d.l.	1.25	d.l.	d.l.	d.l.	d.l.	d.l.	d.l.
Eu	3.69	0.43	1.41	1.2	d.l.	0.12	0.07	d.l.	d.l.	0.09
Gd	17.9	1.27	11.1	9.32	d.l.	d.l.	d.l.	d.l.	d.l.	0.69
Tb	3.25	0.28	3.98	2.01	d.l.	d.l.	0.05	d.l.	d.l.	0.12
Dy	16.9	1.07	37.5	12.2	d.l.	d.l.	0.25	d.l.	d.l.	0.58
Ho	3.17	0.18	7.38	2.13	d.l.	d.l.	0.07	d.l.	d.l.	0.14
Er	9.62	0.69	22.9	6.53	d.l.	d.l.	0.27	d.l.	d.l.	0.48
Tm	1.27	0.09	3.33	0.78	d.l.	d.l.	d.l.	d.l.	d.l.	0.07
Yb	10.1	0.85	19.3	5.67	d.l.	d.l.	0.2	d.l.	d.l.	0.32
Lu	1.27	0.13	2.08	0.72	d.l.	d.l.	0.07	d.l.	d.l.	0.05
Hf	0.84	0.35	d.l.	d.l.	d.l.	d.l.	0.09	d.l.	d.l.	d.l.
Ta	1.6	0.38	d.l.	d.l.	d.l.	d.l.	d.l.	d.l.	d.l.	d.l.
Pb	4.8	1.46	d.l.	d.l.	d.l.	13.4	0.30	d.l.	5.13	10.8
Th	d.l.	d.l.	d.l.	d.l.	d.l.	d.l.	d.l.	d.l.	d.l.	d.l.

elements in ppm, d.l. = under detection limit.

### 3.5.1 Whole rock major and trace elements

The most pristine eclogite from the Tian Shan (sample FTS 9–1.5A) has a basaltic composition with 49.8 wt.%  $\text{SiO}_2$ , 5.9 wt.%  $\text{Na}_2\text{O}$  and 0.1 wt.%  $\text{K}_2\text{O}$ . The  $\text{SiO}_2$  content decreases to values of 41.2 wt.% with increasing intensity of the blueschist-facies overprint, but  $\text{SiO}_2$  loss is not correlated with the distance from the relict eclogite as the one that is farthest away from the pristine eclogite contains still 47.2 wt.%  $\text{SiO}_2$  (sample FTS 9–1.1, Table 3.2). As  $\text{SiO}_2$  and the alkali concentrations are quite ambiguous in metamorphic rocks, the Co and Th concentrations of the undisturbed eclogite (samples FTS 9–1.5 A and B) show more convincingly that the precursor rocks developed in the tholeiitic basalt serie (Hastie et al., 2007, Figure 3.6).  $\text{Al}_2\text{O}_3$ ,  $\text{TiO}_2$ ,  $\text{Fe}[\text{tot}]$ ,  $\text{P}_2\text{O}_5$ , and  $\text{Na}_2\text{O}$  concentrations are relatively constant in all samples, whereas those of  $\text{MgO}$  and  $\text{K}_2\text{O}$  increase with increasing blueschist-facies overprint and those of  $\text{CaO}$  and  $\text{MnO}$  decrease (Table 3.2). The LOI increases strongly from 1.8 in eclogites up to 12.8 wt.% in blueschists.

The Tian Shan eclogite shows a flat chondrite-normalised (Boynton, 1984) REE pattern with  $(\text{Ce}/\text{Yb})_N = 1$  and a slightly positive Eu-anomaly (Figure 3.7). REE and HFSE are slightly depleted compared to N-MORB composition (Hart et al., 1999). The Nb/Ta and Zr/Hf ratios are 25 and 30, respectively, and the HFSE are highly depleted and form distinct troughs in the MORB-normalised multi-element diagram (Figure 3.8A). N-MORB normalised LILE (Cs, Rb, Ba, Sr and Pb) are slightly enriched compared to REE with  $(\text{Ba}/\text{La})_N = 4$  and HFSE with  $(\text{Pb}/\text{Zr})_N = 12$ ; Figure 3.8A).

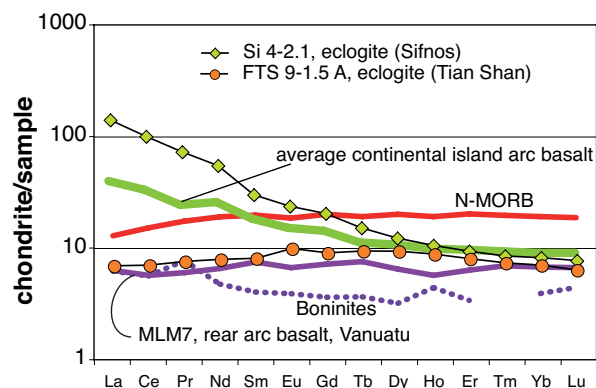


**Figure 3.7:** Chondrite-normalised (Boynton, 1984) eclogite of Sifnos and Tian Shan. For comparison composition of boninite, average continental island arc basalt (Kelemen et al., 2003) and rear-arc basalt of Vanuatu (Peate et al., 1997).

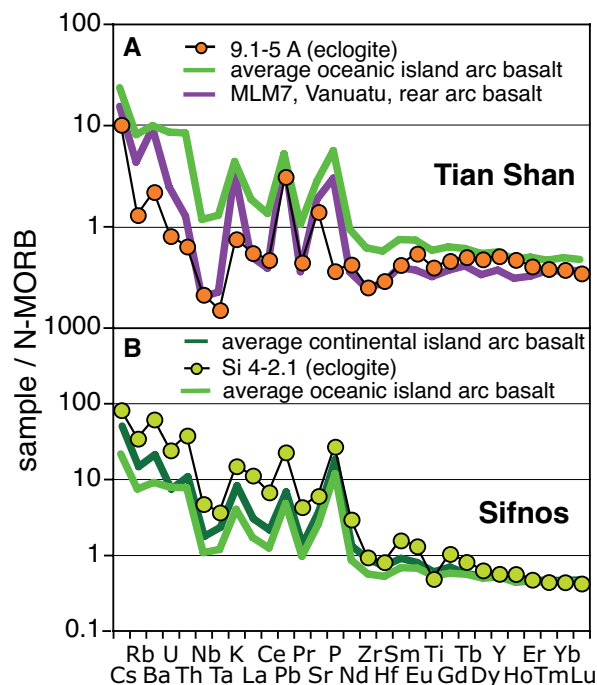


**Figure 3.8:** N-MORB normalised (Hart et al., 1999) eclogite compositions from Sifnos and the Tian Shan. A) Tian Shan eclogite shows correlations to REE-depleted rear-arc basalt of Vanuatu (Peate et al., 1997) indicating back-arc basalt affinity. B) Sifnos eclogite correlates to continental island arc basalts, which can be assumed as protholith.

**Table 3.2:** Major and trace element analyses of the eclogite-blueschist sequence from the South Tian Shan (E 81°18'49.6", N 42°30'59.4") and Sifnos (E 24°39'10.0", N 37°01'24.9").

Sample	Eclogite		Ec/Bs		Ec/Bs		Ec/Bs		Eclogite		blueschist		blueschist		Ec/Bs		Ec/Bs		Ec/Bs		Blueschist						
	FTS 9-1-6	FTS 9-1-5a	FTS 9-1-5b	FTS 9-1-4	FTS 9-1-3a	FTS 9-1-2	FTS 9-1-1	Si 4-2-1	Si 4-2-2	Si 4-2-3	Si 4-2-4	Si 4-2-5	Si 4-2-6	Si 4-2-1	Si 4-2-2	Si 4-2-3	Si 4-2-4	Si 4-2-5	Si 4-2-6	Si 4-2-1	Si 4-2-2	Si 4-2-3	Si 4-2-4	Si 4-2-5	Si 4-2-6		
SiO <sub>2</sub>	55.14	49.75	43.62	41.17	41.99	39.35	47.22	46.25	45.29	44.24	42.86	43.77	43.57	46.25	45.29	44.24	42.86	43.77	43.57	46.25	45.29	44.24	42.86	43.77	43.57	43.57	
TiO <sub>2</sub>	0.23	0.64	0.59	0.68	0.58	0.76	0.65	0.78	0.76	0.72	0.72	0.77	0.82	0.78	0.76	0.72	0.72	0.72	0.77	0.78	0.76	0.72	0.72	0.77	0.82	0.82	
Al <sub>2</sub> O <sub>3</sub>	10.66	12.52	11.88	12.60	12.12	12.80	13.26	12.79	12.81	12.77	12.81	13.26	13.29	12.79	12.81	12.77	12.81	12.81	12.77	12.79	12.81	12.77	12.81	12.81	13.29	13.29	
Fe <sub>2</sub> O <sub>3</sub>	7.33	7.94	8.30	8.66	8.66	10.80	8.20	7.97	8.04	8.03	8.49	8.50	8.77	7.97	8.04	8.03	8.49	8.50	8.03	7.97	8.04	8.03	8.49	8.50	8.77	8.77	
FeO [calc.]	6.60	7.14	8.37	7.93	7.79	9.72	7.38	7.17	7.23	7.23	7.64	7.65	7.89	7.17	7.23	7.23	7.64	7.65	7.23	7.17	7.23	7.23	7.64	7.65	7.89	7.89	
MnO	0.14	0.20	0.24	0.22	0.17	0.35	0.11	0.19	0.21	0.21	0.24	0.21	0.25	0.19	0.21	0.21	0.24	0.21	0.21	0.19	0.21	0.21	0.24	0.21	0.25	0.25	
MgO	6.88	7.59	9.27	9.69	11.18	10.29	10.32	7.48	7.57	7.73	7.87	7.96	7.62	7.48	7.57	7.73	7.87	7.96	7.73	7.48	7.57	7.73	7.87	7.96	7.62	7.62	
CaO	11.80	12.28	11.70	11.12	8.61	9.89	6.62	13.87	14.07	13.55	14.03	13.10	12.45	13.87	14.07	13.55	14.03	13.10	13.10	13.87	14.07	13.55	14.03	13.10	12.45	12.45	
Na <sub>2</sub> O	6.05	5.94	5.11	4.78	4.89	4.10	5.57	1.56	1.61	1.64	1.38	3.40	3.40	1.56	1.61	1.64	1.38	3.40	3.40	1.56	1.61	1.64	1.38	3.40	3.40		
K <sub>2</sub> O	0.02	0.08	0.10	0.15	0.24	0.31	0.28	0.32	0.27	0.23	0.22	0.18	1.55	0.32	0.27	0.23	0.22	0.18	0.18	0.32	0.27	0.23	0.22	0.18	1.55	1.55	
P <sub>2</sub> O <sub>5</sub>	0.05	0.01	0.01	0.01	0.05	0.01	0.01	2.97	3.58	5.15	6.18	5.96	2.21	2.97	3.58	5.15	6.18	5.96	6.17	2.97	3.58	5.15	6.18	5.96	2.21	2.21	
CO <sub>2</sub>								2.03	2.04	2.21	2.29	2.21	8.17	2.03	2.04	2.21	2.29	2.21	2.21	2.03	2.04	2.21	2.29	2.21	8.17	8.17	
H <sub>2</sub> O [calc.]	1.84	3.47	9.14	11.44	12.82	12.23	9.02	5.00	5.62	7.54	8.39	8.46		5.00	5.62	7.54	8.39	8.46	8.17	5.00	5.62	7.54	8.39	8.46			
Density	3.26	3.34	3.16	3.19	3.04	3.12	3.10	3.05	3.03	3.01	2.95	2.97	2.95	3.05	3.03	3.01	2.95	2.97	2.95	3.05	3.03	3.01	2.95	2.97	2.95	2.95	
Total	99.41	100.42	100.96	100.67	101.31	99.81	101.26	99.73	99.57	99.93	100.20	100.30	100.07	99.73	99.57	99.93	100.20	100.30	100.07	99.73	99.57	99.93	100.20	100.30	100.07	100.07	
Li		37.7	33.6	35.5	123.7	30.2	42.3	31.9	30.5	27.4	27.0	26.9		31.9	30.5	27.4	27.0	26.9	26.9		31.9	30.5	27.4	27.0	26.9	26.9	26.9
Sc		38.6	32.8	42.8	20.0	63.5	25.7	34.5	34.6	33.8	34.4	36.2		34.5	34.6	33.8	34.4	36.2	36.2		34.5	34.6	33.8	34.4	36.2	36.2	36.2
V		205	176	205	173	173	178	234	235	229	222	229		234	235	229	222	229	229		234	235	229	222	229	229	229
Cr*		1188	993	1147	1076	1212	1119	694	727	736	681	745		694	727	736	681	745	745		694	727	736	681	745	745	745
Co		32.4	47.1	48.4	56.6	50.9	43.2	43.7	43.4	43.3	38.4	42.4		43.7	43.4	43.3	38.4	42.4	42.4		43.7	43.4	43.3	38.4	42.4	42.4	42.4
Ni		231	349	404	420	396	369	213	207	233	224	246		213	207	233	224	246	246		213	207	233	224	246	246	246
Cu		44.9	63.9	63.1	67.4	66.6	19.5	60.0	55.4	56.8	48.8	51.8		60.0	55.4	56.8	48.8	51.8	51.8		60.0	55.4	56.8	48.8	51.8	51.8	51.8
Zn		51.6	64.0	62.1	85.3	75.1	100.3	62.3	59.9	62.0	64.2	66.0		62.3	59.9	62.0	64.2	66.0	66.0		62.3	59.9	62.0	64.2	66.0	66.0	66.0
Ga		15.9	13.3	13.3	13.0	12.3	15.1	14.0	13.8	13.4	13.3	13.5		14.0	13.8	13.4	13.3	13.5	13.5		14.0	13.8	13.4	13.3	13.5	13.5	13.5
Rb		1.65	1.67	2.31	4.81	6.25	5.70	42.8	44.6	45.2	37.4	42.1		42.8	44.6	45.2	37.4	42.1	42.1		42.8	44.6	45.2	37.4	42.1	42.1	42.1
Sr		159	316	412	448	412	301	677	673	781	872	850		677	673	781	872	850	902		677	673	781	872	850	902	902
Y		18.4	16.0	22.2	22.7	28.6	26.7	96.5	93.9	92.2	88.5	93.2		96.5	93.9	92.2	88.5	93.2	100		96.5	93.9	92.2	88.5	93.2	100	100
Zr		26.2	23.5	26.7	26.7	22.7	28.6	16.4	16.2	15.3	14.7	16.7		16.4	16.2	15.3	14.7	16.7	22.8		16.4	16.2	15.3	14.7	16.7	22.8	22.8
Nb		0.75	0.59	0.48	0.48	0.45	0.80	0.23	0.22	0.19	0.18	0.18		0.23	0.22	0.19	0.18	0.18	16.7		0.23	0.22	0.19	0.18	0.18	16.7	16.7
Mo		0.15	0.14	0.13	0.12	0.12	0.14	0.23	0.22	0.19	0.18	0.18		0.23	0.22	0.19	0.18	0.18	16.7		0.23	0.22	0.19	0.18	0.18	16.7	16.7
Sb		0.81	0.55	0.47	0.32	0.39	0.40	0.77	0.74	0.69	0.68	0.65		0.77	0.74	0.69	0.68	0.65	0.70		0.77	0.74	0.69	0.68	0.65	0.70	0.70
Sn		0.05	0.04	0.04	0.06	0.04	0.06	0.12	0.11	0.10	0.10	0.09		0.12	0.11	0.10	0.10	0.09	0.09		0.12	0.11	0.10	0.09	0.09	0.09	0.09
Cs		0.14	0.17	0.16	0.38	0.30	0.25	1.14	1.18	1.18	0.99	0.97		1.14	1.18	1.18	0.99	0.97	1.07		1.14	1.18	1.18	0.99	0.97	1.07	1.07
Ba		30.5	34.1	49.7	92.8	120	102	843	872	870	704	795		843	872	870	704	795	795		843	872	870	704	795	795	795
La		2.14	2.86	1.72	0.41	0.58	0.20	43.3	41.9	40.0	38.4	42.0		43.3	41.9	40.0	38.4	42.0	42.0		43.3	41.9	40.0	38.4	42.0	42.0	42.0
Ce		5.64	7.28	4.47	1.28	1.86	0.64	80.3	76.9	73.7	70.8	77.8		80.3	76.9	73.7	70.8	77.8	77.8		80.3	76.9	73.7	70.8	77.8	77.8	77.8
Pr		0.92	1.19	0.78	0.24	0.36	0.12	8.84	8.62	8.25	7.89	8.63		8.84	8.62	8.25	7.89	8.63	8.63		8.84	8.62	8.25	7.89	8.63	8.63	8.63
Nd		4.73	6.15	4.37	1.45	2.14	0.71	32.6	31.7	30.4	29.0	31.7		32.6	31.7	30.4	29.0	31.7	31.7		32.6	31.7	30.4	29.0	31.7	31.7	31.7
Sm		1.57	2.07	1.73	0.64	0.93	0.32	5.83	5.68	5.42	5.18	5.61		5.83	5.68	5.42	5.18	5.61	5.61		5.83	5.68	5.42	5.18	5.61	5.61	5.61
Eu		0.72	0.95	0.77	0.31	0.43	0.17	1.73	1.65	1.59	1.43	1.61		1.73	1.65	1.59	1.43	1.61	1.61		1.73	1.65	1.59	1.43	1.61	1.61	1.61
Gd		2.33	2.74	2.64	1.31	1.97	0.78	5.24	5.04	4.77	4.65	4.97		5.24	5.04	4.77	4.65	4.97	4.97		5.24	5.04	4.77	4.65	4.97	4.97	4.97
Tb		0.44	0.46	0.54	0.33	0.59	0.24	0.71	0.70	0.64	0.60	0.70		0.71	0.70	0.64	0.60	0.70	0.70		0.71	0.70	0.64	0.60	0.70	0.70	0.70
Dy		3.00	2.79	3.79	2.39	3.40	1.33	3.94	3.97	3.36	3.32	4.21		3.94	3.97	3.36	3.32	4.21	4.21		3.94	3.97	3.36	3.32			

Eclogite and blueschist of the Si 4-2 sequence from Sifnos are  $\text{SiO}_2$ -depleted mafic rocks. The  $\text{SiO}_2$  content decreases from eclogite to blueschist from 46.3 to 43.6 wt.%, whereas concentrations of  $\text{TiO}_2$ ,  $\text{Al}_2\text{O}_3$ ,  $\text{Fe}[\text{tot}]$ ,  $\text{MgO}$ ,  $\text{CaO}$ ,  $\text{Na}_2\text{O}$  and  $\text{K}_2\text{O}$  remain constant during the blueschist-facies overprint. The  $\text{MnO}$  content increases and the  $\text{P}_2\text{O}_5$  content decreases. The LOI increases strongly from 5 to 8.2 wt.%, which is mainly the result of increasing  $\text{CO}_2$  contents (Table 3.2). Co and Th concentrations suggest that the basaltic protholith prior to eclogite formation derived from a high-potassium or shoshonitic serie (Figure 3.6). The Chondrite-normalised (Boynton, 1984) pattern of the eclogite shows a steep enrichment in LREE (120–140 times chondrite) and moderate enrichments in HREE ( $\sim 10$  times chondrite) with  $(\text{Ce}/\text{Yb})_N$  of 47 (Figure 3.7). The eclogite is enriched in LILE (Cs, Rb, Ba, K) compared to N-MORB-normalised (Hart et al., 1999) HFSE and REE values, e.g.  $(\text{Ba}/\text{La})_N = 5$  and  $(\text{Ba}/\text{Zr})_N = 66$  (Figure 3.8B). The eclogite shows extended Nb–Ta and Zr–Hf troughs in the N-MORB-normalised multi-element diagram and has  $\text{Nb}/\text{Ta} = 23$  and  $\text{Zr}/\text{Hf} = 40$  ratios.

## 3.6 Mineral chemistry

### 3.6.1 Garnet

Generally garnet of the Tian Shan eclogite and blueschist is slightly zoned from core to rim with 60–65 mol.% almandine, 13–15 mol.% pyrope, 17–23 mol.% grossular and 3–4 mol.% spessartine compositions (Figure 3.9A, B). The mean core composition is  $\text{alm}_{0.65}\text{-prp}_{0.13}\text{-grs}_{0.18}\text{-sps}_{0.04}$  with  $X_{\text{Fe}} [\text{Fe}^{2+}/(\text{Fe}^{2+} + \text{Mg})] = 0.83$  and the mean rim composition is  $\text{alm}_{0.61}\text{-prp}_{0.15}\text{-grs}_{0.20}\text{-sps}_{0.04}$  with  $X_{\text{Fe}} = 0.80$  (Table 3.3). Occasionally, garnet core compositions show high spessartine contents (Figure 3.9A, B) up to 20 mol.% together with high almandine ( $\sim 70$  mol.%) and low grossular ( $< 1$  mol.%) and pyrope contents ( $\sim 9$  mol.%). The  $X_{\text{Fe}}$  decreases from core to rim from 0.89 to 0.80. The decrease of  $X_{\text{sps}}$  and  $X_{\text{Fe}}$  indicates a preserved prograde growth zonation. Chondrite-normalised (Boynton, 1984) REE patterns (Figure 3.10A) show the highest enrichment at Dy (25–116 times) slightly decreasing towards Lu (9–65 times). The patterns decrease steeply from

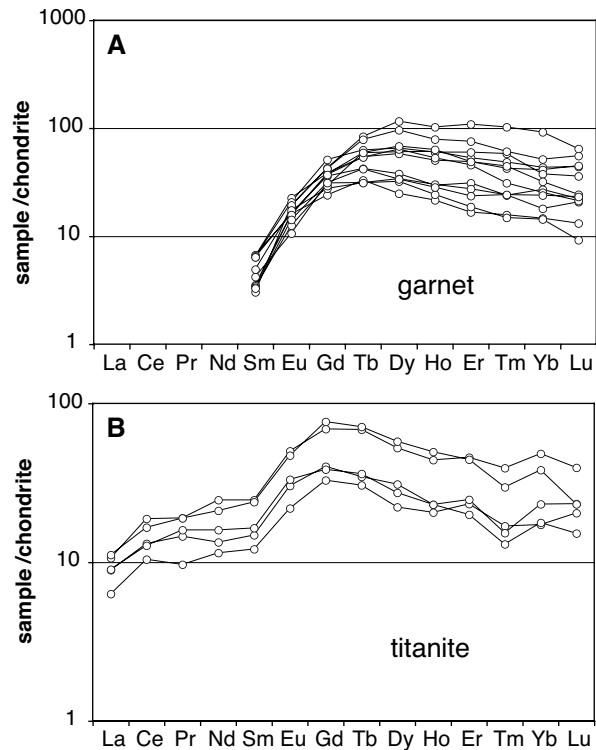


**Figure 3.10:** Chondrite-normalised REE concentrations of garnet (A) and titanite (B) of Tian Shan eclogite, analysed by in-situ LA-ICP-MS.



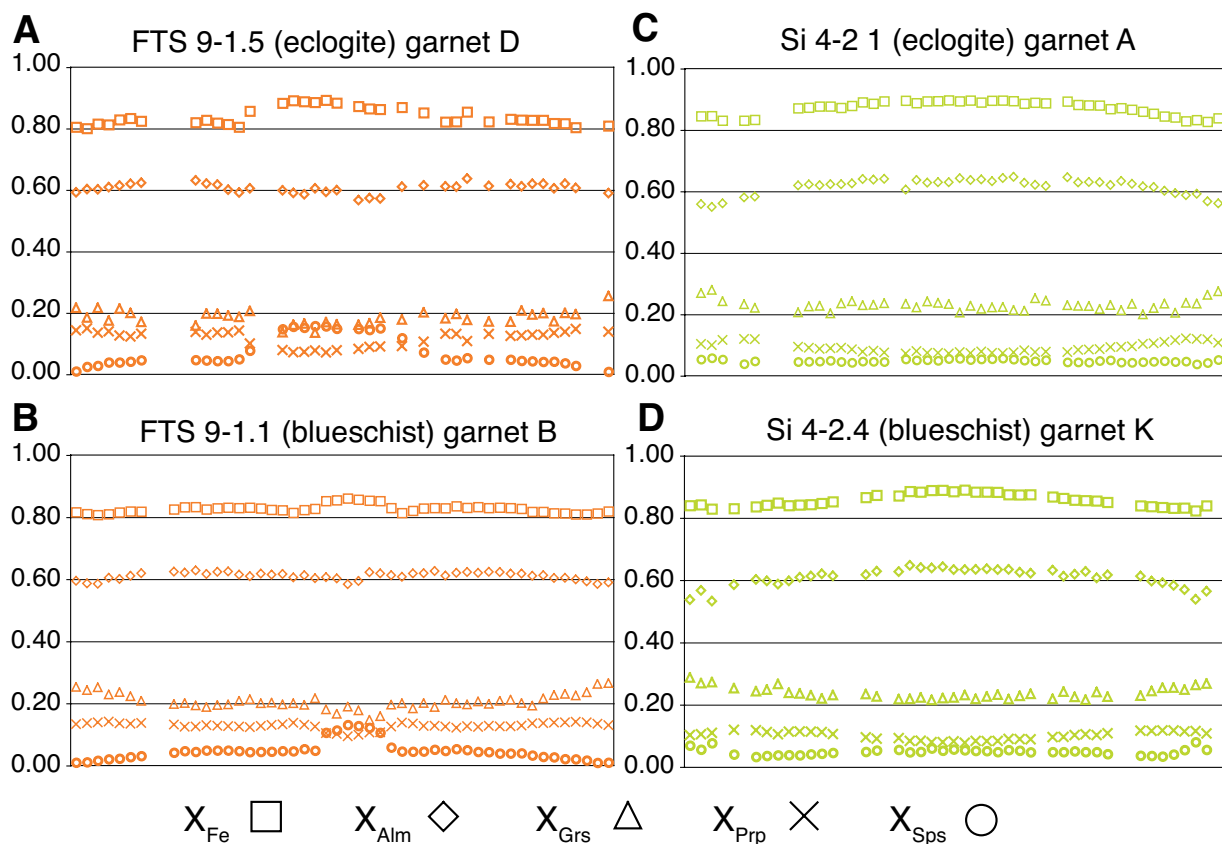


**Figure 3.9:** A + B) Mineral chemical composition of garnet in eclogite (top) and blueschist (bottom) of Tian Shan (sample FTS 9-1.5 and 9-1.1); C + D) Composition of garnet in eclogite (top) and blueschist (bottom) of Sifnos (sample Si 4-2.1 and 4-2.4).

Tb to Sm (3–6 times chondrite). LREE are usually slightly above the detection limit. Most of the incorporated transition metals (Co = ~35, Ni = ~7, Cu = ~2, Zn = ~40 ppm) are moderate in concentrations and are homogeneously distributed, whereas V and Y concentrations decrease from core to rim (~100–33 ppm V and ~200–50 Y, Table 3.1).

Garnets in the Sifnos eclogite and blueschist sequence have similar compositions and zonation pattern with 55–65 mol.% almandine, 4–6 mol.% spessartine, 7–12 mol.% pyrope and 22–29 mol.% grossular (Table 3.3, Figure 3.9C, D). All garnets have a mean core composition of  $alm_{0.65}-sps_{0.05}-prp_{0.08}-grs_{0.22}$  with  $X_{Fe} = 0.89$  and a mean rim composition of  $alm_{0.55}-sps_{0.06}-prp_{0.10}-grs_{0.29}$  of  $X_{Fe} = 0.84$ . The garnets are flatly zoned and show no typical spessartine enrichment in the core.

**Table 3.3:** Electron-microprobe analyses of garnet from Tian Shan and Sifnos samples.

Sample No.	FTS 9-1.5 341	garnet D 367	FTS 9-1.1 501	garnet B 522	Si 4-2.1 24	garnet A 48	Si 4-2.4 3	garnet K 23
Comment	core	rim	core	rim	core	rim	rim	core
SiO <sub>2</sub>	37.58	38.04	37.90	38.42	37.86	38.36	39.04	38.24
TiO <sub>2</sub>	0.16	0.01	0.21	0.06	0.07	0.04	0.02	0.05
Al <sub>2</sub> O <sub>3</sub>	20.80	21.50	21.10	21.51	21.13	21.42	21.51	21.29
Fe[tot]	26.81	28.09	26.43	27.64	28.74	27.56	24.59	29.35
Fe <sub>2</sub> O <sub>3</sub>	0.03	0.04	0.00	0.02	0.01	0.03	0.00	0.01
FeO	26.47	27.52	26.43	27.39	28.57	27.20	24.59	29.27
Cr <sub>2</sub> O <sub>3</sub>	0.28	0.05	0.00	0.15	0.08	0.06	0.25	0.07
MgO	1.81	3.77	2.40	3.62	1.90	3.09	2.84	2.05
MnO	6.90	1.28	5.87	0.95	2.23	1.75	3.51	2.73
CaO	6.37	7.65	6.71	8.50	8.68	8.92	10.10	7.87
Na <sub>2</sub> O	0.05	0.04	0.04	0.06	0.00	0.00	0.00	0.00
Total	100.46	99.90	100.66	100.68	100.54	100.87	101.86	101.58
Si	2.997	2.987	3.006	2.999	3.001	2.997	3.022	3.006
Ti	0.010	0.001	0.013	0.003	0.004	0.002	0.001	0.003
Al [IV]	0.003	0.013	0.000	0.001	0.000	0.003	0.000	0.000
Al [VI]	1.951	1.976	1.972	1.978	1.974	1.970	1.962	1.972
Fe <sup>3+</sup>	0.023	0.037	0.000	0.016	0.011	0.024	0.000	0.005
Fe <sup>2+</sup>	1.765	1.807	1.753	1.788	1.894	1.777	1.592	1.924
Cr	0.018	0.003	0.000	0.009	0.005	0.004	0.015	0.004
Mg	0.215	0.441	0.284	0.421	0.224	0.360	0.328	0.240
Ca	0.544	0.644	0.570	0.711	0.737	0.747	0.838	0.663
Na	0.008	0.005	0.006	0.010	0.000	0.000	0.000	0.000
Mn	0.466	0.085	0.394	0.063	0.150	0.116	0.230	0.182
Sum	8.00	8.00	8.00	8.00	8.00	8.00	7.99	8.00
X <sub>Prp</sub>	0.07	0.15	0.09	0.14	0.07	0.12	0.11	0.08
X <sub>Alm</sub>	0.59	0.61	0.58	0.60	0.63	0.59	0.53	0.64
X <sub>Sps</sub>	0.16	0.03	0.13	0.02	0.05	0.04	0.08	0.06
X <sub>Grs</sub>	0.16	0.20	0.19	0.23	0.24	0.24	0.27	0.22
X <sub>Adr</sub>	0.01	0.02	0.00	0.01	0.01	0.01	0.00	0.00
X <sub>Uva</sub>	0.01	0.00	0.00	0.00	0.00	0.00	0.01	0.00
X <sub>Fe</sub>	0.89	0.80	0.86	0.81	0.89	0.83	0.83	0.89

Fe<sup>3+</sup> calculated assuming stoichiometry. Number of ions on the basis of 12 O.

### 3.6.2 Clinopyroxene

All clinopyroxenes from Sifnos and the Tian Shan are classified as omphacite (Figure 3.11A, Morimoto, 1988). In the Tian Shan the omphacite inclusions in garnet have 45–48 mol.% jadeite [ $Jd = Al^{VI}/(Na + Ca)$ ], 3–6 mol.% acmite [ $Ae = (Na - Al^{VI})/(Na + Ca)$ ] and  $X_{Fe} = Fe^{2+}/(Fe^{2+} + Mg)$  of 0.22–0.28 (Table 3.4). Matrix omphacite has slightly higher jadeite contents of 46–52 mol.% and lower acmite contents of 0–3 mol.% than inclusions. The  $X_{Fe}$  values are similar at 0.21–0.25. The ratio of the jadeite component to the quadrilateral (Ca-Fe-Mg) pyroxene component ( $Jd/Q$ ) increases from 0.70 in omphacite inclusions in garnet to 1.00 in matrix omphacite (Figure 3.11). This means there is a slightly higher jadeite content in the matrix omphacite compared to the omphacite included in garnet. Omphacite inclusions and matrix omphacite show moderate Cr concentrations of ~900 ppm but sometimes up to 3.1 wt.% (Table 3.4).

**Table 3.4:** Electron-microprobe analyses of omphacite from Tian Shan and Sifnos samples.

Sample No.	FTS 9-1.5					Si 4-2.1	Si 4-2.2	Si 4-2.3	Si 4-2.4	Si 4-2.4
	108	45	423	462	566	107	244	326	269	300
Comment	in Grt	in Grt	matrix	matrix	matrix	in Grt	in Grt	matrix	matrix	matrix
SiO <sub>2</sub>	55.94	55.68	55.44	56.84	55.91	54.98	54.80	55.44	55.39	53.96
TiO <sub>2</sub>	0.06	0.00	0.08	0.06	0.06	0.04	0.12	0.05	0.06	0.01
Al <sub>2</sub> O <sub>3</sub>	10.65	8.89	10.49	12.91	12.45	8.00	6.92	9.93	9.08	9.64
Fe [tot]	5.39	5.90	3.31	3.43	3.47	7.18	8.22	4.67	5.44	7.35
Fe <sub>2</sub> O <sub>3</sub>	1.30	1.91	0.25	0.39	0.00	4.87	4.94	3.89	4.24	5.25
FeO	4.22	4.18	3.09	3.08	3.47	2.80	3.77	1.17	1.62	2.62
Cr <sub>2</sub> O <sub>3</sub>	0.14	0.10	3.10	0.49	0.72	0.03	0.00	0.14	0.12	0.12
MgO	7.73	8.37	6.96	6.92	6.91	8.51	8.48	8.32	8.31	7.29
MnO	0.12	0.13	0.01	0.01	0.00	0.10	0.14	0.08	0.09	0.10
CaO	12.67	13.73	11.42	11.08	11.31	13.83	14.16	13.47	13.76	14.47
Na <sub>2</sub> O	7.01	6.42	7.81	8.28	7.79	5.86	5.78	6.35	5.95	5.06
K <sub>2</sub> O	0.00	0.00	0.00	0.00	0.01	0.00	0.01	0.00	0.01	0.01
SrO	0.10	0.02	0.05	0.00	0.03	0.07	0.07	0.08	0.10	0.10
BaO	0.02	0.04	0.03	0.00	0.01	0.00	0.02	0.01	0.04	0.00
NiO	0.03	0.00	0.00	0.00	0.02	0.04	0.02	0.02	0.03	0.02
Total	99.99	99.47	98.72	100.06	98.70	99.12	99.24	98.94	98.79	98.65
Si	1.997	2.008	2.000	2.001	2.000	2.009	2.009	2.007	2.018	1.990
Ti	0.002	0.000	0.002	0.002	0.002	0.001	0.003	0.001	0.002	0.000
Al [IV]	0.003	0.000	0.000	0.000	0.000	0.000	0.000	0.000	0.000	0.010
Al [VI]	0.445	0.378	0.446	0.536	0.525	0.344	0.299	0.424	0.390	0.409
Fe <sub>3+</sub>	0.035	0.052	0.007	0.010	0.000	0.050	0.088	0.001	0.000	0.000
Fe <sub>2+</sub>	0.126	0.126	0.093	0.091	0.104	0.169	0.164	0.141	0.166	0.227
Cr	0.004	0.003	0.088	0.014	0.020	0.001	0.000	0.004	0.003	0.003
Mg	0.411	0.450	0.374	0.363	0.369	0.464	0.463	0.449	0.451	0.401
Mn	0.004	0.004	0.000	0.000	0.000	0.003	0.004	0.002	0.003	0.003
Ca	0.485	0.530	0.441	0.418	0.434	0.541	0.556	0.523	0.537	0.572
Na	0.485	0.449	0.546	0.565	0.540	0.415	0.411	0.446	0.420	0.362
K	0.000	0.000	0.000	0.000	0.000	0.000	0.000	0.000	0.000	0.000
Sr	0.000	0.000	0.000	0.000	0.000	0.001	0.002	0.002	0.002	0.002
Ba	0.000	0.000	0.000	0.000	0.000	0.000	0.000	0.000	0.001	0.000
Ni	0.001	0.000	0.000	0.000	0.001	0.001	0.001	0.000	0.001	0.001
Sum	4.00	4.00	4.00	4.00	4.00	4.00	4.00	4.00	3.99	3.98
X <sub>Ae</sub>	0.46	0.39	0.45	0.54	0.54	0.36	0.31	0.44	0.41	0.44
X <sub>Jd</sub>	0.04	0.07	0.10	0.03	0.02	0.07	0.12	0.02	0.03	0.00
X <sub>Fe</sub>	0.23	0.22	0.20	0.20	0.22	0.27	0.26	0.24	0.27	0.36

Fe<sup>3+</sup> calculated assuming stoichiometry.  $X_{Ae} = (Na - Al^{VI}) / (Na + Ca)$ ;  $X_{Jd} = Al^{VI} / (Na + Ca)$ . Number of ions on the basis of 6 O.

Omphacite with these high Cr concentrations usually occurs close to Cr-muscovite (fuchsite). Concentrations of MnO, Ni and V are moderate with <0.22 wt.%, ~300 ppm and 200–300 ppm, respectively. Locally, matrix omphacite has HREE concentrations near chondritic values (1–2 times chondrite) but most of the REE concentrations are below the detection limit (Table 3.1).

In the samples of Sifnos, omphacite inclusions in garnet have a jadeite content of mean 33 mol.% with a range between 25 and 40 mol.% and a acmite content of up to 13 mol.% (Figure 3.11B). The Jd/Q ratio is ~0.58. Matrix omphacite as well as omphacite grains occurring as inclusions in glaucophane, phengite or clinozoisite have jadeite contents of 29–46 mol.% (mean 39 mol.%) and acmite contents of up to 13 mol.% (mean 5 mol.%). The Jd/Q ratio increases to 0.71. The SrO (0.07–0.10), NiO (~0.02) and MnO (~0.10) concentrations in both omphacite types are very similar, whereas the Cr<sub>2</sub>O<sub>3</sub> concentration

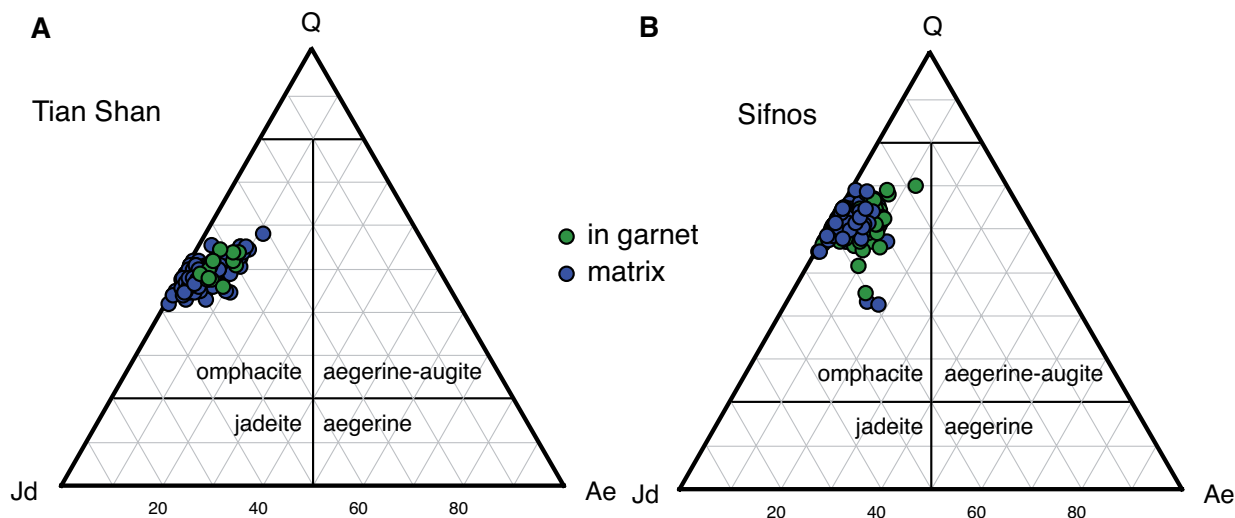


**Figure 3.11:** Clinopyroxene classification after (Morimoto, 1988). A) Clinopyroxene in Tian Shan samples is omphacite. Matrix omphacite tends to jadeite-rich composition in contrast to omphacite inclusions in garnet. B) Clinopyroxene composition of Sifnos samples is omphacite. Matrix omphacite and inclusions in garnet are similar.

increases from mean 0.05 to 0.12 wt.% and the NiO decreases from mean 0.035 to 0.024 wt.% in the matrix omphacite. The  $X_{Fe}$  value is around 0.20 to 0.30 in both omphacite types (Table 3.4).

### 3.6.3 Amphibole

Amphibole classification follows Leake et al. (1997), Figure 3.12. Glaucophane is the dominant amphibole in the Tian Shan rocks. It forms porphyroblasts in the matrix of the eclogite and blueschist, with  $X_{Fe} = 0.18\text{--}0.30$  and  $X_{Fe^{3+}} [Fe^{3+}/(Fe^{3+} + Al^{VI})] = 0.07\text{--}0.12$  (Table 3.5). Na on the B position ranges between 1.665 and 1.824 (based on 23 O, Figure 3.12A). Some porphyroblasts show a zonation with higher NiO (0.10 wt.%) and  $X_{Fe^{3+}} = 0.13$  contents in the core that are decreasing towards the rim (NiO > 0.01,  $X_{Fe^{3+}} = 0.04$ ), whereas the MnO concentration of 0.07 wt.% in the core increases towards the rim to 0.22 wt.%. Sodic-calcic amphibole with composition between barroisite, katophorite and edenite (Figure 3.12B) replaces glaucophane marginally or completely. This replacement is obvious where amphibole is in contact with garnet and omphacite. The sodic-calcic amphibole has lower NiO contents (<0.02 wt.%) but higher  $Cr_2O_3$ , MnO and  $X_{Fe^{3+}}$  contents (0.16 wt.%, 0.28 wt.% and 0.24, respectively). Glaucophane and barroisite contain both up to 100–200 ppm V, 3–6 ppm Cu and ~100 ppm Zn (Table 3.1). REE concentrations are usually below the detection limit.

The amphibole composition of the Sifnos sample varies between glaucophane, winchite and actinolite (Figure 3.12C, D; Leake et al., 1997). Isolated porphyroblastic amphibole grains are glaucophane with occasionally occurring cores of winchite and actinolite (type 1) or glaucophane cores have a rim of glaucophane of slightly different composition (type

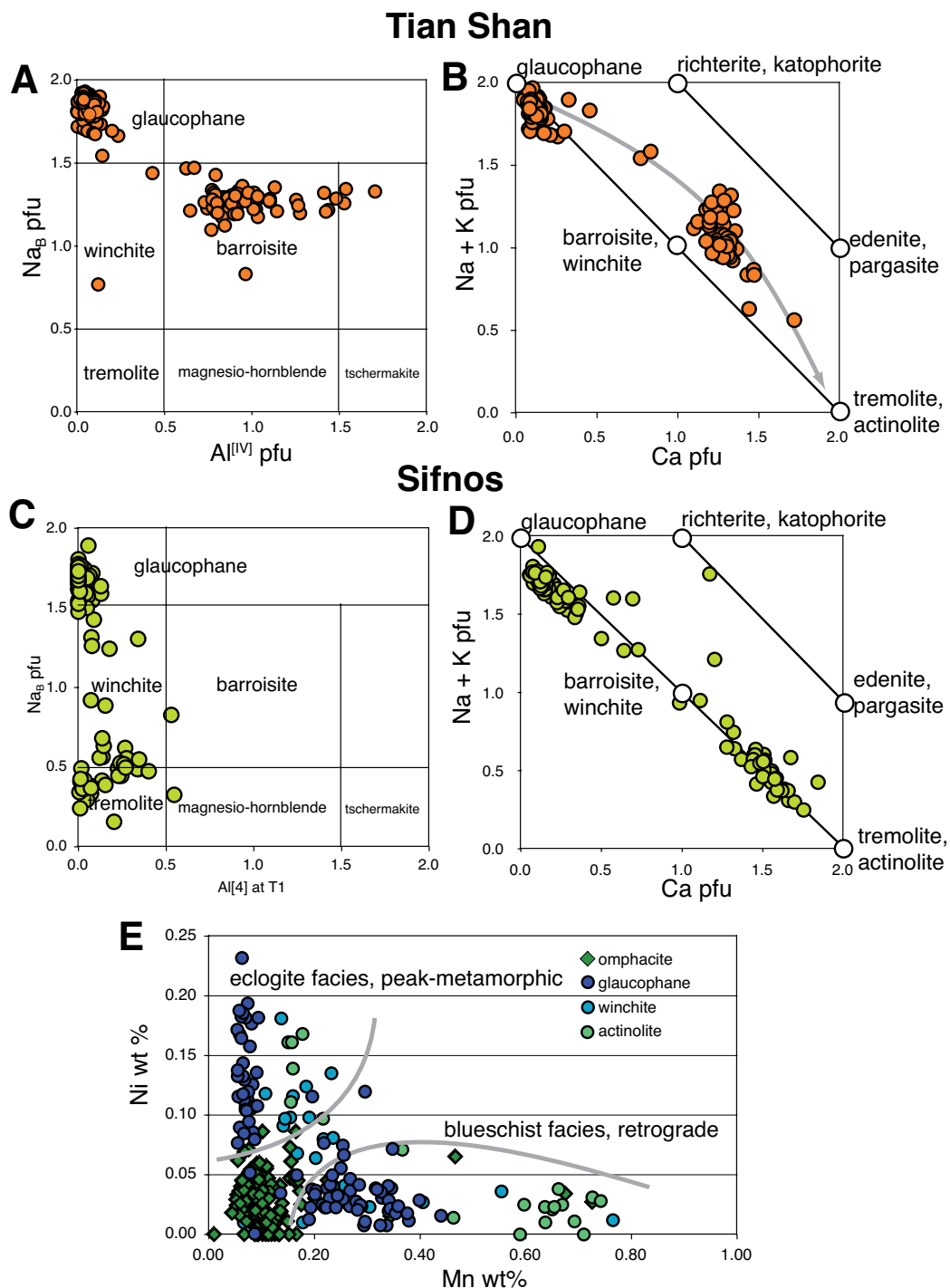


**Figure 3.12:** Amphibole classification and composition diagrams. A + B) Primary amphibole in Tian Shan samples is glaucophane. Amphibole formed during retrogression grains in contact with omphacite and garnet are sodic-calcic amphibole. Its composition is between barroisite, edenite and kataphorite (B). C + D) Amphibole in Sifnos samples ranges between glaucophane, winchite and actinolite. E) Prograde metamorphosed formed glaucophane and actinolite with high NiO and low MnO contents differ from retrograde glaucophane, winchite and actinolite with low NiO but high MnO contents.

1). Fine-grained matrix amphibole is also glaucophane (type 2). Locally, glaucophane rims are replaced by actinolite (type 2), particularly if the glaucophane is in contact with either calcite or with the relic omphacite. Glaucophane of type 1 has  $X_{Fe}$  of 0.15–0.25 and  $X_{Fe^{3+}}$  of 0.17–0.4. The MnO content is around 0.1 wt.% and the NiO concentrations are between 0.07 and 0.20 wt.% (Figure 3.12E). The  $Na_B$  varies between 1.5 and 1.77 pfu (based on 23 O). Actinolite/winchite of type 1 has  $X_{Fe}$  of 0.17–0.22 and  $X_{Fe^{3+}}$  of 0.22–0.43. MnO and NiO contents are similar in all amphiboles with values of about 0.07–0.20 wt.% and 0.14–0.20 wt.%, respectively.

**Table 3.5:** Electron-microprobe analyses of amphibole from Tian Shan and Sifnos samples.

Sample No. Comment	FTS 9-1.5					Si 4-2.4		Si 4-2.3		
	96 Bar	187 Bar	192 Bar	290 Gln core	271 Gln rim	214 Act (II)	222 Gln (II)	289 Gln (I)	290 Win (I)	294 Act (I)
SiO <sub>2</sub>	46.58	46.41	50.40	58.96	57.48	56.40	57.79	57.99	55.76	54.51
TiO <sub>2</sub>	0.33	0.19	0.19	0.00	0.07	0.06	0.00	0.04	0.03	0.09
Al <sub>2</sub> O <sub>3</sub>	13.44	13.91	10.06	11.12	11.67	1.45	10.51	11.20	6.29	4.36
Fe [tot]	14.53	15.36	12.85	7.90	7.13	7.20	8.43	7.88	8.40	8.56
Fe <sub>2</sub> O <sub>3</sub>	2.85	3.46	2.77	2.15	0.73	2.74	2.50	1.91	0.37	1.93
FeO	11.96	12.25	10.36	5.97	6.47	4.73	6.18	6.16	8.07	6.82
Cr <sub>2</sub> O <sub>3</sub>	0.18	0.20	0.16	0.05	0.21	0.03	0.02	0.01	0.04	0.05
MgO	9.85	9.13	11.86	11.47	11.20	18.56	11.47	11.03	14.75	16.43
MnO	0.12	0.03	0.07	0.03	0.01	0.69	0.08	0.07	0.17	0.16
CaO	8.24	8.00	8.10	0.83	0.81	10.57	1.54	0.78	7.38	9.74
Na <sub>2</sub> O	4.14	4.11	3.65	6.54	6.96	1.40	5.96	6.35	3.42	1.92
K <sub>2</sub> O	0.25	0.30	0.19	0.01	0.00	0.03	0.09	0.01	0.08	0.10
SrO	0.12	0.06	0.13	0.16	0.02	0.10	0.19	0.15	0.16	0.12
BaO	0.03	0.00	0.00	0.00	0.03	0.02	0.00	0.02	0.00	0.00
NiO	0.08	0.00	0.02	0.07	0.00	0.01	0.12	0.14	0.07	0.12
Total	98.17	98.04	97.96	97.35	95.65	96.79	96.45	95.86	96.57	96.35
Si	6.747	6.735	7.199	7.998	7.940	7.931	7.957	7.993	7.847	7.741
Al [IV]	1.253	1.265	0.801	0.002	0.060	0.069	0.043	0.007	0.153	0.259
Al [VI]	1.041	1.114	0.893	1.775	1.839	0.171	1.663	1.812	0.890	0.471
Ti	0.036	0.020	0.021	0.000	0.007	0.006	0.000	0.004	0.003	0.010
Fe <sup>3+</sup>	0.311	0.378	0.298	0.219	0.076	0.290	0.259	0.198	0.039	0.206
Fe <sup>2+</sup>	1.449	1.486	1.237	0.677	0.747	0.556	0.712	0.710	0.949	0.810
Cr	0.020	0.023	0.018	0.005	0.023	0.003	0.002	0.001	0.004	0.006
Mg	2.127	1.975	2.525	2.319	2.306	3.891	2.354	2.266	3.094	3.478
Mn	0.015	0.003	0.009	0.004	0.001	0.082	0.009	0.008	0.020	0.019
Ni	0.010	0.000	0.003	0.007	0.000	0.001	0.013	0.016	0.008	0.013
Ca <sub>B</sub>	1.279	1.244	1.240	0.121	0.119	1.593	0.227	0.116	1.113	1.482
Na <sub>B</sub>	0.721	0.756	0.760	1.720	1.864	0.382	1.591	1.697	0.887	0.518
Na <sub>A</sub>	0.441	0.400	0.251	0.000	0.000	0.000	0.000	0.000	0.046	0.011
K	0.046	0.055	0.035	0.001	0.000	0.005	0.016	0.002	0.015	0.019
Sr	0.010	0.005	0.010	0.013	0.001	0.008	0.015	0.012	0.013	0.029
Ba	0.002	0.000	0.000	0.000	0.002	0.001	0.000	0.001	0.000	0.010
Sum	15.51	15.46	15.30	14.86	14.99	14.99	14.86	14.84	15.08	15.08
$X_{Fe}$	0.41	0.43	0.33	0.23	0.24	0.13	0.23	0.24	0.23	0.19
$X_{Fe^{3+}}$	0.23	0.25	0.25	0.11	0.04	0.63	0.13	0.10	0.04	0.30

$Fe^{3+}$  calculated assuming stoichiometry.  $X_{Fe^{3+}} = Fe^{3+}/(Fe^{3+} + Al^V)$ . Number of ions on the basis of 23 O.

Glaucophane of type 2 differs from type 1 in slightly higher  $X_{Fe}$  but lower  $X_{Fe^{3+}}$  contents of 0.20–0.28 and 0.04–0.18, respectively. The NiO content decreases to maximum con-

centrations of 0.05 wt.%, whereas the MnO content is higher with 0.2–0.4 wt.% (Figure 3.12E). The actinolite/winchite of type 2 has similar  $X_{Fe}$  values as the actinolite/winchite of type 1 but the  $X_{Fe^{3+}}$  value and the MnO concentrations are higher with 0.29–0.71 and 0.27–0.74 wt.%, respectively, whereas the NiO content reaches maximum values of up to 0.05 wt.%, similar to the glaucophane of type 2.

### 3.6.4 White mica

**Table 3.6:** Electron-microprobe analyses of white mica from Tian Shan and Sifnos samples.

Sample No.	FTS 9-1.5 (Tian Shan)					Si 4-2.2 (Sifnos)				
	62	63	69	140	160	74	75	76	77	78
Comment	Fuc rim	Fuc core	Fuc core	Pg core	Pg rim	Phe rim	Phe	Phe	Phe	Phe core
SiO <sub>2</sub>	49.69	48.28	48.66	46.80	46.94	51.68	53.88	53.98	53.41	53.90
TiO <sub>2</sub>	0.18	0.18	0.17	0.09	0.12	0.24	0.29	0.22	0.21	0.17
Al <sub>2</sub> O <sub>3</sub>	26.61	25.29	24.84	39.96	38.44	26.21	27.33	26.67	26.46	26.13
Fe [tot]	1.48	1.55	1.55	0.18	0.49	4.37	2.37	3.35	3.22	3.01
Cr <sub>2</sub> O <sub>3</sub>	2.98	6.20	7.03	0.16	0.36	0.25	0.27	0.27	0.39	0.25
MgO	3.16	2.73	2.80	0.15	0.41	3.65	3.65	3.59	3.59	3.78
MnO	0.01	0.03	0.05	0.02	0.01	0.10	0.01	0.00	0.04	0.00
CaO	0.00	0.00	0.00	0.19	0.11	0.10	0.03	0.13	0.07	0.05
Na <sub>2</sub> O	0.81	0.85	0.77	7.42	7.10	0.49	0.51	0.38	0.39	0.27
K <sub>2</sub> O	9.96	9.84	9.75	0.48	0.95	10.42	10.66	10.10	9.97	10.71
F	0.00	0.00	0.00	0.00	0.00	0.00	0.00	0.00	0.00	0.00
Cl	0.01	0.00	0.00	0.00	0.00	0.02	0.00	0.01	0.01	0.00
Total	94.89	94.94	95.62	95.45	94.93	97.53	99.01	98.69	97.76	98.27
Si	3.347	3.291	3.298	2.981	3.018	3.409	3.454	3.475	3.471	3.491
Ti	0.009	0.009	0.009	0.004	0.006	0.012	0.014	0.010	0.010	0.008
Al [IV]	0.644	0.700	0.693	1.015	0.976	0.579	0.532	0.515	0.519	0.501
Al [VI]	1.468	1.332	1.291	1.986	1.937	1.458	1.533	1.509	1.508	1.494
Fe	0.083	0.088	0.088	0.009	0.026	0.242	0.127	0.181	0.175	0.163
Cr	0.159	0.334	0.377	0.008	0.018	0.013	0.014	0.014	0.020	0.013
Mg	0.317	0.278	0.283	0.014	0.039	0.359	0.349	0.345	0.348	0.365
Mn	0.000	0.002	0.003	0.001	0.001	0.005	0.001	0.000	0.002	0.000
Ca	0.000	0.000	0.000	0.013	0.007	0.007	0.002	0.009	0.005	0.004
Na	0.106	0.113	0.101	0.917	0.885	0.063	0.064	0.047	0.049	0.034
K	0.856	0.855	0.843	0.039	0.078	0.877	0.872	0.830	0.827	0.885
F	0.000	0.000	0.000	0.000	0.000	0.000	0.000	0.000	0.000	0.000
Cl	0.001	0.000	0.000	0.000	0.000	0.002	0.000	0.001	0.001	0.000
Sum	6.99	7.00	6.99	6.99	6.99	7.03	6.96	6.94	6.93	6.96
$X_{Fe}$	0.21	0.24	0.24	0.40	0.40	0.40	0.27	0.34	0.33	0.31
$X_{Na}$	0.11	0.12	0.11	0.95	0.91	0.07	0.07	0.05	0.06	0.04

Fe<sup>3+</sup> calculated assuming stoichiometry.  $X_{Na} = Na/(Na + Ca + K)$ . Number of ions on the basis of 11 O.

White mica in the Tian Shan occurs as I) inclusion in garnet, which is phengite with Si ~3.40 pfu (based on 11 O), II) as light greenish porphyroblast in the matrix, which is fuchsite with up to 7 wt.% Cr<sub>2</sub>O<sub>3</sub>, and III) as colourless porphyroblast in the matrix, which is paragonite with  $X_{Na}$  [Na/(Na + Ca + K)] = 0.86–0.96 (Figure 3.13A,B, Table 3.6). White mica contains up to 50 ppm B. Fuchsite contains high concentrations of Ba (~6000 ppm), Cs (~5 ppm) and Rb (~200 ppm). The values for those elements are much lower in paragonite (Table 3.1). Sr and Pb concentrations are in paragonite and fuchsite about 800

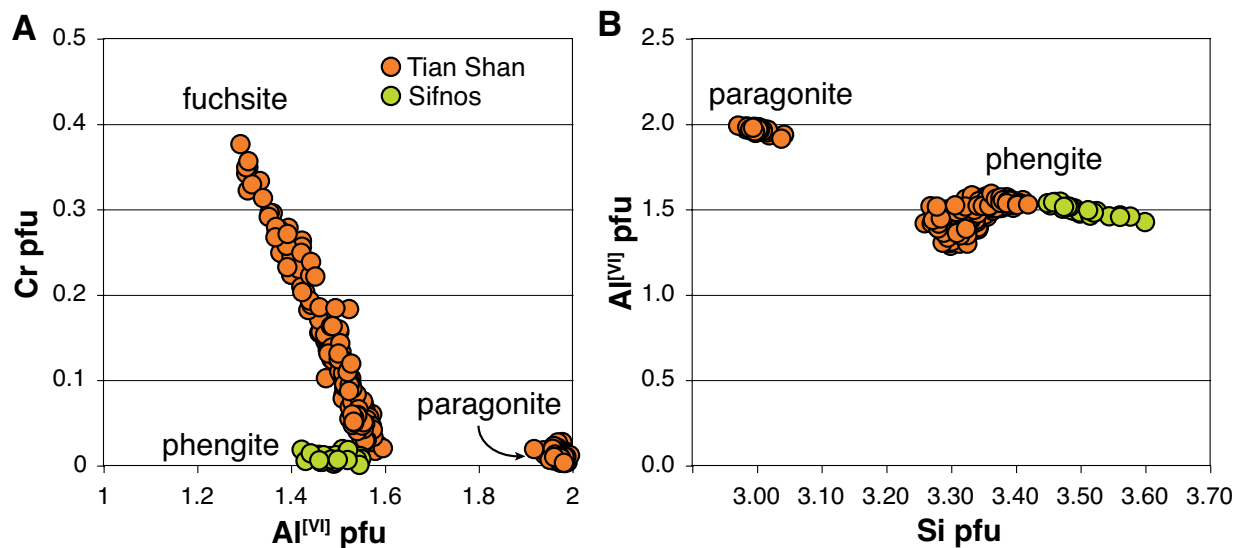


**Figure 3.13:** White mica composition of Sifnos and Tian Shan samples. White mica of Tian Shan samples is phengite (with compositions to fuchsite) and paragonite. White mica of Sifnos samples is phengite.

and 10 ppm, respectively. The Cr concentration in paragonite is  $\sim 800$ – $1000$  ppm and that of V and Ni are  $\sim 50$  ppm and  $\sim 5$  ppm, respectively. They are higher in fuchsite component with 300 ppm V and 60 ppm Ni. REE are usually below the detection limit (Table 3.1). White mica in Sifnos sample is phengite (Figure 3.13A,B) with  $X_{Na}$  [ $Na/(Na + Ca)$ ] between 0.03 and 0.09. The Si content decreases from core to rim from 3.57–3.45 pfu together with increasing  $X_{Fe}$  of 0.23–0.40 (Table 3.6).

### 3.6.5 Epidote mineral

Clinzoisite in the Sifnos samples (nomenclature after Armbruster et al., 2006) can be divided into two texture types. Type 1 occurs as inclusion in garnet and has  $X_{Fe^{3+}}$  [ $Fe^{3+}/(Fe^{3+} + Al^{VI})$ ] of 0.09–0.28 and Sr of 0.008–0.014 pfu (Figure 3.14). Type 2 represents matrix clinzoisite with  $X_{Fe^{3+}}$  of 0.14–0.20 and higher Sr contents of 0.014–0.04 pfu (Table 3.7).

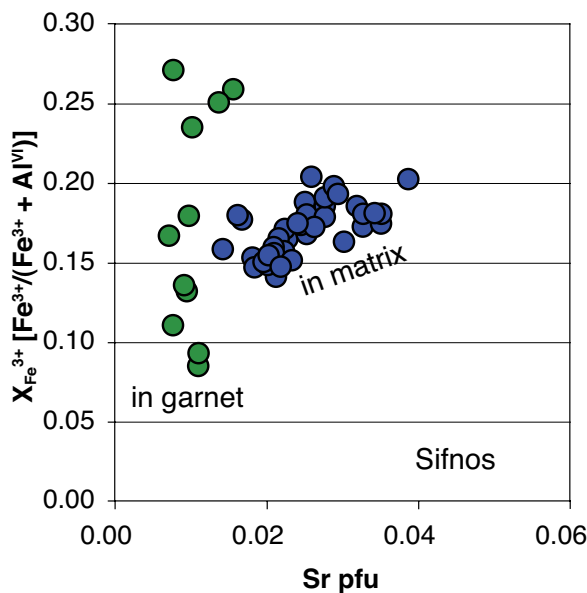


**Figure 3.14:** Clinozoisite of Sifnos eclogite and blueschist. Clinozoisite in garnet has lower SrO contents than clinozoisite in matrix.



### 3.6.6 Other minerals

*Tian Shan*: Carbonate is calcite with mean  $X_{Ca}$  [ $Ca/(Ca + Mg + Fe + Mn)$ ] = 0.94 (Table 3.7). The remaining 6 mol.% of calcite are composed of 3.8–4 mol.% siderite and 2–2.2 mol.% magnesite. Calcite contains ~2000–4000 ppm Mn, 1500–2500 ppm Sr and in minor amounts Co (~35 ppm), Ni (~100 ppm), Zn (80–100 ppm) and Pb (12–16 ppm, Table 3.1). Feldspar is nearly pure albite with  $X_{Na}$  [ $Na/(Na + Ca + K)$ ] = 0.97–0.99 (Table 3.7). Titanite contains some amounts of transition metals (~140 ppm V, ~400 ppm Cr, ~20 ppm Co, <240 ppm Ni, <40 ppm Cu) and 200–500 ppm Mn, which increase to 4000 ppm in contact with garnet. Chondrite-normalised REE patterns show enrichments from Gd to Lu and decreasing slope towards La (Figure 3.10B, Table 3.1). The highest enrichments are in Gd (33–77 times chondrite, ~17 ppm) till Lu (15–39 times chondrite, ~1.27 ppm). La (~3 ppm) is 6–11 times enriched to chondrite.

**Table 3.7:** Electron-microprobe analyses of feldspar, calcite, chlorite and clinzoisite from Tian Shan and Sifnos samples.

Sample No.	FTS 9-1.5		Si 4-2.4		Si 4-2.2	FTS 9-1.5	Si 4-2.1		Si 4-2.5	
	63	164	59	60	194	34	203	207	126	319
Comment	Ab	Ab	Ab	Ab	Cc	Cc	Chl	Chl	Czo	Czo
SiO <sub>2</sub>	69.59	67.70	67.94	67.87	0.03	0.07	29.71	32.13	37.86	39.03
TiO <sub>2</sub>	0.00	0.03	0.04	0.01	0.03	0.00	0.00	0.00	0.05	0.04
Al <sub>2</sub> O <sub>3</sub>	19.18	21.55	19.41	19.18	0.02	0.02	19.15	18.94	26.24	28.37
FeO[tot]	0.40	0.15	0.33	0.39	0.31	2.54	13.19	13.22	8.60	6.78
Cr <sub>2</sub> O <sub>3</sub>	0.03	0.03	0.02	0.00	0.00	0.65	0.05	0.00	0.24	0.22
MgO	0.26	0.03	0.03	0.03	0.26	1.12	23.91	22.09	0.09	0.04
MnO	0.01	0.06	0.04	0.01	0.16	0.00	0.80	0.67	0.13	0.24
CaO	0.54	0.37	0.23	0.17	62.61	57.22	0.08	0.27	22.56	23.74
Na <sub>2</sub> O	11.37	10.75	11.03	10.96	0.02	0.01	0.00	0.64	0.01	0.01
K <sub>2</sub> O	0.01	0.04	0.03	0.02	0.00	0.01	0.01	0.02	0.00	0.01
SrO	0.03	0.06	0.26	0.28	0.00	0.00	0.00	0.00	0.71	0.17
Total	101.50	100.83	99.03	98.52	63.13	59.11	86.91	87.98	96.49	98.64
Si	3.002	2.933	2.991	3.000	0.001	0.002	5.955	6.391	3.013	3.010
Ti	0.000	0.001	0.001	0.000	0.001	0.000	0.000	0.000	0.003	0.002
Al [IV]	0.000	0.067	0.009	0.000	0.000	0.000	2.045	1.609	0.000	0.000
Al [VI]	0.975	1.033	0.998	0.999	0.001	0.001	2.480	2.830	2.461	2.579
Fe*	0.015	0.005	0.012	0.014	0.023	0.096	2.821	2.779	0.515	0.393
Cr*	0.001	0.001	0.001	0.000	0.000	0.016	0.008	0.000	0.015	0.013
Mg	0.017	0.002	0.002	0.002	0.012	0.051	7.145	6.550	0.010	0.004
Mn	0.000	0.002	0.002	0.000	0.004	0.000	0.136	0.113	0.008	0.014
Ca	0.025	0.017	0.011	0.008	1.974	1.865	0.018	0.057	1.924	1.962
Na	0.951	0.903	0.941	0.939	0.001	0.000	0.000	0.245	0.002	0.002
K	0.001	0.002	0.001	0.001	0.000	0.000	0.003	0.006	0.000	0.001
Sr	0.001	0.001	0.007	0.007	0.000	0.000	0.000	0.000	0.033	0.008
Sum	4.986	4.968	4.976	4.971	1.992	1.935	20.61	20.58	7.977	7.975
$X_{Na}$	0.97	0.98	0.99	0.99						
$X_{Ca}$					0.98	0.93				
$X_{Fe^{2+}}$					0.66	0.66	0.28	0.30	0.98	0.99
$X_{Fe^{3+}}$									0.17	0.13

Fe<sup>3+</sup> calculated assuming stoichiometry.  $X_{Na} = Na/(Na + Ca + K)$ ;  $X_{Ca} = Ca/(Ca + Mg + Fe^{2+} + Mn)$ ;  $X_{Fe^{3+}} = Fe^{3+}/(Fe^{3+} + Al^{VI})$ . Number of ions on the basis of 8 O (feldspar), 6 O (carbonate), 36 O (chlorite) and 11.5 O (clinzoisite).

*Sifnos*: Carbonate is calcite with minor siderite, magnesite and rhodochrosite components. The  $X_{Ca}$  is around 0.94–1.00 (Table 3.7), whereas the remaining 0–6 mol.% is composed of 3.2–5.2 mol.% siderite, followed by 0.4–1.9 mol.% magnesite and 0.3–1.1 mol.% rhodochrosite component. Calcite rims in contact with glaucophane show higher amounts of (1.4–2.9 mol.%) of rhodochrosite, siderite (2.5–3.7 mol.%) and magnesite (1–1.3 mol.%) component. Chlorite is a Mg-dominated Fe-Mg-chlorite with  $X_{Fe}$  of 0.27 to 0.30. Feldspar is nearly pure albite with  $X_{Na}$  of 0.96–1.00 (Table 3.7).

## 3.7 Discussion

### 3.7.1 Nature of the eclogite protholiths

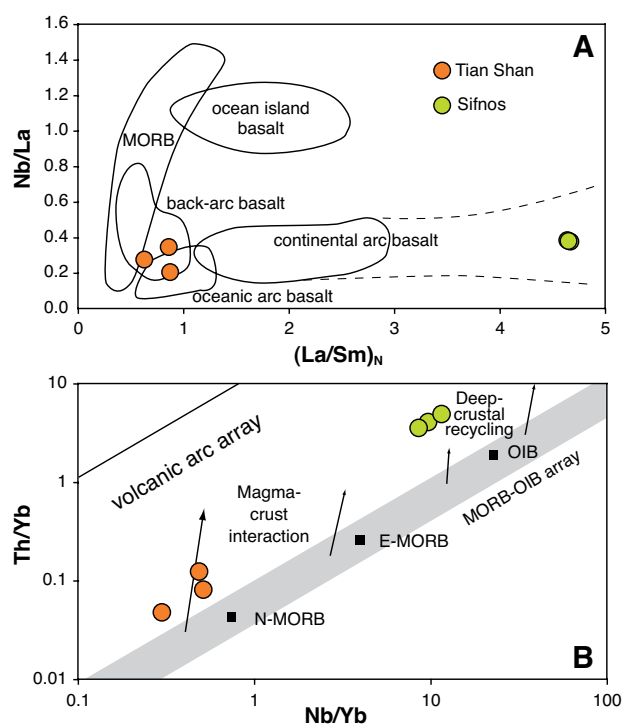


**Figure 3.15:** Chondrite-normalised (Boynton, 1984) La/Sm vs. Nb/La diagram modified after John et al. (2003). Eclogites of Sifnos plot in the continental island arc field, whereas the eclogites of the Tian Shan indicate back-arc basalt affinities. B) Nb/Yb vs. Th/Yb plot, modified after (Pearce, 2008), indicate deep-crustal recycling in the island arc array for eclogites of Sifnos and magma-crust interaction for eclogites from South Tian Shan.

The Tian Shan and Sifnos eclogites are formed from basaltic precursors. Both eclogites differ in their trace element chemistries. Their chemical characteristics allow for suggestions in which geodynamic setting their basaltic precursor melts have been generated. The chondrite-normalised (Boynton, 1984) REE pattern of the Tian Shan eclogite shows similarities in MREE and HREE to the pattern of average oceanic island arc basalt (Kelemen et al., 2003), whereas the LREE are better resembling those of average boninites (Kelemen et al., 2003, Figure 3.7). The N-MORB-normalised (Hart et al., 1999) REE of the eclogite differs from the average island arc basalt, as it is too flat and the Nb-Ta anomaly is very pronounced. Instead, the N-MORB-normalised trace element pattern of the eclogite is similar to depleted oceanic basalts from the rear-arc in the Pacific Vanuatu archipelago (Peate et al., 1997), with which they coincide in most of the trace elements (Figure 3.8A). Low  $(La/Sm)_N$  and Nb/La point on an oceanic island arc and back-arc basalt affinity (Figure 3.15A). Hence, the eclogite protholiths likely derive from magma generated in the back-arc area. Low Nb/Yb and

Th/Yb ratios of the eclogites, which plot at the transition of N-MORB and the island arc array, a feature that may be caused by magma-crust interaction are also in agreement with a back-arc setting (Figure 3.15B, Pearce, 2008).

The N-MORB-normalised trace element pattern of the Sifnos eclogite is more enriched than the pattern of average oceanic island arc basalt, except for the HREE. A better correlation is given in the HFSE contents (Zr-Hf, TiO<sub>2</sub> and Nb-Ta) of the eclogites with those of the average continental island arc basalt (CIAB Kelemen et al., 2003), but the LREE and LILE are still more enriched compared to CIAB. High LREE concentrations result in high (La/Sm)<sub>N</sub> = 4.8 at low La/Nb ~0.4 indicating magma-crust interaction (John et al., 2003). The Sifnos eclogite plots at higher (La/Sm)<sub>N</sub> ratios outside of the continental island arc field in Figure 3.15A, but might nevertheless be attributed to the continental arc setting. The high Nb/Yb at high Th/Yb values support the interpretation of strong crustal assimilation (Pearce, 2008, Figure 3.15B). In summary, a continental island arc basalt can be assumed as the precursor of the Sifnos eclogite.

### 3.7.2 P-T path and metamorphic evolution

*Tian Shan:* The most pristine eclogite (sample FTS 9–1.5A) is best suitable for estimating the prograde P-T conditions and to reconstruct the P-T path of the Tian Shan eclogite-blueschist sequence, as the mineral assemblage of FTS 9–1.5A shows only minor features for metasomatism. The P-T path has been reconstructed on the basis of P-T pseudosections calculated with *Perple\_X* (Table A.5, Connolly, 1990) in the TiKCNMnFMASH system with a water activity of 1 (Figure 3.16A). Prograde metamorphic conditions can be estimated from inclusions of white mica, amphibole, omphacite, minor clinozoisite, rutile, titanite and quartz in garnet. Lawsonite or pseudomorphs after lawsonite were found neither as inclusion nor in the matrix. Thus a metamorphic evolution through the lawsonite stability field (<400°C at 11 kbar and <600°C at 22 kbar) seems to be unlikely. The Fe–Mg exchange thermometer calibration of Powell (1985) applied to omphacite inclusions in garnet and garnet cores, results in prograde temperatures of 560±20°C at 10 kbar (Figure 3.16F). Phengite inclusions are present in garnet but paragonite inclusions are lacking. The stability field of white mica + amphibole + garnet + zoisite + titanite + albite restricts the burial from 500–575°C at 10 to 14 kbar (Figure 3.16A). Burial at higher temperatures than 525°C at 8kbar and 800°C at 16kbar can be excluded, as at these conditions biotite would be a stable phase (Figure 3.16A); however, biotite was not found in the investigated samples. Omphacite growth indicates conditions of P >14 kbar and T <700°C, at which the jadeite content increases immediately to values above 40 mol.%, corresponding to X<sub>Na</sub> [Na/(Na + Ca)] isopleths in omphacite of 0.40 (Figure 3.16C). Jadeite contents of matrix omphacite reach values of up to 54 mol.% (Table 3.4). This corresponds to a condition of >650°C and 16kbar in the P-T pseudosections. Prograde burial is documented by decreasing X<sub>Fe</sub> values of 0.90 to 0.80 in garnet cores corresponding to decreasing X<sub>Fe</sub> [Fe<sup>2+</sup>/(Fe<sup>2+</sup> + Mg)] isopleths (Figure 3.9, 3.16B) up to peak-metamorphic temperatures <700°C. Peak-metamorphic pressures are difficult to estimate, as Si isopleths in white mica (Figure 3.16D) and calculated whole rock density isopleths (Figure 3.16E) are the only pa-

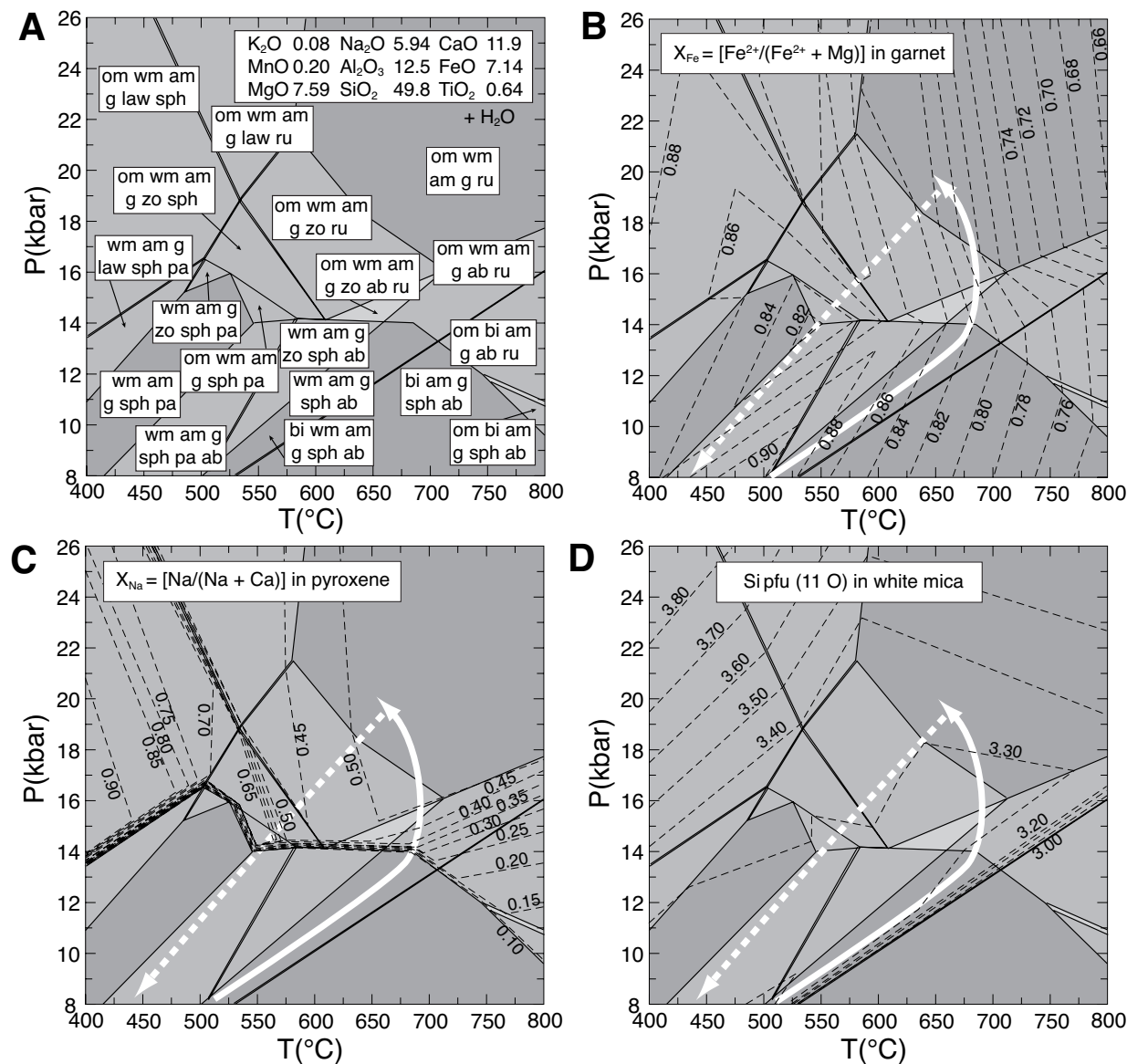


**Figure 3.16:** P-T pseudosection for the Tian Shan eclogite FTS 9–1.5 A calculated with the given whole rock composition in the TiKCNMnFMASH system (ab = albite, am = amphibole, bi = biotite, chl = chlorite, g = garnet, law = lawsonite, om = omphacite, pa = paragonite, ru = rutile, sph = titanite, wm = white mica of phengite and muscovite composition, zo = zoisite). Increasing grey-scale corresponds to higher variance (quadri-, five-, six- and seven-variance); white arrow indicates the deduced P-T path. B)  $X_{Fe}$  isopleths of garnet, C)  $X_{Na}$  isopleths of clinopyroxene, nearly identical to jadeite content, D) Si pfu isopleths of white mica.

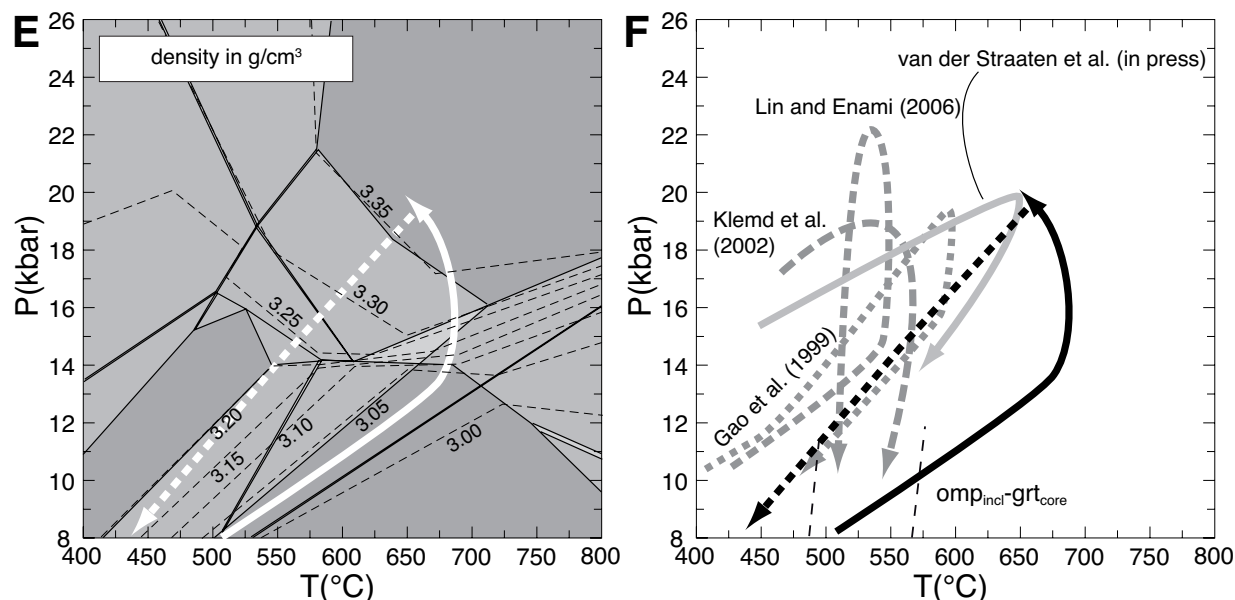


**Figure 3.16:** (cont.) P-T pseudosection for the Tian Shan eclogite FTS 9–1.5 A calculated with the given whole rock composition in the TiKCNMnFMASH system. Increasing grey-scale corresponds to higher variance (quadri-, five-, six- and seven-variance); white arrow indicates the deduced P-T path. E) density isopleths, F) Comparison of published P-T paths from the Tian Shan. Thin dashed lines are temperature calibration by Fe–Mg exchange thermometry (Powell, 1985) from omphacite inclusions and garnet compositions.

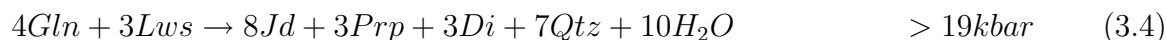
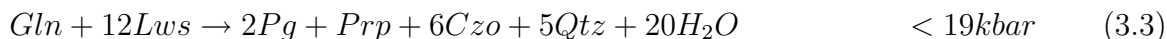
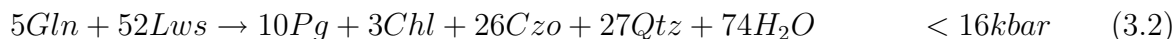
rameters for pressure estimates. Phengite in matrix and phengite inclusions in garnet show maximum Si contents of 3.40 pfu (based on 11 O), which would imply 22 kbar at 650°C in the P-T pseudosections. The measured density of 3.34 g/cm<sup>3</sup> of sample FTS 9-1.5A would imply 21 kbar at 600°C at the corresponding density isopleth in the P-T pseudosection. In summary, peak-metamorphic conditions of ~20 kbar and ~650°C can be assumed in the stability field of the assemblage omphacite + white mica + amphibole + garnet + rutile (Figure 3.16A). Titanite and paragonite in the matrix of sample FTS 9–1.5A imply retrograde cooling and decompression to conditions <16 kbar and <600°C (Figure 3.16A), which is in the stability field of the assemblage omphacite + white mica + amphibole + garnet + titanite + paragonite. A very rapid isothermal decompression might explain the formation of poikiloblastic titanite that includes the fine-grained omphacite matrix (Figure 3.4A). The breakdown of the eclogite-facies assemblage omphacite and garnet (Figure 3.3B) can be described e.g. with the following simplified reaction after Bucher and Frey (2002):



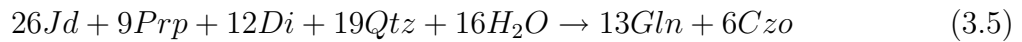
This reaction is poorly developed in the eclogite but distinctly in the blueschist. Albite grows due to the breakdown of the jadeite component in omphacite (Figure 3.3C). The retrograde uplift path can be assumed to have taken place within the stability field of the assemblage white mica + amphibole + garnet + titanite + paragonite + albite at <550°C

and 14 kbar (Figure 3.16).

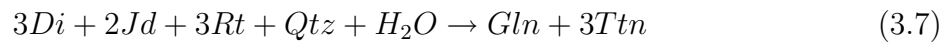
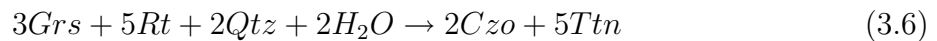
*Sifnos*: The bulk composition of the eclogite sample Si 4-2.1 together with the mineral chemical data have been used to reconstruct the P-T path for the eclogite-blueschist sequence. Fe–Mg exchange thermometers, the garnet-pyroxene-phengite barometer and the jadeite-albite-quartz barometers were applied and combined with P-T pseudosections and isopleth diagrams (calculated with Perple\_X Connolly, 1990, in the TiKCNMnFMASH system with  $a_{H_2O} = 1$ ) to obtain the P-T path shown in Figure 3.17A. Calcite as the only carbonate is not considered in the calculation. Hence, the bulk rock CaO content was reduced for about 3.70 wt.%, related to the measured 2.97 wt.% CO<sub>2</sub> content. Temperatures were estimated by the omphacite-garnet thermometer calibration (Powell, 1985) at  $610 \pm 15^\circ\text{C}$  and by the garnet-phengite thermometry calibration (Green and Hellman, 1982) at  $550 \pm 15^\circ\text{C}$  (Figure 3.17B). Application of the jadeite-albite-quartz barometer calibrations (Gasparik and Lindsley, 1980; Holland, 1980), point to minimum pressures of 13–14.5 kbar at  $600^\circ\text{C}$  and ca 11 kbar at  $450^\circ\text{C}$ . The garnet-pyroxene-phengite barometer calibration (Waters and Martin, 1993) gives pressures of around  $20.5 \pm 2$  kbar for the omphacite<sub>inclusion</sub>–garnet<sub>core</sub>–matrix phengite<sub>core</sub> composition at Si contents of 3.50–3.59 pfu (based on 11 O), and  $16.5 \pm 1$  kbar for omphacite<sub>matrix</sub>–garnet<sub>rim</sub>–matrix phengite<sub>rim</sub> compositions at Si contents of 3.40–3.46 pfu. Peak-metamorphic conditions can be estimated at  $600^\circ\text{C}$  and  $< 20$  kbar, related to the observed mineral assemblage omphacite + garnet + amphibole + white mica + rutile and the applied thermometers and barometers (Figure 3.17B). Within the stability field of the latter assemblage the  $X_{Na}$  [Na/(Na + Ca)] isopleth of 0.42 in omphacite correlates with the highest measured jadeite content in omphacite indicating a metamorphic pressure at 20 kbar (Figure 3.17C). A prograde temperature increase from 400 to  $600^\circ\text{C}$  is indicated by the garnet core to rim  $X_{Fe}$  [ $\text{Fe}^{2+}/(\text{Fe}^{2+} + \text{Mg})$ ] values of 0.89 to 0.80 and indicated by the corresponding  $X_{Fe}$  isopleths in Figure 3.17D. Decreasing Si contents from core to rim in phengite (3.50 to 3.40 Si pfu based on 11 O) at a constant  $X_{Na}$  [(Na/(Na + K))] value of 0.02 in phengite constrain the burial path to peak-metamorphic conditions (Figure 3.17E, F). The prograde low-temperature assemblage chlorite + white mica + amphibole + garnet + lawsonite + titanite obtained in the P-T pseudosection calculation is in accordance with the petrographically observed mineral inclusions in garnet. However, lawsonite occurs only as pseudomorphs consisting of chlorite, clinozoisite and white mica described already by former workers (Okrusch et al., 1978; Schmädicke and Will, 2003). The lawsonite breakdown can occur through several reactions (Evans, 1990), three of which are listed in order of increasing pressure conditions:



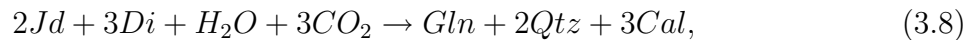
Since lawsonite occurs only as pseudomorphs in garnet and not as relics in the matrix, we assume an early prograde breakdown of lawsonite below 17 kbar. Thus, the rock has left the lawsonite stability field at around 500°C (Figure 3.17A) during burial. At the same conditions rutile becomes stable. Prograde rutile crystallisation temperatures of 445-505°C were determined by (Spear et al., 2006) on Sifnos samples from the same area, which correlates with our P-T pseudosection calculations (Figure 3.17A). Retrograde conditions can be constrained by  $\text{Na}_B$  pfu isopleths in amphibole,  $X_{Na}$  isopleths in white mica and by density isopleths.  $\text{Na}_B$  contents of amphibole porphyroblasts, having a calcic amphibole core and a sodic amphibole rim, correlate with  $\text{Na}_B$  isopleths in amphibole core of 0.90 pfu (based on 23 O) at peak metamorphic conditions, and increasing  $\text{Na}_B$  contents (1.80 pfu at rim) during uplift (Figure 3.17G). Measured  $X_{Na}$  in phengite (core to rim) are in accordance to increasing  $X_{Na}$  isopleths of 0.02 to 0.04 in phengite. The bulk rock density calculated in the P-T pseudosection would decrease from  $>3.30 \text{ g/cm}^3$  to  $<3.20 \text{ g/cm}^3$  during retrogression (Figure 3.17H). These calculated densities cannot be correlated with the measured densities, as calcite has not been included in the calculation, which would reduce the density. The retrograde P-T path can be constructed until the stability field of chlorite + white mica + amphibole + garnet + zoisite + titanite is reached, which is the observed mineral assemblage in the blueschist. The retrograde P-T path is characterised by cooling and decompression. Isothermal decompression can be excluded for the Sifnos samples as biotite and amphibole with Mg-hornblende or tschermakite composition would become stable, minerals that do not occur. During uplift, the eclogite-facies assemblage omphacite and garnet broke down to the blueschist-facies minerals glaucophane, phengite and clinozoisite described by the following reaction (e.g., Evans, 1990):



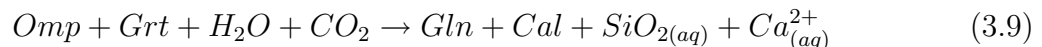
Late-stage glaucophane and clinozoisite growth is verified in the Sifnos sample, whereas the new growth of phengite, as it is described by Reaction 3.1 can be excluded here, because the amount of phengite is similar in the eclogite and the blueschist. During progressive uplift, at  $<550^\circ\text{C}$  and  $<16 \text{ kbar}$ , as indicated by the P-T pseudosection and petrographic evidence, rutile becomes unstable and will be consumed by titanite formation:



Released  $\text{Ca}^{2+}$ , e.g. due to the breakdown of omphacite or garnet, may react with  $\text{CO}_2$ -rich fluids to form calcite. A possible calcite forming reaction can be expressed stoichiometrically:



or by unbalanced equation, in which Ca and Si ions are assumed to be removed from the system:



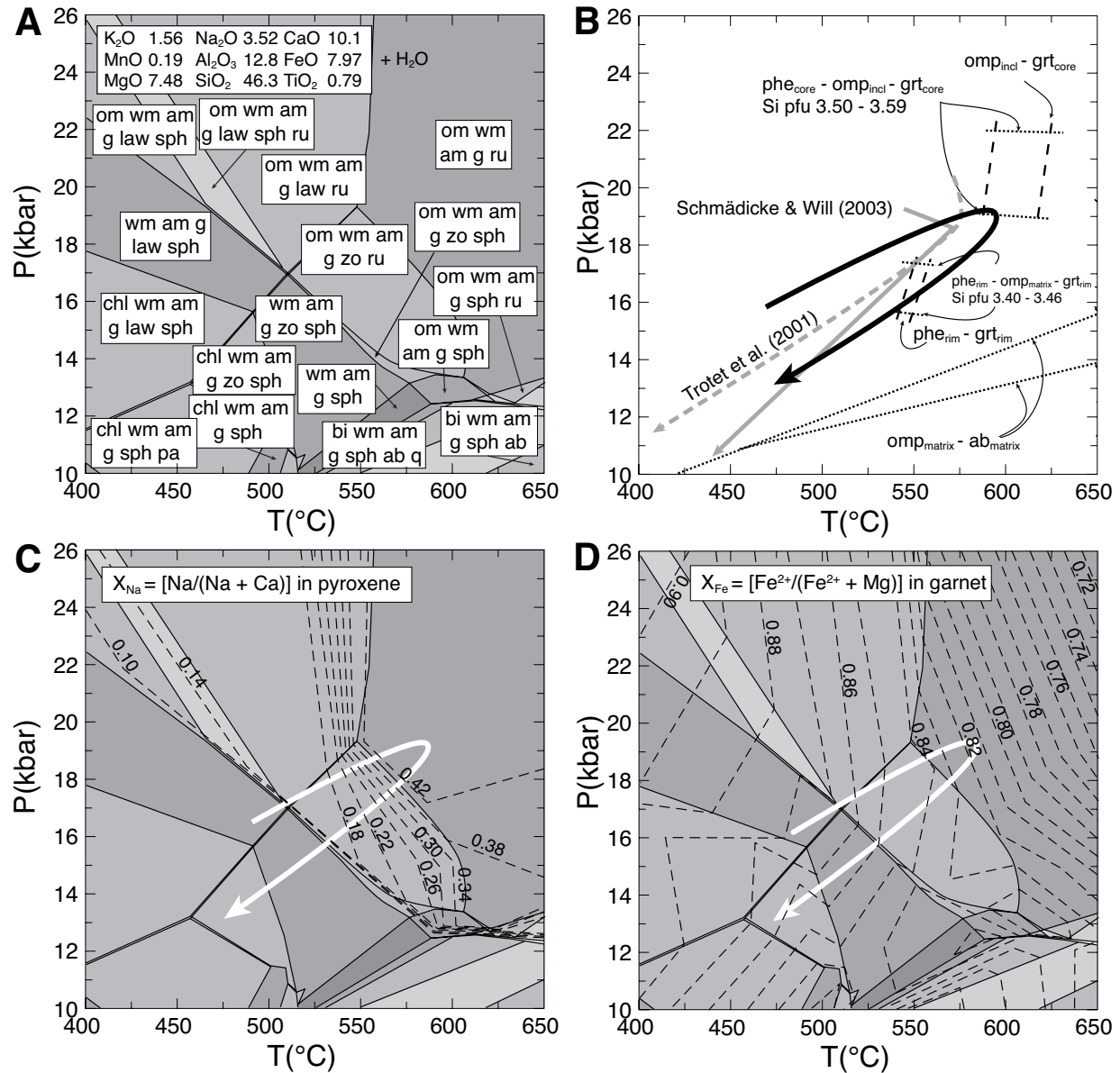


**Figure 3.17:** A) P-T pseudosection of Sifnos eclogite Si 4-2.1 calculated with the given whole rock composition in the TiKCNMnFMASH system (same mineral abbreviations than in Figure 3.16). The CaO content is recalculated concerning 2.97 wt%  $CO_2$  in Calcite. Increasing grey-scale corresponds to higher variance (quadri-, five-, six- and seven-variance); white arrow indicates the deduced P-T path. B) results of applied geothermometer and -barometer (see text for used calibrations) and selected P-T paths of Sifnos from literature for comparison, C)  $X_{Na}$  isopleths of clinopyroxene, similar to jadeite content, D)  $X_{Fe}$  isopleths of garnet.



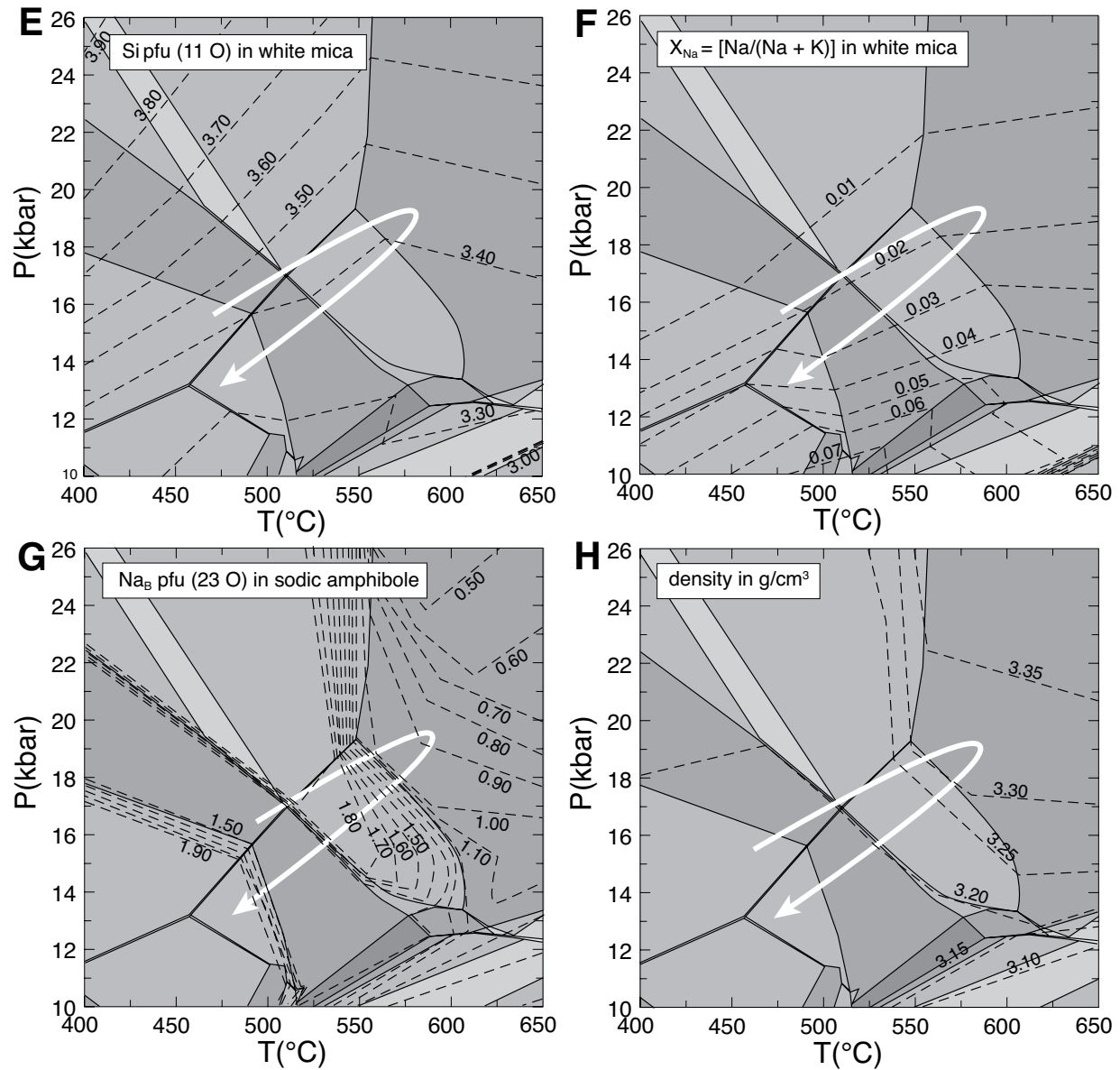
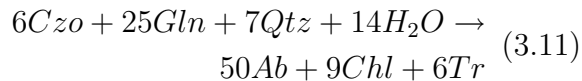
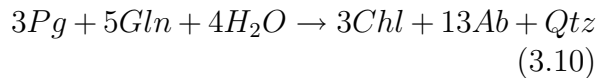


**Figure 3.17:** (cont.) P-T pseudosection of Sifnos eclogite Si 4-2.1 calculated with the given whole rock composition in the TiKCNMnFMASH system. The CaO content is recalculated concerning 2.97 wt% CO<sub>2</sub> in Calcite. Increasing grey-scale corresponds to higher variance (quadri-, five-, six- and seven-variance); white arrow indicates the deduced P-T path. E) Si pfu isopleths of white mica, F)  $X_{Na}$  isopleths of white mica, G)  $Na_B$  pfu isopleths of amphibole, H) density isopleths.

The formation of chlorite and albite is an indication for the blueschist-greenschist transformation. It can be expressed by reactions after [Bucher and Frey \(2002\)](#) and [Evans \(1990\)](#):



The calculated P-T path (Figure 3.17B) of the Sifnos sample is in agreement with similar published P-T reconstructions ([Trotet et al., 2001](#); [Schmädicke and Will, 2003](#)). All P-T path calculations for HP rocks of Sifnos show narrow P-T loops with contemporaneous cooling and decompression during uplift. Published P-T paths for the subduction mélangé in the Chinese South Tian Shan vary slightly (Figure 3.16F). This results from the fact that different lithologies have been analysed that are spatially separated from each other on a large scale. In addition, it correlates with the nature of subduction mélangés, which represent mixtures of different lithologies deriving from different parts of a disintegrated subduction slab (e.g. [Bebout and Barton, 2002](#)). Most of the published P-T paths are clockwise with retrograde cooling and decompression. The here calculated P-T path of the back-arc basalt (FTS 9–1 sequence) has an anticlockwise sense, but it is also similar as retrograde cooling and decompression after distinct higher peak-metamorphic temperatures is indicated. The numerical modelling of [Gerya et al. \(2002\)](#) shows that oceanic rocks subducted in young and hot subduction zones undergo anticlockwise P-T paths and experience isobaric cooling after peak-metamorphism, whereas rocks, which were buried in mature and cooler subduction

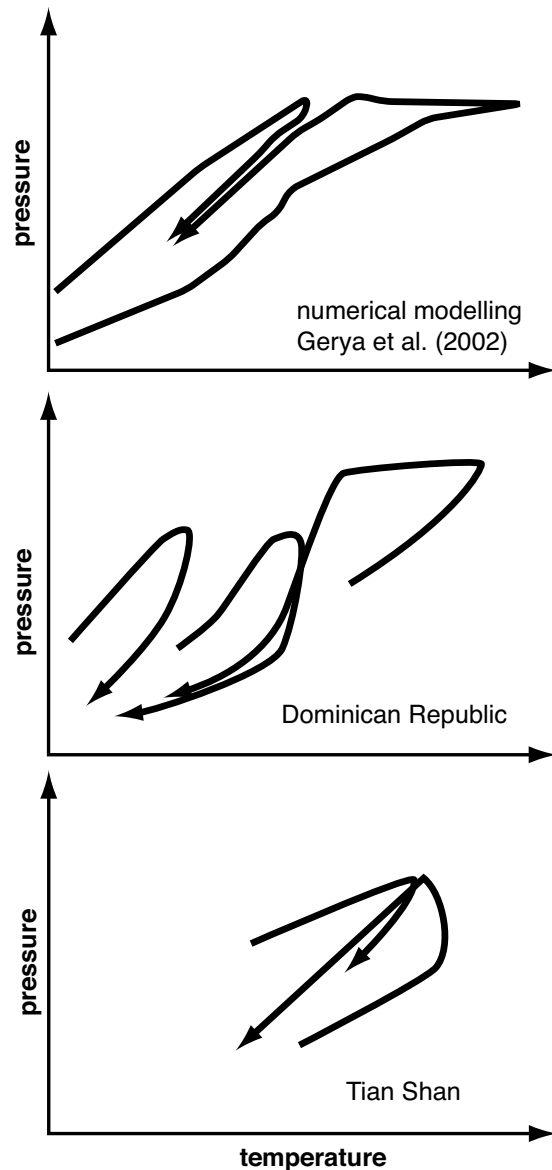


**Figure 3.18:** Comparison of published and modelled P-T paths in subduction channel. A: numerical modelling after [Gerya et al. \(2002\)](#). Basaltic rock in young and hot subduction zone describes anticlockwise P-T path at higher temperatures with isobaric cooling after peak-temperature. Rocks subducted in mature subduction zones describe a clockwise P-T path at lower temperature conditions. Uplift is characterised by cooling and decompression. B: P-T paths from HP-rocks of the tectonic mélangé in the Dominican Republic, after ([Krebs et al., 2008](#)). C: Clockwise P-T path from van der Straaten et al. (in press) from Tian Shan; anticlockwise P-T path is the FTS 9-1 sequence from the Tian Shan of this study.

zones, show clockwise P-T loops at lower temperatures (Figure 3.18A). This numerical modelling is supported by field observations of Krebs et al. (2008), who analysed jadeite-gneiss, blueschist and eclogite from the tectonic mélange of the Dominican Republic (Figure 3.18B). Anti-clockwise P-T paths with retrograde cooling and decompression are also reported by Willner et al. (2004) from the Andean and Garcia-Casco et al. (2008) from Cuba. The anticlockwise P-T path of the eclogite from Tian Shan described here, reflect the burial and exhumation history in a young and hot oceanic subduction setting, whereas most of the basaltic rocks in the Tian Shan subduction mélange describe clockwise, cooler P-T paths (Gao et al., 1999; Klemd et al., 2002; Lin and Enami, 2006; van der Straaten et al., 2008). However, most of the retrograde paths of the described tectonic unit are similar and describe more or less the same retrograde cooling and decompression as it is modelled for uplift in a subduction channel (Figure 3.18A, Gerya et al., 2002).

### 3.7.3 Element mobility, mass-balance and metasomatism during the eclogite-blueschist transformation

The bulk rock data of the Sifnos and Tian Shan samples show that chemical changes were associated with the transformation of eclogites into blueschists (Table 3.2). Due to the element mobility in such open systems, the decrease and/or increase of element concentrations finally results either in an overall mass loss or gain. Mass-balance calculations based on the assumption of immobility of certain elements or element groups (Gresens, 1967; Ague and van Haren, 1996) provide informations about element mobility during the studied eclogite-blueschist transformation processes. The proper choice of the immobile reference elements is crucial and should be selected carefully in accordance to the petrographical observations. For details of the mass-balance calculations and its use for blueschist-overprinted eclogites see Ague (2003) and van der Straaten et al. (2008). We discuss for every eclogite-blueschist sequence of Sifnos and the Tian Shan, three possible immobile reference frames (Figure 3.19A, B), which are: HFSE (Zr, Ti, Nb), HREE, and Al–O. HFSE are predominantly incorporated into accessory phases like zircon, titanite, and rutile and are usually rather immobile with regard to fluid processes in most metamorphic settings (e.g. Floyd and Winchester, 1978; Corfu and Davis, 1991; John et al., 2004). HREE are usually incorporated in garnet (e. Stalder et al., 1998) or in accessory phases such as titanite (e.g. Gao et al., 2007) and can be assumed to behave fluid-immobile if their carrier mineral keeps stable or is just slightly affected by a metasomatic process (John et al., 2008). The P-T estimates discussed in the previous sections indicate peak-metamorphic conditions ( $\sim 21$  kbar) and subsequent growth of hydrous minerals at pressures  $< 20$  kbar and provide some constrains for the kind of mass and volume changes that might be reasonable in the studied samples. At those high pressures an overall mass and volume loss or moderate volume gain can be expected, but a significant volume increase seems unlikely. On these considerations we evaluate among the suggested immobile element groups the most reasonable one. By considering the HREE as the immobile reference frame, the calculated mass and volume change would be +23 and +26 (Sifnos) and +27 and +36 (Tian Shan), respectively, which

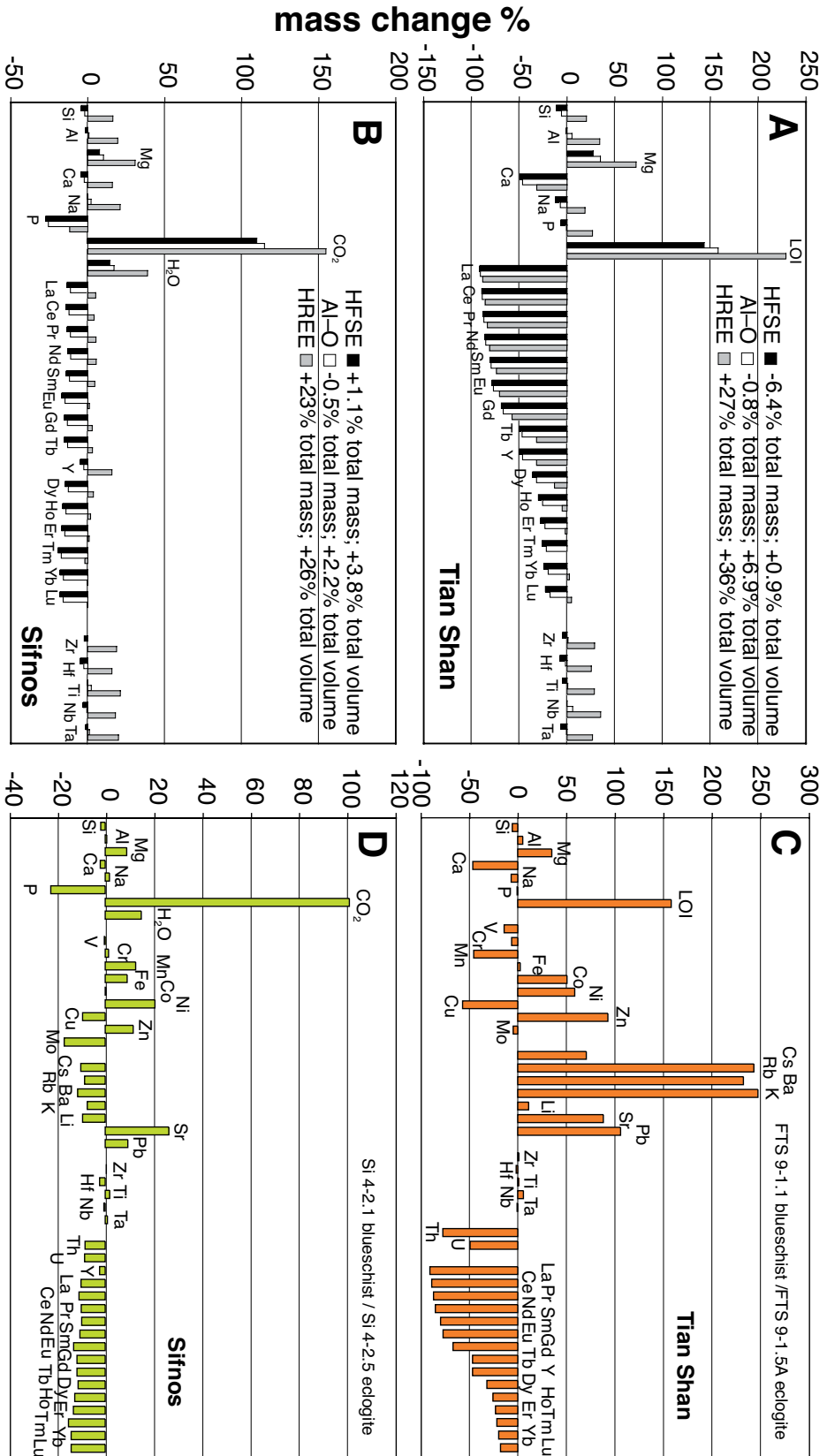


**Figure 3.19:** Element mobility estimated by mass-balance calculations for blueschist samples compared to their precursor eclogite sample from Sifnos and Tian Shan. A+B): Comparison of three different immobility references. purple: HFSE, green: Al-O, orange: HREE. Calculated associated overall volume and mass loss is given in legend. C+D): Element mobility for all major and trace elements based on HFSE and Al-O immobility (gain in white, loss in blue).

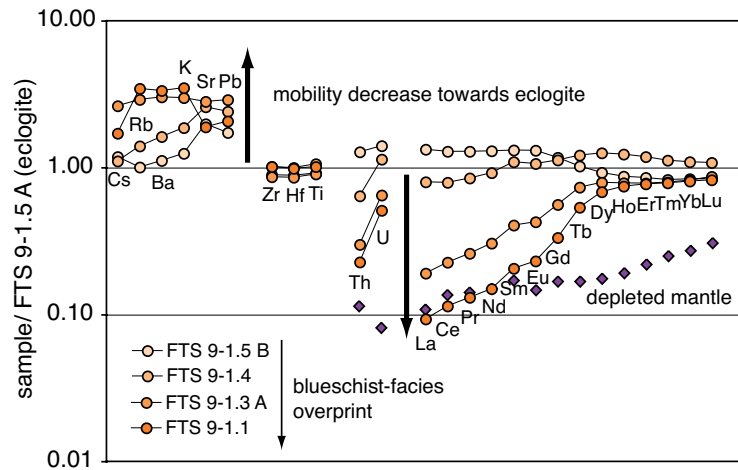


**Figure 3.20:** Element mobility based on mass-balance calculation of blueschists compared to their precursor eclogite composition of the FTS 9-1 sequence (Tian Shan). HFSE are taken as immobile. Sample FTS 9-1.1 represents the blueschist with highest alteration and is farthest of eclogite (see Figure 3.2 for comparison). LREE loss and LILE gain decrease towards the eclogite, which is correlated with alleviated fluid-infiltration towards the eclogite.

would have been accompanied by a gain of  $\sim 30\%$  in HFSE. The calculated volume change is by far too high to be realistic, as we cannot verify a gain of HFSE by petrographic observations. HFSE and Al–O as immobile references result in minor changes of mass and volume during the eclogite-blueschist transformation. On the basis of Al–O immobility the obtained mass loss for the Tian Shan eclogite-blueschist transformation is  $-0.8\%$  and the volume change is  $+6.9\%$ ; in the case of HFSE immobility the mass loss is  $-6.4\%$  and the volume change is  $+0.9\%$ . The mass gain for the Sifnos blueschist/eclogite is  $-0.5\%$  and the volume change is  $+2.2\%$  on the basis of Al–O (HFSE: mass change =  $+1.1\%$ , volume change =  $+3.8\%$ ). Associated minor changes in the HFSE at Al–O immobility is negligible considering the analytical error of 1 %. Minor changes in major elements, that are important on a quantity basis, result in higher mass changes compared to changes of trace element concentrations. Immobility of Al is in accordance to petrological observations. For instance, Al in garnet and jadeite is released by breakdown reactions or by dissolution of these phases and is directly incorporated into alumina-rich minerals like white mica and albite. Based on these considerations we regard Al–O and HFSE as immobile during the Sifnos and Tian Shan eclogite-blueschist transformations. Figure 3.19C and D show the results of the mass-balance calculations. The Sifnos blueschist shows only minor element gains ( $\sim 20\%$ ) compared to the eclogite, except for the distinct gain of  $\sim 115\%$   $\text{CO}_2$ . About 4% of Si and Ca and  $\sim 15\text{--}20\%$  of REE, Y, Th, U, Ba, Cs, Rb, K, Cu, Mo and P seem to be mobilised and removed from the system, in contrast to a gain of 15–25% of Mg,  $\text{H}_2\text{O}$ , Mn, Fe, Ni, Zn, Sr and Pb. The Tian Shan blueschist shows a calculated significant gain of around 50–100% of Mg, Ni, Co, Zn, Cs, Sr and Pb and a 150–250% gain of LOI, Ba, Rb and K. Contrary, there is distinct losses of around 50–100% of REE, Th, U, Cu, Mn and Ca compared to its precursor eclogite. On Sifnos the loss of REE and P is probably related to some dissolution of apatite and garnet. Incorporation of Cs, Rb, Ba and K is usually associated with the formation of white mica (Zack et al., 2001) and the loss of these LILE might be related to the mica breakdown reaction (Reaction 3.10), indicating the blueschist-greenschist facies transition. Gain of  $\text{CO}_2$  is indicated by the growth of calcite. Sr and Pb are distinct trace elements in clinozoisite (Enami et al., 2004; Feinman

et al., 2007) and also occur in significant concentrations in carbonates (Gao et al., 2007). Hence, the gain of Sr and Pb can be related to the growth of clinozoisite and carbonates in the blueschist. Mg, Mn, Fe, and Zn gains are probably associated with the formation of sodic amphibole. Late-stage amphibole formed during the blueschist-facies overprint shows higher Mn contents (Figure 3.12E). The eclogite to blueschist transformation in the Tian Shan sample indicates an increasing release of LREE from the pristine eclogite towards the blueschist and an increasing gain of Cs, Rb, Ba and K (Figure 3.20). Sample FTS 9–1.1 shows the strongest blueschist-facies overprint and according to the chemical data it experienced the most intensive fluid influx. This fits well with the field observation, as this part of the blueschist has the greatest distance from the relict eclogite. We assume that dissolution of omphacite is the main reason for the very high LREE loss, as other typical LREE-bearing phases like apatite or clinozoisite are absent (e.g. John et al., 2004). If omphacite serves as the main carrier of LREE, although contents of LREE in omphacite are rather low (Table 3.1), a significant loss of LREE would occur if this phase would be replaced by a sodic-amphibole during alteration. 20–50% loss of HREE is probably related to the partial breakdown of garnet, which can be assumed as the dominant HREE carrier. Increasing gain of CO<sub>2</sub>, Cs, Rb, Ba and K correlates with increasing formation of white mica (paragonite) and calcite. Both eclogite-blueschist sequences show similarities in the loss of REE, U, Th, Ca and Si, and in the gain of CO<sub>2</sub>, H<sub>2</sub>O, Mg and some transition metals, particularly of Ni. This indicates in both cases an infiltration of a CO<sub>2</sub>-rich aqueous fluid characterised by relatively high Mg and transition metal concentrations at low concentrations of Si, Ca and REE. In addition, the Tian Shan samples indicate a significant LILE infiltration.

### 3.7.4 Exhumation processes in the subduction channel

The chemical changes associated with the eclogite-blueschist transformation suggest that the infiltrating fluids during this transformation were low in Si, Ca and REE but high in Mg, Co and Ni concentrations. Such fluid compositions suggest that they have been in equilibrium with peridotitic rocks prior to infiltration (Barnes et al., 2004; Miller et al., 2008; van der Straaten et al., 2008). Altered and unaltered peridotite is present within the subducting slabs below the oceanic crust and in the mantle wedge above the slab. High gain of CO<sub>2</sub> is likely related to a carbonate source. This could be the marble sequence above and below the eclogites and blueschists in Sifnos (Davis, 1966) and possibly the Silurian marbles in the Tian Shan (Gao et al., 1999). According to the model of the presence of subduction channels the different petrophysical properties of the partially serpentinised mantle peridotite, compared to the unaltered peridotite, are responsible for movement and uplift of the serpentinite itself and of the incorporated rocks (Hermann et al., 2000; Schwartz et al., 2001; Gerya et al., 2002). According to Schwartz et al. (2001) 10–50% serpentinisation in the subduction channel is suitable to carry eclogites from depths of around 100 km up to a depth of 40 km, if the density contrast ranges between 0.1 and 0.4 g/cm<sup>3</sup>. The density calculation for depleted mantle peridotite (composition of Salters and Stracke, 2004) in the CFMASH system ( $a_{H_2O} = 1$ ), indicates a density of <2.9 g/cm<sup>3</sup> at P-

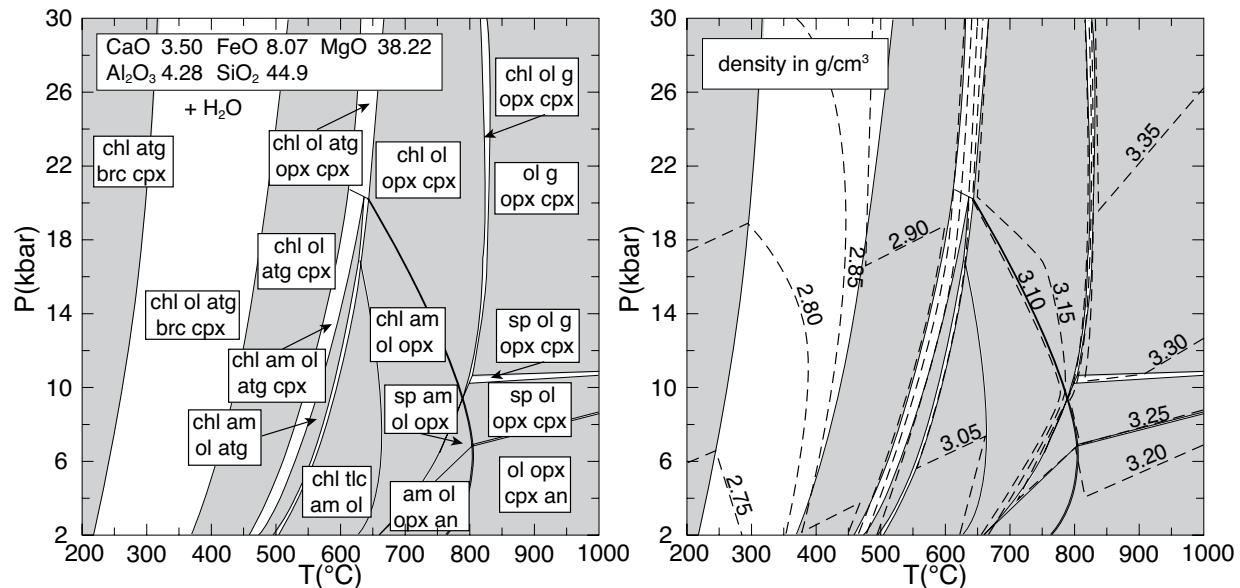


**Figure 3.21:** P-T pseudosection of water-saturated depleted mantle composition (Salters and Stracke, 2004) calculated with the given whole rock composition in the CFMASH system (am = calcic amphibole, an = anorthite, atg = antigorite, brc = brucite, chl = chlorite, cpx = clinopyroxene, g = garnet, ol = olivine, opx = orthopyroxene, sp = spinel, tlc = talc). Increasing grey-scale corresponds to higher variance (di- and tri-variance) B: Dotted lines are calculated density isopleths, given in  $\text{g}/\text{cm}^3$ .

T conditions below  $600^\circ\text{C}$  and 18 kbar, and of  $<2.8 \text{ g}/\text{cm}^3$  below  $400^\circ\text{C}$  (Figure 3.21). The resulting density contrast among the blueschist-facies overprinted eclogite from Sifnos and the calculated serpentinite is max  $0.4 \text{ g}/\text{cm}^3$  at peak-metamorphic conditions of  $<600^\circ\text{C}$  and  $<20$  kbar. This results from the calculated  $3.30 \text{ g}/\text{cm}^3$  in eclogite and  $<2.85 \text{ g}/\text{cm}^3$  in serpentinite (Figure 3.22). The density contrast decreases to  $<0.30 \text{ g}/\text{cm}^3$  during late-stage metamorphic conditions of  $<550^\circ\text{C}$  and 16 kbar. The density contrast will increase up to  $\sim 0.5 \text{ g}/\text{cm}^3$  if marble with 2.6 to  $2.8 \text{ g}/\text{cm}^3$  is taken as the carrier rock. The estimated density contrast of the Tian Shan sequence is  $\sim 0.20 \text{ g}/\text{cm}^3$  corresponding to  $3.34 \text{ g}/\text{cm}^3$  of the eclogite and  $3.15 \text{ g}/\text{cm}^3$  in serpentinite at peak-metamorphic conditions of around  $650^\circ\text{C}$  and 21 kbar. Retrograde density contrasts are similar to those of the Sifnos samples (Figure 3.22). HP rocks that were uplifted in a subduction channel and are displaying a lower density contrast of  $0.10\text{--}0.40 \text{ g}/\text{cm}^3$  with its matrix point to the existence of a wide subduction channel of up to 40 km (Schwartz et al., 2001). This correlates with the open subduction channel theory due to a slab-roll back and extension, as it was proposed for the Cyclades (e.g. Trotet et al., 2001; Jolivet et al., 2003). In contrast, a closed and narrow subduction channel is supposed to be related to contraction tectonics (Jolivet et al., 2003), as it is proposed for the Alps or the Himalayas. Higher density contrasts between HP rocks and their matrix with values of up to  $>0.70 \text{ g}/\text{cm}^3$  are supposed to be associated with narrow subduction channels (Schwartz et al., 2001). Serpentinites as transport matrix in the subduction channel have been present in the Alps (Hermann et al., 2000; Schwartz et al., 2000; Barnes et al., 2004) and in the Himalayas (Guillot et al., 2000), but serpentinite

is only locally present in outcrops of Sifnos and the Tian Shan. Consequently, it has to be assumed that the HP rocks have been tectonically separated from the serpentinite matrix during the final stages of the uplift if serpentinites were the transporting matrix as it was proposed by [Dixon and Ridley \(1987\)](#) for the tectonic *mélange* on Syros (Cyclades). However, rocks with petrophysical properties similar to those of serpentinite may have facilitated the uplift of HP rocks instead. Possible low density and viscosity rocks that are occurring beside serpentinite in supposed subduction channel-outcrops are chlorite or talc schists, metasediments or marbles. Marbles are juxtaposed to altered and unaltered high-pressure rocks on Sifnos as it is on most other islands in the Cycladic archipelago. Buoyancy driven uplift of eclogites facilitated by marble is reasonable: The low density of 2.6–2.8 g/cm<sup>3</sup> of marble in contrast to 3.3 g/cm<sup>3</sup> of the peridotite results in a suitable buoyancy force, which is necessary for migration and transport in the subduction channel ([Gerya et al., 2002](#); [Schwartz et al., 2001](#)). Alternatively, the presence of metapelites (shale: 2.4–2.8 g/cm<sup>3</sup>, slate: 2.7–2.8 g/cm<sup>3</sup>, [www.mininglife.com](#)) and metasediments (sandstone: 2.2–2.8 g/cm<sup>3</sup> and mica schist: 2.5–2.9 g/cm<sup>3</sup>, [www.mininglife.com](#)) can have taken over the role of serpentinite in a subduction channel ([Jolivet et al., 2003](#)). These are associated to the eclogites in adequate amounts in the Tian Shan. Also chlorite and talc schist (talc: 2.6–2.8 g/cm<sup>3</sup>, [www.mininglife.com](#)) satisfy the requested low density and viscosity and are abundantly present in the tectonic *mélange* of the Tian Shan ([Gao et al., 1995, 1998](#); [Klemd et al., 2002](#)).

### 3.7.5 Conclusions

The minerals that formed in the blueschist-facies overprinted eclogites from Sifnos and from the South Tian Shan have similar compositions. Garnet of eclogites and associated blueschists are flatly zoned and almandine-rich. Clinopyroxene is zoned omphacite with a prograde increase of the jadeite component during burial. Peak-metamorphic garnet, omphacite and rutile are replaced by glaucophane, titanite, calcite and white mica, which is paragonite in the Tian Shan and phengite in the Sifnos case. Clinozoisite is only present in the Sifnos samples and shows higher Sr concentrations in the retrograde clinozoisite compared to the prograde one.

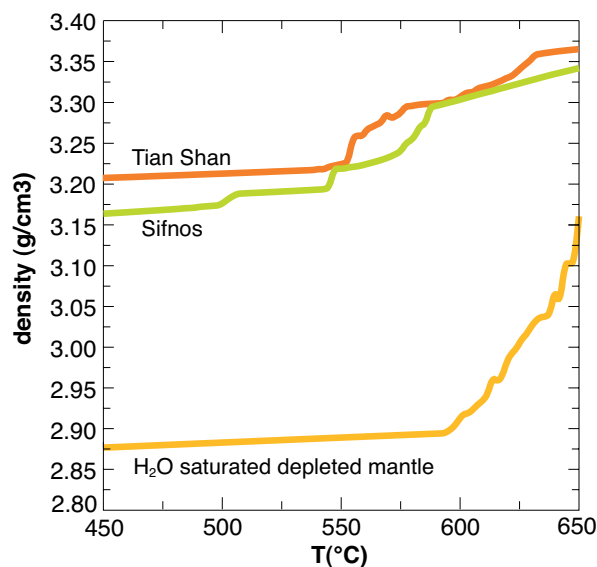


**Figure 3.22:** Density gradient of Sifnos and Tian Shan eclogite-blueschist samples and the calculated hydrated depleted mantle composition following the retrograde P-T conditions.



The chemical bulk composition of the Sifnos eclogite and blueschist point to oceanic island basalt as protholith, whereas that of the Tian Shan eclogite-blueschist sequence points to a back-arc derived oceanic basalt. The Sifnos eclogite experienced a clockwise P-T path and the Tian Shan sample an anticlockwise P-T path at distinct higher temperatures. Both samples are characterised by a retrograde contemporaneous cooling and decompression, which typically results from uplift and exhumation in a subduction channel.

During retrograde fluid infiltration and associated metamorphism and metasomatism Mg, transition metals, and LILE (Tian Shan) were gained in the blueschist compared to the eclogite, while HFSE and Al behaved immobile. Si, Ca and REE were mobilised and removed from the rock during this transformation process. These chemical changes together with the nearly complete loss of LREE in the Tian Shan sample indicate that the fluid prior to infiltration has been in equilibrium with a peridotitic composition, most likely with rocks of the partially serpentinised mantle wedge, i.e. with the rocks of the subduction channel.

The fluid induced element loss and a slight volume increase during the blueschist formation result in a decreased density of the overprinted eclogite. Compared to the assumed serpentinite matrix in the subduction channel, the calculated density contrast to the HP rocks of Sifnos and the Tian Shan is high enough to carry HP rocks in a serpentinite matrix to shallower depths. Serpentinite with incorporated low-density rocks in a matrix of unaltered and thus denser mantle peridotite is able to rise up, driven by buoyancy forces.

The metasomatism associated with the eclogite-blueschist transformation points to infiltration of a fluid that was in equilibrium with a peridotitic composition. However, occurrences of outcropping serpentinite on Sifnos and in the Tian Shan are very rare. Alternative to serpentinite, the marble stratification of Sifnos and the metasediments of the Tian Shan are suitable to overtake the role of the serpentinite as the carrier matrix during exhumation near the surface.

## 3.8 Acknowledgement

The Deutsche Forschungsgemeinschaft (grant Sche 265/S1–2) and the State Key Project for Basic Research of China (2001CB409803), the “Funds for Hundred Outstanding Talents Plan” of the Chinese Academy of Sciences financially supported this study. This publication is contribution no. 160 of the Sonderforschungsbereich 574 “Volatiles and Fluids in Subduction Zones” at Kiel University. We like to thank P. Appel, B. Mader, A. Fehler, A. Weinkauff, C. Kusebauch, U. Westernströer, P. Fiedler, D. Garbe-Schönberg (University of Kiel) and H. Brätz (University of Würzburg) for analytic help. Mark Caddick (ETH Zrich) is thanked for solving technical problems with Perple\_X. R. Halama and S. Brandt are thanked for discussion, which helped to clarify critical points.

## References

- Ague, J. J., 2003. Fluid infiltration and transport of major, minor, and trace elements during regional metamorphism of carbonate rocks, Wepawaug Schist, Connecticut, USA. *American Journal of Science* 303, 753–816.
- Ague, J. J., van Haren, J. L. M., 1996. Assessing metasomatic mass and volume changes using the bootstrap, with application to deep crustal hydrothermal alteration of marble. *Economic Geology and the Bulletin of the society of economic geologists* 91 (7), 1169–1182.
- Altherr, R., Kreuzer, H., Wendt, I., Lenz, H., Wagner, G., Keller, J., Harre, W., Hoehndorf, A., 1982. A late Oligocene/ early Miocene high temperature belt in the Attic-Cycladic crystalline complex (SE Pelagonian, Greece). *Geologisches Jahrbuch* E23, 97–164.
- Altherr, R., Schliestedt, M., Okrusch, M., Seidel, E., Kreuzer, H., Harre, W., Lenz, H., Wendt, I., Wagner, G. A., 1979. Geochronology of high pressure rocks on Sifnos (Cyclades, Greece). *Contributions to mineralogy and petrology* 70 (3), 245–255.
- Armbruster, T., Bonazzi, P., Akasaka, M., Bermanec, V., Chopin, C., Gieré, R., Heuss, A. S., Liebscher, A., Menchetti, S., Pan, Y., Pasero, M., 2006. Recommended nomenclature of epidote-group minerals. *European Journal of Mineralogy* 18 (5), 551–567.
- Aubouin, J., 1957. Essai de corrélation stratigraphique de la Grèce occidentale. *Bulletin de la Société Géologique de France* 7, 281–304.
- Avigad, D., Matthews, A., Evans, B. W., Garfunkel, Z., 1992. Cooling during the exhumation of a blueschist terrane; Sifnos (Cyclades), Greece. *European Journal of Mineralogy* 4 (3), 619–634.
- Avigad, D., Matthews, A., Garfunkel, Z., 1988. The Alpine evolution of the Cyclades: introduction and excursion guide to the geology of the islands of Sifnos and Tinos. *Geol. Soc. Israel. Sec. Publ.*, Jerusalem, p. 66.
- Barnes, J. D., Selverstone, J., Sharp, Z. D., 2004. Interactions between serpentinite devolatilization, metasomatism and strike-slip strain localization during deep-crustal shearing in the Eastern Alps. *Journal of Metamorphic Geology* 22 (4), 283–300.
- Bebout, G. E., Barton, M. D., 2002. Tectonic and metasomatic mixing in a high-T, subduction-zone melange; insights into the geochemical evolution of the slab-mantle interface. *Chemical Geology* 187 (1-2), 79–106.
- Bornovas, I., Rontogianni-Tsiabaou, T., 1983. Geological map of Greece. Institute of Geology and Mineral exploration.
- Boynton, W. V., 1984. Cosmochemistry of the rare earth elements; meteorite studies. In: Henderson, P. (Ed.), *Rare earth element geochemistry*. Vol. 2. Elsevier Sci Publ, Amsterdam, Netherlands, pp. 63–114.
- Bucher, K., Frey, M., 2002. *Petrogenesis of Metamorphic Rocks*. Springer, Berlin Heidelberg.
- Burg, J. P., Philippot, P., 1991. Asymmetric Compositional Layering of Syntectonic Metamorphic Veins as Way-up Criterion. *Geology* 19 (11), 1112–1115.
- Bykadorov, V. A., Bush, V. A., Fedorenko, O. A., Filippova, I. B., Miltenko, N. V., Puchkov, V. N., Smirnov, A. V., Uzhkenov, B. S., Volozh, Y. A., 2003. Ordovician-Permian palaeogeography of Central Eurasia: Development of Paleozoic petroleum-bearing basins. *Journal of Petroleum Geology* 26 (3), 325–350.
- Chemenda, A. I., Mattauer, M., Bokun, A. N., 1996. Continental subduction and a mechanism for exhumation of high-pressure metamorphic rocks: New modelling and field data from Oman. *Earth and Planetary Science Letters* 143 (1-4), 173–182.
- Cloos, M., 1982. Flow Melanges - Numerical Modeling and Geologic Constraints on Their Origin in the Franciscan Subduction Complex, California. *Geological Society of America Bulletin* 93 (4), 330–345.
- Cloos, M., 1983. Comparative-Study of Melange Matrix and Metashales from the Franciscan Subduction Complex with the Basal Great Valley Sequence, California. *Journal of Geology* 91 (3), 291–306.
- Cloos, M., Shreve, R. L., 1988a. Subduction-channel model of prism accretion, melange formation, sediment subduction, and subduction erosion at convergent plate margins; Part I, Background and description. *Pure and Applied Geophysics* 128 (3-4), 455–500.
- Cloos, M., Shreve, R. L., 1988b. Subduction-channel model of prism accretion, melange formation, sediment subduction, and subduction erosion at convergent plate margins; Part II, Implications and discussion. *Pure and Applied Geophysics* 128 (3-4), 501–545.
- Connolly, J. A. D., 1990. Multivariable phase diagrams; an algorithm based on generalized thermodynamics. *American Journal of Science* 290 (6), 666–718.
- Corfu, F., Davis, D. W., 1991. Archean Hydrothermal Zircon in the Abitibi Greenstone-Belt - Constraints on the Timing of Gold Mineralization - Comment. *Earth and Planetary Science Letters* 104 (2-4), 545–552.
- Davis, E. N., 1966. Der geologische Bau der Insel Siphnos. *Geological Geophysical Research* 10, 161–220.
- Dixon, J. E., Ridley, J., 1987. Syros. In: Helgeson, H. C. (Ed.), *Chemical transport in metasomatic processes*. Vol. 218. of NATO ASI Series C, Mathematical and Physical Sciences, Dordrecht, pp. 489–501.
- Dürr, S., 1986. Das Attisch-kykladische Kristallin. In: Jacobshagen, V. (Ed.), *Geologie von Griechenland*. Gebrüder Borntraeger, Stuttgart, pp. 116–149.

- Enami, M., Liou, J. G., Mattinson, C. G., 2004. Epidote minerals in high P/ T metamorphic terranes; subduction zone and high- to ultrahigh-pressure metamorphism. In: Liebscher, A. (Ed.), *Epidotes*. Vol. 56. Mineralogical Society of America and Geochemical Society, Washington, DC, United States, pp. 347–398.
- Ernst, W. G., Maruyama, S., Wallis, S., 1997. Buoyancy-driven, rapid exhumation of ultrahigh-pressure metamorphosed continental crust. *Proceedings of the National Academy of Sciences of the United States of America* 94 (18), 9532–9537.
- Evans, B. W., 1990. Phase relations of epidote-blueschists. *Lithos* 25 (1-3), 3–23.
- Federico, L., Capponi, G., Crispini, L., Scambelluri, M., 2004. Exhumation of alpine high-pressure rocks; insights from petrology of eclogite clasts in the Tertiary Piedmontese basin; Ligurian Alps, Italy. *Lithos* 74 (1-2), 21–40.
- Federico, L., Crispini, L., Scambelluri, M., Capponi, G., 2007. Ophiolite melange zone records exhumation in a fossil subduction channel. *Geology* 35 (6), 499–502.
- Feineman, M. D., Ryerson, F. J., DePaolo, D. J., Plank, T., 2007. Zoisite-aqueous fluid trace element partitioning with implications for subduction zone fluid composition. *Chemical Geology* 239 (3-4), 250–265.
- Fergusson, C. L., 1984. The Gundahl Complex of the New-England Fold Belt, Eastern Australia - a Tectonic Melange Formed in a Palaeozoic Subduction Complex. *Journal of Structural Geology* 6 (3), 257–271.
- Flanagan, F. J., 1976. Description and analyses of eight new USGS rock standards. USGS Professional Paper 840, 1–192.
- Floyd, P. A., Winchester, J. A., 1978. Identification and discrimination of altered and metamorphosed volcanic-rocks using immobile elements. *Chemical Geology* 21 (3-4), 291–306.
- Ganor, J., Matthews, A., Schliestedt, M., Garfunkel, Z., 1996. Oxygen isotopic heterogeneities of metamorphic rocks; an original tectonostratigraphic signature, or an imprint of exotic fluids? A case study of Sifnos and Tinos islands (Greece). *European Journal of Mineralogy* 8 (4), 719–732.
- Gao, J., He, G., Li, M., Xiao, X., Tang, Y., Wang, J., Zhao, M., 1995. The mineralogy, petrology, metamorphic P-T trajectory and exhumation mechanism of blueschists, South Tianshan, northwestern China. *Tectonophysics* 250 (1-3), 151–168.
- Gao, J., John, T., Klemd, R., Xiong, X., 2007. Mobilization of Ti-Nb-Ta during subduction: evidence from rutile-bearing dehydration segregations and veins hosted in eclogite, Tianshan, NW China. *Geochimica et Cosmochimica Acta* 71, 4974–4996.
- Gao, J., Klemd, R., 2003. Formation of HP-LT rocks and their tectonic implications in the western Tianshan Orogen, NW China; geochemical and age constraints. *Lithos* 66 (1-2), 1–22.
- Gao, J., Klemd, R., Zhang, L., Wang, Z., Xiao, X., 1999. P-T path of high-pressure/ low-temperature rocks and tectonic implications in the western Tianshan Mountains, NW China. *Journal of Metamorphic Geology* 17 (6), 621–636.
- Gao, J., Li, M., Xiao, X., Tang, Y., He, G., 1998. Paleozoic tectonic evolution of the Tianshan Orogen, northwestern China. *Tectonophysics* 287 (1-4), 213–231.
- Garbe-Schönberg, C. D., 1993. Simultaneous determination of thirty-seven trace elements in twenty-eight international rock standards by ICP-MS. *Geostandards Newsletter* 17 (1), 81–97.
- Garcia-Casco, A., Lazaro, C., Rojas-Agramonte, Y., Kroner, A., Torres-Roldan, R. L., Nunez, K., Neubauer, F., Millan, G., Blanco-Quintero, I., 2008. Partial melting and counterclockwise P-T path of subducted oceanic crust (Sierra del Convento Melange, Cuba). *Journal of Petrology* 49 (1), 129–161.
- Gasparik, T., Lindsley, D. H., 1980. Phase equilibria at high pressure of pyroxenes containing monovalent and trivalent ions. In: Prewitt, C. T. (Ed.), *Pyroxenes*. Vol. 7. Mineralogical Society of America, Washington, DC, United States, pp. 309–339.
- Gerya, T. V., Stöckhert, B., Perchuk, A. L., 2002. Exhumation of high-pressure metamorphic rocks in a subduction channel; a numerical simulation. *Tectonics* 21 (6), 1056, doi:10.1029/2002TC001406.
- Gorczyk, W., Gerya, T. V., Connolly, J. A. D., Yuen, D. A., Rudolph, M., 2006. Large-scale rigid-body rotation in the mantle wedge and its implications for seismic tomography. *Geochemistry, Geophysics, Geosystems* (G3) 7, DOI: 10.1029/2005GC001075.
- Green, T. H., Hellman, P. L., 1982. Fe-Mg partitioning between coexisting garnet and phengite at high pressure, and comments on a garnet-phengite geothermometer. *Lithos* 15 (4), 253–266.
- Gresens, R. L., 1967. Composition-volume relationships of metasomatism. *Chemical Geology* 2 (1), 47–65.
- Guillot, S., Hattori, K. H., de Sigoyer, J., 2000. Mantle wedge serpentinization and exhumation of eclogites: Insights from eastern Ladakh, northwest Himalaya. *Geology* 28 (3), 199–202.
- Hacker, B. R., Ratschbacher, L., Webb, L., Shuwen, D., 1995. What Brought Them up - Exhumation of the Dabie-Shan Ultrahigh-Pressure Rocks. *Geology* 23 (8), 743–746.
- Hart, S. R., Blusztajn, J., Dick, H. J. B., Meyer, P. S., Muehlenbachs, K., 1999. The fingerprint of seawater circulation in a 500-meter section of ocean crust gabbros. *Geochimica et Cosmochimica Acta* 63 (4), 4059–4080.
- Hastie, A. R., Kerr, A. C., Pearce, J. A., Mitchell, S. F., 2007. Classification of altered volcanic island arc rocks using immobile trace elements: Development of the Th-Co discrimination diagram. *Journal of Petrology* 48 (12), 2341–2357.

- Hermann, J., Muntener, O., Scambelluri, M., 2000. The importance of serpentinite mylonites for subduction and exhumation of oceanic crust. *Tectonophysics* 327 (3-4), 225–238.
- Hill, E. J., Baldwin, S. L., 1993. Exhumation of High-Pressure Metamorphic Rocks during Crustal Extension in the Dentrecasteaux Region, Papua-New-Guinea. *Journal of Metamorphic Geology* 11 (2), 261–277.
- Holland, T. J. B., 1980. The reaction albite = jadeite+quartz determined experimentally in the range 600-1200C. *American Mineralogist* 65 (1-2), 129–134.
- John, T., Klemd, R., Gao, J., Garbe-Schönberg, C.-D., 2008. Trace-element mobilization in slabs due to non steady-state fluid-rock interaction: constraints from an eclogite-facies transport vein in blueschist (Tianshan, China). *Lithos* 103 (1-2), 1–24.
- John, T., Schenk, V., Haase, K., Scherer, E., Tembo, F., 2003. Evidence for a Neoproterozoic ocean in south-central Africa from mid-oceanic-ridge-type geochemical signatures and pressure-temperature estimates of Zambian eclogites. *Geology (Boulder)* 31 (3), 243–246.
- John, T., Scherer, E. E., Haase, K., Schenk, V., 2004. Trace elements fractionation during fluid-induced eclogitization in a subducting slab: trace element and Lu-Hf-Sm-Nd isotope systematics. *Earth and Planetary Science Letters* 227, 441–456.
- Jolivet, L., Faccenna, C., Goffe, B., Burov, E., Agard, P., 2003. Subduction tectonics and exhumation of high-pressure metamorphic rocks in the Mediterranean orogens. *American Journal of Science* 303 (5), 353–409.
- Keiter, M., Piepjohn, K., Ballhaus, C., Lagos, M., Bode, M., 2004. Structural development of high-pressure metamorphic rocks on Syros island (Cyclades, Greece). *Journal of Structural Geology* 26 (8), 1433–1445.
- Kelemen, P. B., Hanghøj, K., Greene, A. R., 2003. One view of the geochemistry of subduction-related magmatic arcs, with an emphasis on primitive andesite and lower crust. In: Rudnick, R. L. (Ed.), *The Crust*. Vol. 3 of *Treatise on Geochemistry*. Elsevier-Pergamon, Oxford, pp. 593–659.
- Klemd, R., Bröcker, M., Hacker, B. R., Gao, J., Gans, P., Wemmer, K., 2005. New Age Constraints on the Metamorphic Evolution of the High-Pressure/Low-Temperature Belt in the Western Tianshan Mountains, NW China. *Journal of Geology* 113, 157–168.
- Klemd, R., Schröter, F. C., Will, T. M., Gao, J., 2002. P-T evolution of glaucophane-omphacite bearing HP-LT rocks in the western Tianshan Orogen, NW China; new evidence for "Alpine-type" tectonics. *Journal of Metamorphic Geology* 20 (2), 239–254.
- Krebs, M., Maresch, W. V., Schertl, H.-P., Mnker, C., Baumann, A., Draper, G., Idleman, B., Trapp, E., 2008. The dynamics of intra-oceanic subduction zones: A direct comparison between fossil petrological evidence (Rio San Juan Complex, Dominican Republic) and numerical simulation. *Lithos* 103 (1-2), 106–137.
- Leake, B. E., Wooley, A. R., Arps, C. E. S., Birch, W. D., Gilbert, M. C., Grice, J. D., Hawthorne, F. C., Kato, A., Kisch, H. J., Krivovichev, V. G., Linthout, K., Laird, J., Mandarino, J., Maresch, W. V., Nickel, E. H., Rock, N. M. S., Schumacher, J. C., Smith, D. C., Stephenson, N. C. N., Ungaretti, L., Whittaker, E. J. W., Youzhi, G., 1997. Nomenclature of amphiboles; report of the Subcommittee on Amphiboles of the International Mineralogical Association Commission on New Minerals and Mineral Names. *European Journal of Mineralogy* 9 (3), 623–651.
- Lin, W., Enami, M., 2006. Prograde pressure-temperature path of jadeite-bearing eclogites and associated high-pressure/low-temperature rocks from western Tianshan, northwest China. *Island Arc* 15, 483–502.
- Lister, G. S., Raouzaïos, A., 1996. The tectonic significance of a porphyroblastic blueschist facies overprint during Alpine orogenesis: Sifnos, Aegean Sea, Greece. *Journal of Structural Geology* 18 (12), 1417–1435.
- Maluski, H., Bonneau, M., Kienast, J. R., 1987. Dating the metamorphic events in the Cycladic area;  $^{39}\text{Ar}/^{40}\text{Ar}$  data from metamorphic rocks of the Island of Syros (Greece). *Bulletin de la Societe Geologique de France, Huitieme Serie* 3 (5), 833–842.
- Mattauer, M., Ritz, J. F., 1996. Geological arguments for a continental subduction model to explain exhumation of high-pressure metamorphism in Oman. *Comptes Rendus De L Academie Des Sciences Serie Ii Fascicule a-Sciences De La Terre Et Des Planetes* 322 (10), 869–876.
- Miller, D. P., Marschall, H. R., Schumacher, J. C., 2008. Metasomatic formation and petrology of blueschist-facies hybrid rocks from syros (greece): implications for reactions at the slab-mantle interface. *Lithos*, doi:10.1016/j.lithos.2008.07.015.
- Mocek, B., 1994. Geochemische Untersuchungen zur Identifizierung der Protholithe der Hochdruckeinheit von Siphnos, Kykladen (Griechenland). *Berichte der deutschen Mineralogischen Gesellschaft, Beiheft zum European Journal of Mineralogy* 6 (1), 1–179.
- Morimoto, N., 1988. Nomenclature of pyroxenes; Subcommittee on Pyroxenes, Commission on New Minerals and Mineral Names (CNMMN), International Mineral Association (IMA). *Schweizerische Mineralogische und Petrographische Mitteilungen = Bulletin Suisse de Mineralogie et Petrographie* 68 (1), 95–111.
- Okrusch, M., Seidel, E., Davis, E. N., 1978. The assemblage jadeite - quartz in the glaucophane rocks of Sifnos (Cyclades Archipelago, Greece). *Neues Jahrbuch fuer Mineralogie Abhandlungen*. 132 (3), 284–308.
- Peacock, S. M., 1993. The importance of blueschist to eclogite dehydration reactions in subducting oceanic crust. *Geological Society of America Bulletin* 105 (5), 684–694.
- Pearce, J. A., 2008. Geochemical fingerprinting of oceanic basalts with applications to ophiolite classification and the search for Archean oceanic crust. *Lithos* 100 (1-4), 14–48.

- Pearce, N. J. G., Perkins, W. T., Westgate, J. A., Gorton, M. P., Jackson, S. E., Neal, C. R., Chenery, S. P., 1997. A compilation of new and published major and trace element data for NIST SRM 610 and NIST SRM 612 glass reference materials. *Geostandards Newsletter-the Journal of Geostandards and Geoanalysis* 21 (1), 115–144.
- Peate, D. W., Pearce, J. A., Hawkesworth, C. J., Colley, H., Edwards, C. M. H., Hirose, K., 1997. Geochemical variations in Vanuatu arc lavas: the role of subducted material and a variable mantle wedge composition. *Journal of Petrology* 38 (10), 1331–1358.
- Pilchin, A., 2005. The role of serpentinization in exhumation of high- to ultra-high-pressure metamorphic rocks. *Earth and Planetary Science Letters* 237 (3–4), 815–828.
- Platt, J. P., 1993. Exhumation of High-Pressure Rocks - a Review of Concepts and Processes. *Terra Nova* 5 (2), 119–133.
- Poli, S., Schmidt, M. W., 1995. H<sub>2</sub>O transport and release in subduction zones; experimental constraints on basaltic and andesitic systems. *Journal of Geophysical Research, B, Solid Earth and Planets* 100 (11), 22299–22314.
- Powell, R., 1985. Regression diagnostics and robust regression in geothermometer/ geobarometer calibration; the garnet-clinopyroxene geothermometer revisited. *Journal of Metamorphic Geology* 3 (3), 231–243.
- Salters, V. J. M., Stracke, A., 2004. Composition of the depleted mantle. *Geochemistry, Geophysics, Geosystems* (G3) 5, doi:10.1029/2003GC000597.
- Savov, I. P., Ryan, J. G., D, A. M., Kelley, K., Mattie, P., 2005. Geochemistry of serpentinized peridotites from the Mariana forearc Conical Seamount, ODP Leg 125; implications for the elemental recycling at subduction zones. *Geochemistry, Geophysics, Geosystems* (G3) 6 (4), doi:10.1029/2004GC000777.
- Schliestedt, M., 1980. Phasengleichgewichte in Hochdruckgesteinen von Sifnos, Griechenland. PhD thesis, Technischen Universität Carolo-Wilhelmina zu Braunschweig, p. 143.
- Schliestedt, M., Okruch, M., 1988. Meta-acidites and silicic meta-sediments related to eclogites and glaucophanites in northern Sifnos, Cycladic Archipelago, Greece. In: Smith, D. C. (Ed.), *Eclogites and eclogite-facies rocks*. Vol. 12. Elsevier, Amsterdam-New York, International, pp. 291–334.
- Schmädicke, E., Will, T. M., 2003. Pressure-temperature evolution of blueschist facies rock from Sifnos, Greece, and implications for the exhumation of high-pressure rocks in the central Aegean. *Journal of Metamorphic Geology* 21 (8), 799–811.
- Schwartz, S., Allemand, P., Guillot, S., 2001. Numerical model of the effect of serpentinites on the exhumation of eclogitic rocks; insights from the Monviso ophiolitic massif (Western Alps). *Tectonophysics* 342 (1–2), 193–206.
- Schwartz, S., Lardeaux, J., Guillot, S., Tricart, P., 2000. Diversité du métamorphisme clogitique dans le massif ophiolitique du Monviso (Alpes Occidentales, Italie). *Geodin. Acta* 13, 169–187.
- Sengör, A. M. C., Natal'In, B. A., 1996. Paleotectonics of Asia: fragments of a synthesis. In: Yin, A., Harrison, M. (Eds.), *The Tectonic Evolution of Asia*. World and Regional Geology Series. Cambridge University Press, Cambridge, New York, Melbourne, pp. 486–640.
- Shreve, R. L., Cloos, M., 1986. Dynamics of sediment subduction, melange formation, and prism accretion. *Journal of Geophysical Research*. B 91 (10), 10229–10245.
- Sobolev, N. V., Dobretsov, N. L., Bakirov, A. B., Shatsky, V. S., 1986. Eclogites from various types of metamorphic complexes in the USSR and the problems of their origin. In: Evans, B., Brown, E. (Eds.), *Blueschists and eclogites*. Vol. 164; Geological Society of America (GSA), Boulder, CO, United States, pp. 349–363.
- Spear, F. S., Wark, D. A., Cheney, J. T., Schumacher, J. C., Watson, B. E., 2006. Zr-in-rutile thermometry in blueschists from Sifnos, Greece. *Contributions to mineralogy and petrology* 152, 375–385.
- Stalder, R., Foley, S. F., Brey, G. P., Horn, I., 1998. Mineral-aqueous fluid partitioning of trace elements at 900–1200 degrees C and 3.0–5.7 GPa; new experimental data for garnet, clinopyroxene, and rutile, and implications for mantle metasomatism. *Geochimica et Cosmochimica Acta* 62 (10), 1781–1801.
- Trotet, F., Vidal, O., Jolivet, L., 2001. Exhumation of Syros and Sifnos metamorphic rocks (Cyclades, Greece); new constraints on the P-T paths. *European Journal of Mineralogy* 13 (5), 901–920.
- van der Straaten, F., Schenk, V., John, T., Gao, J., 2008. Blueschist-facies rehydration of eclogites (Tian Shan, NW-China): implications for fluid-rock interaction in the subduction channel. *Chemical Geology* 255 (1–2), 195–219.
- van Hinsbergen, D. J. J., 2004. The evolving anatomy of a collapsing orogen. *Geologica Ultraiectina* 243, p. 280.
- Warren, C. J., Beaumont, C., Jamieson, R. A., 2008. Modelling tectonic styles and ultra-high pressure (UHP) rock exhumation during the transition from oceanic subduction to continental collision. *Earth and Planetary Science Letters* 267 (1–2), 129–145.
- Waters, D. J., Martin, H. N., 1993. Geobarometry in phengite-bearing eclogites. Seventh meeting of the European Union of Geosciences; abstract supplement 5 (1), 410–411.
- Wijbrans, J. R., Schliestedt, M., York, D., 1990. Single grain argon laser probe dating of phengites from the blueschist to greenschist transition on Sifnos (Cyclades, Greece). *Contributions to mineralogy and petrology* 104 (5), 582–593.

- Willner, A. P., Glodny, J., Gerya, T. V., Godoy, E., Massonne, H., 2004. A counterclockwise PTt path of high-pressure/low-temperature rocks from the Coastal Cordillera accretionary complex of south-central Chile: constraints for the earliest stage of subduction mass flow. *Lithos* 75 (3-4), 283–310.
- Winchester, J. A., Floyd, P. A., 1977. Geochemical discrimination of different magma series and their differentiation products using immobile elements. *Chemical Geology* 20, 325–343.
- Yang, Z., Cheng, Y., Wang, H., 1986. *The geology of China*. Clarendon Press, Oxford, United Kingdom.
- Zack, T., Rivers, T., Foley, S. F., 2001. Cs-Rb-Ba systematics in phengite and amphibole; an assessment of fluid mobility at 2.0 GPa in eclogites from Trescolmen, Central Alps. *Contributions to Mineralogy and Petrology* 140 (6), 651–669.
- Zhang, H., Niu, H., Sato, H., Yu, X., Shan, Q., Zhang, B., Ito, J. i., Nagao, T., 2005. Late Paleozoic adakites and Nb-enriched basalts from northern Xinjiang, northwest China; evidence for the southward subduction of the paleo-Asian oceanic plate. *Island Arc* 14 (1), 55–68.

# Chapter 4

## THE CHEMICAL AND Sr-Nd-O ISOTOPIC COMPOSITIONS OF SUBDUCTION CHANNEL FLUIDS: CONSTRAINTS FROM ECLOGITES PARTIALLY TRANSFORMED TO BLUESCHISTS

### 4.1 Abstract

Eclogites from Sifnos (Greece) and the Tian Shan (China) have been uplifted as tectonic blocks in a serpentinite matrix interpreted to represent a paleo-subduction channel. They show a partial, fluid-induced blueschist-facies overprint, where predominantly glaucophane and white mica replace omphacite and garnet. Chemical changes associated with this overprint were calculated by mass-balance. These show a gain of Mg, Ni and Co and the loss of Si, Ca and REE in the blueschists compared to the eclogites. This points to a fluid source that was in equilibrium with peridotites or rocks with similar bulk chemistry, and that had added a sediment-derived flavour. For a better determination of the possible source(s) of this infiltrating fluid and to characterise the effect of this fluid on the rocks, mineral oxygen isotope analyses and whole rock Sr and Nd isotope analyses were performed from three small scale (dm–m) sequences, where a gradual transition from eclogite to retrograde blueschist is observed. In all three sequences the peak-metamorphic mineral assemblage omphacite and garnet (plus phengite in two sequences) are in oxygen isotope equilibrium ( $\Delta_{Omp-Grt} = 0.89\text{--}1.20\text{‰}$ ). Retrograde glaucophane ( $\delta^{18}\text{O} = +8.8$  to  $+9.8\text{‰}$ ), paragonite and phengite ( $\delta^{18}\text{O} = +9.2$  to  $+11.6\text{‰}$ ) are in oxygen isotope equilibrium as well. The values for glaucophane and white mica are about  $1.8\text{‰}$  higher than expected for equilibration with garnet and omphacite at eclogite-facies conditions and indicate the late-stage incorporation of a heavy O isotope signature that derived from the infiltrating fluid during the blueschist-facies overprint. Higher whole rock initial Nd isotopic compositions of the newly formed blueschist ( $\epsilon\text{Nd} = +10$ ) compared to the eclogite ( $\epsilon\text{Nd} = +7.3$ ) of one Tian Shan sequence supports the hypothesis that the fluids derived from a source of peridotitic composition. It is most likely that major elements control the characteristics of the subduction channel fluids. This feature mainly derives from the intense fluid-rock

interaction of slab-derived fluids with the peridotitic matrix within the subduction channel. The elevated Sr isotope composition points to a fluid-source signature either derive from the seawater-induced formation of serpentinite in the lithospheric slab mantle or from the altered oceanic crust. The sediment-derived LILE addition and the CO<sub>2</sub> component of these fluids may derive from the fluid-flow through the oceanic slab and the overlying sediment layer.

## 4.2 Introduction

Oceanic lithosphere, which has been subducted to great depths and metamorphosed under high-pressure conditions, is occasionally transported in fragments back to the surface by uplift in the subduction channel. The subduction channel is the partially serpentinitised mantle peridotite between the down going slab and the dry mantle wedge in the fore arc (Cloos and Shreve, 1988a,b). It develops by reaction of slab fluids with the mantle wedge peridotite (Peacock, 1993; Bebout, 1995; Poli and Schmidt, 1995; Fisher, 1996; Gerya et al., 2002). The fluid-induced changes in rheology, viscosity and buoyancy of the serpentinite compared to the unaltered mantle peridotite affect migration and transportation of incorporated slab-rocks to shallower levels (Gerya et al., 2002; Schwartz et al., 2001; Warren et al., 2008). The slab fluids are not only affecting the mantle peridotite, resulting in serpentinitisation and the formation of the subduction channel, but they also react with high-pressure rocks, which are transported within the serpentinitised matrix (Gerya et al., 2002; van der Straaten et al., 2008). This is of particular importance as recent research centres on the debate which subduction reservoir releases fluids that contribute most to the chemical budget of arc signatures (e.g., Scambelluri et al., 2001; Hermann et al., 2006; King et al., 2006; Bebout, 2007; Feineman et al., 2007; Zack and John, 2007). The subduction channel fluids may originate from different reservoirs: (I) the partly serpentinitised, subducted mantle peridotite underneath the oceanic crust (Hyndman and Peacock, 2003; Ranero et al., 2003; Ivandic et al., 2008), (II) the altered oceanic crust (e.g., Becker et al., 2000; Staudigel, 2003; Kelley et al., 2005; John et al., 2008), (III) marine subducted sediments (Plank and Langmuir, 1993; Rüpke et al., 2002), (IV) the mélange zone of the slab-wedge interface (King et al., 2006), which is similar to the mélange of the subduction channel above the slab. The partially serpentinitised subducted mantle peridotite is considered to represent the largest reservoir of fluids that can be released into the wedge, followed by the altered basaltic crust and the overlying sediments (Schmidt and Poli, 1998; Rüpke et al., 2002, 2004). In the subduction channel, fluids might inherit the chemical and isotopic signatures of these three reservoirs and might get overprinted by the signature of the partly serpentinitised peridotites of the mantle wedge as a fourth component. Eclogites ideally have a rather dry mineral assemblage and a well-defined basaltic composition. Thus, details about the fluid composition and fluid related metasomatic and metamorphic processes that are taking place in the fluid-rich environment of the subduction channel can be obtained from dry eclogites that have been transformed in this setting to wet blueschists (van der Straaten et al., 2008, in review). Radiogenic isotope ratios are a particularly useful tracer for the



identification of the fluid sources, since they, in contrast to trace element abundances, are not affected by chemical processes (e.g., mineral dissolution and precipitation), but reflect the signature of their source (Baxter and DePaolo, 2000). Oxygen isotope studies can place constraints on the nature and extent of pre- and post-metamorphic fluid-rock interactions (Baker et al., 1997; Zheng et al., 1999; Yui et al., 1997) and are of fundamental importance in understanding geochemical processes in metamorphic rocks (e.g. Chamberlain and Conrad, 1991; Zheng et al., 2003). Oxygen isotope compositions of minerals might indicate fluid-induced changes in the isotopic composition between late-stage blueschist-facies minerals and early eclogite-facies minerals, whereas the Sr and Nd isotopic signatures of fluids differ if they originate either from peridotites, oceanic or continental fragments or marine sediments. Relics of paleo-subduction zones and paleo-subduction channels are represented by subduction mélanges, which occur at the surface today. From such subduction mélanges on the island of Sifnos in Greece and in the Chinese part of the South Tian Shan, we investigated three dm to m scale sequences displaying gradual transitions from eclogite to retrograde blueschist. Newly formed minerals like glaucophane and white mica are formed at the expense of the eclogite-facies mineral assemblage omphacite and garnet ( $\pm$  phengite) during retrograde blueschist-facies metamorphism (van der Straaten et al., 2008, in review). Investigations about the fluid composition, based on major and trace elements, mass-balance calculations in combination with petrographical observations, were made in previous studies (van der Straaten et al., 2008, in review). Here we combine and enhance these results with O, Sr and Nd isotopic analyses to put additional constraints on the possible sources of the fluids acting at the slab-wedge interface and in the subduction channel. Although some information about the chemical budget for rocks in the hybridised mélange zone in the slab-wedge interface (e.g. Bebout, 2003; King et al., 2006; Spandler et al., 2008) or for HP rocks in the subduction channel (van der Straaten et al., 2008, in review) exists, we discuss isotopic data here, to constrain relevant fluid sources and the evolution of the fluid composition during the rehydration process of the eclogites.

### 4.3 Eclogite-blueschist transformation on Sifnos (Greece)

Exhumed and retrograde metasomatised mafic and ultramafic HP rocks juxtaposed in subduction mélanges occur in the Cyclades, e.g. on the island of Syros and in the northern part of Sifnos (Dixon, 1968; Schliestedt, 1980; Okrusch and Broecker, 1990; Keiter et al., 2004). The ophiolites are related to the Jurassic Pindos Ocean, which was divided in many deep basins and became subducted during several tectonic impulses (Bonneau, 1982). Exhumation of the HP units resulted from slab roll back and the formation of extensional faults in the Aegaen arc (Jolivet et al., 2003; van Hinsbergen, 2004). The roll back of the slab induced the opening of the “Cycladic window” and thus the exposure of the Cycladic islands (van Hinsbergen, 2004) within the Pindos zone (Jacobshagen, 1986) associated with the formation of an open subduction channel (Jolivet et al., 2003). The crustal thinning by extensional faulting caused the rapid and cool uplift of subducted high-pressure rocks (Schliestedt, 1990; van Hinsbergen, 2004).

The island of Sifnos is composed of a metamorphosed volcano-sedimentary sequence interlayered with marbles (Davis, 1966; Schliestedt, 1980, Figure 4.1). After a HP metamorphism in the Eocene, preserved in the northern part of the island, a greenschist-facies metamorphism followed in the Miocene, now dominantly occurring in the central and the southern units (Altherr et al., 1979; Schliestedt and Matthews, 1987; Okrusch and Broecker, 1990; Wijbrans et al., 1990). HP mafic rocks of Sifnos describe a burial P-T path under prograde lawsonite-blueschist-facies conditions, preserved by lawsonite pseudomorphs in the matrix of blueschists (Syros, e.g. Brady et al., 2001; van der Straaten et al., in review) or enclosed in garnet of blueschists and eclogites (Fry and Fyfe, 1971; Okrusch et al., 1978; Schmädicke and Will, 2003). Peak-metamorphic conditions reached temperatures of 600°C and pressures of 20 kbar and were followed along

a retrograde uplift path nearly opposite to the prograde burial path, characterised by contemporaneous cooling and decompression (Schliestedt and Okrusch, 1988; Trotet et al., 2001; Schmädicke and Will, 2003; Spear et al., 2006; van der Straaten et al., in review). The lawsonite pseudomorphs and undeformed needles of calcite forming pseudomorphs after aragonite on Syros are interpreted as hints for rapid (0.15 cm/a Schliestedt, 1990) and undisturbed uplift (Brady et al., 2004; Keiter et al., 2004). The HP rocks in north-Sifnos (blueschist, eclogite, chlorite-actinolite gneiss, glaucophane-jadeite gneiss) comprise metamorphosed calc-alkaline basalts, andesites and Fe-rich tholeiitic basalts with protolith characteristics related to MORB, island arc basalt, back-arc basalt or even boninite basalt (Mocek, 1994). In the bay of Vroulidia of northern Sifnos (Figure 4.1, eclogites display a blueschist-facies overprint. Sample Si 4-2 is a partly well preserved eclogite that passes laterally into a retrograde blueschist-facies rock (Figure 4.2A). The whole sequence contains garnet + omphacite + sodic, sodic-calcic and calcic amphibole + clinozoisite + phengite + rutile + quartz ± apatite ± chlorite ± albite ± calcite ± titanite ± opaque phases. Garnet and omphacite are the dominant minerals in the eclogite. Sodic amphibole, phengite and albite replace partly the matrix omphacite, which may become complete with increasing degree of blueschist-facies overprint. Garnet breaks down to amphibole, phengite and Fe-rich chlorite. Rutile in the matrix is partially replaced by titanite. Fluid-derived CO<sub>2</sub> has facilitated calcite growth during the breakdown of garnet and omphacite.

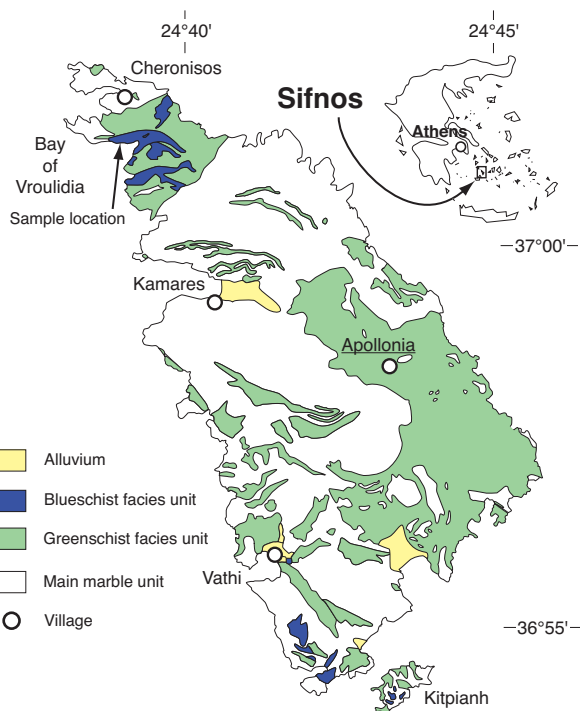


**Figure 4.1:** Simplified geological map of Sifnos modified after (Davis, 1966). The sample area is the northern branch of the Bay of Vroulidia as indicated.

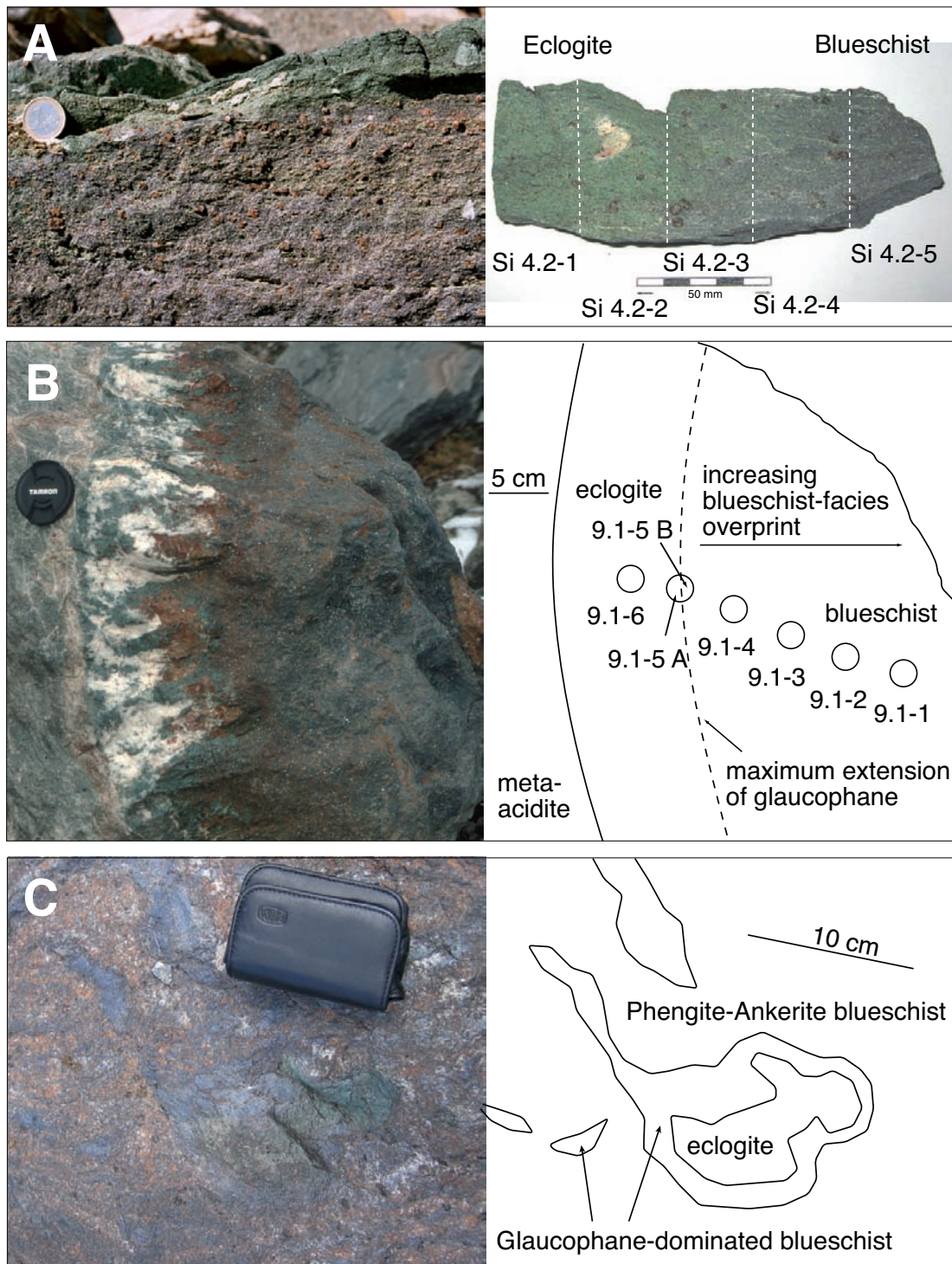


**Figure 4.2:** Blueschist-facies overprinted eclogite samples of A) Sifnos (Greece): photograph of sample Si 4-2 in the Bay of Vroulidia (left) and detail of the sample (right); B) Eclogite and blueschist sequence of sample FTS 9-1 in the Akanzayi River valley of the Chinese South Tian Shan (left) and schematic illustration of token drill holes (right); C) Photograph of an example of the pillow-meta basalts in the Atantayi River valley of the Tian Shan (left) and schematic differentiation between eclogite and two blueschist shells (right). Used samples are not displayed in Figure.

The whole rock composition of the eclogite and the associated blueschist indicates an oceanic mafic rock as precursor. REE and HFSE concentrations of the eclogite indicate an affinity to continental island arc basalt (van der Straaten et al., in review). Mass-balance calculations (following Gresens, 1967; Ague, 2003), based on fluid-immobility of HFSE, Al and O suggest overall volume increase of 2–4% and significant element mobility during the eclogite-blueschist transformation (van der Straaten et al., in review, Figure 4.3A). Loss of REE, Y, U, Th, Cs, Rb, Ba, K, Li, P, Ca and Si is related to the breakdown of garnet, omphacite, phengite and apatite, whereas the gain of Mg, Mn, Fe, Ni, Zn, Sr, Pb, CO<sub>2</sub> and H<sub>2</sub>O is related to the growth of newly formed glaucophane, clinozoisite, chlorite and calcite (van der Straaten et al., in review). A pervasive fluid infiltration on a large scale is not known for the eclogite-blueschist transition on Sifnos (Putlitz et al., 2000; Ganor et al., 1996; Schliestedt and Matthews, 1987), but the presence of a grain boundary film of fluids was postulated to facilitate isotopic and element equilibration between minerals (Putlitz et al., 2000). Hints for infiltration of  $\delta^{18}\text{O}$  enriched channelised fluids, probably in exchange with the associated marbles are described for the blueschist-greenschist transition in the central and southern units of Sifnos (Schliestedt and Matthews, 1987) and is also relevant for the eclogite-blueschist transformation in the northern part. Higher  $\delta^{18}\text{O}$  isotope compositions than that of the average oceanic crust is interpreted as low-temperature seawater alteration that typically occurs within the oceanic crust at modern spreading centres (Putlitz et al., 2000).

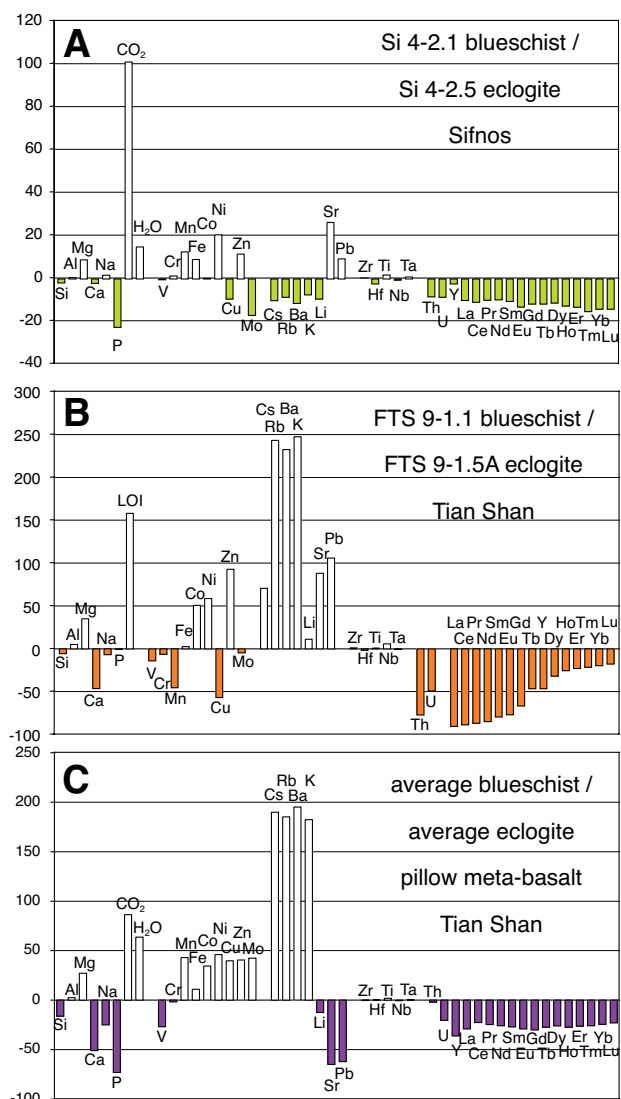


**Figure 4.3:** Element mobility of Tian Shan and Sifnos eclogite and blueschist sequences based on mass-balance calculation in percent. A) Element mobility of the eclogite-blueschist transformation of the Sifnos sample calculated based on immobility of HFSE (Zr, Hf, Ti, Nb and Ta), Al and O (van der Straaten et al., in review). B) Eclogite-blueschist transformation of the FTS 9–1 sequence of the Tian Shan calculated based on the immobility of HFSE, Al and O (van der Straaten et al., in review). C) Eclogite-blueschist transformation of the pillow metabasalts from Tian Shan calculated based on the immobility of HFSE and Th (van der Straaten et al., 2008).

## 4.4 Blueschist-facies overprint of eclogites in Tian Shan (China)

Fluid-induced prograde and retrograde metamorphic and metasomatic features in HP-rocks can be studied at the well-preserved subduction mélangé of the South Tian Shan Fold Belt. The high-pressure metamafic, -ultramafic and -sedimentary rocks are interpreted as relics of the Palaeozoic South Tian Shan Ocean, a marginal basin of the Turkestan Ocean, subducted and incorporated into the South Tian Shan orogen during Silurian and Carboniferous time (Ren et al., 1987; Bykadorov et al., 2003; Sobolev et al., 1986; Sengör and Natal'In, 1996). The predominantly metamafic rocks occur as greenschist-, blueschist- or eclogite-facies rocks, and, together with Silurian marbles, meta-sediments and peridotitic lenses, form the mélangé zone (Figure 4.4, Gao et al., 1995, 1998). Peak metamorphic conditions in eclogites reached pressures of about 20 kbar and temperatures of about 600°C, locally up to 700°C (Gao et al., 1998; Klemm, 2003; Lin and Enami, 2006; van der Straaten et al., 2008, in review). Some of the eclogites describe a P–T path with retrograde cooling and decompression (Gao et al., 1998; van der Straaten et al., 2008, in review), which is characteristic for uplift in a subduction channel (Cloos and Shreve, 1988a,b; Gerya et al., 2002). The Tian Shan high-pressure belt exhibits prograde dehydration related to fluid-induced eclogitisation, which is associated with vein and selvage formation (Gao and Klemm, 2001; Gao et al., 2007; John et al., 2008), as well as retrograde fluid-induced transformation of eclogites to blueschists (van der Straaten et al., 2008, in review). Peak metamorphism was reached at around  $343\pm 44$  Ma (Gao and Klemm, 2003) and retrograde cooling, metamorphism and uplift are interpreted to have lasted until Late Carboniferous times, between 320 and 300 Ma (dominantly 310–311 Ma, Klemm et al., 2005) based on white mica cooling ages (K–Ar, Ar–Ar, Rb–Sr).

Two different sequences comprising a gradual transition from eclogite to blueschist were investigated in this study: I) A lithologically layered sequence of eclogite that is laterally transformed to blueschist (Samples FTS 9–1.1 to 9–1.6, Figure 4.2B, in the following labelled as “FTS 9–1 sequence”, van der Straaten et al., in review) II) Meta-basalts with pillow structure (in the following labelled as “pillow meta-basalt”) with eclogite-facies mineralogy preserved in the pillow cores showing marginal transformation to blueschist (samples FTS 4–3.5, 4–3.3, 4–2.4, 4–1.1, Figure 4.2C, van der Straaten et al., 2008). Eclogite of the FTS 9-1 sequence contains omphacite + garnet + rutile + Cr-rich phengite + glaucophane + titanite ± calcite. In the blueschist-facies overprinted parts, omphacite and garnet are replaced by newly formed glaucophane and paragonite. Glaucophane in the matrix and in contact with the relict garnet and omphacite is transformed into sodic-calcic amphibole. With increasing blueschist-facies alteration the garnet is more and more replaced by chlorite and calcite and may even be totally consumed. Trace element concentrations of the eclogite show affinities to boninites or REE- and HFSE-depleted oceanic back arc basalts. The precursor rock of the eclogite presumably derived from a back-arc related regime (van der Straaten et al., in review). Distinct loss of up to 99 % of the LREE were obtained in mass-balance calculations (based on the assumption of immobility of HFSE and Al–O,

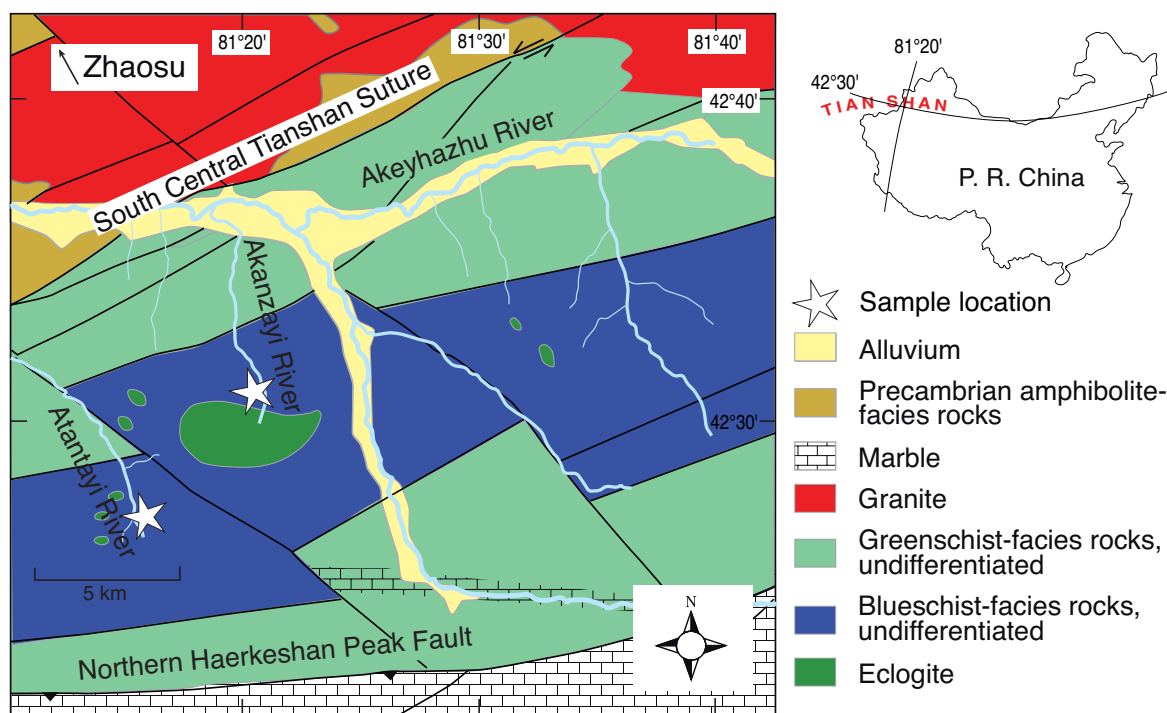


**Figure 4.4:** Simplified geological and metamorphic map of the Chinese South Tian Shan modified after Gao et al. (1999). Stars indicate sample areas.

following Gresens (1967); Ague and van Haren (1996); Ague (2003), Figure 4.3B) This loss is most likely related to the complete replacement of omphacite. Minor loss of HREE is related to resorption of garnet during the eclogite-blueschist transformation. The mineral assemblage of the pillow meta-basalts is garnet + omphacite + clinozoisite + rutile + apatite in the eclogite, which is transformed by fluid-induced retrograde metamorphism to a mainly phengite-glaucophane-ankerite-titanite-bearing blueschist. The eclogites of the pillow meta-basalts show an affinity to ocean island basalt (OIB). Based on the mass-balance calculations (Figure 4.3C) an overall volume and mass loss accompanied the blueschist-facies transformation. The eclogite-blueschist transformation is characterised by the loss of REE and Y due to dissolution and breakdown of apatite, clinozoisite (mainly LREE) and garnet (mainly HREE) as well as by the loss of P, Ca, U (breakdown of apatite) and Sr and Pb (breakdown of clinozoisite). Si, Ca and Na losses are associated with the replacement of omphacite and garnet. Gain of Mg, transition metals (Mn, Fe, Co, Ni, Zn), CO<sub>2</sub> and H<sub>2</sub>O is related to in the formation of glaucophane and ankerite. Cs, Rb, Ba and K gains (Figure 4.3C) were accompanied with the formation of white mica. The loss of REE and Si as well as the gain of Mg, Ni, Co and Zn in both sequences indicates that the fluid inducing the blueschist formation has been in equilibrium with a rock of peridotitic composition prior to infiltration. Strong enrichments of Cs, Rb, Ba, K and CO<sub>2</sub> in the blueschist compared to the eclogite are related to newly grown paragonite and calcite (van der Straaten et al., 2008, in review). The fluids are either derived from the partially serpentinised lithospheric

slab mantle or equilibrated with the mantle peridotite in the subduction channel above the slab. Because of the observed LILE enrichments (Cs, Rb, Ba and K) the fluids must have contained a sediment component, which is most likely derived from the subducted sediments (van der Straaten et al., 2008, in review).

## 4.5 Analytical methods

O isotope measurements of separated, hand picked, minerals were made at the Geowissenschaftliches Zentrum, University of Göttingen. Details of the analytical process are described by (Pack et al., 2007): 1–2 mg of the separated minerals are loaded in a Ni sample holder and evacuated overnight. Samples are melted with 50 W CO<sub>2</sub> laser ( $\lambda = 10.6 \mu\text{m}$ ) and fluorinated with purified F<sub>2</sub> gas ( $\sim 20$  mbar). Excess F<sub>2</sub> reacts with heated NaCl ( $\sim 150^\circ\text{C}$ ) to NaF and Cl<sub>2</sub> is trapped with liquid nitrogen at  $-196^\circ\text{C}$ . O<sub>2</sub> is trapped for 6–10 min on a 5 Å molecular sieve at  $-196^\circ\text{C}$  before being transferred into the sample bellows of the spectrometer by heating up the molecular sieve to  $+80^\circ\text{C}$ . Isotopic analyses are carried out using a Finnigan Delta plus mass spectrometer, which is equipped with three Faraday cups with  $3 \times 10^8$ ,  $3 \times 10^{11}$  and  $1 \times 10^{11} \Omega$  feedback resistors for simultaneous measurement of oxygen with m/z 32, 33 and 34. Samples are analysed by the conventional dual inlet system using bottled reference O<sub>2</sub> of known  $\delta^{18}\text{O}_{VSMOW}$  ( $+12.5\text{‰}$ ). Garnet (UWG–2, N = 9) was used as reference material and was measured with  $+5.66 \pm 0.08\text{‰}$  ( $+5.74 \pm 0.1\text{‰}$ , Valley et al., 1995).

Bulk rock Sr–Nd isotope analyses were carried out at the IFM–GEOMAR, University of Kiel on sample dissolutions previously analyzed by ICP–MS for trace element concentrations. Details of the sample dissolution procedure are given by van der Straaten et al. (2008). Ion chromatography followed established standard procedures (Hoernle et al., 2008). Isotopic ratios were determined by thermal ionization mass spectrometry (TIMS) on a MAT262 RPQ+ (Sr) and TRITON TIMS (Nd). Both instruments operate in static multi-collection mode. Sr and Nd isotopic ratios are normalized within each run to  $^{86}\text{Sr}/^{88}\text{Sr} = 0.1194$  and  $^{146}\text{Nd}/^{144}\text{Nd} = 0.7219$ , respectively, and all errors are reported as 2 sigma of the mean. Reference material measured along with the samples were normalized and gave  $^{87}\text{Sr}/^{86}\text{Sr} = 0.710250 \pm 0.000016$  (N = 4) for NBS987 and  $^{143}\text{Nd}/^{144}\text{Nd} = 0.511850 \pm 0.000003$  (N = 5) for La Jolla. Total chemistry blanks are  $<50$  pg for Sr and Nd and are considered negligible.

## 4.6 Isotope geochemistry results

The  $\delta^{18}\text{O}_{\text{mineral}}$  values measured in garnet, omphacite, amphibole, white mica and clinozoisite of Sifnos (Si 4.2 sequence) and Tian Shan (FTS 9.1 sequence and pillow metabasalts) are presented in Figure 4.5 and Table 4.1. All minerals from the three analysed eclogite–blueschist sequences have  $\delta^{18}\text{O}$  values that are higher than typical mantle values ( $5.3\text{–}6.2\text{‰}$ , e.g. Hart et al., 1999; Eiler et al., 2000). The  $\delta^{18}\text{O}$  values of garnet, om-

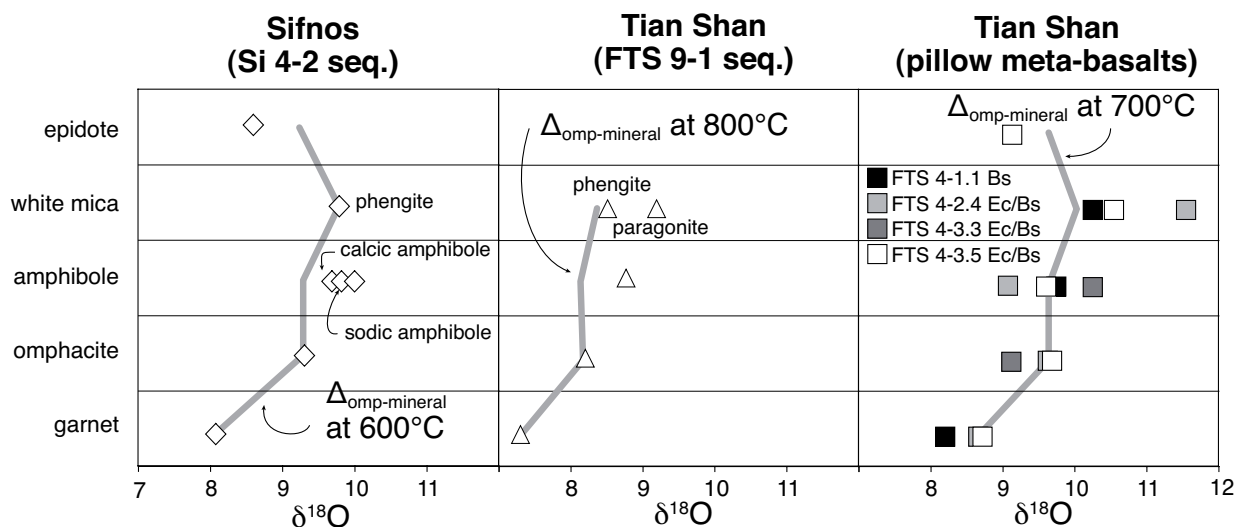


**Figure 4.5:** Mineral oxygen isotope composition of the three eclogite-blueschist sequences: (left to right) Si 4–2 (Sifnos), FTS 9–1 sequence and pillow meta-basalts (Tian Shan). Oxygen isotopic data from the pillow meta-basalts are measured from four different drill cores, each showing the direct eclogite-blueschist transformation, except FTS 4–1.1, which is pure blueschist. Grey lines show calculated equilibrium at shown temperatures of  $\Delta_{Omp-mineral}$  following the calculation of Zheng (1993a,b), see Table 4.1 and text for details.

phacite, clinozoisite and glaucophane (8–10‰) from the Sifnos sequence are in accordance to those values, presented by Putlitz et al. (2000) for minerals from meta-basalts from Sifnos (9–13‰). The  $\delta^{18}O$  of glaucophane, tremolite and phengite (9.6–9.9‰) are higher than those of garnet, clinozoisite and omphacite (8.1–9.3‰) in the Sifnos sequence. The FTS 9–1 sequence in the Tian Shan shows slightly lower  $\delta^{18}O$  of omphacite and garnet (7.3–8.2‰) compared to the Sifnos values. The  $\delta^{18}O$  of the blueschist-facies glaucophane is slightly higher (8.8‰) than those of garnet and omphacite, whereas the eclogite-facies phengite has a lower  $\delta^{18}O$  (8.5‰) than the blueschist-facies paragonite (9.2‰). The pillow meta-basalts have  $\delta^{18}O$  values of eclogite-facies omphacite and garnet between 8.2 and 9.7‰ and high values of blueschist-facies glaucophane (9.1–9.7‰) and highest values in blueschist-facies phengite (10.2–11.6‰). The only analysed clinozoisite from sample FTS 4–3.5 (pillow meta-basalts) has  $\delta^{18}O = 9.1‰$ . Sr and Nd isotopic compositions of whole rocks from the Sifnos and the Tian Shan are listed in Table 4.2 and shown in Figure 4.6. Initial isotopic compositions of  $(^{87}Sr/^{86}Sr)_i$  and  $(^{143}Nd/^{144}Nd)_i$  were calculated for 42 Ma for the Sifnos samples (Altherr et al., 1979; Wijbrans et al., 1990). Eclogite and blueschist of the Sifnos sequence show no significant difference in  $(^{87}Sr/^{86}Sr)_{42}$  and  $\epsilon Nd_{42}$ , with both ratios plotting close to the composition of the Bulk Silicate Earth (BSE) at that time. Cooling ages based on white mica Ar–Ar and K–Ar dating and on Rb–Sr isochrons cluster mostly around  $310 \pm 10$  Ma for blueschists in the Tian Shan (Klemd et al., 2005). Figure 4.7A, B show two Rb–Sr whole-rock isochrons for eclogites and blueschists of the pillow meta-basalts of the Tian Shan (calculated with Isoplot v3.0; Ludwig, 2003).



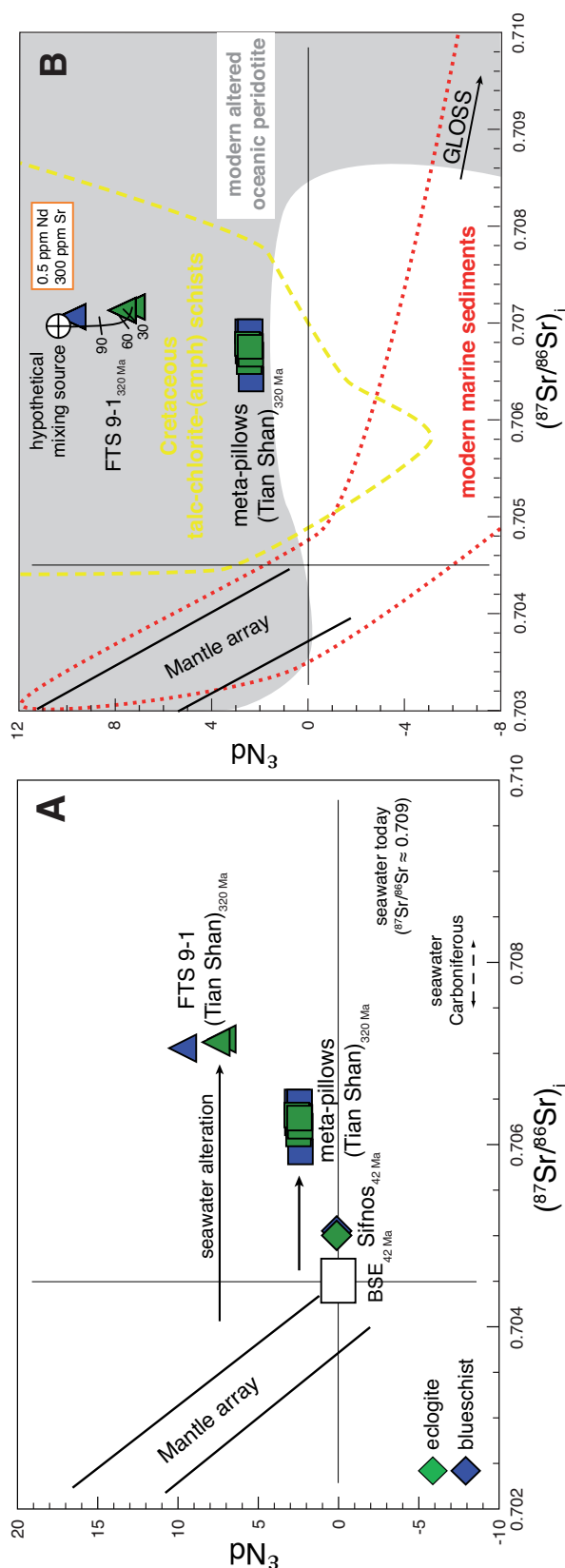


**Figure 4.6:** A) Radiogenic isotope composition of eclogites (grey) and blueschist (white) of the Sifnos (diamonds) and the two Tian Shan sequences FTS 9-1 (triangles) and pillow meta-basalts (squares). Uncertainties in the isotopic values are smaller than the symbol size (Table 4.2). Data sources:  $^{87}\text{Sr}/^{86}\text{Sr}$  seawater values of Carboniferous and today from [Veizer \(1989\)](#); mantle array from [Rollinson \(1993\)](#). Initial isotopic composition recalculated for Sifnos sample with 42Ma ([Altherr et al., 1979](#); [Wijbrans et al., 1990](#)) and for Tian Shan with 320 Ma (see text for detail and Figure 4.7A); Sr, Rb, Nd and Sm concentrations for recalculation of the initial age are taken from [van der Straaten et al. \(2008\)](#). The Nd isotopic composition is expressed as  $\epsilon\text{Nd}$ , calculated using  $(^{143}\text{Nd}/^{144}\text{Nd})_{\text{CHUR,today}}=0.512638$  and  $(^{147}\text{Sm}/^{144}\text{Nd})_{\text{CHUR,today}}=0.1966$  ([Goldstein et al., 1984](#)). Bulk silicate earth (BSE) composition recalculated to 42 Ma using  $(^{87}\text{Sr}/^{86}\text{Sr})_{\text{BSE,today}}=0.7045$  and  $(^{87}\text{Rb}/^{86}\text{Sr})_{\text{BSE,today}}=0.0827$  ([DePaolo, 1988](#)). B) Modelled mixing line between hypothetical fluid source composition and the average eclogite composition of the FTS 9-1 sequence of the Tian Shan. Tick marks reflect 30% mixing. Parameters used in the calculations are as follows: FTS 9-1 seq.: 0.5 ppm Nd, 300 ppm Sr (altered marine peridotite from [Snow et al., 1994](#); [Snow and Reisberg, 1995](#)),  $^{87}\text{Sr}/^{86}\text{Sr}=0.707$  and  $\epsilon\text{Nd}=+10$ , chosen near the blueschist composition which reflects strong equilibrium with peridotite (van der Straaten et al., in review). Data sources: light grey shaded area: extensively altered oceanic peridotites (PetPD Petrological database of the oceanfloor, <http://www.petdb.org>; [Snow et al., 1994](#); [Snow and Reisberg, 1995](#)); dark grey dashed line area: Cretaceous (110-115Ma) talc-chlorite-(amph) schists of the Catalina Schist, California ([King et al., 2006](#)); dark grey dotted line area: modern marine sediment array from GEOROC, <http://georoc.mpch-mainz.gwdg.de>; GLOSS ([Plank and Langmuir, 1993](#)).

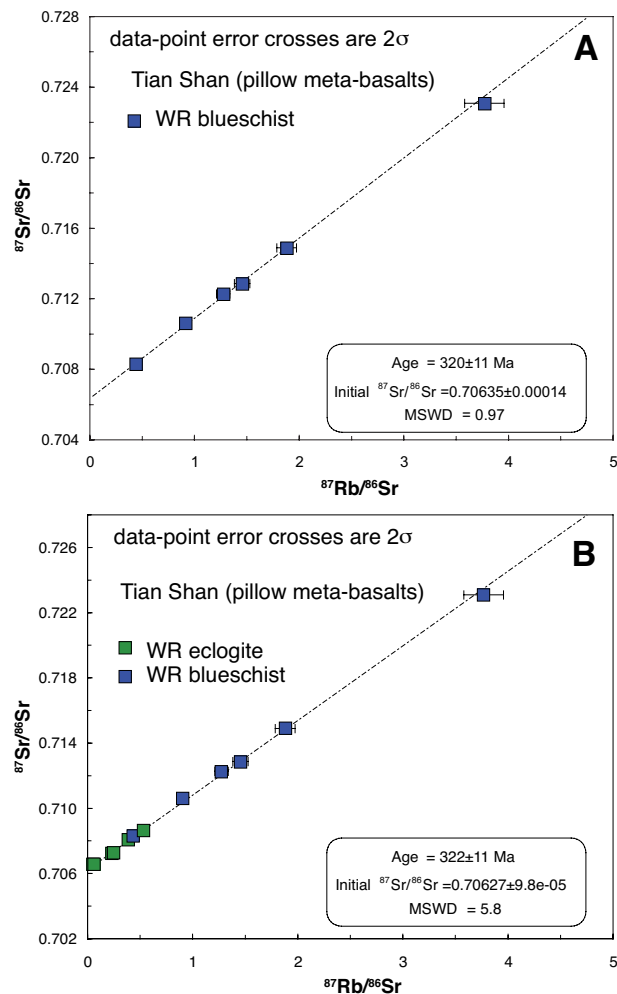


**Figure 4.7:** A)  $^{87}\text{Rb}/^{86}\text{Sr}$  isochron from whole rock blueschists of the pillow meta-basalts, (Tian Shan). B)  $^{87}\text{Rb}/^{86}\text{Sr}$  isochron from whole rock blueschists and eclogites of the pillow meta-basalts (Tian Shan). Eclogites and blueschists show the same isochron age (input errors for both:  $^{87}\text{Sr}/^{86}\text{Sr} = 5\%$ ,  $^{87}\text{Sr}/^{86}\text{Sr} = 0.0024\%$ ).

The blueschist samples are plotting on a well-defined isochron (MSWD = 0.97) and show an initial  $^{87}\text{Sr}/^{86}\text{Sr}$  value of  $0.70635 \pm 0.00014$  with an age of  $320 \pm 11$  Ma ( $2\sigma$ ; Figure 4.7A). This age overlaps with errors with the predominant cooling ages of 310-311 Ma and is in good agreement with the provided overall age range of 323-303 Ma (Klemd et al., 2005). The pillow meta-basalt eclogites have lower  $^{87}\text{Rb}/^{86}\text{Sr}$  ratios than the associated blueschists (Figure 4.7B). Together, eclogite and blueschists provide an isochron age of  $322 \pm 11$  Ma (MSWD = 5.8) with a similar initial  $^{87}\text{Sr}/^{86}\text{Sr}$  of  $0.70627 \pm 0.000098$  (Figure 4.7B). Based on 320Ma values the eclogites and blueschists of the pillow meta-basalts do not show significant differences in the  $(^{87}\text{Sr}/^{86}\text{Sr})_{320\text{Ma}}$  and  $(\epsilon\text{Nd})_{320\text{Ma}}$  values. Calculation of an isochron age for the FTS 9.1 sequence of Tian Shan failed as the  $^{87}\text{Rb}/^{86}\text{Sr}$  values of this sequence are very low ( $<0.05$ ) and a reliable age is not provided. The  $(^{87}\text{Sr}/^{86}\text{Sr})_i$  and the  $\epsilon\text{Nd}$  values for the FTS 9-1 sequence are also calculated for 320 Ma. The eclogite-blueschist transformation of the FTS 9-1 sequence shows increasing  $\epsilon\text{Nd}$  values of +7.3 to +10 at relatively constant  $(^{87}\text{Sr}/^{86}\text{Sr})_{320\text{Ma}}$  values of about  $0.70712 \pm 0.00005$ . Both Tian Shan sequences have Sr isotopic compositions that are displaced from the mantle array towards higher values, whereas Nd isotopic compositions overlap with those of typical mantle-derived rocks (Figure 4.6A).

## 4.7 Discussion

### 4.7.1 Stable oxygen isotopes: constraints on metamorphic equilibrium and metamorphic temperatures

The oxygen isotopic composition of a certain mineral is dependent on the isotopic composition of the bulk rock, the minerals that are equilibrium with the mineral of interest and temperature of formation (Zheng, 1993a,b). To test oxygen isotopic equilibrium conditions between minerals of the investigated eclogites and blueschists and to determine metamorphic temperatures, the temperature dependent theoretical isotope fractionation between all isotopically analysed mineral pairs have been calculated after the method of Zheng (1993a,b) in the temperature range 300–800°C (Table 4.1). For solid solution minerals omphacite, garnet and sodic amphibole, fractionations were calculated for the known endmember proportions based on the microprobe mineral chemical data (van der Straaten et al., 2008, in review). The average core composition of matrix glaucophane, the core composition of matrix omphacite and the rim composition of garnet were used in the calculations (Table 4.1). In the Sifnos Si 4–2 sequence, the green amphibole, which is a calcic amphibole of winchite to tremolite composition, was measured beside the blue sodic amphibole, which is glaucophane. These results of these calculations will be discussed and compared with the measured isotopic mineral data and the petrological observations and P-T estimates. The results are given in Figure 4.5 and Table 4.1.

Garnet and omphacite as major phases in eclogites should have the O-isotope composition of the peak metamorphic stage. The calculated fractionation of  $\Delta_{Omp-Grt} = 1.21\text{‰}$  at 600°C of sample Si 4–2 from Sifnos agrees with the measured fractionation (1.20‰, Table 4.1) and the peak-metamorphic temperature estimate of 600°C calculated with the P-T pseudosections (van der Straaten et al., in review). In addition, the measured  $\Delta_{Omp-Phe} = -0.53\text{‰}$  is similar to the calculated  $\Delta_{Omp-Phe} = -0.47$  to  $-0.57\text{‰}$  at 500 and 600°C, indicating equilibrium of phengite, omphacite and garnet during eclogite-facies conditions. However, equilibrium between the eclogite-facies mineral assemblage and the blueschist-facies glaucophane or epidote cannot be verified (Figure 4.5). Moreover, glaucophane and epidote are not in isotopic equilibrium. The calculated  $\Delta_{Omp-Gln} = -0.04\text{‰}$  at 600°C differ from the measured  $\Delta_{Omp-Gln} = -0.37$  to  $-0.52$  (Table 4.1). The measured  $\Delta_{Omp-Ep}$  differs for about 0.6‰ from the calculated  $\Delta_{Omp-Ep} = 0.05\text{‰}$  (600°C). However, the measured  $\Delta_{Ep-Tr} = -0.91\text{‰}$  is in fair agreement with the calculated  $\Delta_{Ep-Tr} = -0.74$  to  $-0.95\text{‰}$  at 300 and 400°C, which might indicate a late-stage equilibrium between epidote and Ca-amphibole during a greenschist-facies overprint. A retrograde greenschist-facies metamorphism has been described for most lithologies on Sifnos (Altherr et al., 1979; Schliestedt and Matthews, 1987; Okrusch and Broecker, 1990; Wijbrans et al., 1990).

The FTS 9-1 sequence in the Tian Shan displays a measured  $\Delta_{Omp-Grt} = 0.89\text{‰}$ , which is similar to the calculated fractionation of 0.89‰ at 800°C. In this case the temperature estimate based on the oxygen isotope fractionation is around 100°C higher than the peak-metamorphic temperature calculated with Perple\_X in P-T pseudosections (van der Straaten et al., in review). An oxygen isotope fractionation of  $\Delta_{Omp-Grt} = 1.06\text{‰}$  is

**Table 4.1:** Measured mineral oxygen isotope composition in eclogites and blueschists of Sifnos and Tian Shan and calculated temperatures.

Sample		$\delta^{18}\text{O}$ (‰)	Pair	$\Delta^{18}\text{O}$ (‰)	T(°C)*
<b>Sifnos</b>					
Si 4-2.1					
Eclogite	Omp	+9.31	Omp-Grt	1.2	611 ± 43
	Grt	+8.11	Phe-Omp	0.53	549 ± 94
	Gln	+9.83	Omp-Gln	-0.52	-
Si 4-2.6					
Blueschist	Phe	+9.84			
	Gln	+9.68	Tr-Czo	0.91	322 ± 42
	Tr	+9.57			
	Czo	+8.66			
<b>Tian Shan</b>					
FTS 9-1.5 A					
Eclogite	Omp	+8.2	Omp-Grt	0.89	803 ± 64
	Grt	+7.31	Phe-Omp	0.32	752 ± 180
	Phe	+8.52	Phe-Grt	1.21	780 ± 47
FTS 9-1.5 B					
Blueschist	Gln	+8.81	Pg-Gln	0.39	643 ± 139
	Pg	+9.2			
FTS 4-3.5					
Eclogite and Blueschist	Omp	+9.68	Omp-Grt	0.97	729 ± 57
	Grt	+8.71	Omp-Ep	0.55	-
	Czo	+9.13	Omp-Gln	0.07	-
	Gln	+9.61			
	Phe	+10.54			
FTS 4-2.4					
Eclogite and Blueschist	Omp	+9.63	Omp-Grt	0.97	729 ± 57
	Grt	+8.66	Omp-Gln	0.55	-
	Gln	+9.08			
	Phe	+11.55			
FTS 4-3.3					
Eclogite and Blueschist	Omp	+9.12	Omp-Gln	-1.13	-
	Gln	+10.25			
FTS 4-1.1					
Blueschist	Phe	+10.25	Gln-Grt	1.52	479 ± 30
	Gln	+9.72	Phe-Grt	2.05	504 ± 23
	Grt	+8.2	Phe-Gln	0.53	587 ± 99

Minerals: Omp, omphacite (Si 4-2.X,  $\text{Jd}_{39}\text{Ac}_{05}\text{Di}_{39}\text{Hd}_{17}$ ; FTS 9-1.X,  $\text{Jd}_{50}\text{Di}_{38}\text{Hd}_{12}$ ; FTS 4-X.X,  $\text{Jd}_{37}\text{Ac}_{08}\text{Di}_{39}\text{Hd}_{16}$ ); Grt, garnet (Si 4-2.X,  $\text{Alm}_{55}\text{Sps}_{05}\text{Grs}_{30}\text{Prp}_{10}$ ; FTS 9-1.X,  $\text{Alm}_{60}\text{Sps}_{05}\text{Grs}_{20}\text{Prp}_{15}$ ; FTS 4-X.X,  $\text{Alm}_{62}\text{Sps}_{01}\text{Grs}_{25}\text{Prp}_{12}$ ); Gln, glaucophane (Si 4-2.X,  $\text{Gln}_{75}\text{Rbk}_{05}$ ; FTS 4-X.X,  $\text{Gln}_{75}\text{Rbk}_{25}$ ); Tr, tremolite; Phe, phengite; Pg, paragonite; Czo, clinozoisite. \* Calculated in terms of the calibration of [Zheng \(1993a,b\)](#), error used =  $0.1\text{‰}(1\sigma)$ .

**Table 4.1:** (cont.) Comparison of measured and calculated mineral oxygen isotopic compositions dependent on temperature. Calculations for certain isotopic mineral pair compositions follows the description of Zheng (1993a,b).

<b>Sifnos (Si 4-2 sequence)</b>								
T (°C)	Pair* $\Delta^{18}\text{O}$ (‰)	Omp–Grt	Omp–Gln	Omp–Tr	Omp–Phe	Omp–Ep	Ep–Tr	Phe–Tr
300		2.40	-0.06	0.62	-0.92	0.10	-0.95	-1.71
400		1.86	-0.05	0.49	-0.71	0.08	-0.74	-1.33
500		1.49	-0.04	0.39	-0.57	0.06	-0.59	-1.07
600		1.21	-0.04	0.32	-0.47	0.05	-0.48	-0.87
700		1.00	-0.03	0.27	-0.39	0.04	-0.40	-0.72
800		0.84	-0.21	0.42	-0.32	0.03	-0.33	-0.61
	observed:	1.20	-0.37	-0.26	-0.53	0.65	-0.91	0.27
			-0.52					

---

<b>Tian Shan (FTS 9–1 sequence)</b>						
T (°C)	Pair* $\Delta^{18}\text{O}$ (‰)	Omp–Grt	Omp–Gln	Omp–Pg	Omp–Phe	Pg–Gln
300		2.54	0.25	-0.54	-0.78	0.79
400		1.97	0.20	-0.42	-0.61	0.62
500		1.58	0.16	-0.33	-0.49	0.49
600		1.28	0.13	-0.27	-0.40	0.40
700		1.06	0.11	-0.22	-0.33	0.34
800		0.89	0.09	-0.19	-0.28	0.28
	observed:	0.89	-0.61	-1.00	-0.32	0.39

---

<b>Tian Shan (Pillow meta-basalts)</b>								
T (°C)	Pair* $\Delta^{18}\text{O}$ (‰)	Omp–Grt	Omp–Gln	Omp–Phe	Omp–Ep	Gln–Ep	Phe–Gln	Phe–Ep
300		2.43	0.09	-0.89	0.08	0.16	0.98	0.81
400		1.88	0.07	-0.69	0.06	0.13	0.76	0.64
500		1.50	0.06	-0.56	0.05	0.11	0.62	0.51
600		1.23	0.05	-0.45	0.04	0.09	0.50	0.42
700		1.01	0.04	-0.38	0.03	0.07	0.42	0.35
800		0.85	0.04	-0.31	0.02	0.06	0.35	0.29
	observed:							
	FTS 4–3.5	0.97	0.07	-0.86	0.55	0.48	0.93	1.37
	FTS 4–2.4	0.97	0.55	-1.92			2.47	
	FTS 4–3.3		-1.13					
	FTS 4–1.1						0.53	

\* Mineral composition as above, magenta: similarity in calculated and measured oxygen isotopic fractionation.

Table 4.2: Sr and Nd isotope data.

Sample rock type	Si 4-2.1 eclogite	Si 4-2.6 blueschist	F <sup>T</sup> S 9-1.6 eclogite	F <sup>T</sup> S 9-1.5A+B eclogite	F <sup>T</sup> S 9-1.1 blueschist	F <sup>T</sup> S 4-1.1 blueschist	F <sup>T</sup> S 4-1.5 blueschist	F <sup>T</sup> S 4-1.5 eclogite
Rb (ppm)	30.6	39.2	0.64	1.65	5.7	69.2	57.2	29.8
Sr (ppm)	917	738	84.5	159	301	138	44.0	356
( <sup>87</sup> Rb/ <sup>86</sup> Sr)	0.10	0.15	0.02	0.03	0.05	1.45	3.77	0.24
( <sup>87</sup> Sr/ <sup>86</sup> Sr) <sub>m</sub>	0.705065±06	0.705104±05	0.707266±06	0.707268±06	0.707315±06	0.712869±07	0.723093±05	0.707226±06
( <sup>87</sup> Sr/ <sup>86</sup> Sr) <sub>i*</sub>	0.705010	0.705016	0.707166	0.707131	0.707065	0.706244	0.705925	0.706123
Sm (ppm)	5.86	4.89	0.67	1.57	0.32	2.61	5.52	6.88
Nd (ppm)	32.2	27.7	2.23	4.73	0.71	11.2	23.5	28.4
( <sup>147</sup> Sm/ <sup>144</sup> Nd)	0.1095	0.1064	0.1808	0.1998	0.2717	0.1403	0.1414	0.1458
( <sup>143</sup> Nd/ <sup>144</sup> Nd) <sub>m</sub>	0.512623±02	0.512624±01	0.512980±04	0.513039±03	0.513297±03	0.512654±02	0.512647±03	0.512662±03
( <sup>143</sup> Nd/ <sup>144</sup> Nd) <sub>i*</sub>	0.512594	0.512596	0.512601	0.512621	0.512728	0.512361	0.512351	0.512357
ε(Nd) <sub>i*</sub>	0.15	0.18	7.33	7.70	9.79	2.62	2.43	2.55
Sample rock type	F <sup>T</sup> S 4-2.4 eclogite	F <sup>T</sup> S 4-2.4 blueschist	F <sup>T</sup> S 4-3.1 blueschist	F <sup>T</sup> S 4-3.1 eclogite	F <sup>T</sup> S 4-3.3 blueschist	F <sup>T</sup> S 4-3.3 eclogite	F <sup>T</sup> S 4-3.5 eclogite	F <sup>T</sup> S 4-3.5 blueschist
Rb (ppm)	46.4	63.7	55.4	24.8	56.9	7.23	4.97	25.8
Sr (ppm)	251	98.2	126	183	180	402	246	170
( <sup>87</sup> Rb/ <sup>86</sup> Sr)	0.54	1.88	1.27	0.39	0.91	0.05	0.06	0.44
( <sup>87</sup> Sr/ <sup>86</sup> Sr) <sub>m</sub>	0.708644±05	0.714895±05	0.712275±06	0.708084±06	0.710629±06	0.706567±05	0.706563±05	0.708318±05
( <sup>87</sup> Sr/ <sup>86</sup> Sr) <sub>i*</sub>	0.706207	0.706335	0.706474	0.706305	0.706474	0.706330	0.706396	0.706321
Sm (ppm)	6.55	8.68	3.68	4.45	4.17	5.24	4.58	4.94
Nd (ppm)	27.3	38.3	15.5	18.7	16.9	21.6	18.7	19.9
( <sup>147</sup> Sm/ <sup>144</sup> Nd)	0.1444	0.1364	0.1429	0.1434	0.1485	0.1460	0.1474	0.1494
( <sup>143</sup> Nd/ <sup>144</sup> Nd) <sub>m</sub>	0.512654±03	0.512642±03	0.512661±03	0.512653±02	0.512665±02	0.512668±02	0.512663±02	0.512672±03
( <sup>143</sup> Nd/ <sup>144</sup> Nd) <sub>i*</sub>	0.512351	0.512356	0.512361	0.512352	0.512353	0.512362	0.512354	0.512359
ε(Nd) <sub>i*</sub>	2.45	2.55	2.64	2.47	2.48	2.66	2.49	2.59

m = measured; i\* initial age recalculated to 42Ma (Atherton et al., 1979; Wijbrans et al., 1990) for Si 4-2.1 and Si 4-2.6; for F<sup>T</sup>S samples (Tian Shan) 320Ma, this study, see text for detail. Recalculation based on Sr, Rb, Sm and Nd concentrations (van der Straeten et al., 2008, in review); εNd calculated using (<sup>143</sup>Nd/<sup>144</sup>Nd)<sub>CHUR-today</sub>=0.512638 and (<sup>147</sup>Sm/<sup>144</sup>Nd)<sub>CHUR-today</sub>=0.1966 (Goldstein et al., 1984); (<sup>87</sup>Sr/<sup>86</sup>Sr)<sub>i</sub> calculated based on Faure (1986).

calculated assuming peak-metamorphic temperatures of around 700°C as obtained from pseudosections (van der Straaten et al., 2008). Taking into account the errors in temperature estimates for oxygen isotope thermometry ( $803 \pm 64^\circ\text{C}$ ) and pseudosections ( $\pm 50^\circ\text{C}$ ), near equilibrium between omphacite and garnet can be assumed during the eclogite-facies stage. In addition, the calculated fractionation of  $\Delta_{Omp-Phe} = -0.33\text{‰}$  at 700 °C is similar to the measured  $\Delta_{Omp-Phe}$  ( $-0.32\text{‰}$ ), indicating equilibrium between omphacite and phengite at these temperatures. Equilibrium between omphacite, garnet and phengite during eclogite-facies conditions is in agreement with petrographical observations and with the results of P–T pseudosections (van der Straaten et al., in review). Measured  $\Delta_{Omp-Gln} = -0.61\text{‰}$  and  $\Delta_{Omp-Pg} = -1.00\text{‰}$  differ significantly from the calculated fractionations of these pairs ( $\Delta_{Omp-Gln} = 0.11\text{--}0.16\text{‰}$  and  $\Delta_{Omp-Pg} = -0.22$  to  $-0.33\text{‰}$  at 500–700°C), suggesting that glaucophane and paragonite have not been in equilibrium with omphacite and garnet. The measured  $\Delta_{Pg-Gln} = 0.39\text{‰}$  is similar to the calculated fractionation of  $0.40\text{‰}$  at 600°C, indicating that paragonite and glaucophane have been in equilibrium at 600°C, which is consistent with the stability of the assemblage glaucophane-paragonite calculated in the P–T pseudosection (van der Straaten et al., in review).

Samples of the pillow meta-basalts of the Tian Shan contain of pure blueschist (Sample FTS 4–1.1) and three drill cores contain of relict eclogite with domains of blueschist overprinting the eclogite (Samples FTS 4–2.4, FTS 4–3.3 and FTS 4–3.5). Two measured oxygen isotope fractionations between omphacite and garnet ( $\Delta_{Omp-Grt} = 0.97\text{‰}$ ) point to an equilibration temperature of  $728 \pm 57^\circ\text{C}$  (FTS 4–3.5 and 4–2.4, Table 4.1), which is somewhat higher, but within errors identical to the peak-metamorphic temperature of omphacite and garnet of around 650°C obtained with P–T pseudosections (van der Straaten et al., 2008). The measured  $\Delta_{Omp-Gln}$  shows high variations, which is in sample FTS 4–2.4 around 0.50‰ lower and in sample FTS 4–3.3 around 1.10‰ higher than the calculated equilibrium values (Table 4.1, Figure 4.5C). The measured  $\Delta_{Omp-Gln}$  value of sample FTS 4–3.5 is similar to the calculated  $\Delta_{Omp-Gln} = 0.04\text{--}0.07\text{‰}$  at 400–700°C. This suggests equilibrium for sample FTS 4–3.5 between glaucophane and omphacite even though the glaucophane derives from the blueschist and the omphacite derives from the enclosed eclogite domain (Figure 4.5C) and thus we do not consider equilibrium and ignore the coincident and apparent oxygen isotope equilibrium.  $\Delta_{Omp-Phe}$  of samples FTS 4–3.5 and 4–2.4 differ for about 0.5‰ and 1.5‰, respectively, compared to the calculated  $\Delta_{Omp-Phe} = -0.45$  at 600°C. Moreover, the measured  $\Delta_{Omp-Ep} = 0.55$  in Sample FTS 4–3.5 is about 0.50‰ lower than the calculated equilibrium fractionation at 600°C. Hence, glaucophane, phengite and epidote were probably not in equilibrium with omphacite during the peak-metamorphic eclogite facies stage. Equilibrium has been achieved between phengite and glaucophane in the phengite-ankerite blueschist (sample FTS 4–1.1), as the measured  $\Delta_{Phe-Gln} = 0.53\text{‰}$  is similar to the calculated  $\Delta_{Phe-Gln} = 0.50\text{--}0.62\text{‰}$  at 500–600°C. Clinozoisite in sample FTS 4–3.5 shows no oxygen isotope equilibrium with none of the associated minerals, which may derive from the fact that it was not possible to obtain a clean mineral separate of the inclusion rich clinozoisite. In summary, equilibrium is preserved between omphacite and garnet during peak-metamorphic conditions in the eclogite domains of the pillow meta-basalts and between glaucophane and phengite of

the blueschist domain, which are the dominant and stable minerals in the blueschist under retrograde conditions. The FTS 9–1 sequence and the pillow meta-basalts of the Tian Shan show therefore similarities in oxygen equilibrium under peak-metamorphic conditions between omphacite and garnet, and under retrograde blueschist-facies conditions between glaucophane and white mica, which is phengite in the pillow meta-basalts and paragonite in the FTS 9–1 sequence.

#### 4.7.2 Evidence for inherited seawater alteration?

All eclogites that are partially overprinted by a blueschist-facies metasomatism and metamorphism derive from oceanic basalts. It has to be evaluated if and to which extent they have been affected by seawater alteration prior to this overprint. Especially pillow-basalts are susceptible for alteration, since the space between the pillows serves as fluid pathways and alleviate seawater access. Mobility and enrichment of K and Rb are distinct features of seawater alteration in oceanic basalts (Becker et al., 2000; Staudigel, 2003). Bebout (2003) used changes in trace element concentrations and trace element ratios to distinguish between seawater alteration and mobility during metamorphic fluid/rock interaction. The eclogites of all studied sequences do not show characteristic enrichments that follow the seawater alteration trend, as they plot near their precursor composition of N-MORB or OIB on various discrimination diagrams. Thus a significant chemical alteration prior to metamorphism can be excluded. The Tian Shan blueschists are highly enriched in Rb, K, Cs and Ba, whereas the Sifnos blueschist are only slightly enriched. Cs and Ba are usually not enriched due to seawater alteration (e.g. Bebout, 2003). Figure 4.8A shows that K and Rb enrichment of blueschists and eclogites follows the seawater alteration trend, but this enrichment is also typical for additions during HP/UHP metamorphism (Bebout, 2007). However, the enrichment of Ba and K cannot be related to seawater alteration, since the relevant trace element ratios (K/Th vs. Ba/Th) follow the HP/UHP-metamorphic addition trend (Figure 4.8B, C). A further strong indication for seawater alteration would be the gain of Uranium (Bebout, 2007; Staudigel, 2003), but the here described blueschists show a loss of U compared to the precursor eclogite (Figure 4.8D). Therefore an alteration of LILE concentrations by seawater is unlikely.

It is well established that seawater alteration on the ocean floor increases the  $\delta^{18}\text{O}$  values at low temperatures ( $<150^\circ\text{C}$ ). Only at greater depth and higher temperatures (100–400°C)  $\delta^{18}\text{O}$  values decrease to values lower than that of the typical mantle composition (Mühlenbachs and Clayton, 1976; Gregory and Taylor, 1981). An oxygen isotope signature indicative for seawater alteration was proposed for HP metamorphic rocks from Sifnos by Putlitz et al. (2000), because of higher whole rock  $\delta^{18}\text{O}$  values (11–14‰) in the HP rocks compared to that of fresh MORB. The  $\delta^{18}\text{O}$  of an eclogitic whole rock can be derived from the omphacite and garnet compositions, as these minerals are the main components in the rock. Putlitz et al. (2000) assumed that  $\delta^{18}\text{O}_{\text{omphacite}}$  reflects the whole rock  $\delta^{18}\text{O}$  composition and calculated a whole rock  $\delta^{18}\text{O}$  value of +5.8‰ at 500°C for a model eclogite with 60% omphacite, 20% garnet and 20% glaucophane. In case of the eclogites from the Tian Shan and from Sifnos omphacite is always the dominant mineral ( $>60$  vol.%) and thus the



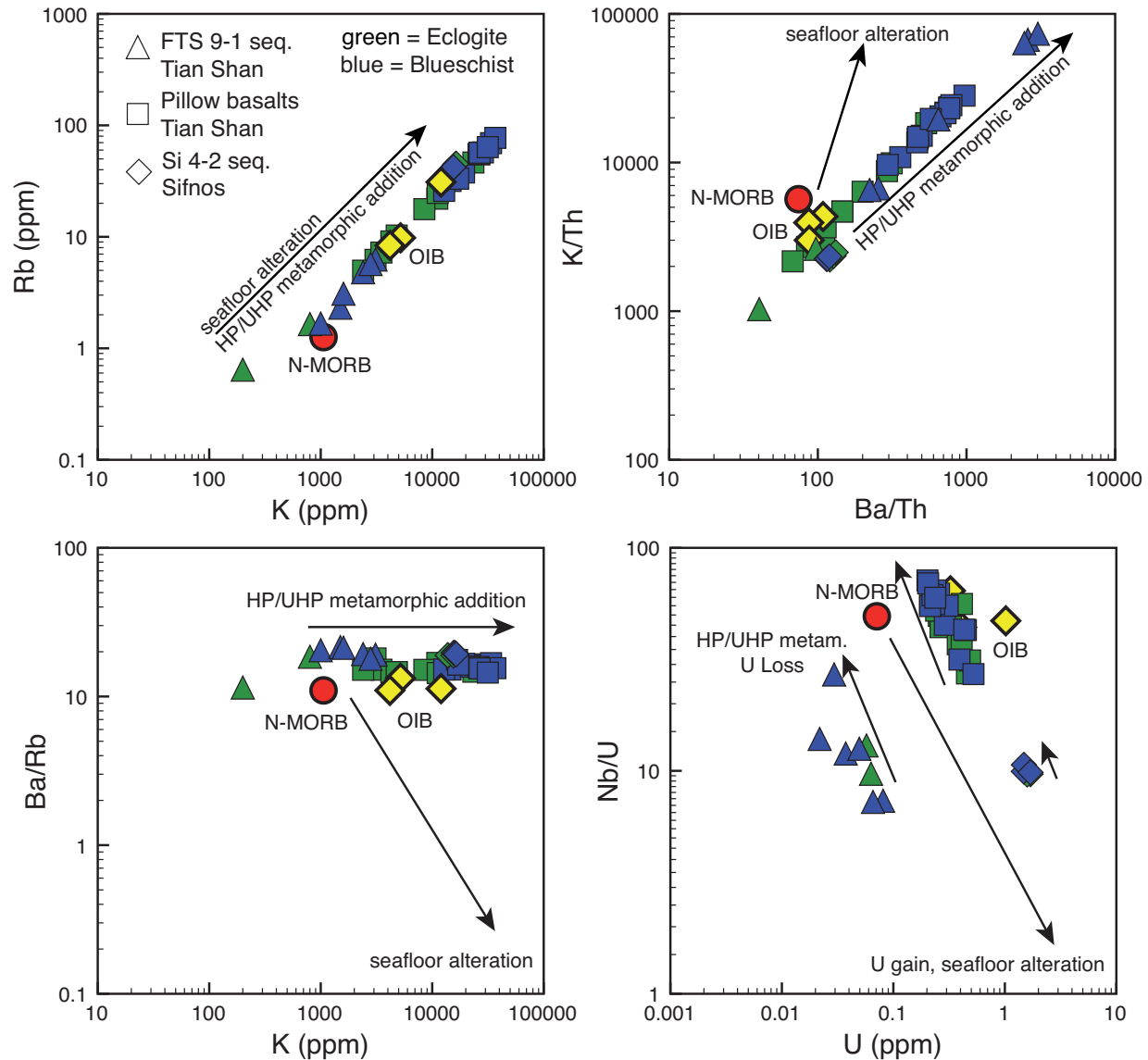


**Figure 4.8:** A) Rb and K gain in blueschists compared to the eclogites from the sequences of Sifnos and the Tian Shan. The Rb–K addition follows the seawater alteration as well the HP/UHP metamorphic fluid trend. B) High concentrations of Ba and K correlated to immobile Th in blueschists compared to the eclogites indicate gain of K and Ba due to HP/UHP metamorphic fluid rather than by seawater alteration. C) HP/UHP metamorphic fluid addition is also true for increasing K concentrations at constant Ba/Rb ratios. D) U concentrations correlated to immobile Nb show that U was not added during seawater alteration in blueschists prior to the eclogite facies of the Sifnos and Tian Shan sequences. Note that all sequences are derived from basalts of different oceanic settings and plot therefore inconsistent (FTS 9–1: back-arc, pillow meta-basalts: ocean island, Sifnos 4–2: island arc).

whole rock  $\delta^{18}\text{O}$  composition can be estimated to range between 8 and 9‰ based on the isotopic composition of omphacite in these rocks (Figure 4.5, Table 4.1). Compared to the average  $\delta^{18}\text{O} = 5.71\text{‰}$  of the oceanic crust (Hart et al., 1999) and mantle-derived basaltic rocks (5.2–6.3‰; Eiler et al., 1997, 2000), the eclogites of all sequences show higher  $\delta^{18}\text{O}$  values, which might be related to inherited low-temperature seawater alteration (reported for Sifnos by Gregory and Taylor, 1981; Putlitz et al., 2000). Alternatively, elevated  $\delta^{18}\text{O}$  values can result from fluid-rock interaction during burial and prograde metamorphism (Chamberlain and Conrad, 1991). Chamberlain and Conrad (1991) concluded that increasing  $\delta^{18}\text{O}$  values in zoned garnet of metamorphic rocks from Vermont, are related to prograde breakdown of chlorite and the release of an isotopically light fluid, since chlorite has formed during seawater alteration in basaltic rocks and was consumed by garnet forming reactions during burial to greater depth. Consequently, the higher  $\delta^{18}\text{O}$  values in omphacite and garnet of the Tian Shan and Sifnos might reflect either seawater alteration or devolatilisation during burial and metamorphic equilibration of the oxygen isotopic composition. To constrain further the possibility of seawater alteration, the radiogenic isotope chemistry has to be considered. The Nd isotope composition will not be affected by seawater alteration (Staudigel et al., 1995; Hoernle, 1998), whereas the Sr isotopic composition reacts very sensitive to seawater alteration by increasing ratios (e.g. Staudigel, 2003). The eclogites and blueschists of Sifnos are only slightly higher in  $(^{87}\text{Sr}/^{86}\text{Sr})_{42\text{Ma}}$  than the Bulk Silicate Earth (BSE) $_{42\text{Ma}}$  (Figure 4.6), indicating a lack of a strong seawater alteration. However, seawater alteration might be a reasonable explanation for the Tian Shan samples. Eclogites and blueschists from the Tian Shan are shifted to higher Sr isotopic values compared to the mantle array in the  $(^{87}\text{Sr}/^{86}\text{Sr})_{320\text{Ma}}$  and  $(\epsilon\text{Nd})_{320\text{Ma}}$  diagram (Figure 4.6). But, at least the eclogites and associated blueschists of the pillow meta-basalts from Tian Shan show similar values in  $^{87}\text{Sr}/^{86}\text{Sr}$  (Figure 4.7B) composition and thus suggest that they have been in equilibrium with the same fluid during blueschist-facies conditions. The blueschists show higher  $^{87}\text{Rb}/^{86}\text{Sr}$  values than the eclogites, which is related to the observed phengite growth in the blueschists. As discussed before, the oxygen isotopes of the eclogite-facies minerals indicate a preserved peak-metamorphic equilibrium, but the initial  $^{87}\text{Sr}/^{86}\text{Sr}$  value of the eclogites seems to be overprinted by a metamorphic fluid infiltration event, since the eclogites have the same initial  $^{87}\text{Sr}/^{86}\text{Sr}$  value as the blueschists. The Sr isotopic signature of the eclogites was reset by this fluid in contrast to the O isotope composition. The breakdown of the Sr bearing minerals clinozoisite and apatite and the new formation of carbonate could be responsible for the change of the bulk Sr isotopic composition of the eclogites. Garnet and omphacite were unaffected by the re-equilibration of the Sr isotopes as both minerals still show their  $\delta^{18}\text{O}$  peak equilibrium. In summary, metamorphic fluids, which infiltrated and metasomatised the eclogites subsequently to peak metamorphism seems to have increased the Sr isotope composition in the Tian Shan rocks. The  $^{87}\text{Rb}/^{86}\text{Sr}$  isochron of the blueschists may reflect the time of resetting of the isotopic equilibrium of eclogites and blueschists during the fluid infiltration event, before the rock became closed against further infiltration and metasomatism. Early seawater alteration of the rocks prior to burial seems unlikely, as the mobility of the LILE (K, Rb, Ba) clearly indicates their enrichment by HP/UHP metamorphic fluids (Figure 4.8A, B). As these

LILE had not been mobilised by seawater alteration it seems implausible that Sr has been exchanged with seawater prior to subduction. The Sr concentration is relatively low in the bulk rock and very sensitive to seawater alteration compared to the isotopic composition, as oxygen makes approximately half of the bulk rock atoms. If it is correct that seawater alteration did not affect the Sr isotopic composition, we would not expect alteration of the oxygen isotope composition as well. This is at least valid in the case of the two Tian Shan sequences. The few samples of the Sifnos sequence are not representative enough, to allow the conclusion that seawater alteration has effected the oxygen isotope composition. However, this has been well documented by [Putlitz et al. \(2000\)](#), although the Sr isotope composition has only changed to a minor degree. If seawater alteration has occurred, the Sr isotope composition that has to be expected in the case of complete equilibration with Tertiary seawater ( $^{87}\text{Sr}/^{86}\text{Sr} = 0.7077$ ; [Veizer, 1989](#)) was not reached in the Sifnos sequence, which has a value of only  $(^{87}\text{Sr}/^{86}\text{Sr})_{42Ma} = 0.705$  (Figure 4.6). Summing up, we suggest that HP metamorphic fluids affected the Sr and the O isotope compositions and the element budget in the two sequences of the Tian Shan. It is reasonable to assume that the stable and radiogenic compositions of the eclogites and the blueschists reflect also the signature of the fluid composition and its source. Before we discuss their isotopic features, we will first look at the fluid source composition given by the elemental signature.

### 4.7.3 Evidence for serpentinite-derived fluids

A fluid that was in equilibrium with a rock of a specific composition might adopt the chemical characteristic of the rock in its major and trace element composition: e.g. a fluid that was in equilibrium with peridotites may also obtain a composition that is dominated by those elements that are typical for peridotites. On the other hand, in a fluid-dominated system, a fluid saturated with certain elements could react with a rock, whose chemical composition would shift towards the composition of the fluid and thus the rock would inherit a fingerprint of the infiltrating fluid ([Zack and John, 2007](#)). The here described blueschists, both from Sifnos and from the Tian Shan, show gains of Mg,  $\text{CO}_2$ ,  $\text{H}_2\text{O}$ , Ni, Co, Zn and LILE (Cs, Ba, Rb, K), locally also of Sr and Pb, whereas REE, Si, Ca, and in cases also of P, Na, V, U and Th, were partly lost (Figure 4.3). In respect to the element concentrations and mobility it is obvious that the dominating major elements show a high effect on the total mass change of the system. The loss of Si and Ca and the contemporaneous gain of Mg and volatiles imply a fluid that was in equilibrium with a rock of peridotitic composition, since peridotites are relatively poor in Si and Ca but highly enriched in Mg, compared to basaltic or granitic compositions. It can be assumed that the initial chemical composition of the infiltrating fluid was in equilibrium with the altered mantle wedge peridotite or the subducted altered mantle peridotite of the slab ([van der Straaten et al., 2008](#)). In addition, two distinct features point to peridotitic fluid sources: (I) the gain of Mg and transition metals Ni and Co and (II) the overall loss of the REE (Figure 4.9). The gain of Ni and Co is always distinct in all three investigated eclogite-blueschist transformation sequences. The enrichment of Ni and Co in blueschists follows a trend towards the composition of the depleted mantle ([Salters and Stracke, 2004](#)) and of the average serpentinite

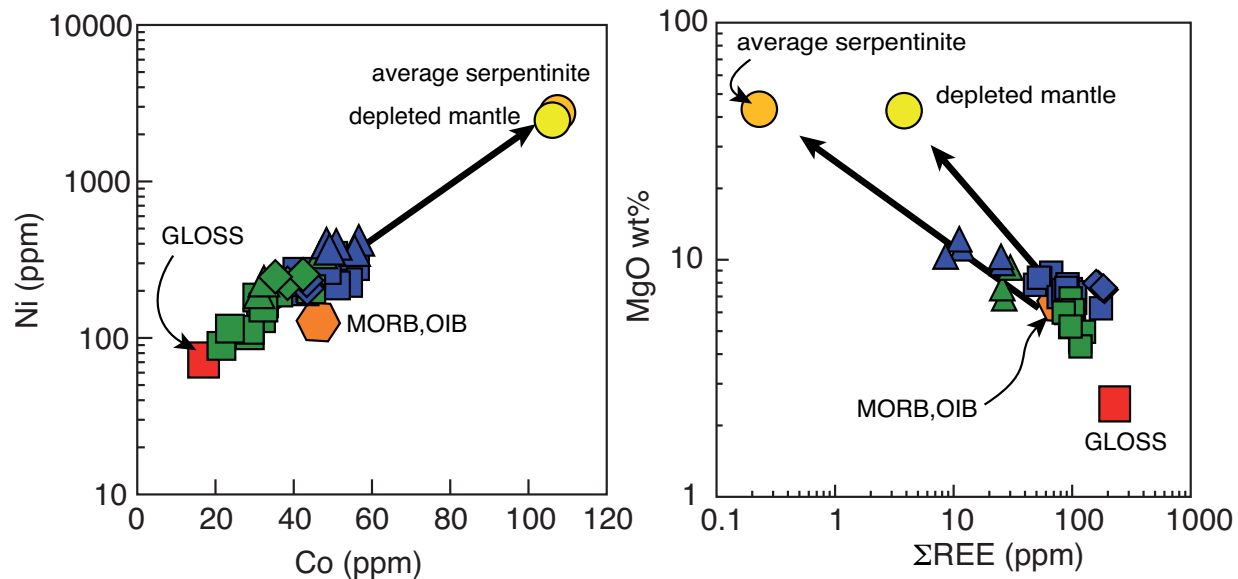


**Figure 4.9:** Composition diagrams of all three eclogites to blueschist sequences from Sifnos and the Tian Shan, same symbol signs than in Figure 4.5, 4.6, 4.8. A: Co ppm vs. Ni ppm: blueschist-facies overprinted eclogites are enriched in both elements and show a tendency to the average serpentinite (Hattori and Guillot, 2003; Savov et al., 2005; Paulick et al., 2006) or depleted mantle composition (Salters and Stracke, 2004). B:  $\Sigma$ REE in ppm vs. MgO wt%: Blueschist are enriched in Mg but concordantly depleted in REE and tend to the composition of serpentinites or the depleted mantle.

(Hattori and Guillot, 2003; Savov et al., 2005; Paulick et al., 2006). Although some marine sediments may show high concentrations in transition metals (e.g. recent Tonga sediments clay cherts, GEOROC database, <http://georoc.mpch-mainz.gwdg.de>), the composition of the global oceanic subducted sediments (GLOSS, Plank and Langmuir, 1993) and most of the modern marine sediments (GEOROC database) are too low to induce such high enrichments of Ni and Co, as it is observed in the blueschists (Figure 4.9A). Additionally, the loss of REE ( $\Sigma$ REE) in combination with the gain of MgO in the blueschists follows also the trend towards peridotitic compositions. Blueschists from Sifnos and from the pillow meta-basalts in Tian Shan trend to the depleted mantle composition whereas the FTS 9-1 sequence of the Tian Shan trends to the average serpentinite composition, which has similar MgO contents to the depleted mantle but lower REE contents (Figure 4.9B) indicating that the fluid infiltrating the eclogite-blueschists was in equilibrium with an altered mantle peridotite (serpentinite).

Moreover, a contamination of the peridotite-derived fluid with LILE and  $\text{CO}_2$  is indicated by mass balance calculations (van der Straaten et al., 2008). The LILE is assumed to partition into the fluid phase during dehydration processes and reactive fluid flow within the altered oceanic crust and sediments (Kessel et al., 2005; Scambelluri et al., 2007; Zack and John, 2007). LILE have been gained during the eclogite-blueschist transformation and were incorporated into white mica (van der Straaten et al., 2008, in review). In addition, the very high gain of  $\text{CO}_2$  in all three sequences cannot be explained with a simple

peridotite-derived fluid. Several sources for CO<sub>2</sub> are possible: (I) subducted carbonate-rich sediments or limestones: some marbles are present in the south of the ophiolitic mélangé in the South Tian Shan (Figure 4.4) and marbles are dominant on Sifnos (Figure 4.1), (II) carbonate-bearing altered oceanic crust (Rosner et al., 2007): John et al. (2008) reported that up to 95% of the total CO<sub>2</sub> was released from carbonate-bearing blueschist during the prograde formation of eclogite veins within the blueschists, (III) carbonates in the serpentinised slab mantle peridotite (Schroeder et al., 2002; Alt and Shanks, 2006; Nasir et al., 2007; Da Costa et al., 2008). In the case of Sifnos, the occurrence of marble in association with the blueschist- and greenschist-facies rocks (Davis, 1966) suggests that the marble may have acted as a carbon source. Altered oceanic crust and sediments might be the CO<sub>2</sub> sources in the Tian Shan, but carbonate-bearing slab serpentinite could have acted as source as well.

#### 4.7.4 Fluid-rock interaction and isotope constraints on fluid source

The measured  $\delta^{18}\text{O}$  of glaucophane in all three blueschist domains is up to 1.2‰ higher than it is expected if it were in equilibrium with omphacite at  $T = 600^\circ\text{C}$ . Paragonite in the FTS 9–1 sequence, is about 0.8‰ higher and phengite in the pillow meta-basalts of the Tian Shan is about 0.4–1.5‰ higher than the calculated equilibrium values at 600°C (Figure 4.5, Table 4.1). The oxygen isotope compositions of the newly formed glaucophane and of the white micas point to a fluid infiltration, in which the oxygen isotopic composition of the fluid was higher than that of the eclogites, resulting in an increase of  $\delta^{18}\text{O}$  in glaucophane and white micas. Seawater ( $\delta^{18}\text{O} = 0\text{‰}$ ) and meteoric water ( $\delta^{18}\text{O} \leq 0\text{‰}$ ) are unlikely fluid sources because they are relatively light. However, fluids produced by dehydration during metamorphism have an adequate O isotopic signature (10‰) (e.g. Baker et al., 1997). Possible sources of high  $\delta^{18}\text{O}$  fluids could be carbonate rocks, sediment components or crustal rocks within the downgoing slab. High gains of CO<sub>2</sub> in all three eclogite-blueschist sequences suggests 1) an addition from devolatilising marbles, carbonate-bearing sediments or calcareous gneisses (Cartwright and Barnicoat, 1999) in the rehydration fluids, or 2) devolatilisation of calcareous serpentinites or ophicarbonates within the downgoing slab. Carbonate phases in serpentinite increase significantly the  $\delta^{18}\text{O}$  (10–25‰) of the whole rock due to the high  $\delta^{18}\text{O}$  (16–24‰) of carbonate (mostly aragonite) in the rocks (e.g. Burkhard and O’Neil, 1988; Schandl and Naldrett, 1992; Alt and Shanks, 2006; Da Costa et al., 2008). Carbonate-bearing serpentinites with high  $\delta^{18}\text{O}$  would explain both, heavy <sup>18</sup>O contents in the infiltrating fluid and the high CO<sub>2</sub> concentrations. Marble derived CO<sub>2</sub> increased the  $\delta^{18}\text{O}$  value in the serpentinite-derived fluid is most likely the case for the Sifnos sequence, as marbles are in tectonic contact with the HP rocks (Figure 4.1). A one-source model for the Tian Shan seems unrealistic, since CO<sub>2</sub> mobilisation during prograde eclogitisation of the blueschists was found (John et al., 2008) and a lot of sediments occur in close proximity to the sample localities (Figure 4.4).

It is possible that the seawater altered lithospheric slab peridotite represented the source for the Sr that led to the elevated isotopic composition in the two Tian Shan sequences. The maximum  $^{87}\text{Sr}/^{86}\text{Sr}$ -value of this metasomatic Sr can be estimate from the Sr isotopic composition of seawater in the Carboniferous, which was between 0.7075 and 0.7082 (Figure 4.6, Veizer, 1989) and may have determined the Sr isotopic composition of the seawater altered serpentinitised oceanic mantle prior to subduction. Both Tian Shan eclogite-blueschist sequences plot in the range of Sr and Nd isotopic composition that are associated to altered oceanic peridotites and overlap with talc- and chlorite-rich schists, regarded as representative for the mélangé zone at the slab-wedge interface (Figure 4.6B, Bebout, 2003; King et al., 2006). Sediment-derived fluids are also likely to provide high  $^{87}\text{Sr}/^{86}\text{Sr}$  ratios, but marine sediments show usually negative  $\epsilon\text{Nd}$  values (Figure 4.6B). Sediment-derived fluids would therefore change the Nd isotope composition of the infiltrated rocks to lower  $\epsilon\text{Nd}$  values. From all three sequences only the FTS 9–1 sequence of the Tian Shan shows distinct changes in the Nd isotopic composition during the eclogite-blueschist transformation (Figure 4.6). The pillow meta-basalt and the Sifnos sequence do not show any changes. The FTS 9–1 sequence is used to discuss a simple mixing model between the eclogite and a hypothetical fluid source, which affected the blueschist isotopic composition of this sequence. To determine the possible fluid source composition the mobility of Sr and Nd during the fluid infiltration has to be considered too. Figure 4.6B shows the hypothetical fluid source and the mixing curve from this possible source with the eclogite of the FTS 9–1 sequence. A mixing of this fluid composition with the eclogite of the FTS 9–1 sequence requires a low Nd load but a relatively high Sr load in the fluid, as Nd was lost and Sr was gained during the eclogite-blueschist transformation (Figure 4.3B, van der Straaten et al., 2008). We assume a fluid that is close to the element and isotopic composition of peridotites, as the blueschist shows a strong affinity to peridotites in the Co and Ni gain and nearly complete loss of LREE (van der Straaten et al., 2008, in review, Figures 4.3, 4.9). Unaltered peridotites have usually low  $^{87}\text{Sr}/^{86}\text{Sr}$  values (today 0.702–0.704, Salters and Stracke, 2004) and low Nd (0.7 ppm) and Sr (9.8 ppm) concentrations. In this case a possible fluid source requires a higher  $\epsilon\text{Nd}$  value and higher Sr (> 300 ppm) and lower Nd concentrations (<1 ppm) than the eclogite ( $\epsilon\text{Nd} = 7.3$ , Sr = 159 ppm Nd = 4.7 ppm) to induce the increase of the Sr and the decrease of the Nd concentrations at a contemporaneous increase of the Nd isotopic composition. These chemical features are present in modern seawater-altered peridotites, which have elevated Sr isotopic compositions and occasionally higher Sr contents (up to 311 ppm) as well ([www.petdb.org](http://www.petdb.org); Snow et al., 1994; Snow and Reisberg, 1995; Senda et al., 2006, Figure 4.6B). The occurrence of the seawater-altered peridotites occurs dominantly in the range of high  $^{87}\text{Sr}/^{86}\text{Sr}$  values (> BSE) and high  $\epsilon\text{Nd}$  values (> 0, Figure 4.6B). The  $\epsilon\text{Nd}$  values are similar to those of the mantle array, as the Nd isotope composition is mostly unchanged by seawater alteration (Staudigel, 2003; Hoernle et al., 2008). Sediments, the altered oceanic crust and the mantle provide possible sources for  $\text{CO}_2$  and Sr. In addition, the Sr and Nd isotopic composition of talc- and chlorite-rich schists, formed either from basaltic or peridotitic protholiths, represents a similar source and provides also high Sr (<328 ppm) concentrations but variable Nd concentrations (0.08–35 ppm) (Catalina Schists, California; King et al., 2006, Figure

4.6B). All subduction related rock types separately, like marine or continental sediments, crustal gneisses, the altered oceanic crust or the mantle peridotite, would not provide all the chemical requirements as mentioned, but a mixture of fluids from all these different sources would do. The high  $\epsilon\text{Nd}$  value of +10 and the chemical trend of the blueschists towards a peridotitic chemistry imply that the altered peridotites from either the slab mantle or the hydrated mantle of the subduction channel are the most important source for the fluids that infiltrated during the eclogite-blueschist transformation.

#### 4.7.5 Implications for element budget of subduction zones

From the above discussion it seems most likely, that the metamorphic fluids infiltrating during blueschist formation were equilibrated with a peridotitic composition. Elevated Sr isotope compositions in the eclogite-blueschist sequences and the high  $\delta^{18}\text{O}$  values in the blueschist-facies minerals may be related to inherited signatures of the infiltrating fluid, which was probably derived from the subducted and dehydrating, seawater-altered oceanic crust and/or the mantle peridotite. The enrichment of LILE indicates the addition of a sediment-derived component, whereas the  $\text{CO}_2$  may derive either from the subducted altered oceanic crust or from the subducted marine sediments. All sediment-derived features might have been incorporated during a reactive fluid-flow through the dehydrating oceanic slab (Gorman et al., 2006; Zack and John, 2007; John et al., 2008). Thus, it is obvious that the fluids at the slab-wedge interface are mixtures of components derived from different sources. The occurrence of highly metasomatised rocks, like talc and chlorite schists in the mélangé zone from Catalina Island (Bebout and Barton, 2002; King et al., 2006) or blueschist-facies overprinted eclogites from Sifnos or the Tian Shan are the proof of the highly reactive behaviour of the subduction channel fluids. In that respect, it is interesting to note that, although the major element composition of the subduction channel fluids seems to be dominated by intense fluid-rock interaction with the serpentinite-dominated subduction channel matrix, information about the evolution of the fluid before it enters the slab-wedge interface are still possible to track. Whatever chemical composition the incoming slab fluids have, in the subduction channel environment, most major and trace element concentrations in the fluid, apart from LILE, are finally controlled by the equilibration with the ultramafic matrix. Malaspina et al. (2006) showed that in a high-pressure metasomatic sequence of eclogites from the Dabie Shan, hosted by a lherzolite matrix, mainly LILE and light elements have been transported. Most likely, all other trace elements of the fluid precipitated in the serpentinite matrix during fluid rock interaction so that the more pervasive flow in the subduction channel produce a kind of filter system for the elements that are less mobile.

## 4.8 Conclusions

The isotopic composition of oxygen in minerals of three eclogite-blueschist associations that show laterally (dm to m scale) a retrograde blueschist-facies overprint on pre-existing

eclogites indicate isotopic equilibrium between omphacite and garnet (plus phengite in Sifnos and FTS 9–1, Tian Shan) during HP peak-metamorphic condition. During the retrograde blueschist-facies overprint, equilibrium has been attained between glaucophane and white mica (paragonite: FTS 9–1; phengite: pillow meta-basalts). Heavier  $\delta^{18}\text{O}$  values in glaucophane and white mica of the blueschists support the petrological observation that the eclogite-blueschist transformation was caused by infiltration of external fluids. In addition, the Sifnos sequence indicates an even late-stage, greenschist-facies equilibrium between newly grown epidote and calcic amphibole.

Elevated  $\delta^{18}\text{O}$  values in the peak-metamorphic mineral assemblage compared to unmodified mantle values are interpreted to derive from the prograde reaction history involving dewatering of chlorite during garnet formation, whereas the elevated whole rock Sr isotope composition seems to derive from seawater-altered peridotites and infiltrated metasomatic processes in the subduction channel fluid.

The major element composition of the metasomatic fluids entering the eclogites during uplift mainly derives from an intense fluid-rock interaction with a peridotite supposed to form the matrix of the uplifting HP rocks. The combined Sr-Nd isotope data suggest, that the elevated Sr isotopic composition is likely a fluid source signature of either the serpentinised lithospheric slab mantle or the altered oceanic crust. The sediment-derived flavour (gain of LILE) and the added  $\text{CO}_2$ -component (formation of carbonates) of the subduction channel fluids may derive from a reactive fluid-flow through the oceanic slab and the overlying sediment layer.

The fluid-rock interaction at the slab-wedge interface or within the subduction channel causes that only the most fluid mobile elements and the isotopic composition of the entering slab fluids remain preserved as a flavour, whereas the bulk composition of the subduction channel fluid is controlled by the ultramafic rocks building up the mantle wedge.

## 4.9 Acknowledgements

The Deutsche Forschungsgemeinschaft supported this study by grant Sche 265/S1–2. This publication is contribution no. 161 of the Sonderforschungsbereich 574 “Volatiles and Fluids in Subduction Zones” at Kiel University. J. Gao is thanked for the support and management of the fieldwork in the Tian Shan. We like to thank A. Pack and R. Przybilla (University of Göttingen) for analytic determining the isotopic composition of oxygen. F. Hauff (GEOMAR, University of Kiel) is thanked for contributing Sr and Nd isotope analyses. The petrological working group of Kiel is thanked for stimulating discussions.



## References

- Ague, J. J., 2003. Fluid infiltration and transport of major, minor, and trace elements during regional metamorphism of carbonate rocks, Wepawaug Schist, Connecticut, USA. *American Journal of Science* 303, 753–816.
- Ague, J. J., van Haren, J. L. M., 1996. Assessing metasomatic mass and volume changes using the bootstrap, with application to deep crustal hydrothermal alteration of marble. *Economic Geology and the Bulletin of the society of economic geologists* 91 (7), 1169–1182.
- Alt, J. C., Shanks, W. C., 2006. Stable isotope compositions of serpentinite seamounts in the Mariana forearc: Serpentinization processes, fluid source and sulfur metasomatism. *Earth and Planetary Science Letters* 242 (3-4), 272–285.
- Altherr, R., Schliestedt, M., Okrusch, M., Seidel, E., Kreuzer, H., Harre, W., Lenz, H., Wendt, I., Wagner, G. A., 1979. Geochronology of high pressure rocks on Sifnos (Cyclades, Greece). *Contributions to mineralogy and petrology* 70 (3), 245–255.
- Baker, J., Matthews, A., Matthey, D., Rowley, D., Xue, F., 1997. Fluid-rock interactions during ultra-high pressure metamorphism, Dabie Shan, China. *Geochimica et Cosmochimica Acta* 61 (8), 1685–1696.
- Baxter, E. F., DePaolo, D. J., 2000. Field measurement of slow metamorphic reaction rates at temperatures of 500C to 600C. *Science* 288, 1411–1414.
- Bebout, G. E., 1995. The impact of subduction-zone metamorphism on mantle-ocean chemical cycling. *Chemical Geology* 126 (2), 191–218.
- Bebout, G. E., 2003. Trace Element and Isotopic Fluxes/Subducted Slab. In: Rudnick, R. L. (Ed.), *The Crust*. Vol. 3 of *Treatise on Geochemistry*. Elsevier-Pergamon, Oxford, pp. add. 1–50.
- Bebout, G. E., 2007. Metamorphic chemical geodynamics of subduction zones. *Earth and Planetary Science Letters* 260 (3-4), 373–393.
- Bebout, G. E., Barton, M. D., 2002. Tectonic and metasomatic mixing in a high-T, subduction-zone melange; insights into the geochemical evolution of the slab-mantle interface. *Chemical Geology* 187 (1-2), 79–106.
- Becker, H., Jochum, K. P., Carlson, R. W., 2000. Trace element fractionation during dehydration of eclogites from high-pressure terranes and the implications for element fluxes in subduction zones. *Chemical Geology* 163 (1-4), 65–99.
- Bonneau, M., 1982. Tectonic Evolution of Central Aegean Hellenides from Upper Jurassic to Miocene Times. *Bulletin De La Societe Geologique De France* 24 (2), 229–242.
- Brady, J. B., Able, L. M., Cheney, J. T., Sperry, A. J., Schumacher, J. C., 2001. Prograde lawsonite pseudomorphs in blueschist from syros, greece. Abstracts of the GSA Annual Meeting, GSA, 105.
- Brady, J. B., Markley, M. J., Schumacher, J. C., Cheney, J. T., Bianciardi, G. A., 2004. Aragonite pseudomorphs in high-pressure marbles of Syros, Greece. *Journal of Structural Geology* 26 (1), 3–9.
- Burkhard, D. J. M., O'Neil, J. R., 1988. Contrasting serpentinization processes in the eastern Central Alps. *Contributions to mineralogy and petrology* 99, 498–506.
- Bykadorov, V. A., Bush, V. A., Fedorenko, O. A., Filippova, I. B., Miltenko, N. V., Puchkov, V. N., Smirnov, A. V., Uzhkenov, B. S., Volozh, Y. A., 2003. Ordovician-Permian palaeogeography of Central Eurasia: Development of Paleozoic petroleum-bearing basins. *Journal of Petroleum Geology* 26 (3), 325–350.
- Cartwright, I., Barnicoat, A. C., 1999. Stable isotope geochemistry of Alpine ophiolites; a window to ocean-floor hydrothermal alteration and constraints on fluid-rock interaction during high-pressure metamorphism. *International Journal Earth Sciences* 88, 219–235.
- Chamberlain, C. P., Conrad, M. E., 1991. Oxygen Isotope Zoning in Garnet. *Science* 254 (5030), 403–406.
- Cloos, M., Shreve, R. L., 1988a. Subduction-channel model of prism accretion, melange formation, sediment subduction, and subduction erosion at convergent plate margins; Part I, Background and description. *Pure and Applied Geophysics* 128 (3-4), 455–500.
- Cloos, M., Shreve, R. L., 1988b. Subduction-channel model of prism accretion, melange formation, sediment subduction, and subduction erosion at convergent plate margins; Part II, Implications and discussion. *Pure and Applied Geophysics* 128 (3-4), 501–545.
- Da Costa, I. R., Barriga, F. J. A. S., Taylor, R. N., 2008. Late seafloor carbonate precipitation in serpentinites from the Rainbow and Saldanha sites (Mid-Atlantic Ridge). *European Journal of Mineralogy* 20 (2), 173–181.
- Davis, E. N., 1966. Der geologische Bau der Insel Siphnos. *Geological Geophysical Research* 10, 161–220.
- DePaolo, D. J., 1988. Neodymium isotope geochemistry: An introduction. Springer Verlag, New York.
- Dixon, J. E., 1968. The metamorphic rocks of Syros, Greece. Ph.d. thesis, St. John's College, Cambridge.
- Eiler, J. M., Farley, K. A., Valley, J. W., Hauri, E., Craig, H., Hart, S. R., Stolper, E. M., 1997. Oxygen isotope variations in ocean island basalt phenocrysts. *Geochimica et Cosmochimica Acta* 61 (11), 2281–2293.
- Eiler, J. M., Schiano, P., Kitchen, N., Stolper, E. M., 2000. Oxygen-isotope evidence for recycled crust in the sources of mid-ocean-ridge basalts. *Nature* 403 (6769), 530–534.
- Faure, G., 1986. Principles of isotope geology, 2nd Edition. John Wiley & Sons, New York.

- Feineman, M. D., Ryerson, F. J., DePaolo, D. J., Plank, T., 2007. Zoisite-aqueous fluid trace element partitioning with implications for subduction zone fluid composition. *Chemical Geology* 239 (3-4), 250–265.
- Fisher, D. M., 1996. Fabrics and veins in the forearc; a record of cyclic fluid flow at depths of <15 km. In: *Subduction top to bottom*. Vol. 96; American Geophysical Union, Washington, DC, United States, pp. 75–89.
- Fry, N., Fyfe, W., 1971. On the significance of the eclogite facies in alpine metamorphism. *Verhandlungen der geologischen Bundesanstalt, Wien (Vienna)* 2, 257–265.
- Ganor, J., Matthews, A., Schliestedt, M., Garfunkel, Z., 1996. Oxygen isotopic heterogeneities of metamorphic rocks; an original tectonostratigraphic signature, or an imprint of exotic fluids? A case study of Sifnos and Tinos islands (Greece). *European Journal of Mineralogy* 8 (4), 719–732.
- Gao, J., He, G., Li, M., Xiao, X., Tang, Y., Wang, J., Zhao, M., 1995. The mineralogy, petrology, metamorphic PTdt trajectory and exhumation mechanism of blueschists, South Tianshan, northwestern China. *Tectonophysics* 250 (1-3), 151–168.
- Gao, J., John, T., Klemd, R., Xiong, X., 2007. Mobilization of Ti-Nb-Ta during subduction: evidence from rutile-bearing dehydration segregations and veins hosted in eclogite, Tianshan, NW China. *Geochimica et Cosmochimica Acta* 71, 4974–4996.
- Gao, J., Klemd, R., 2001. Primary fluids entrapped at blueschist to eclogite transition; evidence from the Tianshan meta-subduction complex in northwestern China. *Contributions to mineralogy and petrology* 142 (1), 1–14.
- Gao, J., Klemd, R., 2003. Formation of HP-LT rocks and their tectonic implications in the western Tianshan Orogen, NW China; geochemical and age constraints. *Lithos* 66 (1-2), 1–22.
- Gao, J., Klemd, R., Zhang, L., Wang, Z., Xiao, X., 1999. P-T path of high-pressure/ low-temperature rocks and tectonic implications in the western Tianshan Mountains, NW China. *Journal of Metamorphic Geology* 17 (6), 621–636.
- Gao, J., Li, M., Xiao, X., Tang, Y., He, G., 1998. Paleozoic tectonic evolution of the Tianshan Orogen, northwestern China. *Tectonophysics* 287 (1-4), 213–231.
- Gerya, T. V., Stöckhert, B., Perchuk, A. L., 2002. Exhumation of high-pressure metamorphic rocks in a subduction channel; a numerical simulation. *Tectonics* 21 (6), 1056, doi:10.1029/2002TC001406.
- Goldstein, S. L., O’Nions, R. K., Hamilton, P. J., 1984. A Sm-Nd study of atmospheric dusts and particulates from major river systems. *Earth and Planetary Science Letters* 70, 221–236.
- Gorman, P. J., Kerrick, D. M., Connolly, J. A. D., 2006. Modeling open system metamorphic decarbonation of subducting slabs. *Geochemistry, Geophysics, Geosystems (G3)* 7 (4), 1–21.
- Gregory, R. T., Taylor, H. P., 1981. An Oxygen Isotope Profile in a Section of Cretaceous Oceanic-Crust, Samail Ophiolite, Oman - Evidence for  $\delta^{18}\text{O}$  Buffering of the Oceans by Deep (Less-Than 5 Km) Seawater-Hydrothermal Circulation at Mid-Ocean Ridges. *Journal of Geophysical Research* 86 (NB4), 2737–2755.
- Gresens, R. L., 1967. Composition-volume relationships of metasomatism. *Chemical Geology* 2 (1), 47–65.
- Hart, S. R., Blusztajn, J., Dick, H. J. B., Meyer, P. S., Muehlenbachs, K., 1999. The fingerprint of seawater circulation in a 500-meter section of ocean crust gabbros. *Geochimica et Cosmochimica Acta* 63 (4), 4059–4080.
- Hattori, K. H., Guillot, S., 2003. Volcanic fronts form as a consequence of serpentinite dehydration in the forearc mantle wedge. *Geology (Boulder)* 31 (6), 525–528.
- Hermann, J., Spandler, C., Hack, A., Korsakov, A. V., 2006. Aqueous fluids and hydrous melts in high-pressure and ultra-high pressure rocks: implications for element transfer in subduction zones. *Lithos* 92, 399–417.
- Hoernle, K., 1998. Geochemistry of Jurassic oceanic crust beneath Gran Canaria (Canary Islands): Implications for crustal recycling and assimilation. *Journal of Petrology* 39 (5), 859–880.
- Hoernle, K., Abt, D. L., Fischer, K. M., Nichols, H., Hauff, F., Abers, G. A., van den Bogaard, P., Heydolph, K., Alvarado, G., Protti, M., Strauch, W., 2008. Arc-parallel flow in the mantle wedge beneath Costa Rica and Nicaragua. *Nature* 451 (7182), 1094–1098.
- Hyndman, R. D., Peacock, S. M., 2003. Serpentinization of the forearc mantle. *Earth and Planetary Science Letters* 212 (3-4), 417–432.
- Ivandic, M., Grevemeyer, I., Berhorst, A., Flh, E. R., McIntosh, K., 2008. Impact of bending related faulting on the seismic properties of the incoming oceanic plate offshore of Nicaragua. *Journal of Geophysical Research* 113 (B0541), doi: 10.1029/2007JB005291.
- Jacobshagen, V., 1986. *Geologie von Griechenland*. Gebrüder Borntraeger, Stuttgart.
- John, T., Klemd, R., Gao, J., Garbe-Schönberg, C.-D., 2008. Trace-element mobilization in slabs due to non steady-state fluid-rock interaction: constraints from an eclogite-facies transport vein in blueschist (Tianshan, China). *Lithos* 103 (1-2), 1–24.
- Jolivet, L., Faccenna, C., Goffe, B., Burov, E., Agard, P., 2003. Subduction tectonics and exhumation of high-pressure metamorphic rocks in the Mediterranean orogens. *American Journal of Science* 303 (5), 353–409.
- Keiter, M., Piepjohn, K., Ballhaus, C., Lagos, M., Bode, M., 2004. Structural development of high-pressure metamorphic rocks on Syros island (Cyclades, Greece). *Journal of Structural Geology* 26 (8), 1433–1445.

- Kelley, K. A., Plank, T., Farr, L., Ludden, J., Staudigel, H., 2005. Subduction cycling of U, Th, and Pb. *Earth and Planetary Science Letters* 234 (3-4), 369–383.
- Kessel, R., Schmidt, M. W., Ulmer, P., Pettke, T., 2005. Trace element signature of subduction-zone fluid, melts and supercritical liquids at 120–180 km depths. *Nature* 437 (29), 724–727.
- King, R. L., Bebout, G. E., Moriguti, T., Nakamura, E., 2006. Elemental mixing systematics and Sr-Nd isotope geochemistry of melange formation: Obstacles to identification of fluid sources to arc volcanics. *Earth and Planetary Science Letters* 246, 288–304.
- Klemd, R., 2003. Ultrahigh-pressure metamorphism in eclogites from the western Tianshan high-pressure belt (Xinjiang, western China); comment. *American Mineralogist* 88 (7), 1153–1156.
- Klemd, R., Bröcker, M., Hacker, B. R., Gao, J., Gans, P., Wemmer, K., 2005. New Age Constraints on the Metamorphic Evolution of the High-Pressure/Low-Temperature Belt in the Western Tianshan Mountains, NW China. *Journal of Geology* 113, 157–168.
- Lin, W., Enami, M., 2006. Prograde pressure-temperature path of jadeite-bearing eclogites and associated high-pressure/low-temperature rocks from western Tianshan, northwest China. *Island Arc* 15, 483–502.
- Ludwig, K. R., 2003. Isoplot/Ex version 3. A geochronological toolkit for Microsoft Excel. Berkeley Geochronology Center, Spec. Publ. 4, 1–71.
- Malaspina, N., Hermann, J., Scambelluri, M., Compagnoni, R., 2006. Multistage metasomatism in ultrahigh-pressure mafic rocks from the North Dabie Complex (China). *Lithos* 90, 19–42.
- Mocek, B., 1994. Geochemische Untersuchungen zur Identifizierung der Protholithe der Hochdruckeinheit von Siphnos, Kykladen (Griechenland). *Berichte der deutschen Mineralogischen Gesellschaft, Beiheft zum European Journal of Mineralogy* 6 (1), 1–179.
- Mühlenbachs, K., Clayton, R. N., 1976. Oxygen isotope composition of oceanic-crust and its bearing on seawater. *Journal of Geophysical Research* 81 (23), 4356–4369.
- Nasir, S., Al Sayigh, A. R., Al Harthy, A., Al-Khribash, S., Al-Jaaldi, O., Musllam, A., Al-Mishwat, A., Al-Bu'saidi, S., 2007. Mineralogical and geochemical characterization of listwaenite from the Semail Ophiolite, Oman. *Chemie der Erde-Geochemistry* 67 (3), 213–228.
- Okrusch, M., Broecker, M., 1990. Eclogites associated with high-grade blueschists in the Cyclades archipelago, Greece; a review. *European Journal of Mineralogy* 2 (4), 451–478.
- Okrusch, M., Seidel, E., Davis, E. N., 1978. The assemblage jadeite - quartz in the glaucophane rocks of Sifnos (Cyclades Archipelago, Greece). *Neues Jahrbuch fuer Mineralogie Abhandlungen*. 132 (3), 284–308.
- Pack, A., Toulouse, C., Przybilla, R., 2007. Determination of oxygen triple isotope ratios of silicates without cryogenic separation of  $\text{NF}_3$  - technique with application to analyses of technical  $\text{O}_2$  gas and meteorite classification. *Rapid Communications in Mass Spectrometry* 21, 3721–3728.
- Paulick, H., Bach, W., Godard, M., de, H. J. C. M., Suhr, G., Harvey, J., 2006. Geochemistry of abyssal peridotites (Mid-Atlantic Ridge, 15 degrees 20'N, ODP Leg 209); implications for fluid-rock interaction in slow spreading environments. *Chemical Geology* 234 (3-4), 179–210.
- Peacock, S. M., 1993. The importance of blueschist to eclogite dehydration reactions in subducting oceanic crust. *Geological Society of America Bulletin* 105 (5), 684–694.
- Plank, T., Langmuir, C. H., 1993. Tracing trace elements from sediment input to volcanic output at subduction zones. *Nature (London)* 362 (6422), 739–743.
- Poli, S., Schmidt, M. W., 1995.  $\text{H}_2\text{O}$  transport and release in subduction zones; experimental constraints on basaltic and andesitic systems. *Journal of Geophysical Research, B, Solid Earth and Planets* 100 (11), 22299–22314.
- Putlitz, B., Matthews, A., Valley, J. W., 2000. Oxygen and hydrogen isotope study of high-pressure metagabbros and metabasalts (Cyclades, Greece); implications for the subduction of oceanic crust. *Contributions to mineralogy and petrology* 138 (2), 114–126.
- Ranero, C. R., Phipps, M. J., McIntosh, K., Reichert, C., 2003. Bending-related faulting and mantle serpentinization at the Middle American Trench. *Nature (London)* 425 (6956), 367–373.
- Ren, J., Jiang, C., Zhang, Z., Qin, D., 1987. *Geotectonic evolution of China*. Sci, Press. Beijing, China/ Springer-Verlag-Berlin, Federal Republic of Germany.
- Rollinson, H., 1993. *Using geochemical data: evaluation, presentation, interpretation*, 1st Edition. Pearson, Prentice Hall, Harlow.
- Rosner, M., Bach, W., Peucker-Ehrenbrink, B., Erzinger, J., Plessen, B., 2007. Carbonate and anhydrite veins from altered gabbroic oceanic crust (atlantis massif, mar 30 degrees n). *Geochimica Et Cosmochimica Acta* 71 (15), A853–A853.
- Rüpke, L. H., Phipps, M. J., Hort, M., Connolly, J. A. D., 2002. Are the regional variations in Central American arc lavas due to differing basaltic versus peridotitic slab sources of fluids? *Geology (Boulder)* 30 (11), 1035–1038.
- Rüpke, L. H., Phipps, M. J., Hort, M., Connolly, J. A. D., 2004. Serpentine and the subduction zone water cycle. *Earth and Planetary Science Letters* 223 (1-2), 17–34.
- Salters, V. J. M., Stracke, A., 2004. Composition of the depleted mantle. *Geochemistry, Geophysics, Geosystems (G3)* 5, doi:10.1029/2003GC000597.

- Savov, I. P., Ryan, J. G., D., A. M., Kelley, K., Mattie, P., 2005. Geochemistry of serpentinized peridotites from the Mariana forearc Conical Seamount, ODP Leg 125; implications for the elemental recycling at subduction zones. *Geochemistry, Geophysics, Geosystems (G3)* 6 (4), doi:10.1029/2004GC000777.
- Scambelluri, M., Bottazzi, P., Trommsdorff, V., Vannucci, R., Hermann, J., Gomez, P. M. T., Lopez, S. V. V., 2001. Incompatible element-rich fluids released by antigorite breakdown in deeply subducted mantle. *Earth and Planetary Science Letters* 192 (3), 457–470.
- Scambelluri, M., Malaspina, N., Hermann, J., 2007. Subduction fluids and their interaction with the mantle wedge: a perspective from the study of high-pressure ultramafic rocks. *Periodico die Mineralogia* 76 (2-3), 253–265.
- Schandl, E., Naldrett, A. J., 1992. CO<sub>2</sub> metasomatism of serpentinites, South of Timmins, Ontario. *Canadian Mineralogist* 30, 93–108.
- Schliestedt, M., 1980. Phasengleichgewichte in Hochdruckgesteinen von Sifnos, Griechenland. PhD thesis, Technischen Universität Carolo-Wilhelmina zu Braunschweig, p. 143.
- Schliestedt, M., 1990. Occurrences and stability conditions of low-temperature eclogites. In: Carswell, D. A. (Ed.), *Eclogite Facies Rocks*. Chapman & Hall, New York, pp. 160–179.
- Schliestedt, M., Matthews, A., 1987. Transformation of blueschist to greenschist facies rocks as a consequence of fluid infiltration, Sifnos (Cyclades), Greece. *Contributions to mineralogy and petrology* 97 (2), 237–250.
- Schliestedt, M., Okruch, M., 1988. Meta-acidites and silicic meta-sediments related to eclogites and glaucophanites in northern Sifnos, Cycladic Archipelago, Greece. In: Smith, D. C. (Ed.), *Eclogites and eclogite-facies rocks*. Vol. 12. Elsevier, Amsterdam-New York, International, pp. 291–334.
- Schmädicke, E., Will, T. M., 2003. Pressure-temperature evolution of blueschist facies rock from Sifnos, Greece, and implications for the exhumation of high-pressure rocks in the central Aegean. *Journal of Metamorphic Geology* 21 (8), 799–811.
- Schmidt, M. W., Poli, S., 1998. Experimentally based water budgets for dehydrating slabs and consequences for arc magma generation. *Earth and Planetary Science Letters* 163 (1-4), 361–379.
- Schroeder, T., John, B., Frost, B. R., 2002. Geological implications of seawater circulation through peridotite exposed at slow-spreading mid-ocean ridges. *Geology* 30 (4), 367–370.
- Schwartz, S., Allemand, P., Guillot, S., 2001. Numerical model of the effect of serpentinites on the exhumation of eclogitic rocks; insights from the Monviso ophiolitic massif (Western Alps). *Tectonophysics* 342 (1-2), 193–206.
- Senda, R., Kachi, T., Tanaka, T., 2006. Multiple records from osmium, neodymium, and strontium isotope systems of the nikubuchi ultramafic complex in the sambagawa metamorphic belt, central shikoku, japan. *Geochemical Journal* 40 (2), 135–148.
- Sengör, A. M. C., Natal'In, B. A., 1996. Paleotectonics of Asia: fragments of a synthesis. In: Yin, A., Harrison, M. (Eds.), *The Tectonic Evolution of Asia*. World and Regional Geology Series. Cambridge University Press, Cambridge, New York, Melnourne, pp. 486–640.
- Snow, J. E., Hart, S. R., Dick, H. J. B., 1994. Nd and Sr Isotope Evidence Linking Mid-Ocean-Ridge Basalts and Abyssal Peridotites. *Nature* 371 (6492), 57–60.
- Snow, J. E., Reisberg, L., 1995. Os isotopic systematics of the MORB mantle: results from altered abyssal peridotites. *Earth and Planetary Science Letters* 133, 411–421.
- Sobolev, N. V., Dobretsov, N. L., Bakirov, A. B., Shatsky, V. S., 1986. Eclogites from various types of metamorphic complexes in the USSR and the problems of their origin. In: Evans, B., Brown, E. (Eds.), *Blueschists and eclogites*. Vol. 164;. Geological Society of America (GSA), Boulder, CO, United States, pp. 349–363.
- Spandler, C., Hermann, J., Faure, K., Mavrogenes, J. A., Arculus, R. J., 2008. The importance of talc and chlorite "hybrid" rocks for volatile recycling through subduction zones; evidence from the high-pressure subduction mlang of New Caledonia. *Contributions to mineralogy and petrology* 155, 181–198.
- Spear, F. S., Wark, D. A., Cheney, J. T., Schumacher, J. C., Watson, B. E., 2006. Zr-in-rutile thermometry in blueschists from Sifnos, Greece. *Contributions to mineralogy and petrology* 152, 375–385.
- Staudigel, H., 2003. Hydrothermal alteration processes in the oceanic crust. In: Rudnick, R. L. (Ed.), *The Crust*. Vol. 3 of *Treatise on Geochemistry*. Elsevier-Pergamon, Oxford, pp. 511–536.
- Staudigel, H., Davies, G. R., Hart, S. R., Marchant, K. M., Smith, B. M., 1995. Large-Scale Isotopic Sr, Nd and O Isotopic Anatomy of Altered Oceanic-Crust - Dsdp/Odp Sites-417/418. *Earth and Planetary Science Letters* 130 (1-4), 169–185.
- Trotet, F., Vidal, O., Jolivet, L., 2001. Exhumation of Syros and Sifnos metamorphic rocks (Cyclades, Greece); new constraints on the P-T paths. *European Journal of Mineralogy* 13 (5), 901–920.
- Valley, J. W., Kitchen, N., Kohn, M. J., Niendorf, C. R., Spicuzza, M. J., 1995. UWG-2, a garnet standard for oxygen isotope ratios: Strategies for high precision and accuracy with laser heating. *Geochimica et Cosmochimica Acta* 59 (24), 5223–5231.

- van der Straaten, F., Schenk, V., John, T., in review. Fluid-induced chemical and petrophysical changes associated with the retrograde eclogite-blueschist transformation: Constraints for metasomatism and exhumation processes within a subduction channel. *Contribution to Mineralogy and Petrology*.
- van der Straaten, F., Schenk, V., John, T., Gao, J., 2008. Blueschist-facies rehydration of eclogites (Tian Shan, NW-China): implications for fluid-rock interaction in the subduction channel. *Chemical Geology* 255 (1-2), 195–219.
- van Hinsbergen, D. J. J., 2004. The evolving anatomy of a collapsing orogen. *Geologica Ultraiectina* 243, p. 280.
- Veizer, J., 1989. Strontium isotopes in seawater through time. *Annual Review of Earth and Planetary Sciences* 17, 141–167.
- Warren, C. J., Beaumont, C., Jamieson, R. A., 2008. Modelling tectonic styles and ultra-high pressure (UHP) rock exhumation during the transition from oceanic subduction to continental collision. *Earth and Planetary Science Letters* 267 (1-2), 129–145.
- Wijbrans, J. R., Schliestedt, M., York, D., 1990. Single grain argon laser probe dating of phengites from the blueschist to greenschist transition on Sifnos (Cyclades, Greece). *Contributions to mineralogy and petrology* 104 (5), 582–593.
- Yui, T.-F., Rumble, D. I., Chen, C.-H., Lo, C.-H., 1997. Stable isotope characteristics of eclogites from the ultra-high-pressure metamorphic terrain, east-central china. *Chemical Geology* 137, 135–147.
- Zack, T., John, T., 2007. An evaluation of reactive fluid flow and trace-element mobility in subducting slabs. *Chemical Geology* 239, 199–216.
- Zheng, Y. F., 1993a. Calculation of oxygen isotope fractionation in anhydrous silicate minerals. *Geochimica et Cosmochimica Acta* 57 (5), 1079–1091.
- Zheng, Y. F., 1993b. Calculation of oxygen isotope fractionation in hydroxyl-bearing silicates. *Earth and Planetary Science Letters* 120, 247–263.
- Zheng, Y. F., Fu, B., Gong, B., Li, L., 2003. Stable isotope geochemistry of ultrahigh pressure metamorphic rocks from the Dabie-Sulu orogen in China: implications for geodynamics and fluid regime. *Earth-Science Reviews* 62, 105–161.
- Zheng, Y. F., Fu, B., Xiao, Y., Li, Y., Gong, B., 1999. Hydrogen and oxygen isotope evidence for fluid-rock interactions in the stages of pre- and post-UHP metamorphism in the Dabie Mountains. *Lithos* 46, 677–693.



# List of Figures

1.1	Subduction channel model . . . . .	1
1.2	P-T paths in subduction channel . . . . .	2
2.1	Geological map of the Southern Tian Shan . . . . .	10
2.2	Photographs of the pillow meta-basalts (Tian Shan) . . . . .	14
2.3	Modal amounts of eclogites and blueschists (pillow meta-basalts) . . . . .	15
2.4	Photomicrographs of eclogite-blueschist transformation . . . . .	17
2.5	Mn-mapping of eclogite- and blueschist-facies garnet . . . . .	18
2.6	Chondrite-normalised REE concentrations . . . . .	20
2.7	Mineral chemical compositions . . . . .	24
2.8	P-T pseudosections of eclogite . . . . .	28
2.9	P-T pseudosection of blueschist . . . . .	29
2.10	Chondrite-normalised REE of eclogites and blueschists . . . . .	31
2.11	Evidence for seawater alteration? . . . . .	35
2.12	Trace and volatile element variations . . . . .	36
2.13	Mass-balance calculation of pillow meta-basalts) . . . . .	39
2.14	Element mobility during eclogite-blueschist transformation . . . . .	42
2.15	Schematic eclogite-blueschist transformation of pillow meta-basalts . . . . .	45
3.1	Geological map of the Tian Shan (China) . . . . .	55
3.2	Photographs of eclogite-blueschist sequences (Tian Shan, Sifnos) . . . . .	57
3.3	Microphotographs of eclogite-blueschist transformation . . . . .	58
3.4	BSE image of eclogite, sample FTS 9-1.5A (Tian Shan) and Si 4-2.4 (Sifnos) . . . . .	59
3.5	Geological map of Greece and Sifnos . . . . .	61
3.6	WR Co vs. Th of eclogites (Sifnos and FTS 9-1 seq.) . . . . .	62
3.7	Chondrite-normalised REE of eclogites (Sifnos and FTS 9-1 seq.) . . . . .	64
3.8	N-MORB normalised eclogites (Sifnos and FTS 9-1 seq.) . . . . .	64
3.10	Chondrite-normalised REE concentrations, sample FTS 9-1.5A . . . . .	66
3.9	Composition of garnets (Sifnos and FTS 9-1 seq.) . . . . .	67
3.11	Composition of clinopyroxene (Sifnos and FTS 9-1 seq.) . . . . .	70
3.12	Composition of amphiboles (Sifnos and FTS 9-1 seq.) . . . . .	71
3.13	Composition of white mica (Sifnos and FTS 9-1 seq.) . . . . .	74
3.14	Composition of clinozoisite (Sifnos) . . . . .	74
3.15	(La/Sm) <sub>N</sub> vs. Nb/La plot and Nb/Yb vs. Th/Yb plot . . . . .	76

---

3.16	P-T pseudosections for the eclogite, sample FTS 9–1.5A (FTS 9–1 seq.) . . .	79
3.17	P-T pseudosections of eclogite, sample Si 4–2.1 (Sifnos) . . . . .	83
3.18	P-T path in subduction channels . . . . .	84
3.19	Element mobility of Sifnos and FTS 9-1 seq. . . . .	86
3.20	Element mobility of FTS 9-1 seq. . . . .	87
3.21	P-T pseudosection of the depleted mantle . . . . .	89
3.22	Density gradient of eclogites compared to depleted mantle . . . . .	90
4.1	Geological map of Sifnos (Greece) . . . . .	100
4.2	Photographs of eclogite–blueschist sequences (Sifnos and Tian Shan) . . .	101
4.3	Mass–balances of eclogite–blueschist sequences (Sifnos and Tian Shan) . .	102
4.4	Geological map of sample area (Tian Shan, China) . . . . .	104
4.5	$\delta^{18}\text{O}$ values of eclogite–blueschist sequences . . . . .	106
4.6	Sr and Nd isotope composition of eclogite–blueschist sequences . . . . .	107
4.7	WR $^{87}\text{Rb}/^{86}\text{Sr}$ isochrons (pillow meta-basalts) . . . . .	108
4.8	Evidence for seawater alteration? . . . . .	115
4.9	Peridotite affinity of eclogite–blueschist sequences . . . . .	118



# List of Tables

2.1	Representative mineral analyses (cont.) . . . . .	21
2.2	Representative LA-ICP-MS mineral analyses . . . . .	23
2.3	Representative whole rock data (pillow meta-basalts) . . . . .	32
3.1	Representative LA-ICP-MS mineral analyses . . . . .	63
3.2	Representative whole rock data (FTS 9–1 sequence) . . . . .	65
3.3	Representative microprobe analyses of garnet (FTS 9–1 seq. and Sifnos) . . . . .	68
3.4	Representative microprobe analyses of omphacite (Sifnos and FTS 9–1 seq.) . . . . .	69
3.5	Representative microprobe analyses of amphibole (Sifnos and FTS 9–1 seq.) . . . . .	72
3.6	Representative microprobe analyses of white mica (FTS 9–1 seq. and Sifnos) . . . . .	73
3.7	Representative microprobe analyses (Sifnos and FTS 9–1 seq.) . . . . .	75
4.1	Mineral O isotope analyses . . . . .	110
4.2	Whole rock Sr and Nd isotope analyses . . . . .	112
A.1	Analyses of international rock standard by XRF. . . . .	133
A.2	Analyses of blank, standard and duplicate by ICP–MS. . . . .	134
A.3	Analyses of standards by LA–ICP–MS. . . . .	135
A.4	Analyses of international rock standards by ICP-OES. . . . .	136
A.5	Perple_X data . . . . .	136



# Appendix A

## Geochemical analyses of international rock standards and used parameters for Perple\_X (Chapter 2 and 3).

Table A.1: Analyses of international rock standard by XRF.

	BHVO.1			
	n = 12	1 $\sigma$	RSD %	Ref.
SiO <sub>2</sub>	49.9	0.11	0.22	49.8
Al <sub>2</sub> O <sub>3</sub>	13.6	0.04	0.26	13.7
TiO <sub>2</sub>	2.78	0.01	0.27	2.75
MgO	7.01	0.06	0.91	7.22
Fe <sub>2</sub> O <sub>3</sub>	12.2	0.04	0.30	12.4
CaO	11.5	0.03	0.25	11.4
P <sub>2</sub> O <sub>5</sub>	0.28	0.00	1.32	0.27
Na <sub>2</sub> O	2.5	0.03	1.06	2.3
K <sub>2</sub> O	0.53	0.00	0.82	0.53
MnO	0.17	0.00	0.00	0.17

Concentrations given in wt%, RSD = relative standard deviation in %, Ref. = published analytical data: BHVO.1 ([Flanagan, 1976](#)).

**Table A.2:** Analyses of blank, standard and duplicate by ICP-MS.

	blank	BHVO.2				FTS 4-1.1		
	N = 3	N = 3	1 $\sigma$	RSD %	Ref.	N = 5	1 $\sigma$	RSD %
Li	0.001	4.51	0.038	0.84	4.80	43.8	0.183	0.38
Sc	0.000	31.6	0.190	0.60	32.0	24.9	0.915	3.35
V	0.097	316	2.083	0.66	317	204	7.629	3.41
Cr	0.045	193	15.32	7.92	280	235	8.439	3.27
Co	0.000	43.8	0.357	0.82	45.0	41.9	1.322	2.88
Ni	0.013	117	1.028	0.88	119	224	6.100	2.49
Cu	-0.014	124	0.518	0.42	127	66.8	2.046	2.80
Zn	0.127	102	0.588	0.58	103	102	2.440	2.19
Ga	0.000	21.0	0.023	0.11	22.0	19.6	0.469	2.19
Rb	0.001	8.88	0.085	0.96	9.11	69.2	1.445	1.91
Sr	0.007	392	2.494	0.64	396	138	3.906	2.59
Y	0.000	24.5	0.109	0.44	26.0	10.4	0.174	1.53
Zr	0.005	161	1.533	0.95	172	157	5.287	3.08
Nb	0.004	16.9	0.080	0.47	18.1	14.4	0.257	1.63
Mo	0.009	4.23	0.368	8.70	4.00	0.32	0.005	1.40
Cd	0.000	0.15	0.008	5.30	0.06	0.09	0.004	4.45
Sn	0.003	1.55	0.345	22.2	1.70	1.37	0.007	0.44
Sb	0.000	0.10	0.010	10.0	0.13	0.12	0.004	2.87
Cs	0.000	0.10	0.000	0.03	0.10	2.66	0.019	0.65
Ba	0.009	138	0.528	0.38	131	1160	15.74	1.24
La	0.001	15.4	0.099	0.64	15.2	6.72	0.019	0.26
Ce	0.000	38.1	0.250	0.65	37.5	19.2	0.037	0.18
Pr	0.000	5.55	0.050	0.90	5.35	2.60	0.005	0.19
Nd	0.000	25.6	0.279	1.09	24.5	11.22	0.047	0.38
Sm	0.000	6.35	0.066	1.04	6.07	2.61	0.017	0.58
Eu	0.000	2.14	0.011	0.53	2.07	0.80	0.003	0.31
Gd	0.000	6.46	0.053	0.82	6.24	2.52	0.010	0.36
Tb	0.000	0.97	0.012	1.25	0.92	0.43	0.002	0.50
Dy	0.000	5.53	0.053	0.96	5.31	2.62	0.012	0.43
Ho	0.000	1.02	0.007	0.68	0.98	0.50	0.004	0.70
Er	0.000	2.51	0.026	1.02	2.54	1.36	0.006	0.37
Tm	0.000	0.34	0.002	0.73	0.33	0.21	0.001	0.55
Yb	0.000	2.06	0.013	0.64	2.00	1.42	0.003	0.21
Lu	0.000	0.29	0.002	0.87	0.27	0.21	0.002	0.89
Hf	0.000	4.47	0.042	0.95	4.36	3.64	0.017	0.42
Ta	0.000	1.08	0.013	1.16	1.14	0.89	0.005	0.50
W	0.006	0.44	0.014	3.15	0.21	0.57	0.002	0.39
Tl	0.000	0.02	0.001	4.56	0.06	0.23	0.002	0.94
Pb	0.017	1.56	0.210	13.4	1.60	1.35	0.007	0.49
Th	0.000	1.10	0.008	0.69	1.22	1.20	0.008	0.64
U	0.000	0.42	0.005	1.21	0.40	0.20	0.002	0.92

Concentrations in ppm, RSD = relative standard deviation, Ref. = published analytical data: BHVO.2 (Wilson, 1997).

**Table A.3:** Analyses of standards by LA-ICP-MS.

Element	NIST 612				NIST 614				NIST 610			
	N=13	1 $\sigma$	RSD %	Ref.	N=4	1 $\sigma$	RSD %	Ref.	N=4	1 $\sigma$	RSD %	Ref.
Li	41.50	1.71	4.12	41.54	1.95	0.25	12.9	1.74	521	10.1	1.95	485
Be	37.41	1.75	4.67	37.74	0.79	0.05	6.02	0.76	489	19.5	3.99	466
B	33.74	2.26	6.69	34.73	1.79	0.09	5.04	1.13	384	18.3	4.76	356
V	39.32	1.98	5.03	41.05	0.88	0.06	7.13	0.95	455	24.8	5.44	442
Cr	40.05	2.29	5.72	39.88	1.03				430	20.7	4.81	405
Mn	38.72	2.15	5.55	38.43	1.44	0.21	14.6	1.37	426	19.4	4.56	433
Co	34.75	2.05	5.88	35.26	0.78	0.08	9.79	0.74	385	8.27	2.15	405
Ni	37.88	1.74	4.59	38.44	1.04	0.06	5.30		447	20.0	4.49	444
Cu	35.33	2.36	6.69	36.71	2.12	0.36	16.9	1.40	358	37.0	10.3	430
Zn	37.49	3.03	8.09	37.92	<9				420	15.6	3.72	456
Rb	30.58	2.18	7.11	31.63	0.81	0.02	2.68	0.82	424	28.6	6.75	431
Sr	75.92	3.97	5.23	76.15	43.63	1.70	3.90	45.5	470	18.4	3.91	497
Y	39.08	2.21	5.67	38.25	0.76	0.04	4.66	0.79	460	14.4	3.14	450
Zr	37.16	2.27	6.10	35.99	0.82	0.06	6.85	0.81	427	21.1	4.96	440
Nb	38.80	2.34	6.04	38.06	0.84	0.05	6.53	0.85	456	18.4	4.02	419
Mo	37.13	2.30	6.19	38.30	0.85	0.05	6.35	0.73	431	29.7	6.89	377
Cs	40.72	2.92	7.18	41.64	0.63	0.03	4.23	0.65	351	33.5	9.53	361
Ba	38.44	2.20	5.72	37.74	3.00	0.18	6.01	3.29	426	11.5	2.70	424
La	37.27	2.08	5.58	35.77	0.75	0.05	6.98	0.74	440	6.95	1.58	457
Ce	38.94	2.02	5.18	38.35	0.81	0.04	4.33	0.79	454	24.4	5.37	448
Pr	38.68	1.97	5.09	37.16	0.74	0.09	12.3	0.78	447	11.0	2.47	430
Nd	37.19	2.47	6.63	35.24	0.73	0.06	8.06	0.75	451	17.4	3.87	431
Sm	37.90	2.61	6.88	36.72	0.73	0.07	9.59	0.77	463	25.8	5.57	451
Eu	35.65	2.44	6.83	34.44	0.74	0.07	9.15	0.77	438	13.1	3.00	461
Gd	37.41	1.83	4.88	36.95	0.74	0.08	10.3	0.73	447	27.1	6.06	420
Tb	36.54	2.09	5.71	35.92	0.70	0.04	5.30	0.77	427	17.1	4.01	443
Dy	36.83	2.01	5.45	35.97	0.71	0.04	6.12	0.76	452	23.4	5.19	427
Ho	38.52	2.42	6.28	37.87	0.74	0.04	6.07	0.78	460	24.2	5.26	449
Er	37.51	1.72	4.60	37.43	0.75	0.06	7.90	0.78	464	21.0	4.53	426
Tm	38.03	2.12	5.58	37.55	0.77	0.05	6.75	0.77	450	20.3	4.51	420
Yb	39.62	2.22	5.61	39.95	0.85	0.08	9.41	0.76	472	23.3	4.95	462
Lu	38.17	2.30	6.03	37.71	0.70	0.03	3.72	0.78	475	16.3	3.42	435
Hf	35.60	2.28	6.40	34.77	0.75	0.06	8.05	0.66	432	20.6	4.77	418
Ta	40.55	2.32	5.72	39.77	0.80	0.07	8.82	0.79	492	14.4	2.93	377
Pb	38.54	3.68	9.54	38.96	2.40	0.17	7.14	2.30	421	33.5	7.94	413
Th	37.95	2.26	5.95	37.23	0.73	0.05	7.08	0.78	469	15.4	3.30	451

Concentrations given in ppm, RSD = relative standard deviation in %, Ref. = published analytical data: NIST 610,612 (Pearce et al., 1997), NIST 614 (Horn et al., 1997).

**Table A.4:** Analyses of international rock standards by ICP-OES.

	AC_E granite			BHVO_1 basalt			JDo_1 dolomite		
	Meas.	Ref.	Dev.	Meas.	Ref.	Dev.	Meas.	Ref.	Dev.
TiO <sub>2</sub>	0.10	0.11	0.01	2.74	2.75	-0.03	0.01	0.01	0.01
Al <sub>2</sub> O <sub>3</sub>	14.85	14.70	-0.15	14.52	13.70	-0.72	0.01	0.02	0.01
Fe[ <i>tot</i> ]	2.45	2.53	0.08	12.30	12.40	-0.07	0.02	0.02	0.00
MnO	0.06	0.06	0.00	0.18	0.17	-0.01	0.01	0.01	0.00
MgO	0.03	0.03	0.00	7.55	7.22	-0.32	17.82	18.47	0.65
CaO	0.31	0.34	0.03	10.71	11.40	0.69	30.42	33.96	3.54
Na <sub>2</sub> O	6.58	6.54	-0.04	2.28	2.30	-0.02	0.01	0.01	0.00
K <sub>2</sub> O	4.55	4.49	-0.06	0.56	0.53	-0.04	0.01	0.00	-0.01
P <sub>2</sub> O <sub>5</sub>	0.02	0.01	0.00	0.26	0.27	0.01	0.04	0.03	-0.01
	MAG_1 marine sediment			JLs_1 limestone			BCS_CRM393 limestone		
	Meas.	Ref.	Dev.	Meas.	Ref.	Dev.	Meas.	Ref.	Dev.
TiO <sub>2</sub>	0.66	0.75	0.09	0.00	0.02	0.02	0.00	0.01	0.01
Al <sub>2</sub> O <sub>3</sub>	15.66	16.40	0.74	0.01	0.02	0.01	0.13	0.12	-0.01
Fe[ <i>tot</i> ]	6.42	6.80	0.38	0.02	0.02	0.00	0.05	0.05	0.00
MnO	0.09	0.10	0.01	0.00	0.00	0.00	0.01	0.01	0.00
MgO	2.98	3.00	0.02	0.70	0.61	-0.09	0.18	0.15	-0.03
CaO	1.25	1.37	0.12	56.49	55.09	-1.40	56.32	55.40	-0.92
Na <sub>2</sub> O	3.74	3.83	0.09	0.00	0.00	0.00	0.01		
K <sub>2</sub> O	3.47	3.55	0.08	0.01	0.00	0.00	0.02	0.02	0.00
P <sub>2</sub> O <sub>5</sub>	0.18	0.16	-0.02	0.04	0.03	-0.01	0.01		

Meas. = analysed concentrations in wt%, Ref. = published analytical data: AC\_E (Potts and Holbrook, 1987), BHVO\_1 and Mag\_1 (Flanagan, 1976), BCS\_CRM393 (Jochum et al., 2005), JLs\_1 and JDo\_1 (Terashima et al., 1990), Dev. = deviation between Ref. and Meas.

**Table A.5:** Solid solution models and endmember parameters of mineral phases used in Perple.X.

solution name [abbr. in Figure]	endmember	
Gt(HP) [g] garnet $\text{Fe}_{3x}\text{Ca}_{3y}\text{Mg}_{3z}\text{Mn}_{3(1-x-y-z)}\text{Al}_2\text{Si}_3\text{O}_{12}$ , $x+y+z \leq 1$	alm grs py sps	$\text{Fe}_3\text{Al}_2\text{Si}_3\text{O}_{12}$ $\text{Ca}_3\text{Al}_2\text{Si}_3\text{O}_{12}$ $\text{Mg}_3\text{Al}_2\text{Si}_3\text{O}_{12}$ $\text{Mn}_3\text{Al}_2\text{Si}_3\text{O}_{12}$
Omph(HP) [om] omphacite $\text{Na}_{1-y}\text{Ca}_y\text{Mg}_{xy}\text{Fe}_{(1-x)y}\text{Al}_y\text{Si}_2\text{O}_6$	jd di hed	$\text{NaAlSi}_2\text{O}_6$ $\text{CaMgSi}_2\text{O}_6$ $\text{CaFeSi}_2\text{O}_6$
Cpx(HP) [cpx] clinopyroxene $\text{Na}_{1-y}\text{Ca}_y\text{Mg}_{xy}\text{Fe}_{(1-x)y}\text{Al}_y\text{Si}_2\text{O}_6$	jd di hed cats	$\text{NaAlSi}_2\text{O}_6$ $\text{CaMgSi}_2\text{O}_6$ $\text{CaFeSi}_2\text{O}_6$ $\text{CaAlAlSiO}_6$
Opx(HP) [opx] orthopyroxene $[\text{Mg}_x\text{Fe}_{1-x}]_{2-y}\text{Al}_2\text{ySi}_{2-y}\text{O}_6$	en fs mgts fets	$\text{Mg}_2\text{Si}_2\text{O}_6$ $\text{Fe}_2\text{Si}_2\text{O}_6$ $\text{MgAlSi}_2\text{O}_6$ $\text{FeAlSi}_2\text{O}_6$
Sp(HP) [sp] spinel $\text{Mg}_x\text{Fe}_{1-x}\text{Al}_2\text{O}_4$	sp hc	$\text{MgAl}_2\text{O}_4$ $\text{FeAl}_2\text{O}_4$
O(HP) [ol] olivine $\text{Mg}-2x\text{Fe}_{2y}\text{Mn}_{2(1-x-y)}\text{SiO}_4$ , $x+y \leq 1$	fo fa teph	$\text{Mg}_2\text{SiO}_4$ $\text{Fe}_2\text{SiO}_4$ $\text{Mn}_2\text{SiO}_4$

Amph(DPW) [(c,n)am] amphibole	tr	$\text{Ca}_2\text{Mg}_5\text{Si}_8\text{O}_{22}(\text{OH})_2$
$\text{Ca}_{2-2w}\text{Na}_z+2w[\text{Mg}_x\text{Fe}_{1-x}]_{3+2y+z}\text{Al}_{3-3y-w}\text{Si}_{7+w+y}\text{O}_{22}(\text{OH})_2$ , $w+y+z \leq 1$	ftr	$\text{Ca}_2\text{Fe}_5\text{Si}_8\text{O}_{22}(\text{OH})_2$
	gl	$\text{Na}_2\text{Mg}_3\text{Al}_2\text{Si}_8\text{O}_{22}(\text{OH})_2$
	fgl	$\text{Na}_2\text{Fe}_3\text{Al}_2\text{Si}_8\text{O}_{22}(\text{OH})_2$
	ts	$\text{CaNaMg}_3\text{Al}_2\text{Si}_6\text{Al}_2\text{O}_{22}(\text{OH})_2$
	fts	$\text{CaNaFe}_3\text{Al}_2\text{Si}_6\text{Al}_2\text{O}_{22}(\text{OH})_2$
	parg	$\text{NaCa}_2\text{Mg}_4\text{AlSi}_6\text{Al}_2\text{O}_{22}(\text{OH})_2$
	fparg	$\text{NaCa}_2\text{Fe}_4\text{AlSi}_6\text{Al}_2\text{O}_{22}(\text{OH})_2$
GlTrTs [nam] sodic-calcic amphibole	tr	$\text{Ca}_2\text{Mg}_5\text{Si}_8\text{O}_{22}(\text{OH})_2$
$\text{Ca}_{2-2w}\text{Na}_{2w}[\text{Mg}_x\text{Fe}_{1-x}]_{3+2y}\text{Al}_{3-3y-w}\text{Si}_{7+w+y}\text{O}_{22}(\text{OH})_2$ , $w+y \leq 1$	ftr	$\text{Ca}_2\text{Fe}_5\text{Si}_8\text{O}_{22}(\text{OH})_2$
	gl	$\text{Na}_2\text{Mg}_3\text{Al}_2\text{Si}_8\text{O}_{22}(\text{OH})_2$
	fgl	$\text{Na}_2\text{Fe}_3\text{Al}_2\text{Si}_8\text{O}_{22}(\text{OH})_2$
	ts	$\text{CaNaMg}_3\text{Al}_2\text{Si}_6\text{Al}_2\text{O}_{22}(\text{OH})_2$
	fts	$\text{CaNaFe}_3\text{Al}_2\text{Si}_6\text{Al}_2\text{O}_{22}(\text{OH})_2$
Bio(HP) [bi] biotite	phl	$\text{KMg}_6\text{Si}_6\text{Al}_2\text{O}_{20}(\text{OH})_4$
$\text{K}[\text{Mg}_x\text{Fe}_y\text{Mn}_{1-x-y}]_{3-w}\text{Al}_{1+2w}\text{Si}_{3-w}\text{O}_{10}(\text{OH})_2$ , $x+y \leq 1$	ann	$\text{KFe}_6\text{Si}_6\text{Al}_2\text{O}_{20}(\text{OH})_4$
	east	$\text{KMg}_4\text{Al}_2\text{Si}_4\text{Al}_4\text{O}_{20}(\text{OH})_4$
	sdph	$\text{KFe}_4\text{Al}_2\text{Si}_4\text{Al}_4\text{O}_{20}(\text{OH})_4$
	mmbi	$\text{KMn}_6\text{Si}_6\text{Al}_2\text{O}_{20}(\text{OH})_4$
	mmts	$\text{KMn}_4\text{Al}_2\text{Si}_4\text{Al}_4\text{O}_{20}(\text{OH})_4$
Pheng(HP) [wm] phengite	pa	$\text{NaAl}_2\text{Si}_3\text{AlO}_{10}(\text{OH})_2$
$\text{K}_x\text{Na}_{1-x}\text{Mg}_y\text{Fe}_z\text{Al}_{3-2(y+z)}\text{Si}_{3+y+z}\text{O}_{10}(\text{OH})_2$	cel	$\text{KMgAlSi}_4\text{O}_{10}(\text{OH})_2$
	fcel	$\text{KFeAlSi}_4\text{O}_{10}(\text{OH})_2$
	mu	$\text{KAl}_2\text{Si}_3\text{AlO}_{10}(\text{OH})_2$
Chl(HP) [chl] chlorine	daph	$\text{Fe}_5\text{Al}_2\text{Si}_3\text{O}_{10}(\text{OH})_8$
$[\text{Mg}_x\text{Fe}_w\text{Mn}_{1-x-w}]_{5-y+z}\text{Al}_{2(1+y-z)}\text{Si}_{3-y+z}\text{O}_{10}(\text{OH})_8$ , $x+w \leq 1$	clin	$\text{Mg}_5\text{Al}_2\text{Si}_3\text{O}_{10}(\text{OH})_8$
	ames	$\text{Mg}_4\text{Al}_4\text{Si}_2\text{O}_{10}(\text{OH})_8$
	afchl	$\text{Mg}_6\text{Si}_4\text{O}_{10}(\text{OH})_8$
	mnchl	$\text{Mn}_5\text{Al}_2\text{Si}_3\text{O}_{10}(\text{OH})_8$
T [tlc] talc	ta	$\text{Mg}_3\text{Si}_4\text{O}_{10}(\text{OH})_2$
$[\text{Mg}_x\text{Fe}_{1-x}]_{3-y}\text{Al}_2\text{Si}_4\text{O}_{10}(\text{OH})_2$	fta	$\text{Fe}_3\text{Si}_4\text{O}_{10}(\text{OH})_2$
	tats	$\text{Mg}_2\text{Al}_2\text{Si}_3\text{O}_{10}(\text{OH})_2$
	ftat	$\text{tats} + \frac{2}{3}\text{fta} - \frac{2}{3}\text{ta}$
Atg [atg] serpentine	atg	$\text{Mg}_3\text{Si}_2\text{O}_5(\text{OH})_2$
$\text{Mg}_{48x}\text{Fe}_{48(1-x)}\text{Si}_{34}\text{O}_{85}(\text{OH})_{62}$	fatg	$1\text{atg} - 16\text{ta} + 16\text{fta}$
B [brc] brucite	br	$\text{Mg}(\text{OH})_2$
$\text{Mg}_x\text{Fe}_{1-x}(\text{OH})_2$	fbr	$1\text{br} - \frac{1}{3}\text{ta} + \frac{1}{3}\text{fta}$
Do(HP) (ank)	dol	$\text{CaMg}(\text{CO}_3)_2$
$\text{CaMg}_x\text{Fe}_{1-x}(\text{CO}_3)_2$	ank	$\text{CaFe}(\text{CO}_3)_2$
law [law] lawsonite	law	$\text{CaAl}_2\text{Si}_2\text{O}_7(\text{OH})_2\text{H}_2\text{O}$
pa [pa] paragonite	pa	$\text{NaAl}_2\text{Si}_3\text{AlO}_{10}(\text{OH})_2$
zo [zo] zoisite/clinozoisite	zo	$\text{Ca}_2\text{Al}_3\text{Si}_3\text{O}_{12}(\text{OH})$
ru [ru] rutile	ru	$\text{TiO}_2$
sph [sph] titanite	sph	$\text{CaTiSiO}_5$
q [q] quartz	q	$\text{SiO}_2$

see solut\_07.dat and "Perple\_X Solution Model Glossary" at <http://www.perplex.ethz.ch/> for details and citations of solid solution models.

## References

- Flanagan, F. J., 1976. Description and analyses of eight new USGS rock standards. USGS Professional Paper 840, 1–192.
- Horn, I., Hinton, R. W., Jackson, S. E., Longerich, H. P., 1997. Ultra-trace element analysis of NIST SRM 616 and 614 using laser ablation microprobe-inductively coupled plasma-mass spectrometry (LAM-ICP-MS): a comparison with secondary ion mass spectrometry (SIMS). *Geostandards Newsletter* 21 (2), 191–203.
- Jochum, K. P., Nohl, U., Herwig, K., Lammel, E., Stoll, B., Hofmann, A. W., 2005. GeoReM: A new geochemical database for reference materials and isotopic standards. *Geostandards and Geoanalytical Research* 29 (3), 333–338.
- Pearce, N. J. G., Perkins, W. T., Westgate, J. A., Gorton, M. P., Jackson, S. E., Neal, C. R., Chenery, S. P., 1997. A compilation of new and published major and trace element data for NIST SRM 610 and NIST SRM 612 glass reference materials. *Geostandards Newsletter-the Journal of Geostandards and Geoanalysis* 21 (1), 115–144.
- Potts, P. J., Holbrook, J. R., 1987. Alisa Craig - The history of a reference material. *Geostandards Newsletter* 11, 257–260.
- Terashima, S., Ando, A., Okai, T., Kanai, Y., Taniguchi, M., Takizawa, F., Itho, S., 1990. Elemental concentrations in nine new GSJ rock reference samples "sedimentary rock series". *Geostandards Newsletter* 14, 1–5.
- Wilson, S., 1997. Data compilation for USGS reference material BHVO-2, Hawaiian Basalt. U.S. Geological Survey Open-File Report X, xxx.



# Addendum

## Danksagung

Bei der Erstellung dieser Dissertation bin ich einer Vielzahl von Menschen zu Dank verpflichtet. Prof. Dr. Volker Schenk danke ich für die intensive Betreuung. Seine Begeisterung für Petrologie hat mein fachliches Wissen bereichert. Prof. Dr. Volker Schenk, Dr. Timm John und Dr. Petra Herms, sowie dem Sonderforschungsbereich 574 “Volatiles and Fluids in Subduction zones” danke ich an dieser Stelle für die Antragstellung im Projekt C1, die die Finanzierung der Dissertation ermöglicht hat.

Ich danke auch den drei genannten bei der Probennahme auf den Kykladen und im Tian Shan. Neben der angenehmen Atmosphäre und viel Spaß (der Einfachheit wegen wurde aus der Eklogit-Blauschiefer Überprägung schlicht nur noch grün-blau) habe ich noch sehr viel im Gelände dazu gelernt. An dieser Stelle danke ich auch Prof. Dr. Jun Gao für die Finanzierung und die Ermöglichung der China Expedition in den Tian Shan. Dr. Xiong Xiangming und Herr Zhang haben bei der Organisation und Mithilfe bei der Geländearbeit tatkräftig mitgewirkt. Ich danke den Beiden, dass sie uns den Aufenthalt in China so angenehm wie möglich gemacht haben.

Dr. Timm John danke ich für die unermüdliche Motivation und die geduldigen Diskussionsrunden. Die vorliegende Arbeit hat davon sehr profitiert. Er war mir während der gesamten Zeit ein Wegweiser und Freund.

Ralf Halama danke ich für die Hilfe bei der Interpretation von geochemischen Daten, vor allem der Isotopen-geochemie. Peter Appel und Barbara Mader danke ich für die Betreuung bei der Mikrosonde. Insbesondere danke ich Dieter Garbe-Schönberg für die intensive Betreuung und Hilfestellung bei der ICP-MS und ICP-OES Analytik. Hier seien auch Ulrike, Petra und Karin als treue Laborfeen erwähnt. Andreas Fehler danke ich für die Anfertigung von unzähligen Dünnschliffen. Christof danke ich für die Unterstützung in der Probenaufbereitung und Analytik, während seiner Hiwi-Zeit. Meinen Kollegen: Niels, Denny, Nelson, Peter, Peter, Petra, Wolf-Achim, Timm, Ralf und Sönke und den Studierenden, die mich in der Zeit begleitet haben, mich abgelenkt haben, wenn es sein musste oder mich wieder aufgebaut haben, danke ich recht herzlich.

Meiner Familie und meinen Freunden danke ich für die Unterstützung und Durchhalteparolen und für die erforderliche Ablenkung, die jeder mal braucht. Ich danke auch meinen Freunden, die sich ebenfalls in einer Promotion befinden oder befanden und mit denen ich das “Malefiz” spielen konnte.

## Curriculum vitae

### Persönliche Daten

François van der Straaten

Dorotheenstrasse 19  
24113 Kiel

geboren am 16. April 1976 in Ede (NL)  
deutsche und niederländische Staatsbürgerschaft  
fs@min.uni-kiel.de

### Ausbildung

ab 02/2005	Christian-Albrechts-Universität zu Kiel Promotionsstudent
10/1998–01/2005	Friedrich-Alexander-Universität Erlangen-Nürnberg Studium der Geologie und Paläontologie
08/2004	Abschluss zum Diplom Geologen
03/1998–09/1998	Steigenberger Hotel“Drei Mohren”, Augsburg Empfangssekretär
09/1995–01/1998	Koch’s Hotel, Olpe Ausbildung zum Hotelfachmann
08/1992–06/1995	Städtisches Gymnasium, Olpe schulische Ausbildung mit Abitur

## Erklärung

Hiermit erkläre ich, dass ich, François van der Straaten, die vorliegende Abhandlung in Inhalt und Form selbständig angefertigt, und abgesehen von den wissenschaftlichen Beratungen durch meine akademischen Lehrer nur die angegebenen Hilfsmittel verwendet habe. Ich erkläre ferner, dass ich weder diese noch eine vergleichbare Arbeit an anderer Stelle im Rahmen eines Prüfungsverfahrens vorgelegt habe.

September 2008  
Kiel

François van der Straaten